The Pennsylvania State University

The Graduate School

College of Engineering

SYNTHESIS OF ADVANCED CONTROL STRUCTURES FOR

COMPLEX CHEMICAL PROCESSES USING SENSOR

NETWORKS

A Dissertation in

Chemical Engineering

by

Davood Babaei Pourkargar

Submitted in Partial Fulfillment

of the Requirements

for the Degree of

Doctor of Philosophy

August 2015

The dissertation of Davood Babaei Pourkargar was reviewed and approved* by the following:

Antonios Armaou

Associate Professor of Chemical Engineering

Dissertation Advisor, Chair of Committee

Ali Borhan

Professor of Chemical Engineering

Christopher D. Rahn

Professor of Mechanical Engineering

Kyle Bishop

Assistant Professor of Chemical Engineering

Phillip E. Savage

Professor of Chemical Engineering

Walter L. Robb Chair and Head of the Department of Chemical Engineering

*Signatures are on file in the Graduate School.

ABSTRACT

In recent years the interest in control of distributed parameter systems (DPSs) has significantly increased in the chemical and advanced material process industries. This is due to the need to synthesize control structures for complex transport-reaction processes which are characterized by the coupling of chemical reactions with significant convection, diffusion, and dispersion phenomena. Such processes as exemplified by packed and fluidized bed reactors in chemical plants, reactive distillation in petrochemical industries processes, most lithographic and deposition processes in microelectronics and advanced materials manufacturing, and finally crystal and glass production, exhibit spatial variations that need to be explicitly accounted for by the controller.

An important observation is that the long term behavior of the above chemical processes can be captured by a finite number of degrees of freedom; thus the partial differential equation (PDE) descriptions can be effectively approximated by reduced order models (ROMs) in the form of finite dimensional ordinary differential equations (ODEs). For processes with nonlinear spatial operators and/or complex

process domains, the ODEs can only be obtained via data-driven order reduction methods. Their major shortcoming is that they require a representative ensemble of solutions pre-exists for the process to be properly described, while there isn't a systematic method to ensure this important prerequisite. Currently, there is a lack of systematic and computationally-efficient data-driven methodologies for optimization and control of nonlinear PDE systems with complex spatial domains.

The proposed research will extend the applicability of control-oriented data-driven nonlinear order reduction methods for dissipative nonlinear PDE systems. The intellectual objective is to relax the requirement of a representative ensemble of solutions and develop a systematic data-driven order reduction methodology specifically tailored for control of PDE systems. It will thus resolve a fundamental limitation of data-driven techniques for control synthesis of spatially distributed processes. The main contributions of the proposed research can be classified as (a) deriving a computationally efficient adaptive model order reduction framework to circumvent the limitations of the current model order reduction techniques for control of nonlinear DPSs, and (b) synthesizing advanced output feedback control structures that can guarantee closed-loop stability and performance while (c) identifying criteria to minimize the required information for the controller structure revisions.

TABLE OF CONTENTS

Chapter 8
Adaptive control of distributed parameter systems via model order reduction   **246**

LIST OF FIGURES

xii

LIST OF TABLES

ACKNOWLEDGMENTS

First and foremost, I would like to express my sincere gratitude to my advisor, Professor Antonios Armaou for his motivation, support and guidance throughout my doctoral research work. I am really indebted to him for encouraging and guiding me to become an independent researcher.

I would like to thank Professor Ali Borhan, Professor Christopher Rahn and Professor Kyle Bishop for agreeing to serve on my doctoral committee.

I would like to thank my parents for their encouragement and love. Last but not least, I would like to express my deepest gratitude to my wife, Setareh, for her unconditional love, encouragement, patience and support. Her contribution to my life is so great to fit on this page.

With them the Seed of Wisdom did I sow,

And with my own hand labourd it to grow:

And this was all the Harvest that I reap'd -

I came like Water, and like Wind I go.

Omar Khayyam, 1048-1131

Persian Mathematician, Astronomer, Philosopher, and Poet

INTRODUCTION

1.1 Distributed parameter systems in chemical process industries

In the last twenty years the need for production of high purity chemicals and materials with complex structures, and efficient energy use in chemical and advanced material industries have motivated research on processes development. As fabrication processes become elaborate they necessitate the introduction of advanced mathematical techniques for their modeling, simulation, analysis, optimization and control.

Nonlinear distributed parameter models provide a natural framework for de-

scribing distributed product properties as a function of process conditions in typical complex transport-reaction processes which are characterized by the coupling of chemical reactions with significant convection, diffusion, and dispersion phenomena. Such processes as exemplified by the ones in Table 1.1, exhibit spatial variations that need to be explicitly accounted by the controller. The governing models obtained from balance equations (momentum, material and energy) are usually in the form of partial differential equations (PDEs).

Table 1.1: Complex processes with spatial variation in corresponding industries

1)	Packed and fluidized bed reactors in chemical plants
2)	Reactive distillation in petrochemical industries
3)	Lithographic processes
4)	Chemical vapor deposition, etching processes and plasma discharge reactors in microelectronics manufacturing and complex materials production
5)	Crystallization and polymerization processes
6)	Tin float bath processes in glass production

1.2   Mathematical formulation

We consider highly dissipative distributed parameter systems (DPSs) which can be described by the following general form of input-affine PDEs,

$$
\begin{aligned}
\frac{\partial}{\partial t}\bar{x}(z,t) &= \mathcal{F}_n(z,\bar{x}) + H(z,\bar{x}) + B(z)u(t), \\
\Gamma(\bar{x}, \frac{\partial}{\partial z}\bar{x}, \ldots, \frac{\partial^{n-1}}{\partial z^{n-1}}\bar{x})\Big|_{\partial\Omega} &= 0, \\
\bar{x}(z,0) &= \bar{x}_i(z),
\end{aligned}
\tag{1.1}
$$

where $\bar{x} = [\bar{x}_1 \ \bar{x}_2 \ \cdots \ \bar{x}_k]^T \in \mathbb{R}^k$ denotes the vector of spatially distributed states of the system, $z \in \Omega \subset \mathbb{R}^3$ is the spatial coordinate, Ω is the process domain and t indicates the time. The term $\mathcal{F}_n$ presents the nonlinear differential operator of order n, H denotes an algebraic smooth nonlinear Lipschitz function and $u \in \mathbb{R}^l$ is the vector of manipulated inputs where l denotes the number of inputs. The vector function of $B^T(z)$ describes the spatial distribution of the manipulated inputs. The vector of $\Gamma(\cdot)$ presents the homogeneous boundary conditions defined over the process boundary of $\partial\Omega$, and $\bar{x}_i$ is a smooth function that describes the initial spatial profile.

The general nonlinear PDE system of (1.1) presents a wide range of dissipative DPSs [205]. The PDE system is

1. linear, if and only if H is a linear function and the spatial differential operator of $\mathcal{F}_n(z, \bar{x})$ takes the following linear form,

$$\mathcal{F}_n(z, \bar{x}) = \alpha_n(z)\frac{\partial^n \bar{x}}{\partial z^n} + \alpha_{n-1}(z)\frac{\partial^{n-1}\bar{x}}{\partial z^{n-1}} + \cdots + \alpha_1(z)\frac{\partial \bar{x}}{\partial z},$$

2. semilinear, if and only if it is not linear and the coefficient of derivative of order n in the spatial differential operator of $\mathcal{F}_n$ is only a function of the spatial coordinate as follows,

$$\mathcal{F}_n(z, \bar{x}) = \alpha(z)\frac{\partial^n \bar{x}}{\partial z^n} + g\Big(\frac{\partial^{n-1}\bar{x}}{\partial z^{n-1}}, \frac{\partial^{n-2}\bar{x}}{\partial z^{n-2}}, \ldots, \frac{\partial \bar{x}}{\partial z}, \bar{x}, z\Big),$$

3. quasilinear, if and only if it isn't linear nor semilinear, and the coefficient of derivative of order n in the spatial differential operator of $\mathcal{F}_n$ depends on the spatial coordinate and derivatives of order strictly less than n as described below,

$$\mathcal{F}_n(z,\bar{x}) = \alpha\Big(\frac{\partial^{n-1}\bar{x}}{\partial z^{n-1}}, \frac{\partial^{n-2}\bar{x}}{\partial z^{n-2}}, \ldots, \frac{\partial\bar{x}}{\partial z}, \bar{x}, z\Big)\frac{\partial^n\bar{x}}{\partial z^n} + g\Big(\frac{\partial^{n-1}\bar{x}}{\partial z^{n-1}}, \frac{\partial^{n-2}\bar{x}}{\partial z^{n-2}}, \ldots, \frac{\partial\bar{x}}{\partial z}, \bar{x}, z\Big),$$

4. nonlinear, when it can not be classified as linear, semilinear or quasilinear PDEs in the most general form of (1.1),

$$\mathcal{F}_n(z,\bar{x}) = h\Big(\frac{\partial^n\bar{x}}{\partial z^n}, \frac{\partial^{n-1}\bar{x}}{\partial z^{n-1}}, \frac{\partial^{n-2}\bar{x}}{\partial z^{n-2}}, \ldots, \frac{\partial\bar{x}}{\partial z}, \bar{x}, z\Big),$$

where α and g are possibly nonlinear functions and h is a nonlinear function. According to such classification we obtain that

$$\textit{Linear PDE} \subsetneq \textit{Semilinear PDE} \subsetneq \textit{Quasilinear PDE} \subsetneq \textit{Nonlinear PDE}.$$

There also exists another classification for two dimensional second order linear PDEs in the general form of

$$A\frac{\partial^2\bar{x}}{\partial z_1^2} + B\frac{\partial^2\bar{x}}{\partial z_1\partial z_2} + C\frac{\partial^2\bar{x}}{\partial z_2^2} + D\frac{\partial\bar{x}}{\partial z_1} + E\frac{\partial\bar{x}}{\partial z_2} + F\bar{x} + G = 0, \qquad (1.2)$$

where $A, \ldots, G$ are constant coefficients. The PDE of (1.2) is called elliptic for $B^2 - 4AC < 0$, parabolic for $B^2 - 4AC = 0$ and hyperbolic for $B^2 - 4AC > 0$. Note that a wide range of governing PDEs in the momentum, heat and mass transfer processes can be classified in such standard linear forms.

We assume that the highly dissipative PDE of (1.1) has a unique sufficiently smooth solution for the linear, semilinear, quasilinear and nonlinear forms. The reader may refer to [205] to find the required solutions and detailed existence and uniqueness discussions for different classes of PDEs.

Mathematical models for a wide range of transport-reaction processes and fluid dynamic systems derived by momentum, mass and energy conservation equations take the form of highly dissipative (typically parabolic) PDEs. The notion of dissipativity which arises in a variety of physico-chemical processes indicates the dissipation of some energy associated with the system. Such processes are contrasted with energy conserving systems called Hamiltonian systems [69]. Highly dissipative PDE systems are characterized by dominant dynamics which can be approximated using low-dimensional ordinary differential equation (ODE) models.

The PDE system of (1.1) can be presented as an infinite-dimensional system in a relevant Sobolev space $\mathbf{W}^{(n-1),2}(\Omega, \mathbb{R})$, $\forall i, j \in \mathbb{N}$, $i \geqslant 1$ and $1 \leqslant j < \infty$,

$$\mathbf{W}^{i,j} = \left\{ \bar{x} \in L^j(\Omega) : \ \partial^\alpha \bar{x} \in L^j(\Omega), \forall \alpha \in \mathbb{N}, |\alpha| \leqslant i \right\},$$

where Sobolev spaces are functional subspaces that consider functions for which

all the distributional derivatives can be applied. We can define the inner product

and norm in $L_2(\Omega)$ as

$$(\vartheta_1, \vartheta_2) = \int_\Omega r(z)\vartheta_1^T(z)\vartheta_2(z)dz, \quad \|\vartheta_1\|_2 = (\vartheta_1, \vartheta_1)^{1/2},$$

where ϑ^T denotes the transpose of ϑ and $r(z)$ is the weight function that is assumed

to be 1 in this work. Note that to simplify the notation we will use $\mathbb{W}$ to denote

$\mathbb{W}^{(n-1),2}(\Omega, \mathbb{R})$ in the rest of the thesis.

By defining the infinite-dimensional system state,

$$x(t) = \bar{x}(\cdot, t),$$

the nonlinear differential, nonlinear algebraic and the manipulated input operators,

$$\boldsymbol{\mathcal{F}}(x) = \mathcal{F}_n(z, \bar{x}),$$

$$\mathbf{H}(x) = H(z, \bar{x}),$$

$$\mathbf{B}u = B(z)u,$$

in an appropriate functional Sobolev subspace of $\mathbb{W}$, the PDE system of (1.1) can

be represented in the following infinite-dimensional functional form

$$\dot{x} = \boldsymbol{\mathcal{F}}(x) + \mathbf{H}(x) + \mathbf{B}u, \quad x(0) = x_0, \tag{1.3}$$

where $x \in \mathbb{W}$ and

$$\mathbb{W}(\Omega) = \Big\{ \mathcal{G} \in L_2(\Omega) : \ \forall \alpha \in \mathbb{N}, \ |\alpha| \leqslant n - 1,$$
$$\partial^\alpha \mathcal{G} \in L_2(\Omega), \ \Gamma(\mathcal{G}, \frac{\partial \mathcal{G}}{\partial z}, \dots, \frac{\partial^{n-1} \mathcal{G}}{\partial z^{n-1}}) \Big|_{\partial \Omega} = 0 \Big\}.$$

To present the infinite-dimensional functional form of (1.3) in a normal form and present the idea that is the basis for the proposed work, we have to find the basis functions needed to discretize the system. Such basis functions must be computed from the eigenproblem of the nonlinear operator of $\mathcal{F}$ as

$$\begin{aligned}
&\mathcal{F}(\phi_i) - \lambda_i \phi_i = 0, \\
&\Gamma(\phi_i, \frac{\partial \phi_i}{\partial z}, \dots, \frac{\partial^{n-1} \phi_i}{\partial z^{n-1}}) \Big|_{\partial \Omega} = 0, \\
&i = 1, \dots, \infty,
\end{aligned} \tag{1.4}$$

where ϕ_i denote the ith basis function which corresponds to the ith eigenvalue, λ_i.

Assumption 1.1. *The dynamics of highly dissipative DPS described by the nonlinear PDE of (1.1) with infinite-dimensional representation of (1.3) can be decomposed to two subsystem dynamics; (1) the finite slow subsystem that includes the slow and possibly unstable modes of the system, and (2) the infinite complement fast subsystem that contains the remaining fast and stable modes of the system. We also assume that there is a time scale separation between the slow and fast subsystems and that a modal representation can be derived to capture the local system behavior in a ball of radius $O(\frac{1}{\sigma})$ around current state where σ is a small number*

[76].

Then the system representation can be in practice identified by the sets of slow and fast basis functions computed based on analytical or statistical methods. Based on the assumption which is satisfied by the majority of transport-reaction processes [76], the Sobolev subspace of $\mathbb{W}$ can be decomposed to a slow subspace, $\mathbb{W}_s$ and its complement fast subspace, $\mathbb{W}_f$.

Assumption 1.2. *We assume that the countable corresponding sets of eigenfunctions are strong generators of the defined general, slow and fast Sobolev subspaces, i.e.,*

$$\mathbb{W} \triangleq span\{\phi_i\}_{i=1}^{\infty}, \quad \mathbb{W}_s \triangleq span\{\phi_i\}_{i=1}^{m}, \quad \mathbb{W}_f \triangleq span\{\phi_i\}_{i=m+1}^{\infty}.$$

The projection operator of $\mathcal{P} : \mathbb{W} \rightarrow \mathbb{W}_s$ and its complement operator, $\mathcal{Q} : \mathbb{W} \rightarrow \mathbb{W}_f$, can be defined as

$$\begin{aligned}
\mathcal{P}(\cdot) &= (\cdot, \Phi_s), \\
\mathcal{Q}(\cdot) &= (\cdot, \Phi_f),
\end{aligned} \tag{1.5}$$

to decompose the infinite-dimensional system of (1.3) to the following modal vectorized slow and fast forms,

$$\begin{aligned}
\dot{x}_s &= F_s(x_s, x_f) + H_s(x_s, x_f) + B_s u, \quad x_s(0) = \mathcal{P}x_0, \\
\dot{x}_f &= F_f(x_s, x_f) + H_f(x_s, x_f) + B_f u, \quad x_f(0) = \mathcal{Q}x_0,
\end{aligned} \tag{1.6}$$

where $x = x_s \oplus x_f$, $x_s = \mathcal{P}x \in \mathbb{W}_s$, $x_f = \mathcal{Q}x \in \mathbb{W}_f$, $F_s = \mathcal{P}\mathcal{F}$, $F_f = \mathcal{Q}\mathcal{F}$, $H_s = \mathcal{P}\mathbf{H}$, $H_f = \mathcal{Q}\mathbf{H}$, $B_s = \mathcal{P}\mathbf{B}$, $B_f = \mathcal{Q}\mathbf{B}$, $\Phi_s = [\phi_1 \quad \phi_2 \quad \cdots \quad \phi_m]^T$ and $\Phi_f = [\phi_{m+1} \quad \phi_{m+2} \quad \cdots]^T$. In the modal infinite-dimensional system of (1.6), F_s is a nonlinear bounded and F_f is a nonlinear unbounded differential operator, and H_s and H_f are nonlinear Lipschitz vector functions according to the properties of the nonlinear operator and function in the PDE system of (1.1). In addition according to the assumption, the unbounded operator of F_f is exponentially stable and generates a strongly continuous exponentially stable semigroup [76]. We can compute the set of empirical eigenvalues and corresponding empirical basis functions required to discretize the infinite-dimensional system of (1.3) in the form of a partitioned set of ODEs of (1.6).

Neglecting the fast dynamics of (1.6) we can approximate the infinite-dimensional system by the slow subsystem of

$$\dot{x}_s = F_s(x_s, 0) + H_s(x_s, 0) + B_s u, \quad x_s(0) = \mathcal{P}x_0, \tag{1.7}$$

which can be directly used to design a low-dimensional controller employing standard control methods for ODEs [76]. To employ such finite-dimensional approximation as the basis for the controller synthesis we must show that if the finite-dimensional slow subsystem of (1.7) is exponentially stable, then the infinite-dimensional system of (1.6) is also exponentially stable.

1.3   Background on model reduction and control of nonlinear distributed parameter systems

Over the last thirty years, significant research within the area of process control has focused on analysis and control of lumped chemical processes described by nonlinear ODEs. Excellent reviews of results in the area of nonlinear process control can be found in [2, 61, 130, 153–155, 180, 189, 211]. In the last decade research focus has also encompassed analysis and control of nonlinear DPSs. The research activity in this area has been motivated by a wealth of industrially important processes (e.g., metalorganic vapor phase epitaxy (MOVPE), plasma enhanced chemical vapor deposition (PECVD), Czochralski crystal growth and various fluid dynamic systems) which exhibit significant spatial variations due to the presence of strong diffusive and convective mechanisms.

Focusing on control and optimization, current approaches for PDEs can be broadly classified into direct ones where solutions are obtained based explicitly on the PDEs and indirect ones where nonlinear order reduction methodologies are initially used to discretize the PDEs into an appropriate finite dimensional ordinary differential equation (ODE) representation. Specifically for the latter approaches, well-established optimization and controller design techniques have now been developed. For processes with nonlinear spatial differential operators or complex process domains, these techniques commonly hinge on a data-driven

order reduction methodology. Their main limitation lies on the *ad-hoc* nature of the data-driven order reduction step, that requires a representative ensemble of solutions exists for the PDE to be properly discretized. This problem is usually addressed through extensive simulations, thus increasing the computational cost of the existing methods. Without hoping to present a comprehensive overview of the excellent results in the area of control for spatially distributed systems, we focus on a brief discussion of results in the area of control of dissipative DPSs.

Distributed chemical processes with significant diffusive phenomena can be described by systems of linear or nonlinear PDEs. Parabolic PDEs are characterized by a finite-number of modes that describe their dominant long-term dynamic behavior [244]. As a result, the standard approach to control of parabolic PDEs utilizes modal decomposition techniques to obtain ODEs, which are then used for controller design [44, 46, 80, 89, 117, 212, 229, 266]. A drawback of this approach is the possibly high dimensionality of the resulting ODEs in order to capture the PDE dynamics accurately, thus leading to high dimensionality of the resulting controllers. Motivated by this, in [116] singular functions were employed for linear PDEs to derive ODE models used for controller synthesis. In another approach, the concept of approximate inertial manifolds [107–109] was employed, leading to low-order ODE models that accurately describe parabolic PDEs, that were subsequently used for nonlinear controller design [13, 18, 75, 78] and dynamic optimization [20].

Feedback controllers were also developed based on a combination of geometric and control Lyapunov function techniques [5, 19, 76, 272], that compensate for the effect of model uncertainty and handle constraints on the control action [99]. The developed nonlinear control algorithms were successfully applied to a variety of advanced materials processes [12, 14, 17, 76] and fluid dynamic systems [15, 16, 42, 77]. The reader may refer to [45, 76, 140, 167, 254] for reviews on control of nonlinear DPSs.

1.4 Statistical techniques for mode order reduction

The analytical approaches for model reduction cannot be directly applied to systems which have nonlinear spatial differential operators and/or to problems defined over irregular spatial domains, since the eigenvalue-eigenfunction problem of the spatial operator for these systems cannot be analytically solved in general, and it is thus difficult to derive the basis functions to expand the solution of the PDE systems. To overcome this limitation researchers have focused on data-driven methods, where in data obtained from the system is used to obtain the required basis functions. One such data-driven method, known as the method of snapshots, which uses Karhunen-Loève expansions (KLE) (also known as proper orthogonal decomposition (POD)), was proposed by Sirovich [133, 228]. This method has

been extensively utilized to "empirically" compute the eigenfunctions using an ensemble of solution data obtained either through experimental observations or from detailed numerical simulations. This method has been profusely used in model reduction [24, 113, 122, 134, 210], optimization [20, 22, 49–51, 59, 248], sensor placement [3, 4] and control [16, 27, 224–226] of distributed processes.

Another methodology for model reduction of infinite-dimensional systems is balanced truncation [83, 149, 165, 232, 280]. Balanced POD, which combines ideas from POD and balanced truncation is used to compute balanced truncations, or their approximations with computational cost similar to POD [214]. Balanced POD was originally introduced for high dimensional linear systems and it uses similar ideas to the method of snapshots for standard POD computations, however there are now two separate datasets.

Dynamic mode decomposition (DMD) is also a relatively recently developed method for modal decomposition [72, 215, 220]. DMD approximates the modes of the Koopman operator, which is a linear, infinite-dimensional operator that represents nonlinear, finite-dimensional dynamics without linearization [181, 182]. The method can be used for computing the eigenvalues and eigenvectors of a linear model that approximates the underlying dynamics from empirical data even if those dynamics are nonlinear. Unlike POD and the balanced POD, this decomposition yields growth rates and frequencies associated with each mode, which can be found from the magnitude and phase of each corresponding eigenvalue. Applications of

DMD to experimental and numerical data can be found in [215, 220–222].

Proper generalized decomposition (PGD) is a powerful model reduction technique that computes *a priori* by means of successive enrichment a separated representation of the unknown field. The computational complexity of the PGD scales linearly with the dimension of the space wherein the model is defined, which is in marked contrast with the exponential scaling of standard grid-based methods. First introduced in the context of computational rheology [8, 9], the PGD has since been further developed and applied in a variety of applications ranging from the solution of the Schrödinger equation of quantum mechanics to computational rheology [74].

To handle the situations where in the snapshots or data sets used are incomplete (gappy) [104] proposed a modification for the basic POD based methodology. In the modification, especially focusing on image reconstruction, the basic POD based methodology was combined with the least-squares approach to estimate the necessary modal coefficients from the available incomplete data. The application of this methodology was however extended to aerodynamic [247, 265] & fluid mechanics [258] problems. An extension of the gappy POD methodology was also proposed [258, 269] to eliminate its dependence on the initial guess, used in filling the missing data in a given data vector, while finding the best possible reconstruction.

The POD-based data-driven methods assume an *a priori* availability of a large

ensemble of snapshots to correctly capture the incidence of new trends during the process evolution using the basis functions computed off-line from the *a priori* available snapshot ensemble. However, generating such an ensemble is not straight-forward (and experimentally infeasible) as it necessitates using suitably designed inputs to excite all the modes [122, 255]. This is especially relevant when considering the control problem; there is a need to extend the basis function set *on command* as new trends appear [123, 124].

1.5 Thesis objectives

We propose to extend the applicability of indirect feedback control approaches for dissipative PDE systems. Specifically, the intellectual objective of the proposed research is to develop a systematic data-driven order reduction methodology that is specifically tailored for control of PDE systems. The proposed work will resolve fundamental computational issues associated with data-driven techniques in control policies for spatially distributed process systems. To achieve this objective, the individual aims of the proposed research include:

Aim 1 Develop a computationally efficient data-driven algorithm for the derivation of nonlinear low-order, approximate models. This algorithm will relax central requirements of data-driven model reduction techniques.

Aim 2 Construct practically implementable feedback control systems that can

deal with the issues of nonlinearity, model uncertainty and constraints. Extend the control system applicability to cases when the availability of distributed sensors and actuators is restricted.

Aim 3 Illustrate the applicability of the controller design methods on industrially relevant transport-reaction processes such as chemical reactors with imperfect mixing and a typical physico-chemical process described by Kuramoto-Sivashinsky equation (KSE) and Korteweg-de Vries-Burgers (KdVB) equation.

A wide range of industrial processes will benefit from the proposed control methodologies including: a) microelectronics manufacturing and advanced materials processing, e.g. chemical vapor deposition (CVD), wet deposition processes and etching, b) transport-reaction chemical processes, e.g. advanced catalytic reactors and c) battery production industry. e.g. control of temperature profile in Lithium-Ion (Li-Ion) batteries using proper sensors and actuators placement to avoid thermal runaway and to manage charging and degradation.

1.6 Thesis structure

Chapter 2 briefly explains how adaptive proper orthogonal decomposition (APOD) is used to construct the required empirical basis functions and update them on demand. Such empirical basis functions are essential to develop the reduced order

models (ROMs).

Chapter 3 is a version of Pourkargar D.B., Armaou A., "Design of APOD-based switching dynamic observers and output feedback control for a class of nonlinear distributed parameter systems", *Chemical Engineering Science, Special Issue on Smart Plants*, 2015, in press, $DOI : 10.1016/j.ces.2015.02.032$, which focuses on the output feedback control problem of DPSs with limited measurement sensors. A combination of a robust state feedback controller with a Luenberger-type nonlinear dynamic observer of the system states is applied to synthesize a computationally efficient control structure based on APOD. The stability of the closed-loop system is proved based on Lyapunov stability theorem for hybrid systems. The effectiveness of the proposed control method is successfully employed to stabilize a physicochemical system described by the KSE when the open-loop process exhibits highly nonlinear behavior.

Chapter 4 is a version of Pourkargar D.B., Armaou A., "Modification to adaptive model reduction for regulation of distributed parameter systems with fast transients", *AIChE Journal*, $59(12)$, $4595 - 4611$, 2013, which addresses the dynamic observer based control problem of DPSs with limited state measurements by employing entropic APOD methodology. The stability of the closed-loop system is proven by Lyapunov stability criteria for hybrid systems. The proposed approach is successfully used to regulate the KSE at an spatially invariant steady state profile in the absence and presence of uncertainty when the open loop process exhibits

highly nonlinear and chaotic behavior with fast transients.

Chapter 5 is a version of Pourkargar D.B., Armaou A., "Geometric output tracking of nonlinear distributed parameter systems via adaptive model reduction", *Chemical Engineering Science*, 116, 418 − 427, 2014, which focuses on the output tracking control issue for DPSs with limited state measurements. A computationally efficient regulator and output tracking controller structure is synthesized, by combining a globally linearizing controller (GLC) with a dynamic observer of the system states based on APOD methodology. The proposed synthesis method is successfully employed to address the output tracking problem for a catalytic reactor; specifically, the thermal dynamics of the reactor are controlled to reduce the hot spot temperature across the reactor length using a limited number of actuators and sensors to force the process evolution.

Chapter 6 is a version of Pourkargar D.B., Armaou A., "APOD-based control of general linear distributed parameter systems in the presence of network communication constraints", *AIChE Journal*, 61(2), 434 − 447, 2015, and Pourkargar D.B., Armaou A., "Lyapunov-based control of dissipative distributed parameter systems via adaptive model order reduction with minimum feedback information", *IEEE Transaction on Automatic Control*, 2015, under review, which focuses on model-based controllers designed for linear and nonlinear distributed processes based on restricted communication between the control system elements. We address the modeling component question via APOD algorithm to recursively compute the set

of empirical basis functions. The problem is that due to sub-sampling the empirical basis functions and modes may not be properly ordered. We employ APOD to properly express the system while circumventing extensive off-line computations. The main objective is to minimize snapshots transfer rate from the distributed sensors to the controller, for ROM revisions, considering closed-loop stability. The proposed control structure is illustrated on the temperature regulation problem of a tubular reactor and the spatiotemporal dynamic regulation of a physico-chemical system modeled by the KSE.

Chapter 7 is a version of Pourkargar D.B., Armaou A., "Dynamic shaping of transport-reaction processes with a combined sliding mode controller and Luenberger-type dynamic observer design", *Chemical Engineering Science*, 2015, under review, and Pourkargar D.B., Armaou A., "Spatiotemporal dynamic shaping of nonlinear dissipative distributed parameter systems using empirical eigenfunctions", *Journal of Process Control*, 2015, in preparation, which focuses on the spatiotemporal dynamic shaping of semilinear DPSs by regulating the error dynamics between the ROMs of governing and target PDEs. The required ROMs are derived by applying Galerkin projection to the describing PDEs. The spatiotemporal error dynamics between the governing and target ROMs are stabilized using a sliding mode controller design combined with a Luenberger-type dynamic observer to estimate the required states. The effectiveness of the proposed control structure is illustrated on thermal dynamic shaping of a tubular flow reactor.

Chapter 8 is a version of Pourkargar D.B., Armaou A., "Control of spatially distributed processes with unknown transport-reaction parameters via two layer system adaptations", *AIChE Journal*, 61(8), $2497 - 2507$, 2015, Pourkargar D.B., Armaou A., "Adaptive output feedback control of transport-reaction processes", *Journal of Process Control*, 2015, in preparation, and Pourkargar D.B., Armaou A., "Adaptive wave motion suppression in physico-chemical processes using two layer system adaptations", *Automatica*, 2015, in preparation, which addresses the control problem of dissipative DPSs with unknown parameters which are modeled by semilinear parabolic PDEs via model order reduction. The unknown parametric changes have a significant effect on model order reduction approaches and the resulting ROMs. We use the combination of APOD and Galerkin's method to construct the ROM that is the basis for adaptive controller design. The proposed control strategy is illustrated on thermal regulation in a catalytic chemical reactor in the presence of constant and time-varying unknown parameters and wave motion suppression problem of fluid flow processes described by the KdVB.

ADAPTIVE PROPER ORTHOGONAL DECOMPOSITION

2.1   Preliminaries

As described in previous chapter, spatially distributed processes with reaction and significant diffusion terms can be mathematically modeled by a set of nonlinear dissipative partial differential equations (PDEs) [76]. Consequently, the infinite-dimensional representation of such systems in appropriate Sobolev subspaces, can in principle be decomposed to a finite-dimensional slow and possibly unstable, and an infinite-dimensional fast and stable subsystems. Taking advantage of this decomposition, the governing PDEs can be approximated by a finite-number of

ordinary differential equations (ODEs). In detail, the solution of the PDE system can be presented as an infinite-sum of spatial basis functions times time-varying coefficients called modes. Then the infinite-dimensional ODE system for modes can be derived based on the variants of weighted residual methods. The finite-dimensional reduced order model (ROM) can then be derived by considering a proper number of ODEs corresponding to the basis functions which capture the dominant dynamics of the original PDE system. This standard strategy, named model order reduction (MOR), has been frequently applied to address control, monitoring and optimization problem of dissipative PDEs [44, 89].

On the basis of the above, when the set of basis functions are computed, the PDE systems can be discretized and the ROMs can be constructed. However the applicability of analytical model reduction methods to industrial processes is limited, due to complex nonlinear spatial dynamics and irregular domains. Statistical techniques like proper orthogonal decomposition (POD) are usually used to bypass this limitation and construct empirical basis functions [13, 18, 29, 77, 203, 228]. POD has been applied extensively in model reduction, optimization and control of DPSs [13, 18, 77, 139]. It assumes the a priori availability of a sufficiently large ensemble of PDE solution data in which the most prevalent spatial modes are excited. In practice, it is difficult to generate such an ensemble so that all possible dominant spatial modes are appreciably contained within the corresponding snapshots. Therefore, the resulting basis functions are representative of the

corresponding ensemble only. During closed-loop operation, situations may arise when the existing basis functions fail to accurately represent the dynamics of the PDE system. To circumvent this requirement an efficient recursive computation algorithm, known as adaptive proper orthogonal decomposition (APOD), can be used as additional data from the process becomes available.

As in all data-driven model reduction and control methodologies, initially, snapshots of the state profile during process evolution are gathered to construct an ensemble of snapshots. We note that the initial data can be obtained either experimentally (by allowing the process to evolve with no control action for a short period of time) or from previously obtained historical data, or via off-line numerical simulations of the PDE system of (1.1) by using simulation packages for PDE systems such as Fluent and Comsol. Note that in previous methods, the ensemble of solutions must be constructed by gathering state profile snapshots for different values of $u(t)$, and different initial conditions [20, 59, 122]; APOD disposes of this requirement.

We use the off-line constructed ensemble of snapshots to construct the empirical basis functions necessary for the derivation of finite dimensional ODE models. During this off-line step of the proposed method, POD is used to compute an orthogonal set of empirical basis functions to represent this ensemble, which by extension also are basis functions of (1.1). A measure of the relative contribution of each basis function to the mean square fluctuation of the ensemble is also obtained.

POD yields the most efficient way for computing the basis functions which capture the dominant patterns of the ensemble in a least squares sense [133]. We will briefly present the key features of POD. The reader may refer to [115, 133, 228] for a detailed presentation of POD.

2.2 A brief review to POD algorithm

Let $v(z) = [v_1(z) \; v_2(z) \; \cdots \; v_K(z)]^T$ be the ensemble of K snapshots of the system, where $v_i(z) = \bar{x}(z, t_i)$. The empirical basis functions which are the most characteristic spatial profiles can be obtained by an optimization problem,

$$
\begin{aligned}
&max \; \frac{\overline{(\Psi, v)^2}}{(\Psi, \Psi)}, \\
&s.t. \;\; (\Psi, \Psi) = 1, \;\; \Psi \in L_2(\Omega),
\end{aligned}
\tag{2.1}
$$

where $\overline{(\cdot)}$ denotes the ensemble average. Generally, the solution of this optimization problem of (2.1) is computationally very expensive since the search space is infinite dimensional. To circumvent this issue, Sirovich introduced the method of snapshots [228]. The central idea of this technique is to assume that the requisite empirical basis functions can be expressed as a linear combination of the snapshots themselves. Under this assumption, the optimization problem can actually

be solved algebraically, through the solution of the following integral eigenproblem,

$$\int_\Omega \overline{\big(v(z)v(\xi)\big)}\Psi(\xi)d\xi = \Lambda\Psi(z). \tag{2.2}$$

An efficient approach to solve the above integral eigenproblem is via method of snapshots [228] wherein the optimal set of required empirical basis functions are presented by a linear combination of the snapshots,

$$\Psi(z) = \Lambda^{-1/2}Z^T v(z), \tag{2.3}$$

where Λ indicates the diagonal matrix of the eigenvalues and Z is the matrix of eigenvectors obtained from the solution of the following eigenvalue-eigenvector problem,

$$C_K Z = \Lambda Z, \tag{2.4}$$

the elements of the positive semidefinite covariance matrix can be constructed by obtaining the inner product of each snapshot with the rest of the ensemble snapshots,

$$C_K := \frac{1}{K}\int_\Omega v(\xi)v^T(\xi)d\xi. \tag{2.5}$$

The solution of the eigenproblem of (2.4) (obtained utilizing standard methods from linear algebra [217]) yields K eigenvectors to construct K empirical basis functions $\psi_\kappa(z)$ for $\kappa = 1,\ldots,K$ that form an orthonormal set. By construction,

matrix C_K is symmetric and positive semi-definite, and thus, its eigenvalues, λ_κ for $\kappa = 1, \ldots, K$, are real and non-negative. The relative magnitude of the eigenvalues represents a measure of the fraction of the "energy" embedded in the ensemble captured by the corresponding empirical basis functions. We order the calculated empirical basis functions such that $\lambda_1 > \lambda_2 > \ldots > \lambda_K$. To obtain the dominant empirical basis functions, we only consider the first m basis functions such that their corresponding eigenvalues satisfies the following criteria

$$\frac{\lambda_{m+1}}{\sum_{i=1}^{m} \lambda_i} \geq \epsilon \tag{2.6}$$

where ϵ denotes the desired fraction of the energy of the ensemble. The key steps of the POD algorithm are presented in Table 2.1.

Table 2.1: POD algorithm

1)	**Collect** the available snapshots in an ensemble, v.
2)	**Compute** the covariance matrix of C_K using (2.5).
3)	**Solve** the eigenvalue-eigenvector problem of (2.4).
4)	**Order** the eigenvalues and eigenvectors.
5)	**Keep** the dominant eigenvalues and their corresponding eigenvectors.
6)	**Compute** the dominant empirical basis functions using (2.3).

2.3   APOD

In this section we briefly explain how APOD is used to construct the empirical basis functions required for ROM development and update them on demand.

2.3.1 Algorithm

2.3.1.1 Off-line steps

Let $v(z) = [\bar{x}(z, t_1)\ \bar{x}(z, t_2)\ \cdots\ \bar{x}(z, t_K)]^T$ be the set of K snapshots called the ensemble, where $\bar{x}(z, t_k)$ is the available snapshot at time t_k. The off-line APOD is applied to initialize the set of empirical basis functions that capture the dominant ensemble patterns and to initiate an indicator that shows the relative contribution of such empirical basis functions to the entire energy of patterns inside the ensemble. The covariance matrix of the ensemble, $C_K := (v^T, v^T)$, is computed. The computationally expensive eigenfunction problem of the spatial differential operator is thus replaced by the eigenvector problem for the covariance matrix. Without loss of generality it is assumed that m eigenmodes capture ϵ of patterns energy of the ensemble, i.e. $\sum_{i=1}^{m} \lambda_i / \sum_{i=1}^{K} \lambda_i \geq \epsilon$, where $\lambda_1 > \lambda_2 > \cdots > \lambda_K$. An orthonormal basis obtains as

$$Z = [\omega_1\ \omega_2\ \cdots\ \omega_m],\ Z \in \mathbb{R}^{K \times m}$$
$$\Lambda = [\lambda_i]_{ii},\ i = 1, \ldots, m$$

$$(2.7)$$

where ω_i denotes the ith eigenvector of C_K that corresponds to the ith eigenvalue, λ_i. Then the vector of basis functions, $\Psi = [\psi_1\ \psi_2\ \cdots\ \psi_m]^T$, is computed by a linear combination of the system snapshots,

$$\Psi = \Lambda^{-1/2} Z^T v. \tag{2.8}$$

The resulting eigenspace of C_K used to partition $\mathbb{W}$ into a dominant subspace, $\mathbb{P}$, that contains the empirical basis functions which capture ϵ of pattern energy in the ensemble to approximate $\mathbb{W}_s$ and the orthogonal complement subspace, $\mathbb{Q}$, that contains the rest of the empirical basis functions to approximate the dominant part of $\mathbb{W}_f$ [244]. Such a partition is possible due to the fact that the dominant dynamics of highly dissipative PDEs are finite dimensional. The orthogonal projection operators P and Q onto subspaces $\mathbb{P}$ and $\mathbb{Q}$ are obtained as

$$P = ZZ^T, \quad Q = I_K - ZZ^T, \tag{2.9}$$

onto subspaces $\mathbb{P}$ and $\mathbb{Q}$, respectively, where I_K is the identity matrix. A detailed analysis of the off-line APOD has been presented in [203, 228, 256].

2.3.1.2 On-line steps

During system evolution, the recursive algorithm updates the set of empirical basis functions once new measurements become available from the process. Such orthonormal basis of subspace $\mathbb{P}$ is recursively revised, while the orthonormal basis of $\mathbb{Q}$ is computed from the fact that $\mathbb{Q}$ is the orthonormal complement of $\mathbb{P}$. The mentioned recursive process is computationally efficient as long as the dimension of $\mathbb{P}$ is small (which partly depends on choosing an appropriate value for ϵ and the system characteristics).

Our task is to continuously refine the basis Z as new snapshots of the process

become available. The algorithm we propose to develop will compute an approximation to Z without requiring the solution of the eigenvalue-eigenvector problem of C_K. We assume that the process is observable, i.e. the appearance of new patterns is captured by the snapshots. The algorithm requires the dimensionality of the covariance matrix to remain constant, which we will achieve by discarding the oldest snapshot from the ensemble.

Specifically, when a new snapshot is obtained from the closed-loop process, it is added to the ensemble and the oldest snapshot is removed, i.e., $k = 1 + k \bmod K$ where mod denotes the modulus operator. Thus, the ensemble only includes the most recent snapshots in each time step. Then the covariance matrix of C_K is revised based on the updated ensemble. Due to the covariance matrix updates, the set of eigenvalues is revised, the dominant eigenspace and the set of empirical basis functions are changed when needed. The subspace $\mathbb{P}$ may change in one of the following three ways:

- One mode from $\mathbb{Q}$ becomes necessary to capture the desired ϵ percent of energy in the ensemble, the dimension of the dominant subspace $\mathbb{P}$ must increase.

- Some of the eigenmodes of the subspace $\mathbb{P}$ are no longer be necessary to capture the required ϵ percent of the energy. In this case, the basis Z is updated and its dimension is simultaneously decreased.

- The dimensionality of $\mathbb{P}$ remains unchanged, however the basis Z needs to

be updated in order to account for the newly added snapshot.

The individual steps are discussed below:

Increasing the size of the basis. We first consider the case when one eigenmode of subspace $\mathbb{Q}$ becomes dominant as a new snapshot is added, in the sense that the associated eigenfunction becomes necessary to accurately describe the ensemble of solutions. The eigenmode thus becomes an element of subspace $\mathbb{P}$ and leaves $\mathbb{Q}$. To monitor this eventuality we will observe the dominant eigenmodes which belong to subspace $\mathbb{Q}$. To achieve this we will identify a projection of the ensemble to $\mathbb{Q}$, c_q and monitor the percentage contribution of the dominant eigenvalue of c_q, namely λ_{m+1} towards the total energy of the ensemble. We define the percentage contribution of λ_{m+1} as $\xi = \lambda_{m+1}/\sum_{i=1}^{m+1} \lambda_i$. If ξ increases to more than $(1 - \epsilon)$ we will increase the dimensionality of subspace $\mathbb{P}$. We note that the eigenvalues λ_i $\forall$ i=1,...,m can be computed by solving a small eigenvalue problem, while λ_{m+1} can be efficiently computed from c_q.

Decreasing the size of the basis. As new snapshots are added and old snapshots are eliminated from the ensemble, the dominant eigenspace of C_K continuously changes. It is likely that during the process some of the eigenmodes in subspace $\mathbb{P}$, may no longer be necessary to capture the desired percentage of energy. In such cases, it is required to decrease the dimensionality of $\mathbb{P}$ to include the dominant eigenspace only. To test whether it is required to decrease the size of the basis we will define a projection H from the $\mathbb{P}$ to $\mathbb{P}$ using C_K. If the null space of

H becomes non empty it directly implies that the dimensionality of $\mathbb{P}$ is too large. This can easily be captured by the eigenvalues of H which can be computed with little computational effort as long as m remains small. If only $\hat{m}$, with $\hat{m} < m$, eigenvalues of H are dominant (in a sense that only $\hat{m}$ eigenmodes are required to capture ϵ percent of energy of the ensemble), then the dominant eigenfunctions of H will automatically provide us with the basis for the revised dominant space $\mathbb{P}$ of dimensionality $\hat{m}$.

Maintaining the accuracy of the basis. During the process evolution it may become apparent that even though the basis dimensionality remains the same, there is an increase in the error between the new snapshots and the projection identified using the "old" basis functions. The evaluation of the error is based on the fact that the orthogonal projections P and Q should satisfy $QC_KP = 0$. Hence, the accuracy of the basis can be evaluated by computing the matrix $\mathcal{E} = QC_KP$. In this case, an appropriate orthonormalization of the basis is performed to maintain the accuracy of the basis. When the covariance matrix stops providing the controller with relevant information the re-evaluation of the empirical eigenfunctions is suspended.

A flow chart illustrating the APOD approach and the associated algebraic computations are presented in Figure 2.1, where ξ denotes the contribution of the dominant eigenvalue of $c_q = QC_KQ$, namely λ_{m+1}, towards the total pattern energy of the ensemble, i.e. $\xi = \lambda_{m+1}/\sum_{i=1}^{m+1} \lambda_i$, and $H = Z^TC_KZ$ is an $m \times m$

matrix.

Remark 2.1. *Consider the local subspace of the slow and unstable modes, $\mathbb{W}_s = span\{\phi_1, \phi_2, \ldots, \phi_s\}$ and subspace $\mathbb{P}$ defined as $\mathbb{P} = span\{\psi_1, \psi_2, \ldots, \psi_m\}$, where ϕ_i for $i = 1, 2, \ldots, s$ are the real basis functions of the system and ψ_j for $j = 1, 2, \ldots, m$ are the set of basis functions computed based on APOD. We assumed that $\mathbb{W}_s \subseteq \mathbb{P}$, locally, due to the excitation of the higher modes during the closed-loop process evolution providing richer behavior than the slow subsystem would.*

Remark 2.2. *APOD does not need a high value of ξ as the slow subspace, $\mathbb{P}$, is updated whenever a mode of subspace $\mathbb{Q}$ becomes dominant thus capturing the new trends that appear during closed-loop process evolution. However, during the closed-loop simulation in the next section, we use a higher value $\xi = 0.01$ to emphasize the changes in dimensionality of the slow subspace, $\mathbb{P}$.*

Remark 2.3. *Once a change to the basis of the dominant eigenspace $\mathbb{P}$ is declared, we refine the ROM and reconfigure the controller structure using the updated ROM. This step assures that the ROM captures the impact of the controller on the process and the new trends that appear when the process traverses new regions in the variable state space during closed-loop operation. A further advantage is that as new state information becomes available and the model is refined the model error remains bounded.*
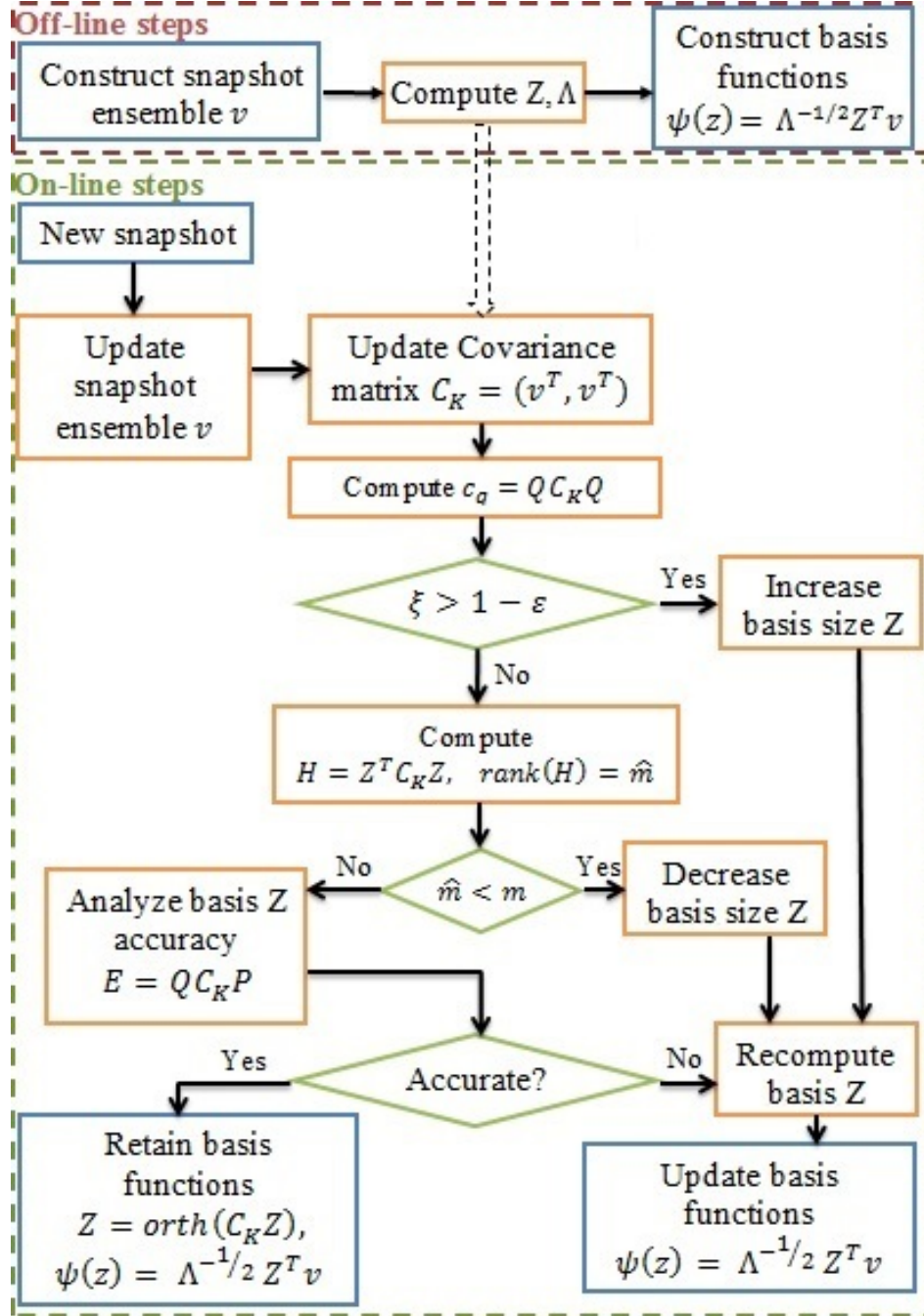
Figure 2.1: Flow chart of APOD. Blue boxes denote algorithm I/Os and green decision steps.

2.3.2 Modifications

As described before, the performance of the controller structure hinges on the local validity of the ROM. To have a valid ROM it is necessary to update the ensemble, used for computation of the basis functions, based on the new snapshots arrived from the system during the process evolution. So far the newest snapshots are considered in the ensemble. In each time step during closed-loop process evolution the oldest snapshot of the system, v_1, will be replaced by the new snapshot obtained by the periodic snapshot measurements. Thus, in each time step the ensemble only includes the most recent snapshots. This data ensembling which previously used is called the "original APOD".

In the original APOD, the ensemble of the snapshots that is used to update the basis functions only possesses the most recent snapshots. The procedure could possibly lead to loss of previously important profiles as the process evolves away from them and they are replaced by profiles that contain new information. If the process revisits a previously accessed state space region, APOD has to recapture the new trends as they reaffirm themselves leading to a lag in the ROM revision that captures the new trends.

2.3.2.1 The most important snapshots approach

The modification analyzes the contribution of snapshots in $\mathbb{P}$ by normalized dominant eigenvectors and search for the one which had the minimum 2-norm per row

and eliminates the corresponding snapshot in the ensemble. To formulate the procedure, consider the contribution column vectors of $D = \{d_j\}$ and standardization column vector of $S = \{s_j\}$, respectively, as follows

$$d_j = (P_A P_A^T)_{jj} \tag{2.10}$$

where $(\cdot)_{jj}$ indicates the diagonal element of $(\cdot)$ and

$$s_j = \|C_{K,j}\|_2, \tag{2.11}$$

where $\| \cdot \|_2$ indicates the 2-norm of vector $(\cdot)$ and $C_{K,j}$ means the jth row of the covariance matrix and $j = 1, \ldots, K$.

The normalized snapshot contribution column vector, $N = \{n_j\}$, is defined based on (2.12)

$$n_j = \frac{d_j}{s_j}, \quad j = 1, \ldots, K. \tag{2.12}$$

We eliminate the snapshot that corresponds to the element in the normalized snapshot contribution vector that has the lowest value.

The ensemble condensation by most dependent snapshot elimination can be performed before or after addition of the new snapshot in C_K. If the elimination takes place after augmenting the new snapshot to the ensemble, there is a possibility to eliminate the new data at each revisions. To circumvent this problem, the least important snapshots are eliminated before adding the new one, in order to

have the most recent snapshot and also the most important ones. This is called the "entropic APOD".

A move to consider the most important snapshots instead of newest ones thus leads to faster and more infrequent revision of the ROM when regions of the state space are previously revisited. Control design based on this ROM leads to larger region of accuracy which is important when dealing with model uncertainty and fast evolving processes. Also the dynamic observer that is constructed based on the basis functions from this entropic APOD is more insensitive to the available number of point measurements and their locations; in most cases we can use only one sensor without being concerned about sensor placement using robust nature of entropic APOD. The other advantage of the refined approach is using smaller ensemble of snapshots during the closed-loop process evolution that leads reduction in load of covariance matrix computation and saving run-time. A flow chart illustrating the revised APOD approach is presented in Figure 2.2.

Remark 2.4. *The entropic data ensembling approach increases the computation time of APOD by* 10%. *However it leads to more robust ROMs that require revisions more infrequently, as will be illustrated in the application section.*

Remark 2.5. *In the proposed approach for model reduction the snapshots used are obtained during closed-loop system evolution as opposed to most other proper orthogonal decomposition-based reduction approaches that are based on open-loop snapshots. Thus, these snapshots and the resulting ROM account for the impact*
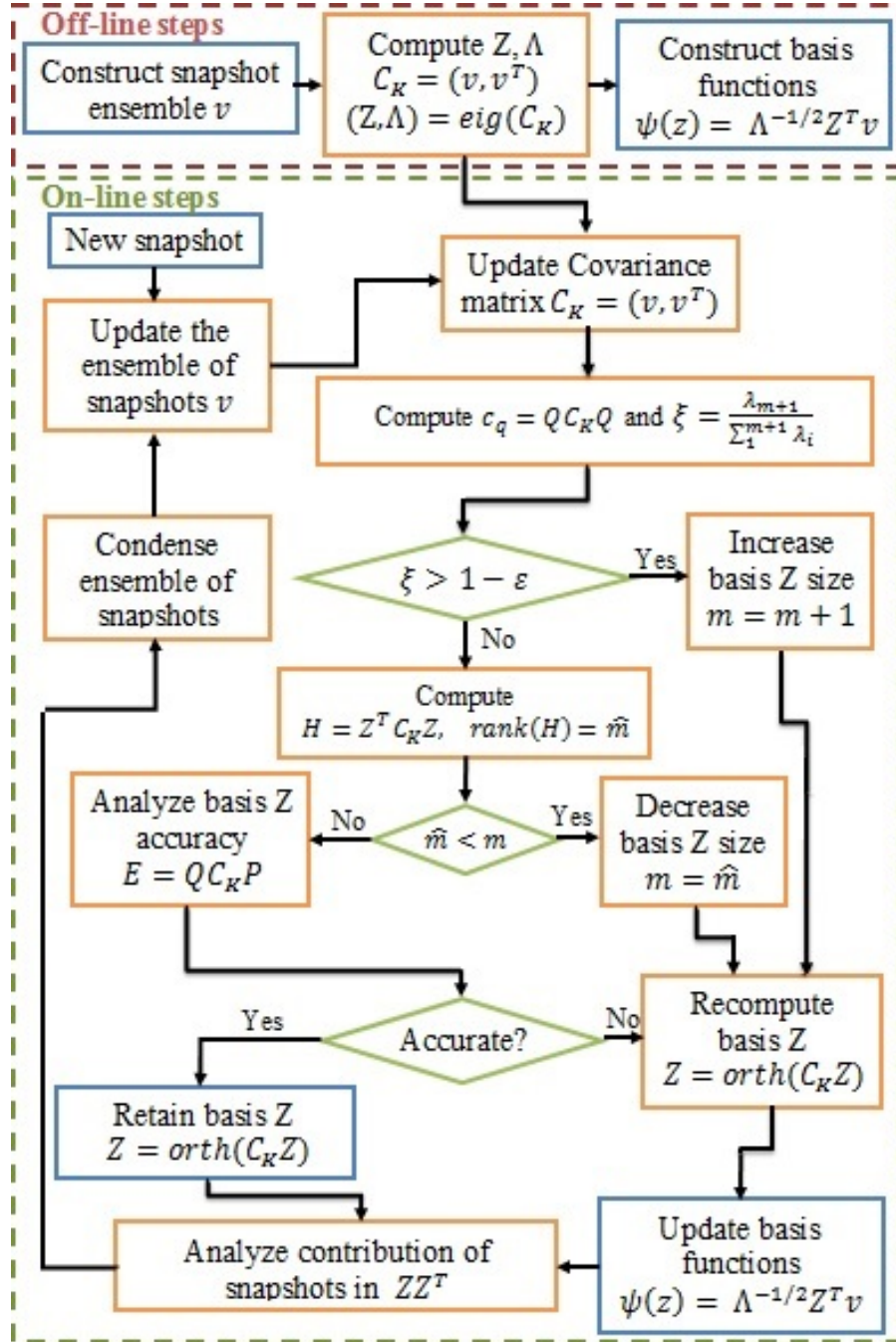
Figure 2.2: Flow chart of entropic APOD. Blue boxes denote algorithm I/Os and green decision steps.

of controller functional form on the process. It is important to note this intimate relation between APOD and the controller.

DESIGN OF LYAPUNOV-BASED SWITCHING DYNAMIC OBSERVERS AND OUTPUT FEEDBACK CONTROL

In this chapter, we investigate the output feedback control problem of dissipative distributed parameter systems (DPSs) using limited number of continuous measurements sensors. Specifically, our effort focuses on the efficient design of switching dynamic observers based on adaptively updating reduced order models (ROMs) and further on-line refinement from measurements during process evolu-

tion. ROM updating is also based on the efficient construction of basis functions. The important static observer requirements of available number of measurement sensors being supernumerary to the ROM dimension and required designs for the measurement sensors placement is circumvented using dynamic observer synthesis that conceptually needs only one measurement output to compute the estimation error and construct the dynamic observer structure.

The combination of adaptive proper orthogonal decomposition (APOD) with a dynamic observer design method that is stable in the Lyapunov sense allows us to synthesize nonlinear robust output feedback controllers that account for model reduction error and uncertainty, and guarantee local regulation of the process and output tracking. The assumption of separation principle is relaxed in controller/observer synthesis.

During the controller/observer synthesis steps, first the design problem of output feedback controller and dynamic observer is investigated between ROM revisions and Lyapunov stability is proved in the time period between two model reconstructions. A supervisory scheme is subsequently designed to enforce closed-loop stability to ROM revisions procedure. The proposed control structure is illustrated on the stabilization problem of the Kuramoto-Sivashinsky equation (KSE) at an open-loop unstable steady state.

3.1 Preliminaries

3.1.1 Class of nonlinear dissipative PDE

We consider processes with a nonlinear dissipative, input-affine, partial differential equation (PDE) description in the following state space representation

$$\frac{\partial}{\partial t}\bar{x}(z,t) = \mathcal{A}(z)\bar{x}(z,t) + \mathcal{F}(z,\bar{x}) + b(z)u(t),$$

$$y_m(t) = \int_\Omega s(z)\bar{x}(z,t)\ dz, \tag{3.1}$$

$$y_r(z,t_k) = \int_0^t \delta(t-t_k)\bar{x}(z,t)\ dt,$$

subject to boundary conditions

$$q(\bar{x}, \frac{\partial \bar{x}}{\partial z}, ..., \frac{\partial^{n_0-1}\bar{x}}{\partial z^{n_0-1}}) = 0 \ \ \text{on} \ \ \partial\Omega, \tag{3.2}$$

and initial condition

$$\bar{x}(z,0) = \bar{x}_0(z). \tag{3.3}$$

In the PDE system of (3.1)-(3.3), t is the time, $z \in \Omega \subset \mathbb{R}^3$ denotes the spatial coordinate, Ω is the process domain with its boundary, $\partial\Omega$. The vector of state variables is denoted by $\bar{x}(z,t) \in \mathbb{R}^n$ and $u(t) \in \mathbb{R}^l$ is the vector of manipulated inputs. $\mathcal{A}(z)$ and $\mathcal{F}(z,\bar{x})$ present the dissipative linear and nonlinear parts of the system spatial differential operator of order n_0, respectively. Note that the nonlinear operator is bounded Lipschitz. $b(z) \in \mathbb{R}^{n \times l}$ is a smooth matrix function

of z that describes spatial distribution of the control actions. $q(\cdot)$ is a smooth vector function, $\frac{\partial^i \bar{x}}{\partial z^i}|_{\partial\Omega}$ for $i = 1, \ldots, n_0 - 1$, presents the spatial derivatives in the direction perpendicular to the process boundary of $\partial\Omega$ and $\bar{x}_0(z)$ is also a smooth vector function of z.

Two types of measurement outputs are assumed to be available for the process: (1) periodic distributed snapshot measurement output, $y_r(z, t_k) \in \mathbb{R}^n$, and (2) continuous measurement output, $y_m \in \mathbb{R}^r$, where r indicates the number of continuous measurement sensors and t_k shows the instance for snapshot measurements. The spatial distribution of the continuous measurement sensors is denoted by $s(z)$. Note that the results of the current work are presented for $\bar{x} \in \mathbb{R}$. We can extend the results for $\bar{x} = [\bar{x}_1 \ \bar{x}_2 \ \cdots \ \bar{x}_n]^T \in \mathbb{R}^n$, by considering each component of $\bar{x}_i$ for $i = 1, \ldots, n$, individually [228]. The control objective is to stabilize the dissipative DPSs described by the PDE system of (3.1)-(3.3) at a desired spatial profile of $\bar{x}_d(z, t)$. To implement the proposed method we consider the spatially uniform steady state of $\bar{x}_d(z, t) = 0$ as the desired profile.

3.1.2 Infinite-dimensional representation

To present the results, we formulated the PDE system of (3.1) as an infinite-dimensional system in an appropriate Sobolev subspace $\mathbb{W}(\Omega, \mathbb{R})$ where the space derivatives' definitions are added to the subspace. We also consider the inner

product and norm in $L_2[\Omega]$ as

$$(\vartheta_1, \vartheta_2) = \int_\Omega r(z)\vartheta_1^T(z)\vartheta_2(z)dz \qquad \text{and} \qquad \|\vartheta_1\|_2 = (\vartheta_1, \vartheta_1)^{1/2}$$

where ϑ^T is the transpose of ϑ and $r(z)$ denotes the spatially distributed weight

function that is considered to be 1 in this work. By defining the state x on $\mathbb{W}(\Omega, \mathbb{R})$

as

$$x(t) = \bar{x}(z, t), \tag{3.4}$$

the differential operators

$$\mathbf{A}x = \mathcal{A}(z)\bar{x},$$
$$\mathbf{F}(x) = \mathcal{F}(z, \bar{x}), \tag{3.5}$$

and the input and measured output operators as $\mathbf{B}u = b(z)u$, $S_m x = \int_\Omega s(z)\bar{x}\,dz$,

the PDE system of (3.1) can be represented in the infinite-dimensional form

$$\dot{x} = \mathbf{A}x + \mathbf{F}(x) + \mathbf{B}u,$$
$$y_m = S_m x, \tag{3.6}$$

with initial condition

$$x(0) = x_0. \tag{3.7}$$

Based on bounded locally Lipschitz assumption for $\mathcal{F}$, we can conclude that

$\mathbf{F}$ is a nonlinear smooth vector function that satisfies $\mathbf{F}(0) = 0$ and is also locally

Lipschitz

$$\left\|\mathbf{F}(x_1) - \mathbf{F}(x_2)\right\|_2 \leq K_L \|x_1 - x_2\|_2 \tag{3.8}$$

where K_L is the Lipschitz gain in the above inequality.

Assumption 3.1. (state-space partitioning) *The infinite-dimensional representation of the system (3.1)-(3.3) in an appropriate Sobolev subspace, $\mathbb{W}$, can be partitioned into a finite number of slow (possibly unstable) and an infinite number of fast and stable subsystems; also a time scale separation can be identified between the two subsystems dynamics.*

The analytical basis functions needed to discretize the infinite-dimensional representation of the system in $\mathbb{W}$, can be computed from the eigenfunction problem of the operator $\mathbf{A}$,

$$\mathbf{A}\phi_i = \lambda_i \phi_i, \quad i = 1, \ldots, \infty \tag{3.9}$$

subject to

$$q(\phi_i, \frac{d\phi_i}{dz}, ..., \frac{d^{n_0-1}\phi_i}{dz^{n_0-1}}) = 0 \ \text{ on } \ \partial\Omega, \tag{3.10}$$

where λ_i and ϕ_i denote the ith eigenvalue and the corresponding eigenfunction, respectively.

Assumption 3.1. (restated) *The ordered eigenspectrum of the operator $\mathbf{A}$, $\{\lambda_1, \lambda_2, \ldots\}$, can be decomposed to a finite-dimensional set of p eigenvalues with possibly positive real parts, $\{\lambda_1, \lambda_2, \ldots, \lambda_p\}$, and an infinite-dimensional complement set of the remaining eigenvalues with negative real parts, $\{\lambda_{p+1}, \lambda_{p+2}, \ldots\}$*

where the corresponding eigenfunctions to the two subsets of eigenvalues can be presented as $\Phi_s = [\phi_1 \ \phi_2 \ \cdots \phi_p]^T$, $\Phi_f = [\phi_{p+1} \ \phi_{p+2} \ \cdots]^T$. *Also a time scale separation can be identified between slow and fast subsets of the eigenvalues as* $\sigma = \dfrac{|Re(\lambda_1)|}{|Re(\lambda_{p+1})|}$ *where Re denotes the real part.*

According to Assumption 3.1, we can decompose the Sobolev subspace, $\mathbb{W}$, to a slow subspace, $\mathbb{W}_s \triangleq span\{\phi_i\}_{i=1}^p$, and a complement fast and stable subspace, $\mathbb{W}_f \triangleq span\{\phi_i\}_{i=p+1}^\infty$, i.e., $\mathbb{W} = \mathbb{W}_s \oplus \mathbb{W}_f$. Then by defining the orthogonal projection operators of $\mathcal{P} : \mathbb{W} \to \mathbb{W}_s$, $\mathcal{P} = (\cdot, \Phi_s)$ and $\mathcal{Q} : \mathbb{W} \to \mathbb{W}_f$, $\mathcal{Q} = (\cdot, \Phi_f)$, we obtain

$$x = x_s + x_f, \tag{3.11}$$

where $x_s = \mathcal{P}x \in \mathbb{W}_s$, $x_f = \mathcal{Q}x \in \mathbb{W}_f$. Using such decomposition, the system of (3.6) can be discretized in the form of a partitioned ODE set of vectorized modes,

$$\begin{aligned}
\dot{x}_s &= A_s x_s + F_s(x_s, x_f) + B_s u, \\
\dot{x}_f &= A_f x_f + F_f(x_s, x_f) + B_f u, \\
y_m &= S_m x_s + S_m x_f, \\
y_r &= S_r x_s + S_r x_f,
\end{aligned} \tag{3.12}$$

subject to the following initial conditions

$$\begin{aligned}
x_s(0) &= \mathcal{P}x(0) = \mathcal{P}x_0, \\
x_f(0) &= \mathcal{Q}x(0) = \mathcal{Q}x_0,
\end{aligned} \tag{3.13}$$

where $A_s = \mathcal{P}\mathbf{A}(x_s + x_f) = \mathcal{P}\mathbf{A}x_s$, $A_f = \mathcal{Q}\mathbf{A}(x_s + x_f) = \mathcal{Q}\mathbf{A}x_f$, $F_s = \mathcal{P}\mathbf{F}$, $F_f = \mathcal{Q}\mathbf{F}$, $B_s = \mathcal{P}\mathbf{B}$, $B_f = \mathcal{Q}\mathbf{B}$.

Assumption 3.2. (Observability and controllability) *The PDE system of (3.1)-(3.3) is assumed to be approximately observable and controllable [84].*

Remark 3.1. *The APOD algorithm requires the spatially distributed profile of the system states (snapshots) at revisions to revise the set of empirical basis functions during closed-loop process evolution. Consequently, we assume the existence of the periodic distributed snapshot measurement output, $y_r(z, t_k) \in \mathbb{R}^n$. Such required snapshots can be accessible from periodic fixed or moving spatially distributed measurement sensors, or be computed using in parallel high fidelity simulator. The required snapshots at each revisions in the presence of partial sensor information can be reconstructed by Gappy-APOD from previous spatially distributed profiles [204]. Gappy-APOD reconstructs the required data via a two tier procedure for a part of the spatial domain which was not measured. We can also address the snapshot construction problem by spatially distributed dynamic observers in the form of PDEs which only use a limited number of fixed point measurement sensors. The on-line snapshot construction problem to circumvent this basic assumption is the subject of the authors' current work.*

Remark 3.2. *The state-space partitioning assumption (Assumption 3.1) is satisfied by the majority of transport-reaction processes (see the catalytic rod example at section 2, the catalytic packed-bed reactor example at section 4 in [75], chemical*

vapor deposition process [1, 178, 248] and plasma discharge reactor [172]). This assumption validates the existence of only a few dominant modes that describe the dynamics of the parabolic PDE system and enables us to approximate the PDE by a finite-dimensional ODE system.

Remark 3.3. *The controllability and observability of DPSs depend on the locations of control actuators and measurement sensors, and specification of control objectives, while the controllability and observability of the ROMs of DPSs additionally depend on the discretization method used and the number and location of discretization nodes [216]. In general chemical engineering processes are over-designed in terms of observability where measurement sensors are placed in appropriate locations. One of the common approaches to actuator and sensor placement is to select the locations based on open-loop considerations to ensure controllability and observability. For further work on different aspects of actuator and sensor placement based on controllability/observability and optimal measurement methods see [21, 88, 251, 252] and the references therein.*

3.2 APOD-based model reduction and controller-observer synthesis

We investigate the design problem of output feedback control and dynamic observer between ROM revisions; Lyapunov stability is proved in the time period between

two consecutive snapshot arrivals and model reconstructions. Contrary to most of the data-driven model reduction approaches which use only open-loop system data, in the proposed APOD-based model reduction approach the required data are obtained during closed-loop system evolution. Thus, the resulting ROM accounts for the effects of controller actions on the process and the possible destabilizing effect they may have even if they were initially neglected. The dynamic observer and controller that are designed in this section will be refined based on stability of hybrid systems adding a supervisory control scheme.

3.2.1 Finite-dimensional approximation using method of weighted residuals

The finite-dimensional approximation of the infinite-dimensional PDE system of (3.1)-(3.3) can be derived by the method of weighted residuals from the empirical basis functions. $\bar{x}(z,t)$ can be generally described by an infinite weighted sum of a complete vectorized set of empirical basis functions $\Psi(z)$. The following approximation can be obtained by truncating the series expansion of $\bar{x}(z,t)$ up to order m:

$$\bar{x}(z,t) \simeq \sum_{k=1}^{m} \psi_k(z) a_k(t) \overset{m \to \infty}{\longrightarrow} \bar{x}(z,t) = \sum_{k=1}^{\infty} \psi_k(z) a_k(t) \qquad (3.14)$$

where $a_k(t)$ are known as system time-varying empirical modes. The following m^{th} order ODEs are derived by substituting (3.14) in the PDE system of (3.1)-(3.3),

multiplying the PDE with the weighting functions, $\varphi(z)$, and integrating over Ω:

$$
\begin{aligned}
\sum_{k=1}^{m} (\varphi_v(z), \psi_k(z))\dot{a}_k(t) = &\sum_{k=1}^{m} (\varphi_v(z), \mathcal{A}(z)\psi_k(z))a_k(t) \\
&+ \left(\varphi_v(z), \mathcal{F}(z, \sum_{k=1}^{m} \psi_k(z)a_k(t))\right) + (\varphi_v(z), b(z))u, \\
& v = 1, ..., m, \\
y_m = &\sum_{k=1}^{m} (s(z), \psi_k(z))a_k(t).
\end{aligned}
\tag{3.15}
$$

The method of weighted residuals reduces to Galerkin's projection when the weighting functions, $\varphi(z)$, are set to be the same as the empirical basis functions, $\psi(z)$. Then (3.15) can be presented in the compact form of

$$
\begin{aligned}
\dot{a} &= Aa + f(a) + Bu, \\
y_m &= Ca.
\end{aligned}
\tag{3.16}
$$

In the above equation, A, B and C denote constant matrices between revisions and f is a Lipschitz nonlinear vector function, i.e.,

$$
\left\| f(a_1) - f(a_2) \right\| \leq K_l \|a_1 - a_2\|,
\tag{3.17}
$$

where K_l indicates the upper bound gain in the Lipschitz inequality. In general, we must employ an overestimator for the range of values that we are interested in, in order to obtain a local bound. We also assume that the reduced order model of (3.16) keeps the observability and controllability properties of the original PDE

system of (3.1)-(3.3) due to the set of globally recursively updated empirical basis functions.

Remark 3.4. *Note that since the basis functions, Ψ, are periodically revised, the approximate systems we obtain are switching systems, i.e., the form and dimensionality of the system changes during process evolution. Furthermore, the designed observer and controller will also be revised as well at each switching, resulting in a switched closed-loop system, even though the process is continuous.*

3.2.2   APOD-based dynamic observer design

For the APOD-based ROM revision and dynamic observer design, we assume the periodic availability of the spatially distributed snapshots and continuous availability of measurements of the process from a limited number of point sensors. A static observer was designed to estimate the modes in the ROM of (3.15) required by the output feedback control structure [203, 256], however in such design the number of required point sensors must be supernumerary to the number of modes, otherwise the observer gives erroneous estimates. In this chapter, we employ a exponentially stable Luenberger-type nonlinear observer design to circumvent this essential issue. Note that the Luenberger-type dynamic observers need only one point measurement sensor to formulate the estimation error and predict the dynamic behavior of the system modes.

We can define the spatially distributed estimation error by neglecting the fast

and stable dynamics of the system as follows

$$E(z,t) = \bar{x}_e(z,t) - \bar{x}_s(z,t), \tag{3.18}$$

where $\bar{x}_s$ denotes the state of the slow subsystem and $\bar{x}_e$ is its estimated value. The slow part of the original system state can be obtained using time-space separation as

$$\bar{x}_s(z,t) = \Phi_s{}^T(z)\, x_s(t), \tag{3.19}$$

and the estimated state

$$\bar{x}_e(z,t) = \Psi^T(z)\, \hat{a}(t), \tag{3.20}$$

where $\Psi = [\psi_1 \ \psi_2 \ \ldots \ \psi_m]^T$, $\Phi_s = [\phi_1 \ \phi_2 \ \ldots \ \phi_p]^T$; m is the number of APOD-based empirical basis functions and p denotes the number of analytical basis functions of the slow subsystem operator and $\hat{a}$ is the vector of estimated modes of (3.16). Note that the set of analytical basis functions of the system are unavailable and are used only for the system analysis and to expose the stability conditions needed. We can not define the observation error as the subtraction of $\hat{a} - x_s$, because the vectors of x_s and $\hat{a}$ in Eqs. (3.19) and (3.20) may have different dimensions due to the possible difference between the numbers of analytical basis functions, Φ_s, and empirical basis functions, Ψ.

Assumption 3.3. *We assume that $\mathbb{W}_s \subseteq \mathbb{P}$, locally, where $\mathbb{W}_s \triangleq span\{\phi_i\}_{i=1}^p$ denotes the local subspace of the slow and possibly unstable modes and $\mathbb{P} \triangleq span\{\psi_i\}_{i=1}^m$*

is empirical dominant subspace.

Note that Assumption 3.3 can be justified from the excitation of the higher order dynamics during the system progression. Based on this assumption, subspace $\mathbb{P}$ includes the slow Sobolev subspace $\mathbb{W}_s$ and may include a part of the fast Sobolev subspace $\mathbb{W}_f$. Then by defining a bounded map in the form of a linear transformation, we can connect the slow Sobolev subspace and subspace $\mathbb{P}$ and find the corresponding states. Such linear transformation changes at ROM revisions to conserve the properties of the subspaces during closed-loop process evolution. The bounded map is defined as follows

$$\bar{x}_s = \Phi_s^T x_s = \Psi^T \mathcal{M} x_s = \Psi^T \tilde{a}, \tag{3.21}$$

where $\tilde{a} = \mathcal{M} x_s$, $\mathcal{M} : \mathbb{W}_s \mapsto \mathbb{P}$ and

$$\mathcal{M} = (\Psi^T, \Phi_s^T). \tag{3.22}$$

Note that based on Assumption 3.3, $\mathcal{M} = (\Psi^T, \Phi_s^T)$, $\mathcal{M} : \mathbb{W}_s \mapsto \mathbb{P}$, is an injective linear transformation, i.e., if $\tilde{a}_1 = \tilde{a}_2, \forall \tilde{a}_1, \tilde{a}_2 \in \mathbb{P}$ then $x_{s,1} = x_{s,2}, \forall x_{s,1}, x_{s,2} \in \mathbb{W}_s$. The reverse transformation can also be defined as $\mathcal{M}^\perp = (\Phi_s^T, \Psi^T)$, $\mathcal{M}^\perp : \mathbb{P} \mapsto \mathbb{W}_s$ such that $\mathcal{I} = \mathcal{M}^\perp \mathcal{M} : \mathbb{W}_s \mapsto \mathbb{W}_s$ is a bijective map. An interesting fact about this transformation is that $\mathcal{M}^\perp = \mathcal{M}^T$.

Using the transformation, the slow dynamics of (3.12) can be represented within

subspace $\mathbb{P}$ as

$$\dot{\tilde{a}} = A\tilde{a} + f(\tilde{a}) + Bu,$$

$$y_m = C\tilde{a},$$

(3.23)

where $A = \mathcal{M}A_s\mathcal{M}^\perp$, $B = \mathcal{M}B_s$ and $C = S_m\mathcal{M}^\perp$ are constant matrices between ROM revisions and $f = \mathcal{M}F_s$ is a Lipschitz nonlinear function. From the transformation and its reverse it is straightforward to show that A, B and C matrices, and f nonlinear function in (3.23) are the same as A, B and C matrices, and f nonlinear function used in (3.16).

Based on (3.23), the Luenberger-type dynamic observer is formulated as

$$\dot{\hat{a}} = A\hat{a} + f(\hat{a}) + Bu + L(C\hat{a} - y_m),$$

(3.24)

where $\hat{a}$ is the vector of estimated modes and L denotes the observer gain. Then based on Assumption 3.1, the observation error can be defined as

$$E = \bar{x}_e - \bar{x}_s \simeq \Psi^T e,$$

(3.25)

where $e = \hat{a} - \tilde{a}$ is the observer error with respect to empirical eigenmodes, and the observer error dynamics can be derived from (3.24) and (3.23)

$$\dot{e} = (A + LC)e + [f(\hat{a}) - f(\hat{a} - e)].$$

(3.26)

The following Lyapunov function is considered

$$V = V_o + V_c = \frac{\zeta_o}{2} e^T P_o e + \frac{\zeta_c}{2} \hat{a}^T P_c \hat{a}, \tag{3.27}$$

where $\tilde{V}_o$ is the observer Lyapunov function (OLF) and V_c denotes the control Lyapunov function (CLF), P_o and P_c are positive definite matrices and P_o has bounded Frobenius norm, $\|P_o\| \leq K_p$; ζ_o and ζ_c are positive numbers. Then we can obtain the time derivative of the mentioned Lyapunov function as $\dot{V} = \dot{V}_o + \dot{V}_c$.

By setting the control objective at dynamic regulation of the observer, $\hat{a} \to 0$, and considering the following CLF $V_c = \frac{\zeta_c}{2} \hat{a}^T P_c \hat{a}$, we assume a controller can be designed that forces the time derivative of the CLF, $\dot{V}_c$ to be negative. Thus we need only consider the OLF to be negative, $\dot{V}_o < 0$, at this point. We will revisit this assumption during the controller design step.

The question thus becomes how to find the observer gain, L, that stabilizes the system of (3.24) in the Lyapunov sense. Three different approaches are proposed as follows to address observer gain computation.

3.2.2.1 Pole placement

As mentioned previously we need only establish that $\dot{V}_o < 0$. For $P_o = I$ we obtain

$$\dot{V}_o = \zeta_o e^T \dot{e} = \zeta_o \left(e^T (A + LC) e + e^T [f(\hat{a}) - f(\hat{a} - e)] \right) < 0. \tag{3.28}$$

From the Lipschitz condition (3.17) we conclude

$$e^T[f(\hat{a}) - f(\hat{a} - e)] \le \|e^T\| \left\|f(\hat{a}) - f(\hat{a} - e)\right\| \le \|e^T\| \|K_l\| \|e\| = K_l \|e\|^2 = K_l e^T e.$$

(3.29)

then using (3.29), the inequality of (3.28) can be stated as follows

$$e^T(A + LC)e + e^T(K_l I)e < 0 \Rightarrow e^T(A + LC + K_l I)e < 0 \Rightarrow A + LC + K_l I < 0.$$

(3.30)

By considering $A_o = A + K_l I$, we can solve the inequality problem to find the observer gain, L, using any pole placement technique. The closed-loop poles of the dynamic observer error (the eigenvalues of $A_c = A_o + LC$), can be placed at arbitrarily locations by solving the following equation

$$\left|sI - (A_o + LC)\right| = p_{des}(s)$$

(3.31)

for the observer gain matrix where I denotes the identity matrix and p_{des} is the characteristic polynomial of the desired observation poles.

3.2.2.2   Linear quadratic regulation (LQR)

Another approach to compute the observer gain is via linear quadratic regulation (LQR). In this approach, Eq. (3.31) can be restated as

$$\left| sI - (A_o + LC) \right| = \left| (sI - (A_o + LC))^T \right| = \left| sI - (A_o^T + C^T L^T) \right| \qquad (3.32)$$

where A_o^T and C^T are the dual system matrices in (3.33) and L^T denotes the gain matrix for the state feedback control problem of the dual system

$$\dot{\tilde{e}} = A_o^T \tilde{e} + C^T \tilde{u},$$
$$\tilde{u} = L^T \tilde{e}. \qquad (3.33)$$

We design a linear quadratic feedback regulator [257] to solve the dual control problem and compute the observer gain. A state feedback regulator law can be synthesized via an optimization problem that minimizes the following quadratic objective function

$$J(\tilde{u}) = \int_0^\infty (\tilde{a}^T Q \tilde{a} + \tilde{u}^T R \tilde{u} + 2\tilde{a}^T N \tilde{u}) dt \qquad (3.34)$$

subject to the dual system dynamics of (3.33) and that Q, R and N are chosen to be positive definite matrices. The optimal gain matrix of L^T then is computed as

$$L^T = -\left(R^{-1}(B^T S + N^T) \right)^T \Rightarrow L = -(N + S^T B)R^{-T} \qquad (3.35)$$

where S is the solution of the associated algebraic Riccati equation

$$A_o S + S A_o^T - (SC^T + N)R^{-1}(CS + N^T) + Q = 0. \tag{3.36}$$

3.2.2.3 Linear matrix inequality (LMI)

In this approach, the time derivative of the OLF of (3.27) is chosen to be

$$\dot{V}_o = \frac{\zeta_o}{2}\left(\dot{e}^T P_o e + e^T P_o \dot{e}\right). \tag{3.37}$$

Using (3.26), the time derivative of $\tilde{V}_o$ (which we derive to be negative) is

$$
\begin{aligned}
\dot{V}_o &= \frac{\zeta_o}{2}\bigg[\left(e^T(A^T + C^T L^T) + [f(\hat{a}) - f(\hat{a} - e)]^T\right)P_o e \\
&\quad + e^T P_o\left((A + LC)e + [f(\hat{a}) - f(\hat{a} - e)]\right)\bigg] \\
&= \frac{\zeta_o}{2}\bigg[e^T\left((A + LC)^T P_o + P_o(A + LC)\right)e \\
&\quad + e^T P_o[f(\hat{a}) - f(\hat{a} - e)] + \left(e^T P_o[f(\hat{a}) - f(\hat{a} - e)]\right)^T\bigg] < 0.
\end{aligned}
\tag{3.38}
$$

Based on the Lipschitz condition (3.17) and bounded norm of P_o we obtain

$$
\begin{aligned}
e^T P_o[f(\hat{a}) &- f(\hat{a} - e)] + \left(e^T P_o[f(\hat{a}) - f(\hat{a} - e)]\right)^T \\
&\leq 2\left\|e^T P_o[f(\hat{a}) - f(\hat{a} - e)]\right\| \leq 2\|e^T\|\|P_o\|\left\|[f(\hat{a}) - f(\hat{a} - e)]\right\| \\
&\leq 2K_l K_p\|e^T\|\|e\| \\
&\leq K_0 e^T e,
\end{aligned}
\tag{3.39}
$$

where $K_0 = 2K_l K_p$. Then inequality (3.38) can be expressed as follows using (3.39)

$$e^T \Big((A + LC)^T P_o + P_o(A + LC) \Big) e + K_0 e^T e < 0$$
$$\Rightarrow e^T \Big((A + LC)^T P_o + P_o(A + LC) + K_0 I \Big) e < 0. \tag{3.40}$$

Since $P_o A_c + A_c^T P_o + K_0 I < 0$ where $A_c = A + LC$, it follows that $\dot{V} < 0$ for all $e \neq 0$ and stability is proved. So P_o and L are chosen so that the following LMI is satisfied

$$A_c^T P_o + P_o A_c + K_0 I < -P_o W P_o - P_o L U L^T P_o \tag{3.41}$$

where W and U are the design weighting matrices and they must symmetric positive definite. From (3.41) we have

$$A_c^T P_o + P_o A_c + P_o W P_o + P_o L U L^T P_o + K_0 I < 0$$
$$\Rightarrow (A^T + C^T L^T) P_o + P_o(A + LC) + P_o W P_o + P_o L U L^T P_o + K_0 I < 0$$
$$\Rightarrow A^T P_o + P_o A + (P_o LC)^T + P_o LC + P_o W P_o + P_o L U L^T P_o + K_0 I < 0. \tag{3.42}$$

Using $Y = P_o L$, (3.42) can be expressed as

$$A^T P_o + P_o A + (YC)^T + YC + P_o W P_o + Y U Y^T + K_0 I < 0$$
$$\Rightarrow P_o A + A^T P_o + (Y^T + U^{-1}C)^T U (Y^T + U^{-1}C) - C^T U^{-1} C + P_o W P_o + K_0 I < 0. \tag{3.43}$$

By setting $Y^T = -U^{-1}C$ we have

$$P_o A + A^T P_o - C^T U^{-1} C + P_o W P_o + K_0 I < 0. \tag{3.44}$$

The above matrix inequality is equivalent to

$$\begin{pmatrix} P_o A + A^T P_o - C^T U^{-1} C + K_0 I & P_o \\ P_o & -W^{-1} \end{pmatrix} < 0 \tag{3.45}$$

using the Schur complement lemma [219].

The observer gain is computed by minimizing $trace(P_o^{-1})$ subject to (3.45). The observer gain then can be directly computed as

$$L = -P_o^{-1} C^T U^{-1}. \tag{3.46}$$

Proposition 3.1. *The observation error using dynamic observer of (3.24) is locally stable while f satisfies the Lipschitz condition (3.17) and (i) The characteristic polynomial roots are negative and feedback gain L is computed from (3.31) for the case when $P_o = I$, (ii) The Riccati equation of (3.36) has a solution, S, for positive definite matrices, Q, R, N and feedback gain L is obtained from (3.35), (iii) W and U are symmetric positive definite matrices and L is obtained from (3.46).*

Proof *See Appendix A.1.1 for proof of the proposition.*

Theorem 3.1. *Consider the nonlinear dissipative, input-affine, PDE system of (3.1)-(3.3) with infinite-dimensional representation of (3.6) and finite-dimensional approximation of (3.23) in subspace $\mathbb{P}$ with APOD-based empirical basis functions when the time interval between ROM updates, δt, is finite and larger than a critical value, t_b. Under Assumptions of 3.1-3.3 and Lipschitz assumption of nonlinear functions, the observation error dynamics is locally asymptotically stable between ROM revisions using dynamic observer of (3.24), with observer gain computed by either (i) Eq. (3.31) where $P_o = I$ and Hurwitz characteristic polynomial, (ii) Eq. (3.35) for positive definite matrices of Q, R and N, (iii) Eq. (3.46) for symmetric positive definite matrices of W and U.*

Proof *See Appendix A.1.2 for proof of the theorem.*

The dynamic observer of (3.24) is redesigned when the ROM is updated by APOD. Thus, stability theorems of hybrid systems are needed to prove that the switching closed-loop system still remains stable during the periodic revisions of the ROM. Then multiple OLFs in the form of (3.27) must be considered for such hybrid system analysis [79]. Considering finite time intervals between ROM revisions, the negative time derivative of the multiple Lyapunov functions of (3.27) guarantees stability of the switching system (Theorem 3.2 in [86]) when the following condition [79, 86] is also satisfied

$$V_o\big(e(t_k)\big) < V_o\big(e(t_{k-1})\big). \tag{3.47}$$

In the above condition, $k > 1$ and $V_o\big(e(t_k)\big)$ corresponds to the value of Lyapunov

function at the beginning of interval $[t_k, t_{k+1}]$. Note that the time interval between ROM revisions, $\delta t = t_{k+1} - t_k$, is chosen to be large enough to relax the fast dynamics of the system to zero. The OLF, $V_o = \dfrac{\zeta_o}{2} e^T P_o e$, may possibly increase during dimensionality changes of the ROM. Thus, value ζ_o must be chosen appropriately from a supervisory logic in the closed-loop process.

We can directly compute the eigenmodes of the system at the revisions when the new snapshot arrives by the periodic snapshot measurements,

$$\bar{x}(z, t_k) = \sum_{j=1}^{m} \psi_j(z)\tilde{a}_j(t_k) \implies \tilde{a}_j(t_k) = \int_{\Omega} \psi_j(z)\bar{x}(z, t_k)dz, \quad j = 1, \ldots, m,$$

where $x(z, t_k) = y_r(z, t_k)$ is the system snapshot at revision instant, t_k, and m denotes the number of eigenmodes. Thus, the following equation is applied to update the value of ζ_o,

$$\zeta_o = \xi \frac{e^T(t_{k-1})\ e(t_{k-1})}{e^T(t_k)\ e(t_k)}, \tag{3.48}$$

where $e = \hat{a} - \tilde{a}$. Alternatively, we initialize ζ_o at value ζ_{in} and reevaluate it using (3.48) only when the criteria of (3.47) is violated. This procedure leads to a less aggressive dynamic observer design that has smaller observer gain while guaranteeing stability of observation error dynamics.

Remark 3.5. *The LMI approach is well defined but computationally expensive. The pole placement technique is fast but it can be ill-conditioned if unrealistic locations have been chosen for closed-loop poles. Generally we should avoid placing*

multiple poles at the same location and typically require high gain, L, when the open-loop poles are weakly observable which in turn sensitizes the entire closed-loop structure to perturbations [142].

Remark 3.6. *For the ROM states to be unobservable the most probable situation is that all point sensors must be located at the zeros of a specific basis function with a corresponding decoupled eigenmode; this can in principle happen but very rarely, and as the number of sensors increases it becomes highly improbable. We can identify such cases on-line by comparing the positions of zeros of the computed basis functions and the placement of the sensors. Another reason for unstable estimates of the process state is the ROM/PDE model mismatch; this is the underlying reason we recursively update the ROM during process evolution.*

3.2.3   APOD-based output feedback controller design

In this section, we now focus on synthesizing a controller structure that achieves the objective of regulating the system of (3.1) to the origin based on an appropriate finite-dimensional approximation of (3.23) using Lyapunov's direct method when the state values' estimates originate from dynamic observer (3.24). As described before, the ROM of (3.16) is an approximation of the main PDE system of (3.1). Due to this fact the model reduction error between ROM and original PDE is considered as system uncertainty that affects controller design. We should note that the assumption of separation principle between the controller and the observer

is relaxed. A simpler controller design under separation principle is presented in [28].

In the proposed control structure, the ROM is used as the basis for output feedback controller synthesis, however, the state values needed by the controller to compute the control action are estimated from the dynamic observer. There is a difference (in the form of the Luenberger term) between the ROM equations used by the controller and the dynamic observer. If we assume principle of separation, there is no need to account for this term in the closed-loop stability analysis, because the principle of separation of observation and control implies the stability properties of the output feedback controller can be deduced from the stability analysis of the dynamic observer and deterministic state feedback controller, separately.

For synthesizing a control structure (a) without assuming separation principle between control and observation, and (b) to compensate for the uncertainty results from model reduction error, first we design the controller to stabilize the dynamic observer and then the stable dynamic observer to guarantee the observation error regulation. We consider the Luenberger term in (3.24) as a general non-vanishing perturbation. We also assume this perturbation can be considered as a summation of possibly time varying but bounded uncertain variables. By considering the internal uncertainty in the observer dynamics we can also circumvent the issues of ignoring the observation of fast and stable dynamics in (3.12) in the time period

of $[0, t_b]$ that is discussed in the proof of Theorem 3.1. In this case the system of

(3.24) can be considered in the following general form

$$\dot{\hat{a}} = F(\hat{a}) + Bu + \sum_{i=1}^{s} w_i(\hat{a})\theta_i(t), \tag{3.49}$$

where $F(\hat{a}) = A\hat{a} + f(\hat{a})$, $L(C\hat{a}(t) - y_m(t)) = \sum_{i=1}^{s} w_i(\hat{a})\theta_i(t)$, $\theta_i(t) \in \Theta$, $\|\theta_i(t)\| \le$

θ_{bi} and $\Theta \subset \mathbb{R}$ is a nonempty compact convex subset. The upper bounds of θ_{bi} can

be approximated based on monitoring the dynamic observer error and the norm

of observer gain.

The vector of uncertain variables in (3.49) can compensate for uncertainty in the

system due to basis functions computation or model mismatch and also can account

for exogenous disturbances. Assuming that the perturbation is non-vanishing, the

origin of the system is no longer an equilibrium point for the uncertain system.

Thus, the objective is to synthesize a robust nonlinear output feedback controller

that guarantees global boundedness in a neighborhood around the desired steady

state.

Theorem 3.2. *Consider the nonlinear dissipative PDE system in (3.1), for which*

Assumptions 3.1-3.3 hold. The following static output feedback control law [100,

235] asymptotically stabilizes the system of (3.1) when the time interval between

ROM updates, δt, is finite and larger than a critical value, t_b.

$$u(t) = -k(\hat{a}, c_o, \rho, \chi, \theta_b)(L_B V_c), \tag{3.50}$$

where $c_o > 0$, $\rho > 0$ and $\chi > 1$ are adjustable parameters and

$$k(\hat{a}, c_o, \rho, \chi, \theta_b) = \begin{cases} c_o + \dfrac{L_F^\S V_c + \sqrt{\left(L_F^\S V_c\right)^2 + \left(\|(L_B V_c)\|\right)^4}}{\left(\|(L_B V_c)\|\right)^2}, & L_B V_c \neq 0 \\[4ex] c_o, & L_B V_c = 0 \end{cases}$$

$$L_F^\S V_c = L_F V_c + \rho \|P_c \hat{a}\| + \chi \sum_{i=1}^{s} \|L_{w_i} V_c\| \theta_{bi}.$$

$V_c = \dfrac{\zeta_c}{2} \hat{a}^T P_c \hat{a}$ *is the CLF, P_c is a positive definite matrix, $L_B V_c = [L_{B_1} V_c \ \ldots \ L_{B_l} V_c]^T$ is a column vector,* $L_F V_c = \dfrac{\partial V_c}{\partial \hat{a}} F$, $L_B V_c = \dfrac{\partial V_c}{\partial \hat{a}} B$ *denote Lie derivatives and* $\theta_b = [\theta_1 \ \theta_2 \ \cdots \ \theta_s]^T$.

Proof *See Appendix A.1.3 for proof of the theorem.*

At the ROM revisions, the same strategy for dynamic observer designs is used for ζ_c because CLF, $V_c = \dfrac{\zeta_c}{2} \hat{a}^T P_c \hat{a}$, also may increase during the ROM dimensionality changes. The value of ζ_c must be chosen appropriately to satisfy the hybrid systems stability criteria [79]. A possible strategy is to automatically adjust ζ_c at every instance of ROM changes as follows

$$\zeta_c = \xi \frac{\hat{a}^T(t_{k-1}) \ \hat{a}(t_{k-1})}{\hat{a}^T(t_k) \ \hat{a}(t_k)} \tag{3.51}$$

in order to retain an aggressive controller throughout the process operation. The strategy used in the current work is to initialize ζ_c at value ζ_{in} and reevaluate it using (3.51) only when constraints of (3.47) are violated. This procedure leads to

less aggressive control action while guaranteeing closed-loop stability.

Theorem 3.3. *The DPS of (3.1) that is described by the switching ROM of (3.23), can be asymptotically stabilized by the output feedback control structure of (3.50) and (3.24) using supervisory strategies of (3.51) and (3.48) to evaluate ζ_c and ζ_o at each time period when the time interval between the ROM revisions, δt, is chosen to satisfy $\delta t > t_b$, where t_b can be obtained from singular perturbation analysis.*

Proof *See Appendix A.1.4 for proof of the theorem.*

By combining the APOD-based dynamic observer and APOD-based controller synthesis with ζ_o and ζ_c updating procedures, we thus obtain a hybrid output feedback control structure that guarantees that the system closed-loop stability at the desired steady state. The block diagram of the closed-loop process is presented in Figure 3.1, where the connections between the proposed control structure components such as continuous point and periodic distributed measurement sensors, model reduction, dynamic observer, controller and actuators are illustrated. The proposed structure redesigns the observer/controller pair to enforce closed-loop stability whenever the ROM is revised to retain accuracy.

Remark 3.7. *The principle of separation of estimation and control, which is relaxed in the proposed output feedback control synthesis, only holds for linear time-invariant (LTI) systems. The important consequence of the separation principle is that the controller and dynamic observer can be designed separately, i.e., the controller gain, k can be computed independently of the observer gain, L. Such*
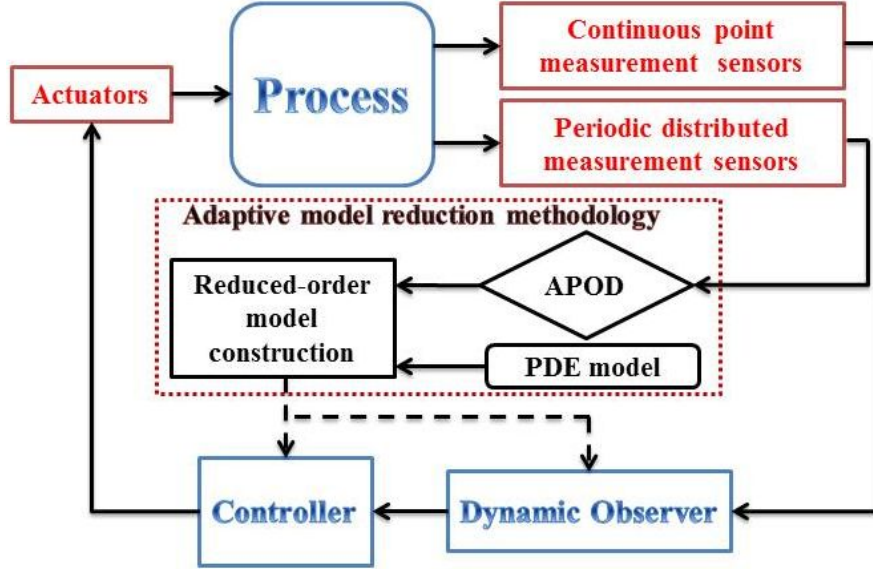
Figure 3.1: Process operation block diagram under the proposed controller structure.

principle does not generally hold for linear time-variant (LTV) and nonlinear systems [68, 148]. Invoking the separation principle is a strong assumption in general nonlinear systems which limits the applicability of the resulting output feedback controller design for nonlinear systems [207]. It may lead to severe deterioration of the nominal closed-loop performance or even to closed-loop instability.

Remark 3.8. *The controller parameters $\rho > 0$ and $\chi > 1$ are tuned to achieve the trade-off between desired stability region and degree of uncertainty attenuation. Using small values for these parameters enlarges the guaranteed closed-loop stability region and using large values achieves a significant degree of uncertainty attenuation in dynamic observer structure. By introducing a sufficiently small positive value of η in the denominator of $k(\cdot)$ we circumvent the control action possible*

chattering behavior near the origin. In the controller structure, c_o is also employed to tune the speed of the system convergence to the steady state.

Remark 3.9. *Based on Assumption 3.3, any basis functions of slow subsystem belong in $\mathbb{P} \oplus \mathbb{Q}$. This assumption is correct only for the time intervals longer than the critical time period of t_b needed for fast dynamics to be stabilized. This condition may fail due to appearance of new trends as time evolves. In such case the APOD updates the set of empirical basis functions then the ROM is revised using updated basis functions. The revised ROM is then used as the basis to redesign the controller/observer pair. These corrections will be repeated to enforce closed-loop stability during process evolution.*

Remark 3.10. *The relative significance of the empirical eigenvalues is a strong indicator that the slow subsystem is included in $\mathbb{P} \oplus \mathbb{Q}$. In general the retained snapshot ensemble size is the maximum size of the slow subsystem we can account for. We assume that at any time there are a number of eigenvalues at zero which is a requirement of all proper orthogonal decomposition (POD) based methods.*

Remark 3.11. *The presence of uncertain parameters and unmodeled dynamics, if not taken into account in the controller design, may lead to severe deterioration of the nominal closed-loop performance or even to closed-loop instability [76]. As discussed in section 3.2.3 the non-vanishing perturbation term in the system approximation of (3.49) accounts for the system parameter uncertainty beside relaxing the separation principle. The typical sources of model uncertainty which can*

be compensated in such non-vanishing form includes unknown or partially known

time-varying process parameters, exogenous disturbances, and unmodeled dynamics

[76].

3.3   Application to physico-chemical systems described by KSE

The effectiveness of the proposed output feedback controller in regulating physico-chemical systems described by the Kuramoto-Sivashinsky equation (KSE) is illustrated in this section. KSE has been independently derived in a wide range of physico-chemical systems, where it can adequately describe incipient instabilities. Such systems as exemplified by phase turbulence in diffusion-reaction systems, long-wave motions of falling liquid thin films, interfacial instabilities between viscous fluids and unstable flame fronts [71, 93]. KSE with periodic boundary conditions shows a variety of dynamic behaviors, from converging to stable and unstable steady states to periodic waves and chaotic behavior, for different parameters [146]. The control problem of physico-chemical processes modeled by KSE was studied in the literature [15, 77, 93, 203].

We consider the integral controlled form of KSE as

$$\frac{\partial \bar{x}}{\partial t} = -v\frac{\partial^4 \bar{x}}{\partial z^4} - \frac{\partial^2 \bar{x}}{\partial z^2} - \bar{x}\frac{\partial \bar{x}}{\partial z} + \sum_{i=1}^{l} b_i u_i(t) \tag{3.52}$$

with periodic boundary conditions

$$\frac{\partial^j \bar{x}}{\partial z^j}(-\pi, t) = \frac{\partial^j \bar{x}}{\partial z^j}(\pi, t), \qquad j = 0, ..., 3 \tag{3.53}$$

and initial condition

$$\bar{x}(z, 0) = \bar{x}_0(z), \tag{3.54}$$

where $\bar{x}(z, t)$ is the system variable, $u(t) \in \mathbb{R}^l$ denotes the vector of manipulated inputs, t is the time, z is the spatial coordinate, $b(z)$ describes the control actuators' distribution and v is the diffusion parameter. Also the length of the spatial domain is 2π and the domain of the process is defined on $(-\pi, \pi)$. In the above form $\mathcal{A}(z)\bar{x} = -v\frac{\partial^4 \bar{x}}{\partial z^4} - \frac{\partial^2 \bar{x}}{\partial z^2}$ and $\mathcal{F}(z, \bar{x}) = -\bar{x}\frac{\partial \bar{x}}{\partial z}$.

Six control actuators were considered at $L_a = [-\pi/2, -\pi/4, -\pi/6, \pi/5, \pi/4, \pi/2]$ to regulate the system dynamics. The actuators distribution function are also set as $b_i(z) = \delta(z - L_{a,i})$ for $i = 1, ..., 6$, where $\delta(\cdot)$ is the Dirac delta function. The periodic sensors distribution function is assumed as $s_r(z, t) = 1$, i.e, the complete state profiles of the system state at ROM revisions. The important static observer requirements of available point measurements being supernumerary to the ROM dimension is circumvented using the proposed dynamic observer design (as discussed in "APOD-based dynamic observer" section). To illustrate such improvement, only one continuous point measurement sensor placed at $L_s = \pi/2$ is assumed to be available. The sensor shape distribution function is chosen to be
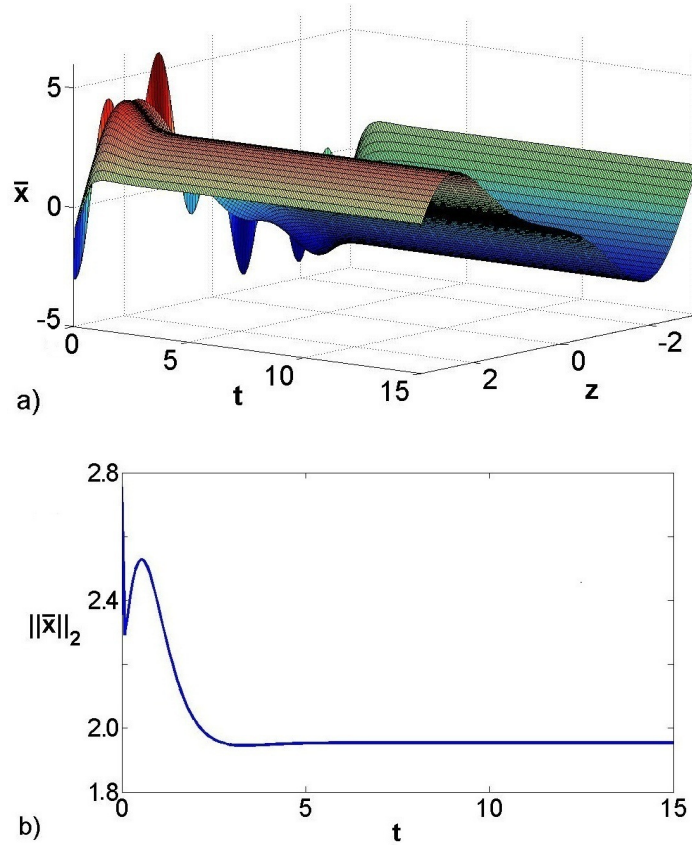
Figure 3.2: Open-loop spatiotemporal profile of (a) state of the system and (b) 2-norm of the state for $v = 0.4$.

$s_m(z) = \delta(z - L_s)$ and $\bar{x}_0 = 3\sin(z) - \cos(2z) - \sin(5z) + 2\cos(5z)$ is considered as the spatially nonuniform initial condition. The open-loop spatiotemporal dynamic behavior of the system and its spatial 2-norm are presented in Figure 3.2 for $v = 0.4$. The control objective is to regulate the KSE at a desired spatial profile. Without loss of generality, we set the spatially uniform unstable steady state [146] of $\bar{x}_d(z, t) = 0$ as the desired profile.

To initiate the set of empirical basis functions we consider the open-loop process $(u(t) = 0)$ and collect 31 snapshots during the initial time interval of $t \in [0, 2]$. By

applying off-line APOD to such ensemble of snapshots we obtain 3 empirical basis

functions that capture 0.99 of the ensemble energy. We consider the availability

of process spatially distributed snapshots every $t_s = 0.5$ while the point measure-

ment from only one sensor is assumed to be available continuously. To construct

the observer we applied three approaches presented in sections "pole placement",

"linear optimal observer" and "linear matrix inequality". The resulting closed-loop

system behavior was almost identical (when using proper sensor pole placement).

For brevity only the pole placement results are presented here.

To implement the proposed APOD-based output feedback control structure on

the KSE we set $\eta = 0.001$, $c_o = 0.8$, $\rho = 0.5$, $\chi = 2$ and $\zeta_{in} = 1$, where ζ_{in} indicates

the initial value for ζ_o and ζ_c. Figure 3.3 presents the closed-loop spatiotemporal

dynamic behavior of the process and its spatial 2-norm. We observe that the con-

troller successfully stabilizes the system of (3.52)-(3.54) at $\bar{x}(z,t) = 0$ and converges

to zero. Figure 3.4(a) shows the monitored 2-norm of error between the process

modes and the estimated modes by the observer in the closed-loop time period,

$t \in [2, 12]$ and Figure 3.4(b) presents the required control action. The monitored

error is estimated based on one point sensor and it converges to zero. It is also

observed that the control action converges to zero without any chattering. In Figs.

3.3(a), 3.3(b) and 3.4(b), $t \in [0, 2]$ indicates the open-loop time period. At the end

of this period, off-line APOD is used to initially construct the basis functions by

collecting the snapshots. Time interval 1 in these figures shows no control action
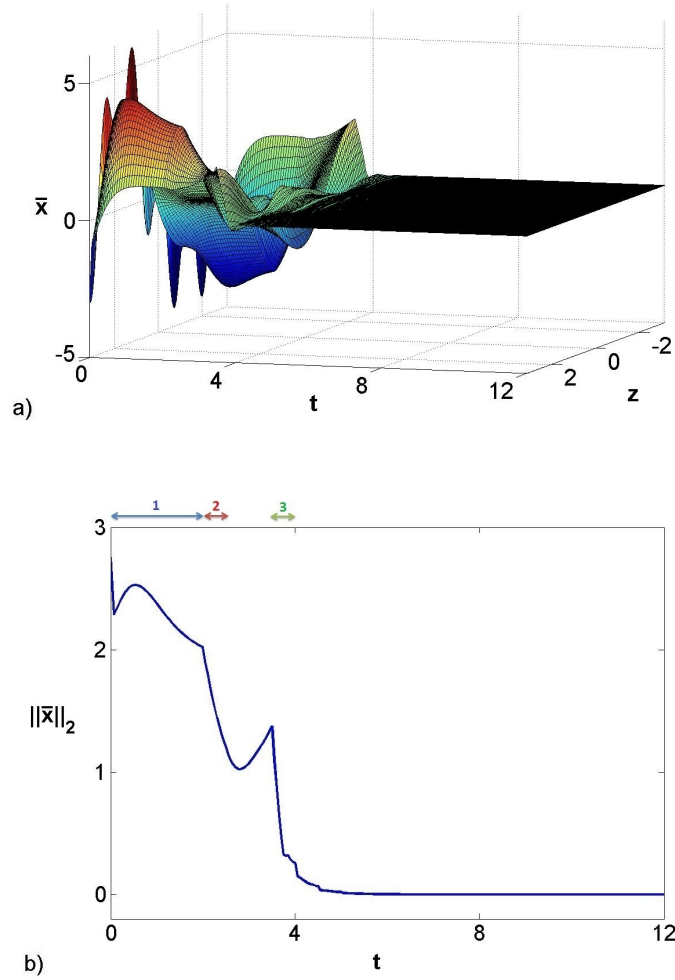
Figure 3.3: Closed-loop system temporal profile of (a) the state spatial profile, (b) 2-norm of the state.

while the system is open-loop. A relatively large control action can be identified at the beginning of time interval 2 that shows the controller attempts to stabilize the process by applying large initial control action. There is another fluctuation in control actions at the beginning of time interval 3 due to ζ_c update. In Figure 3.3(b), the temporal profile of spatial 2-norm converges to zero. We observe a peaking at the beginning of time interval 3 due to the peaking in control action. Generally,
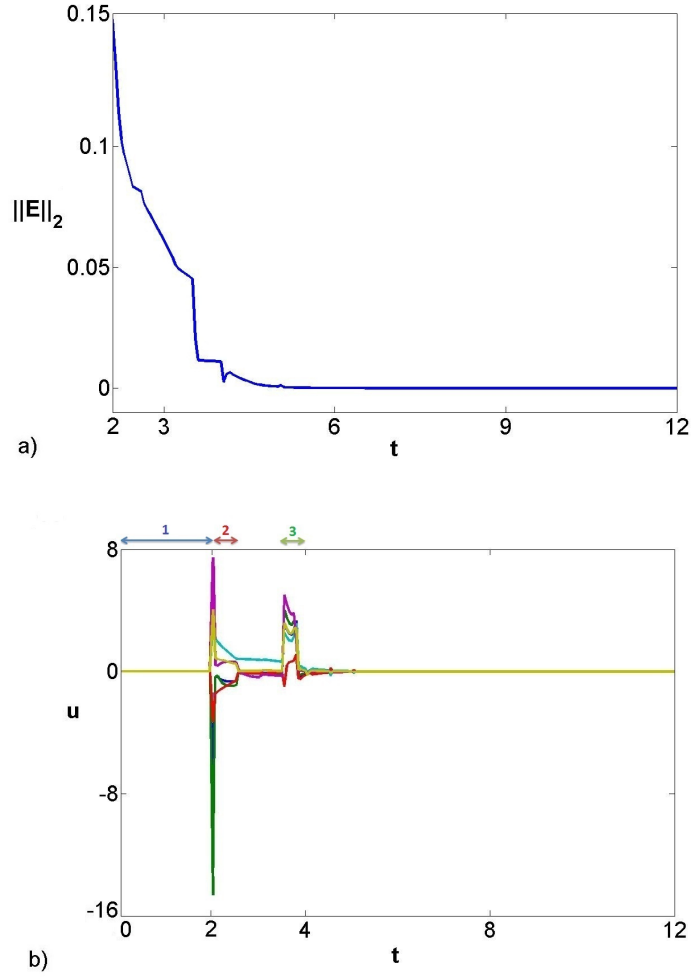
Figure 3.4: Closed-loop system temporal profile of (a) monitored norm of error between the real system and the observer from point measurement sensor, and (b) control action.

the non-smooth behavior of control action, spatial 2-norm and Lyapunov function at specific times can happen due to ROM revisions and ζ_c updating, where ROM revisions could include dimensionality changes. Such non-smooth behavior can be in principle compensated by incorporating input constraints considering closed-loop stability [79, 183] at the same time ensuring that the conditions set by
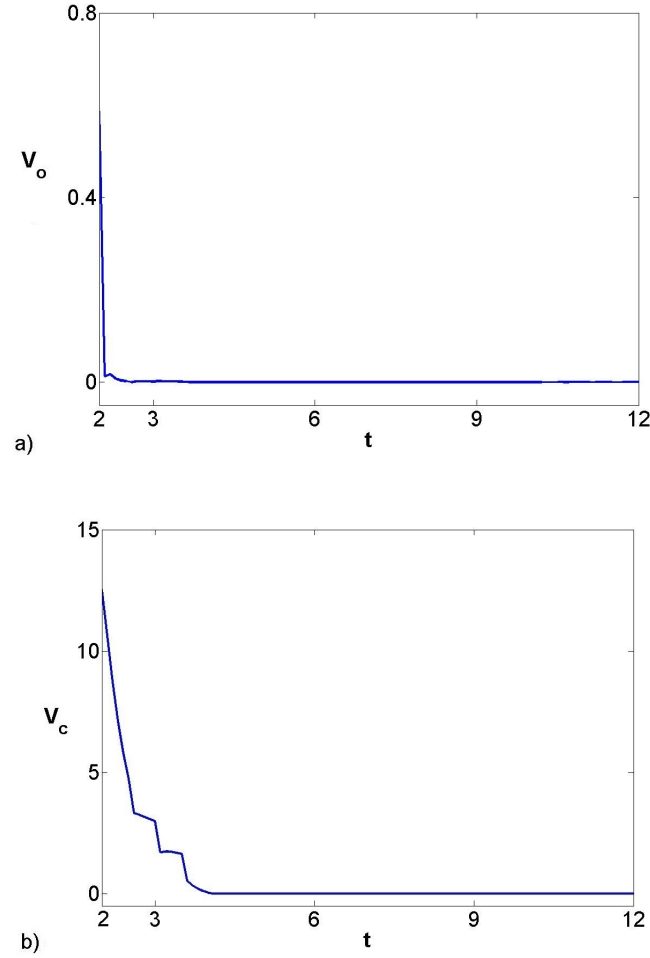
Figure 3.5: Closed-loop system temporal profile of (a) OLF, and (b) CLF.

hybrid system theory are satisfied. Figure 3.5(a) and (b) present the values of the OLF and the CLF, respectively, in the closed-loop time period, $t \in [2, 12]$. Note in Figure 3.5(b) the increase of the CLF is due to the significant change in the behavior of the KSE. If no update was allowed the system would remain unstable. Figure 3.6 shows the change in the number of basis functions during the process. The number of required empirical basis functions to capture the initial open-loop dynamic of the system was three. When new patterns appeared as the process
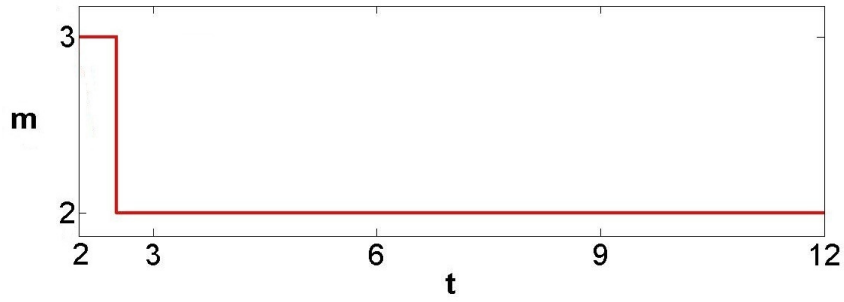
Figure 3.6: Number of basis functions.
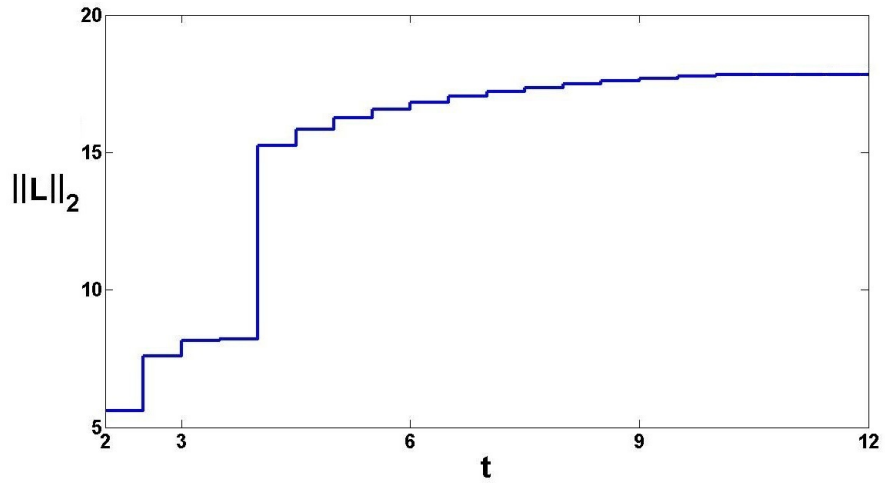
Figure 3.7: The 2-norm of the observer gains.

evolved the dominant empirical basis functions were revised to capture the process behavior. The ROM dimensionality change depends on the closed-loop process evolution and the chosen ROM design parameters, the energy fraction parameter, ξ. Figure 3.7 shows the norm of dynamic observer gain during process evolution that is computed based on the pole placement approach to predict the modes of the system. Figure 3.8 shows the profile of the updated parameters ζ_c and ζ_o based on the supervisory control such that the Lyapunov functions could satisfy the Lya-

punov stability of switching systems conditions, (3.47). Figure 3.8 shows that the CLF violated the criteria (3.47) at $t = 3.5$ and the supervisory control updated ζ_c to satisfy it. Also, it indicates the OLF did not violate the hybrid system stability criteria during the closed-loop process evolution.
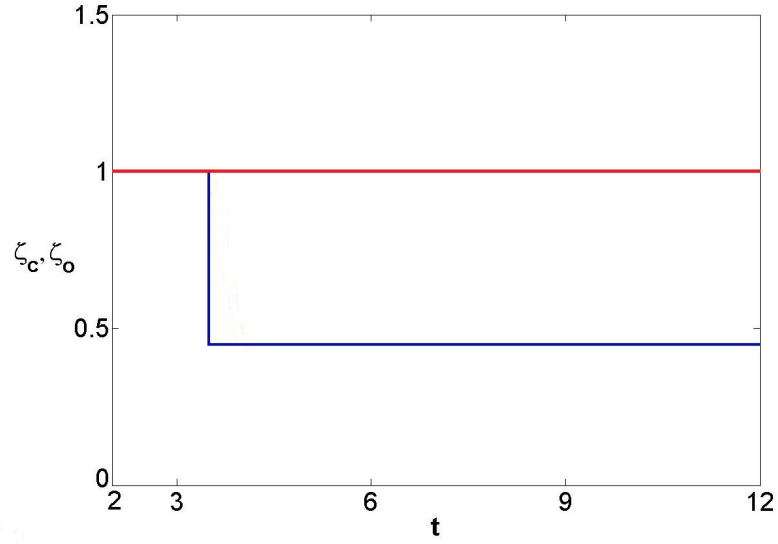
Figure 3.8: Temporal profile of updated parameters ζ_c (blue line) and ζ_o (red line) based on supervisory control.

The temporal profile of the empirical basis functions and corresponding modes that have been estimated using the dynamic observer are presented in Figs. 3.9-3.10. It is observed that the APOD-derived basis functions are adapting with the system during the process evolution. Also, the modes of the system converge to zero; this illustrates the effectiveness of the proposed controller structure to stabilize the system at the desired steady state. The peaks in the first and second eigenmodes profiles indicate the ROM switching. Figure 3.11 presents the tem-
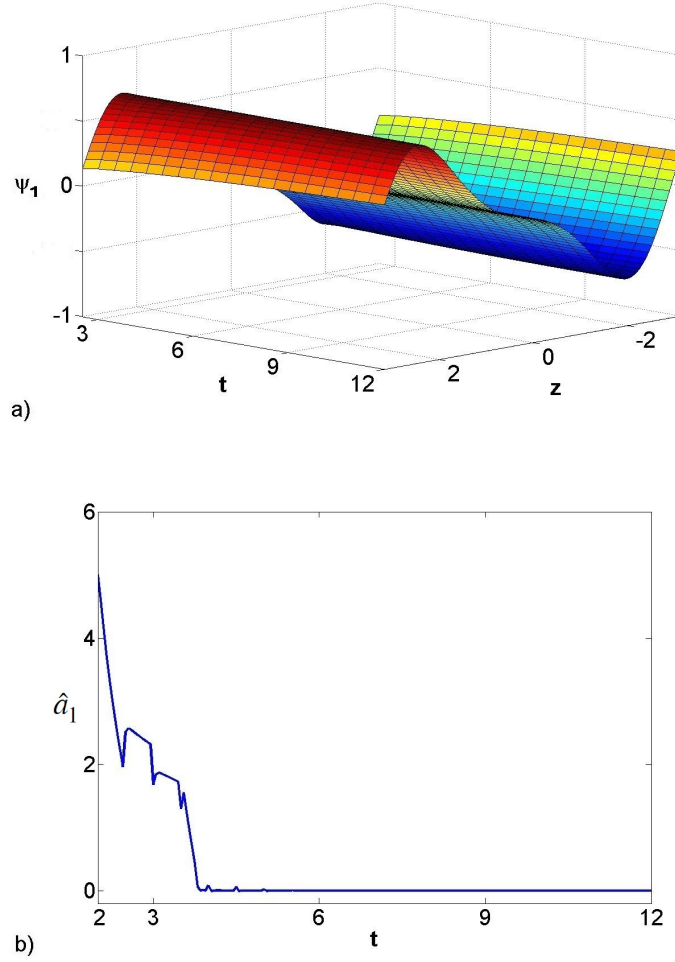
Figure 3.9: Temporal profile of (a) the first basis function and (b) First eigenmode.

poral plot of the inner product of dominant empirical basis functions and their steady state spatial profile that quantifies the changes in the set of empirical basis functions during process evolution. The third basis function is not presented due to the short time-span that it was considered. The small difference for the inner product temporal profile of the first basis function shows that there were minor changes in it. The significant difference for the second temporal profile signifies

a)

b)
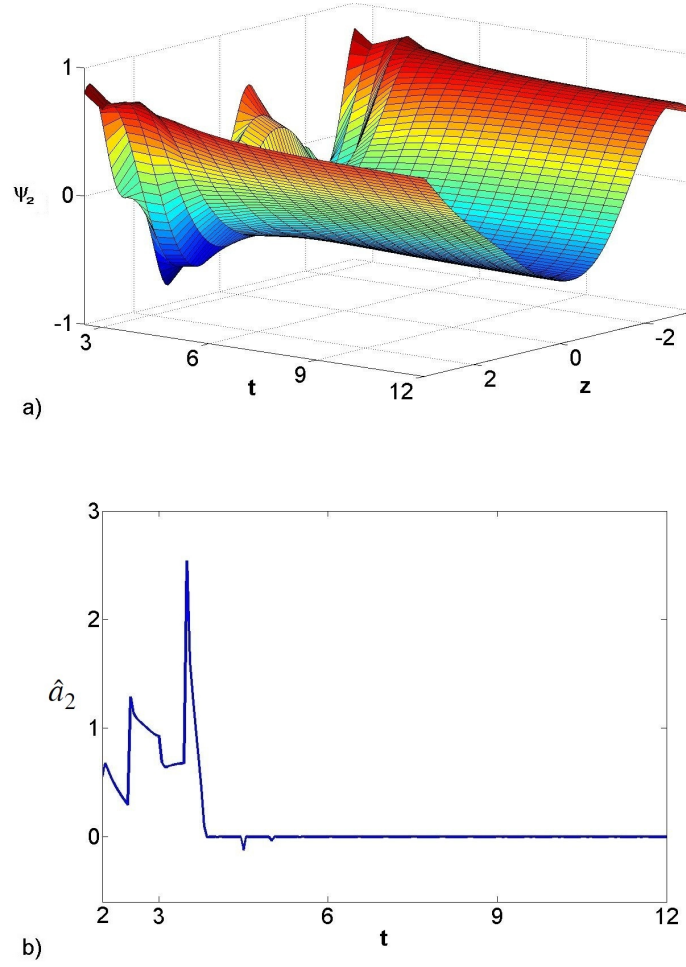
Figure 3.10: Temporal profile of (a) the second basis function and (b) Second eigenmode.

the rapid changes needed in the second dominant empirical basis function during the process evolution, instigated by the nonlinear behavior of the system and the small size of the ensemble of solutions.
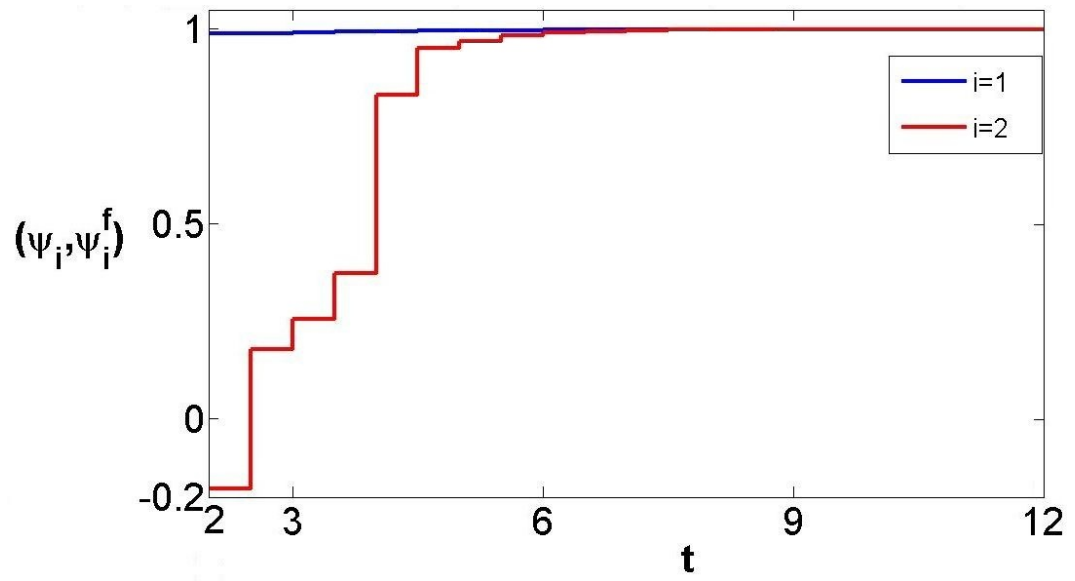
Figure 3.11: Temporal profile of the inner product of dominant empirical basis functions with respect to their final time spatial profile.

ENTROPIC APOD FOR LYAPUNOV-BASED OUTPUT FEEDBACK CONTROL OF FAST EVOLVING SYSTEMS

In this chapter, output feedback controllers are designed for fast evolving distributed parameter systems (DPSs) based on continuous point measurements available from limited number of sensors and infrequent distributed snapshots. The developed methodology for robust output feedback control is based on the successful integration of dynamic observers with static controllers. A refined ensembling ap-

proach is used in adaptive proper orthogonal decomposition (APOD) to recursively update the eigenfunctions as the closed-loop process evolves through different regions of the state space based on maximizing retained information that is received from the infrequent distributed sensor measurements. The proposed controller is illustrated on the Kuramoto-Sivashinsky equation (KSE) with and without uncertainty in the presence of highly nonlinear dynamics and chaotic behavior, where they are called to stabilize the system at an open-loop unstable system steady state. The original and the modified ensemble construction approaches for APOD are compared in different conditions and the robustness of entropic APOD with respect to uncertainty, number of snapshots and number of continuous point sensors and their locations is illustrated.

4.1   Mathematical Preliminaries

We focus on the output feedback regulation problem of spatially distributed processes described by the following state space description of highly dissipative partial differential equations (PDEs)

$$
\frac{\partial \bar{x}}{\partial t} = \mathcal{A}(z)\bar{x} + \mathcal{F}(z, \bar{x}, \frac{\partial \bar{x}}{\partial z}, ..., \frac{\partial^{n_0} \bar{x}}{\partial z^{n_0}}) + b(z)u,
$$
$$
y_m = \int_\Omega s_m(z)\bar{x} \ dz, \tag{4.1}
$$
$$
y_r = s_r(z, t)\bar{x},
$$

subject to the following boundary conditions

$$q(\bar{x}, \frac{d\bar{x}}{d\eta}, ..., \frac{d^{n_0-1}\bar{x}}{d\eta^{n_0-1}}) = 0 \quad \text{on} \quad \partial\Omega \qquad (4.2)$$

and initial condition

$$\bar{x}(z, 0) = \bar{x}_0(z). \qquad (4.3)$$

In the above PDE system, t is the time, $z \in \Omega \subset \mathbb{R}^3$ is the spatial coordinate, Ω is the domain of the process and $\partial\Omega$ is its boundary. $\bar{x}(z, t) \in \mathbb{R}^{n \times 1}$ denotes the vector of state variables. $u \in \mathbb{R}^l$ denotes the vector of manipulated inputs. $\mathcal{A}(z)$ is a linear spatial differential operator of order n_0 (where n_0 is an even number). $\mathcal{F}$ is a bounded purely nonlinear and possibly differential function of order up to n_0. $b(z) \in \mathbb{R}^{n \times l}$ is a smooth matrix function of z of the form $[b_1(z) \ b_2(z) \ ... \ b_l(z)]$, where $b_i(z)$ describes how the ith control action $u_i(t)$ is distributed in the spatial domain Ω, e.g. point actuation could be defined using Dirac delta. In (4.2), $q(\cdot)$ is a sufficiently smooth nonlinear vector function, $\frac{d\bar{x}}{d\eta}|_{\partial\Omega}$ denotes the derivative in the direction perpendicular to the boundary and $\bar{x}_0(z)$ is a smooth vector function of z. The availability of two types of measurement sensors is assumed: periodic snapshot measurements, $y_r(z) \in \mathbb{R}^n$, to measure spatial profiles and continuous measurements, $y_m \in \mathbb{R}^r$, where r is the number of continuous sensors. $s_r(z, t)$ and $s_m(z)$ are the sensor shape functions corresponding to y_r and y_m, respectively. In the remainder of the chapter we present our results for $\bar{x} \in \mathbb{R}$. It is conceptually

straightforward to extend the results to $\bar{x} \in \mathbb{R}^n$, usually by treating each state individually [243].

The control objective is to stabilize the process of (4.1)-(4.3) at a desired spatial profile, $\bar{x}_d(z)$. Without loss of generality, we assume the spatially uniform steady state $\bar{x}_d(z) = 0$ as the desired profile. We also assume that long term and dominant dynamic behavior of the system of (4.1)-(4.3) can be captured by a finite number of degrees of freedom. This implies that, in principle, the long term dynamics of state $\bar{x}$ of the mentioned system can be accurately described by a finite number of appropriately chosen basis functions.

4.2   Problem Formulation

The reduced vector representation of the PDE system of (4.1) can be obtained by applying weighted residual methods and keeping the first m ODEs and neglecting the fast and stable subsystem [76]. The type of weighted residual method could be determined by the weighting functions in the above equation. The method of weighted residuals reduces to Galerkin's method when the weighting functions and the basis functions are the same. Obtained from the basis functions, the reduced order model (ROM) can be summarized as

$$\dot{a} = \mathcal{A}a + \mathcal{F}(a) + \mathcal{B}u,$$
$$y_m = \mathcal{C}a,$$
(4.4)

where $\mathcal{A}$, $\mathcal{B}$ and $\mathcal{C}$ are constant matrices and $\mathcal{F}$ is a nonlinear smooth vector function of the modes. We assume that $\mathcal{F}$ satisfies the Lipschitz condition as follows

$$\left\|\mathcal{F}(a_1) - \mathcal{F}(a_2)\right\|_2 \leq K_l \|a_1 - a_2\|_2,$$

where K_l indicates the upper bound gain in the Lipschitz inequality.

4.2.1 Dynamic observer design

We assume that the snapshots of the process become available only periodically and the point measurements from a restricted number of sensors are continuously available which is quite common in industrial processes. In [203, 256], static output observers based on the continuous point measurements were designed to estimate the system modes that are required for controller design. The number of sensors had to be supernumerary to the number of modes to successfully estimate the system modes using the linear static observers. This implies that numerous measurement sensors are required, otherwise the static observer gives erroneous estimates. Also the static observer existence depends on the location and shape of the measurement sensors. To overcome these issues, we employed a dynamic observer that conceptually needs only one point measurement to predict the dynamic behavior of the modes as long as the process is observable at that position [84].

We can define the observation error based on the Sobolev subspace representa-

tion of the system of (4.1) as follows

$$\varepsilon(z,t) = \hat{\bar{x}}(z,t) - \bar{x}(z,t), \qquad (4.5)$$

where $\hat{\bar{x}}$ and $\bar{x}$ are the observer and system states of (4.1)-(4.3), respectively.

By neglecting the fast and stable part of the process system dynamic behavior and using separation of variables, we can define the observer state

$$\hat{\bar{x}}(z,t) = \Psi^T(z)\hat{a}(t), \qquad (4.6)$$

and the original state

$$\bar{x}(z,t) = \Phi^T(z)a(t), \qquad (4.7)$$

where $\Psi = [\psi_1 \ \psi_2 \ \ldots \ \psi_m]^T$, $\Phi = [\phi_1 \ \phi_2 \ \ldots \ \phi_s]^T$; m is the number of empirical eigenfunctions of the slow subsystems that are computed using APOD and s is the number of real eigenfunctions of the slow subsystem.

The dimension of the system slow modes, a and $\hat{a}$ in equations (4.6) and (4.7), respectively is not necessarily the same because the number of identified slow subsystem basis functions Φ and Ψ may be different; so the observation error can not be defined directly by the simple subtraction, $\hat{a} - a$.

From (4.7) we could define a mapping between two subspaces, $\mathbb{W}_s$ and $\mathbb{P}$ as follows

$$\bar{x} = \Phi^T a = \Psi^T \mathcal{M} a = \Psi^T \tilde{a}, \qquad (4.8)$$

where $\tilde{a} = \mathcal{M}a$, $\mathcal{M} : \mathbb{W}_s \mapsto \mathbb{P}$ and

$$\mathcal{M} = \int_\Omega \Psi\Phi^T \, dz. \tag{4.9}$$

Using the above transformation, the system eigenmode dynamics in (4.4) can be expressed using the basis functions of subspace $\mathbb{P}$ in the following form

$$\dot{\tilde{a}} = A\tilde{a} + f(\tilde{a}) + Bu,$$
$$y_m = C\tilde{a}, \tag{4.10}$$

while the dynamic observer based on (4.10) will have the following structure

$$\dot{\hat{a}} = A\hat{a} + f(\hat{a}) + Bu + L(C\hat{a} - y_m), \tag{4.11}$$

where $\hat{a}$ is the vector of estimated modes, L is the observer gain, C is the output matrix and f is locally Lipschitz continuous. Also the observation error could be defined within subspace $\mathbb{P}$ as follows

$$\varepsilon = \hat{\bar{x}} - \bar{x} \simeq \Psi e, \tag{4.12}$$

where $e = \hat{a} - \tilde{a}$.

Assuming observability and controllability of the system (4.10), we used pole placement approaches to compute the observer gain, L, that stabilizes the system

of (4.11) in the Lyapunov sense. The observer error dynamics can be defined using (4.10) and (4.11) as follows

$$\dot{e} = (A + LC)e + [f(\hat{a}) - f(\hat{a} - e)]. \tag{4.13}$$

If the following Lyapunov function is considered

$$V = \frac{\zeta_o}{2} e^T e + \frac{\zeta_c}{2} \tilde{a}^T \tilde{a}, \tag{4.14}$$

where V_o and V_c are the observer Lyapunov function (OLF) and the control Lyapunov function (CLF), respectively and ζ_o and ζ_c are appropriately chosen positive numbers, the time derivative of Lyapunov function will be $\dot{V} = \zeta_o e^T \dot{e} + \zeta_c \tilde{a}^T \dot{\tilde{a}}$.

Considering the control objective, $\tilde{a} \to 0$ and the CLF, $V_c = \frac{\zeta}{2} \tilde{a}^T \tilde{a}$, we assume a controller can be designed that forces the time derivative of the CLF, $\tilde{a}^T \dot{\tilde{a}}$ to be negative. Then we need only establish that

$$\dot{V} = \zeta_o e^T \dot{e} = \zeta_o \left(e^T (A + LC)e + e^T [f(\hat{a}) - f(\hat{a} - e)] \right) < 0. \tag{4.15}$$

If f satisfies the Lipschitz condition as follows

$$\|f(\hat{a}) - f(\hat{a} - e)\|_2 \leqslant K_l \|e\|_2, \tag{4.16}$$

where K_l indicates the upper bound gain in the Lipschitz inequality, then

$$e^T[f(\hat{a}) - f(\hat{a} - e)] \leqslant \|e^T\|_2 \|f(\hat{a}) - f(\hat{a} - e)\|_2$$

$$\leqslant \|e^T\|_2 K_l \|e\|_2 = K_l \|e\|_2^2 = K_l e^T e. \tag{4.17}$$

Inequality (4.15) can be stated as follows using (4.17)

$$e^T(A + LC)e + e^T(K_l I)e < 0 \Rightarrow e^T(A + LC + K_l I)e < 0 \Rightarrow A + LC + K_l I < 0.$$

$$\tag{4.18}$$

The above inequality problem can be solved using pole placement for $A + K_l I + LC = A_o + LC$. The closed-loop observer error poles are the eigenvalues of $A_c = A_o + LC$, which can be arbitrarily assigned by proper selection of the observer gain matrix, L. The observer gain matrix, L, is chosen such that

$$\left| sI - (A_o + LC) \right| = p_{des}(s) \tag{4.19}$$

where I is the identity matrix and p_{des} is the characteristic polynomial of desired poles.

Proposition 4.1. *For the system of (4.10), the observation error under the observer of (4.11) is locally stable in the Lyapunov sense.*

Proof *See Appendix A.2.1 for proof of the proposition.*

Remark 4.1. *Note that $\mathcal{M} : \mathbb{W}_s \mapsto \mathbb{P}$ is an injective map because subspace $\mathbb{P}$*

contains $\mathbb{W}_s$ and a part of subspace $\mathbb{W}_f$. By construction, when $\tilde{a}_1 = \tilde{a}_2$, $\forall \tilde{a}_1, \tilde{a}_2 \in \mathbb{P}$ implies $a_1 = a_2$, $\forall a_1, a_2 \in \mathbb{W}_s$, which is necessary for observer and controller design purposes. Due to this construction, a reverse map, $\mathcal{M}^\perp : \mathbb{P} \mapsto \mathbb{W}_s$, can be in principle defined such that $\mathcal{M}^\perp \mathcal{M} : \mathbb{W}_s \mapsto \mathbb{W}_s$ is a bijective map [37].

4.2.2 Output feedback controller design

In this section, we focus on the controller structure design using Lyapunov's direct method to achieve the stabilization objective the system of (4.10) in the origin between ROM revisions.

Proposition 4.2. *Assuming separation principle for the system of (4.10), the following static output feedback control law [76, 235] can asymptotically stabilize the system of (4.10).*

$$u(t) = -k(\tilde{a}, c_o)(L_B V_c), \tag{4.20}$$

where

$$k(\tilde{a}, c_o) = \begin{pmatrix} c_o + \dfrac{L_F V_c + \sqrt{\left(L_F V_c\right)^2 + \left(\|(L_B V_c)\|\right)^4}}{\left(\|(L_B V_c)\|\right)^2}, & L_B V_c \neq 0 \\[4ex] c_o, & L_B V_c = 0 \end{pmatrix},$$

$V_c = \dfrac{\zeta_c}{2}\tilde{a}^T \tilde{a}$ is the CLF, $L_B V_c = [L_{B_1} V_c \ \ldots \ L_{B_l} V_c]^T$ is a column vector, $L_F V_c = \dfrac{\partial V_c}{\partial \tilde{a}} F$ and $L_B V_c = \dfrac{\partial V_c}{\partial \tilde{a}} B$ denote Lie derivatives.

Proof *See Appendix A.2.2 for proof of the proposition.*

Remark 4.2. *The positive parameter c_o allows a certain degree of flexibility in shaping the dynamic behavior of the closed-loop system. For example, a large value of c_o will force $\dot{V}_c$ to be more negative and therefore generate a faster transient response. Note that a positive value of c_o is not necessary for stabilization.*

Remark 4.3. *When implementing the controller of (4.20) in closed-loop process simulations, the numerical integrations could result in chattering-like behavior for the control input near origin. This problem is circumvented by adding a sufficiently small positive number η_c to $(L_{\mathcal{G}_i}V_c)^2$ in the denominator of (4.20). The addition of this parameter obviously leads to some offset in the closed-loop response. However, this offset can be made arbitrarily small by choosing a sufficiently small value for η_c. A tradeoff thus exists between the smoothness of the control action (corresponds to large η_c) and the smaller offset in the closed-loop response (corresponds to using small value for η_c).*

4.3   Supervisory control

During system evolution, the ROM may need to be updated to remain accurate. The OLF, the CLF and finally the controller in (4.20) are redesigned based on the updated ROM using APOD when new snapshots arrive during the process evolution. Consequently, we need the stability tools of hybrid systems theory to prove that the closed-loop system remains stable during the periodic updates of the ROM. For this analysis multiple Lyapunov functions (CLFs and OLFs) of the form

(4.14) are considered. Under the assumption of finite time interval between ROM updates, the multiple Lyapunov functions of (4.14) for each ROM guarantee the Lyapunov stability of switching system (Theorem 3.2 in [86]) when the following additional constrain is satisfied

$$V_c\big(\hat{a}(t_k)\big) < V_c\big(\hat{a}(t_{k-1})\big), \quad V_o\big(e(t_k)\big) < V_o\big(e(t_{k-1})\big), \tag{4.21}$$

where $k > 1$, $V_c\big(a(t_k)\big)$ and $V_o\big(e(t_k)\big)$ correspond to the value of Lyapunov function at the beginning of the interval k.

The Lyapunov functions may increase possibly during dimensionality changes of the ROM even when the offset is small. Thus, values of ζ_c and ζ_o need to be chosen appropriately using a supervisory control loop. We can then ascertain that for the chosen controller parameters the Lyapunov functions during controller redesign satisfy the conditions of switching systems stability theorem [79, 86]. In general, higher values of ζ_c lead to more aggressive control action. A possible strategy is to automatically adjust ζ_c as follows

$$\zeta_{c,t_k} = \big(\frac{\epsilon}{100}\big)\big(\frac{\hat{a}(t_{k-1})^T\hat{a}(t_{k-1})}{\hat{a}(t_k)^T\hat{a}(t_k)}\big), \tag{4.22}$$

in order to retain an aggressive controller throughout the process operation. The strategy used in the current work is to initialize ζ_c at value ζ_{in} and reevaluate it only when V_c constraint in (4.21) is violated based on the formula of (4.22)

[204]. The specific strategy leads to less aggressive behavior while guaranteeing closed-loop stability of the system. A non-aggressive representation of (4.22) can be obtained as follows

$$\zeta_{c,t_k} = min\left\{\zeta_{c,t_{k-1}}, \ (\frac{\epsilon}{100})(\frac{\hat{a}(t_{k-1})^T\hat{a}(t_{k-1})}{\hat{a}(t_k)^T\hat{a}(t_k)})\right\}. \tag{4.23}$$

The same strategy is also used for ζ_o because OLF, $V_o = \frac{\zeta_o}{2}e^T P_o e$, may also increase when the ROM dimensionality changes. The value of ζ_o needs be chosen appropriately to satisfy the conditions of switching systems stability theorem in [79]. At the time, t_i, when the periodic snapshot measurements become available, the basis functions computed using APOD locally capture the subspace $\mathbb{W}_s$ and as a result we can directly compute the system state $\tilde{a}$ and the observer error, $e = \hat{a} - \tilde{a}$, at that instant from

$$\bar{x}(z,t_i) = \sum_{k=1}^{m}\tilde{a}_k(t_i)\psi_k(z) \ \Rightarrow \ \tilde{a}_k(t_i) = \int_{\Omega}\bar{x}(z,t_i)\psi_k(z)dz, \quad k = 1,\ldots,m,$$

where $\bar{x}(z,t_i)$ is the snapshot of the system at switching time t_i. Thus, similar to the updating formula for ζ_c the following equation is used for updating ζ_o

$$\zeta_{o,t_k} = (\frac{\epsilon}{100})(\frac{e(t_{k-1})^T e(t_{k-1})}{e(t_k)^T e(t_k)}). \tag{4.24}$$

For a less aggressive policy, similarly to ζ_{c,t_k}, i.e., we may initialize ζ_o at value ζ_{in}

and reevaluate it based on the formula of (4.23) only when V_o constraint in (4.21) is violated. The non-aggressive representation of (4.24) can be obtained as follows

$$\zeta_{o,t_k} = min\left\{ \zeta_{o,t_{k-1}}, (\frac{\epsilon}{100})(\frac{e(t_{k-1})^T e(t_{k-1})}{e(t_k)^T e(t_k)}) \right\}. \tag{4.25}$$

Theorem 4.1. *Consider the nonlinear dissipative PDE system in (4.1) with Sobolev representation and its finite dimensional approximation of (4.4) with APOD obtained basis functions. We assume that*

- *the state modes of (4.1) can be partitioned into a finite number of slow and possibly unstable modes and an infinite number of stable and fast modes and there is a time scale separation between the dynamic behavior of the two subsystems,*

- *nonlinear function, $\mathcal{F}$, in (4.4) is locally Lipschitz,*

- *locally, $\mathbb{W}_s \subseteq \mathbb{P}$,*

- *the time interval between ROM updates, δt, is finite and larger than a critical value, t_b.*

Under these assumptions, the system is locally asymptotically stable under the dynamic observer design of (4.11) and the output feedback controller of (4.20) using supervisory control strategies of (4.22) and (4.24) for appropriately chosen control structure values, c_o, η, ξ, ϵ and δt.
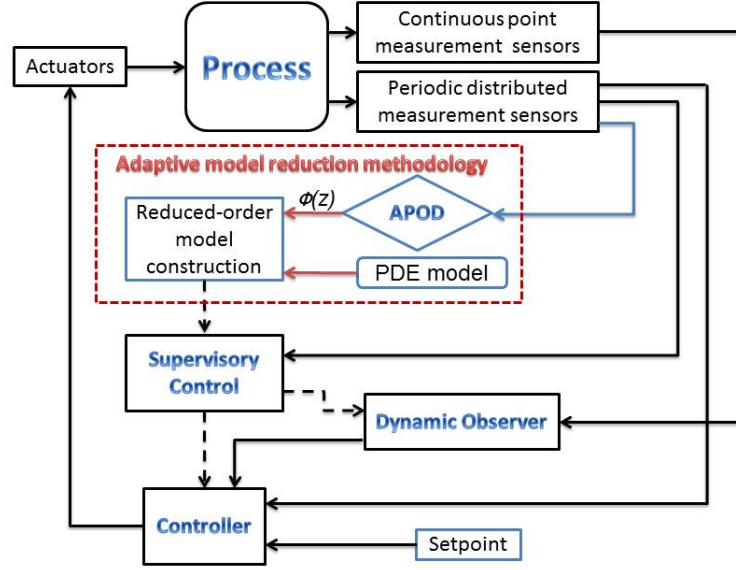
Figure 4.1: Process operation block diagram under proposed controller structure.

Proof *See Appendix A.2.3 for proof of the theorem.*

Combining the model reduction procedure with the dynamic observer and controller synthesis methods, we have obtained an output feedback controller structure that guarantees that the closed-loop system evolves to the desired steady state. In Figure 4.1 the closed-loop process is presented under the proposed control structure in a block diagram form. The specific controller structure recursively redesigns the observer/controller components whenever the ROM is revised to retain relevancy and enforce closed-loop stability.

Remark 4.4. *Note that $\tilde{a}(t_k)$ is the initial condition for the dynamic observer at the beginning of the time interval k after updating procedure of ζ_c and ζ_o. This is*

possible because we obtain process snapshots, and thus state values of the dynamic observer are initiated to be the same as the state of the system.

Remark 4.5. *In principle, the relaxation time periods for convergence of the fast dynamics can become arbitrarily small with the appropriate choice of slow subsystem dimensionality due to the properties of dissipative systems. This directly translates into appropriately choosing parameter, ξ, in APOD.*

4.4 Application

4.4.1 Problem description

In this section, the ability of entropic APOD in stabilizing the KSE is illustrated and compared to the original data ensembling approach in the absence and presence of uncertainty. The dynamic behavior of KSE with periodic boundary conditions has revealed the existence of steady and periodic wave solutions, as well as chaotic behavior [146]. The integral form of the controlled KSE that is considered is

$$\frac{\partial \bar{x}}{\partial t} = -v\frac{\partial^4 \bar{x}}{\partial z^4} - \frac{\partial^2 \bar{x}}{\partial z^2} - \bar{x}\frac{\partial \bar{x}}{\partial z} + \sum_{i=1}^{l} b_i u_i(t), \tag{4.26}$$

with periodic boundary conditions

$$\frac{\partial^j \bar{x}}{\partial z^j}(-\pi, t) = \frac{\partial^j \bar{x}}{\partial z^j}(\pi, t), \qquad j = 0, ..., 3, \tag{4.27}$$

and initial condition

$$\bar{x}(z, 0) = \bar{x}_0(z), \tag{4.28}$$

where $\bar{x}(z, t)$ is the system variable, $u(t) \in \mathbb{R}^l$ is the vector of control variables, t is the time, z is the spatial coordinate, $b(z)$ is a row vector describing the control actuators and v is the diffusion parameter. Also in the above form $\mathcal{A}(z) = -v\dfrac{\partial^4}{\partial z^4} - \dfrac{\partial^2}{\partial z^2}$ and $\mathcal{F}(\bar{x}) = -\bar{x}\dfrac{\partial \bar{x}}{\partial z}$. The Lipschitz condition for the nonlinear term in KSE, $\mathcal{F}(\bar{x})$, is discussed in Appendix A.2.4.

Six control actuators were assumed to be available at locations

$$L = [-\pi/2, -\pi/4, -\pi/6, \pi/5, \pi/4, \pi/2],$$

and the corresponding spatial distribution functions at these locations are $b_i(z) = \delta(z - L_i)$ for $i = 1, ..., 6$. The length of the spatial domain is 2π and continuous point measurement sensors placed uniformly across the domain of the process $(-\pi, \pi)$ are used. The continuous sensors shape distribution function, $s_m(z)$, for all time t, at these respective positions is $s_{m,i}(z) = \delta(z - z_i)$ for $i = 1, ..., 5$, where z_i is the location of ith sensor unless otherwise stated. Also the periodic measurement sensor distribution function is assumed to be $s_r(z, t) = 1$, i.e., the complete profiles of the state as snapshots are available in specific time instants. Note that the specific actuators affect all the modes of the system. The following spatially nonuniform initial condition was considered $\bar{x}_0 = 3\sin(z) - \cos(2z) - \sin(5z) + 2\cos(5z)$. For

both ensembling approaches, 31 snapshots of the process evolution we employed. During the initial stage of populating the ensembles the snapshot interval was $\delta t = 0.067\,s$. After that we assume the availability of snapshots of the process every $\delta t = 2$ units of time during closed loop operation.

4.4.2 Comparison tools

In this section we quantify the qualitative discussion in Chapter 2.3.2.1 and compare the original and entropic APOD. Data sets often store redundant information. In other words, new entries may not convey independent information from other data in a set. In information theory and data mining communities, entropy is a measure of the information contained in a dataset; it quantifies the relative richness of data in the set. By extension there is a direct relationship between entropy and information contained in two similar sets with equal number of data.

A way to compare the efficiency of the original and entropic APOD is through comparing their data ensembles. The ensemble entropy can provide an estimate of complexity of the spatial and temporal variations that illustrates which ensemble contains more independent profiles in their set. Shanon entropy can be defined as [62]

$$S(z) = -\sum_{i=1}^{m} p_i(z) \ln(p_i(z)), \tag{4.29}$$

where m is the number of dominant eigenvalues and p_i is defined using the following

equation

$$p_i(z) = \frac{\mu_i |\psi_i(z)|}{\sum_{j=1}^m \mu_j |\psi_j(z)|}. \tag{4.30}$$

Note that the entropy is maximal and equal to 1 if the ensemble energy captured by the dominant eigenfunctions is distributed equally through all eigenfunctions and it is minimal and equal to 0 if only a single mode is captured. Larger entropy during system evolution indicates that the corresponding ensemble contains more information; thus the corresponding ensembling approach is more efficient in retaining important information and can be used to construct ROMs with a wider range of accuracy.

Additionally, to provide a complete picture when comparing the performance of the two approaches, we define two performance indices: INC, the integral of norm of the control actions and INE, the integral of norm of the error between the real system and the model. The smaller values of INC and INE, the less control effort and more accurate model, respectively.

4.4.3   Simulation results

Figure 4.2 presents the open-loop profile and the spatial norm of the state of the KSE for $v = 0.4$, 0.23 and 0.15, respectively. We observe that KSE exhibits complex behavior for $v < 1$ and the profile $\bar{x} = 0$ is open-loop unstable. Thus, the control objective is to stabilize the system of (4.26)-(4.28) at the spatially uniform steady state $\bar{x}_d(z, t) = 0$.
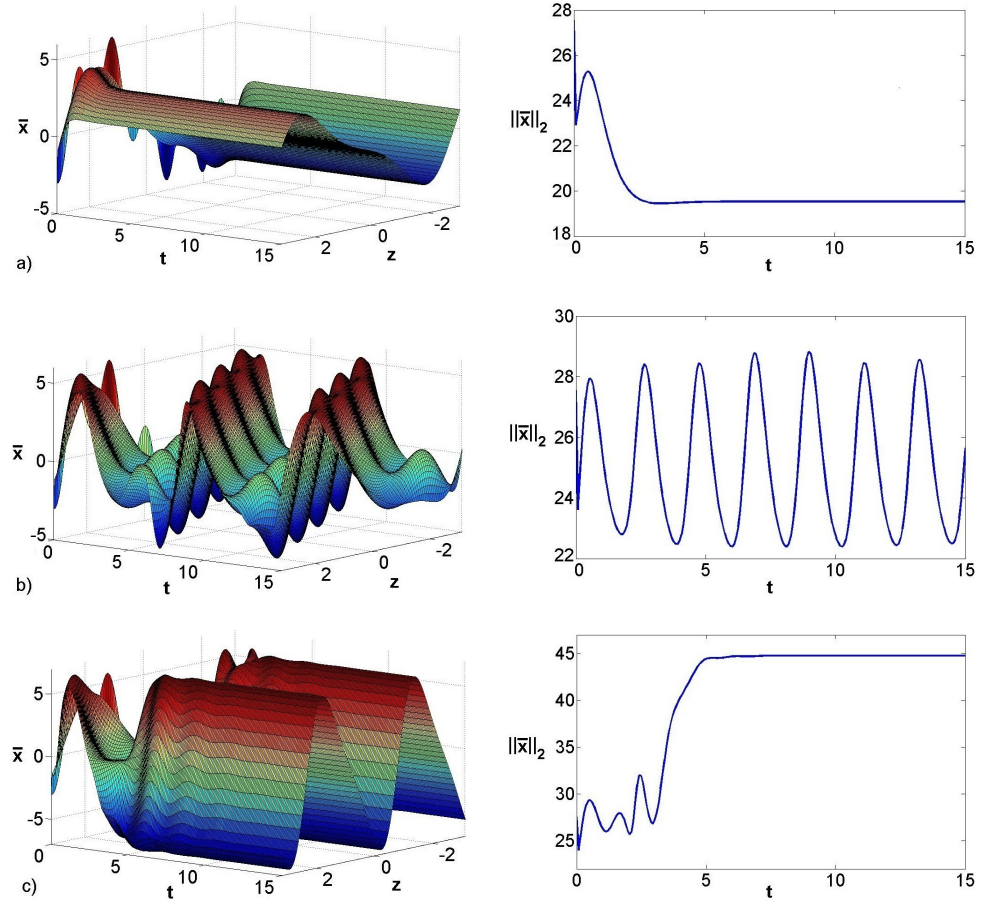
Figure 4.2: Open-loop spatiotemporal state profile (left) and norm of the state (right) for (a) $v = 0.4$, (b) $v = 0.23$ and (c) $v = 0.15$.

Figure 4.3 shows the temporal profile of norm of Shanon entropy when using the two APOD approaches to construct the ensembles. The blue and red lines present the norm of Shanon entropy using original and entropic APOD, respectively. In Figs. 4.3a and 4.3c the Shanon entropy based on original APOD decreases during open-loop system evolution and converges to zero when the system reaches steady state while the entropy based on entropic APOD increases or remains constant as old information is retained. In Figure 4.3b the Shanon entropy based on both ap-

proaches increases due to oscillatory behavior of the open-loop system that causes continuous system excitation during process evolution. These results indicates that the ensemble based on entropic APOD retains more information about the complex dynamics of KSE compared to the original one. As we will see later, this will result in a faster converging ROM to the true KSE dynamic behavior once we excite the system.

Focusing on the closed-loop system, during the initial time period $t = [0, 2]$ of populating the ensembles, the process evolved with $u(t) = 0$ (inactive controller). Application of off-line APOD to this ensemble resulted in 3 eigenfunctions for $\bar{x}$ which captured 99% of the energy embedded in the ensemble. As the availability of snapshots of the process is usually limited, we assume the availability of snapshots of the process every $\delta t = 2$ units of time during closed loop operation. The following design parameter values were used to implement the control structure on the KSE: $\eta = 0.001$, $c_o = 0.8$, $\zeta_{in} = 2$, where ζ_{in} indicates the initial value for ζ_o and ζ_c.

Figure 4.4 presents the closed-loop process profile, number of dominant eigenfunctions and the norm of the state, respectively, for the original and the entropic APOD when the diffusivity parameter, v, changes will be from 0.4 to 0.23 at $t = 40$ and the observer and controller know about the parameter change; this is called "the case without any uncertainty". We observe that for both approaches the controllers successfully stabilize the system of (4.26)-(4.28) at $\bar{x}(z, t) = 0$ while the
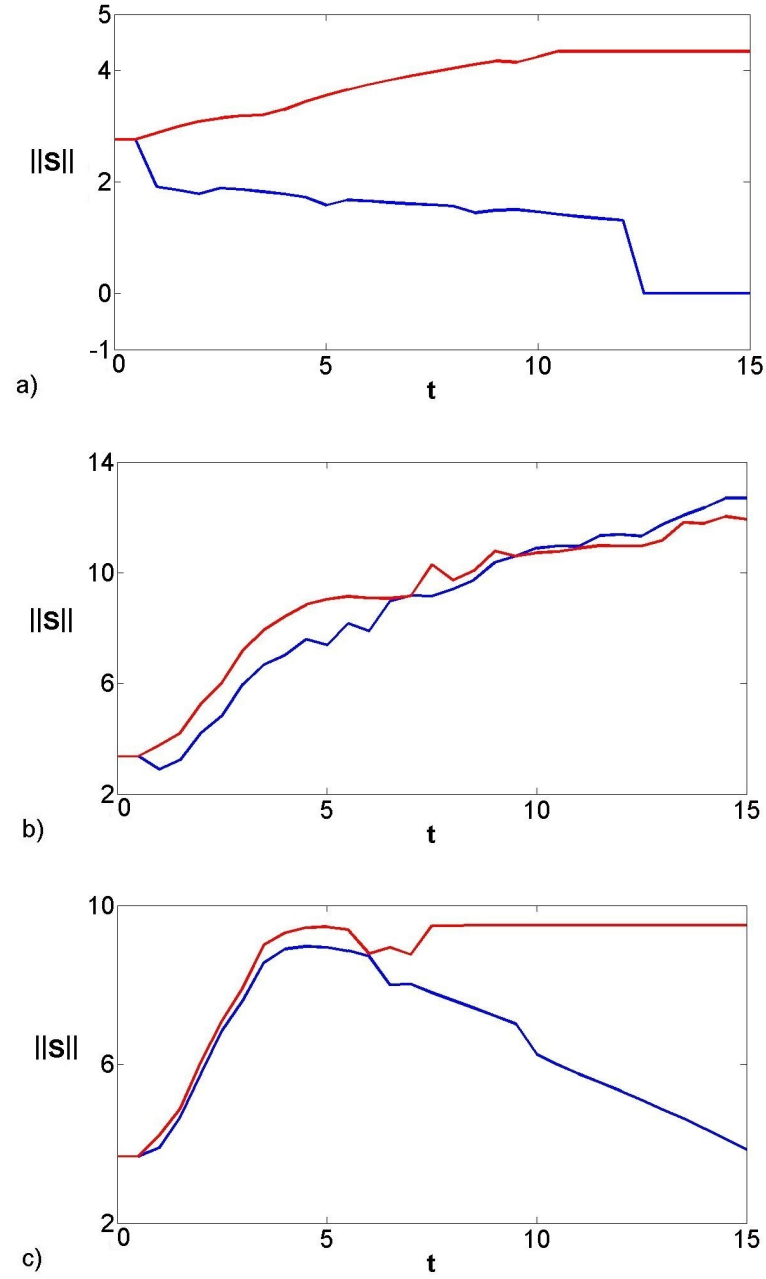
Figure 4.3: Open-loop temporal profile of norm of Shanon entropy using original APOD (blue lines) and entropic APOD (red lines) for (a) $v = 0.4$, (b) $v = 0.23$ and (c) $v = 0.15$ (note the scale differences).
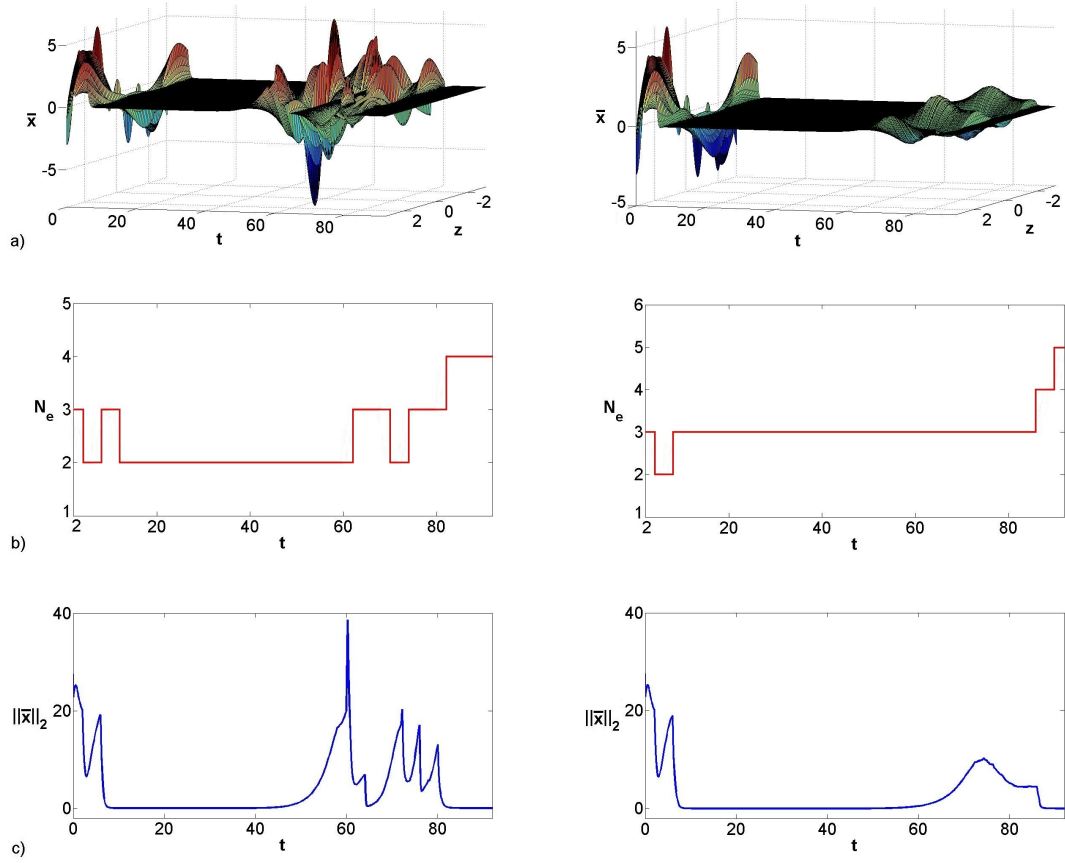
Figure 4.4: Closed-loop temporal profiles of (a) the state spatial profile (note the scale difference), (b) number of dominant eigenfunctions and (c) norm of the state when v changes from 0.4 to 0.23 at $t = 40$. The left figures present results when using original APOD and the right figures present results using entropic APOD.

state 2-norms converge smoothly to zero without any peaking. In both cases the success of the designed controller in stabilizing the process at the desired profile is due to the dominant eigenspace (hence the ROM and the control law) being updated as the process traverses through different regions of the state space during closed-loop operation. The number of eigenfunctions required to capture the initial trends was three. During the closed-loop process operation, when new trends ap-

peared the dominant eigenspace dimension was updated to accurately capture the process behavior, appropriately changing the number of empirical eigenfunctions. In general, the non-smooth behavior of state 2-norm at specific times is due to fast modes' excitation and dimensionality changes. We observe that even though the change in v takes place at 40, it takes 10 seconds for the new trends to become appreciable and another 5 seconds for them to necessitate a ROM dimensionality change in order to capture all the unstable eigenmodes.

Figs. 4.5a and 4.5b show the control actions and error norms between the real system and the ROMs, respectively. Using both approaches, the control actions and the model errors converge to zero and we do not observe any chattering when the parameter of the system changes and the controller/observer pairs is cognizant of this change. We observe a relatively large control action at the beginning of closed-loop region. It indicates that the controller tries to regulate the process using initially large control action. The error 2-norm converges to zero and there is a peaking at the beginning due to a peak in control action. Note that the non-smooth behavior of control action and state 2-norm at specific times is also due to fast modes excitations caused by ROM revisions.

When v changes from 0.4 to 0.23 without any uncertainty the following indices show the improved performance of entropic approach to the original approach in APOD; $INC_{or} = 93.02$, $INC_{mod} = 34.01$, $INE_{or} = 98.63$, $INE_{mod} = 62.01$, where "or" and "mod" indicate the original and the entropic ensembling approach
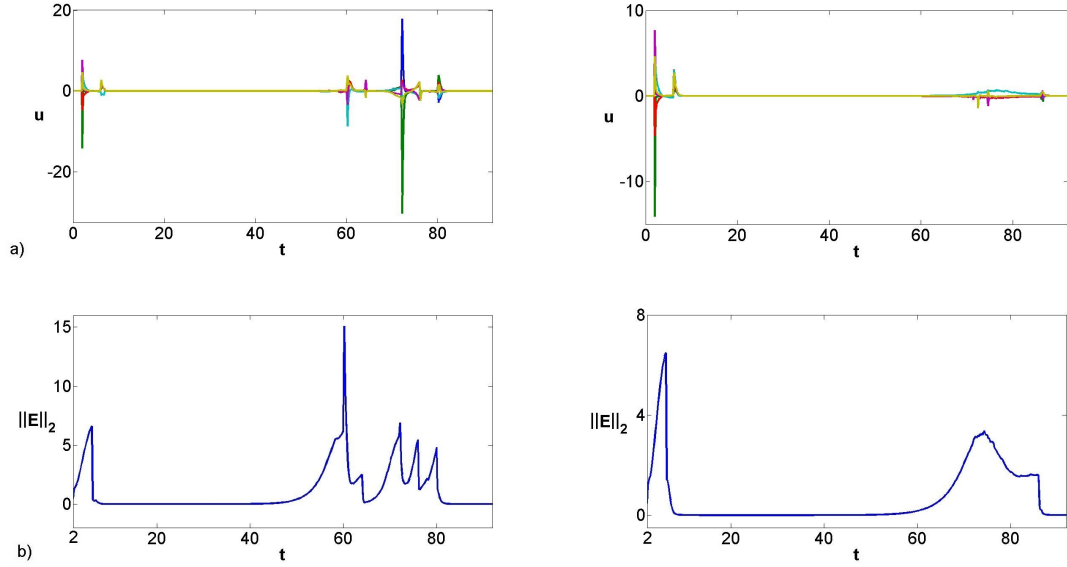
Figure 4.5: Closed-loop temporal profiles of (a) control action and (b) norm of error between the real system and the model when v changes from 0.4 to 0.23 at $t = 40$. The left figures present results when using original APOD and the right figures present results using entropic APOD (note the scale differences).

in APOD. Based on the indices we conclude entropic APOD derived more accurate ROMs and constructed a " better" controller in this case, that required less control action to stabilize the system and responded better to the perturbation.

In the presence of uncertainty the effectiveness of the entropic approach becomes more apparent. Figure 4.6 shows the closed-loop process profile, number of dominant eigenfunctions and the norm of the state, respectively, for the original and the entropic APOD when the diffusivity parameter, v, changes from 0.4 to 0.23 at $t = 40$ and the controller and the dynamic observer are not informed about the parameter change. We observe that the controllers still successfully stabilize the system of (4.26)-(4.28) at $\bar{x}(z, t) = 0$ while the 2-norms converge smoothly to
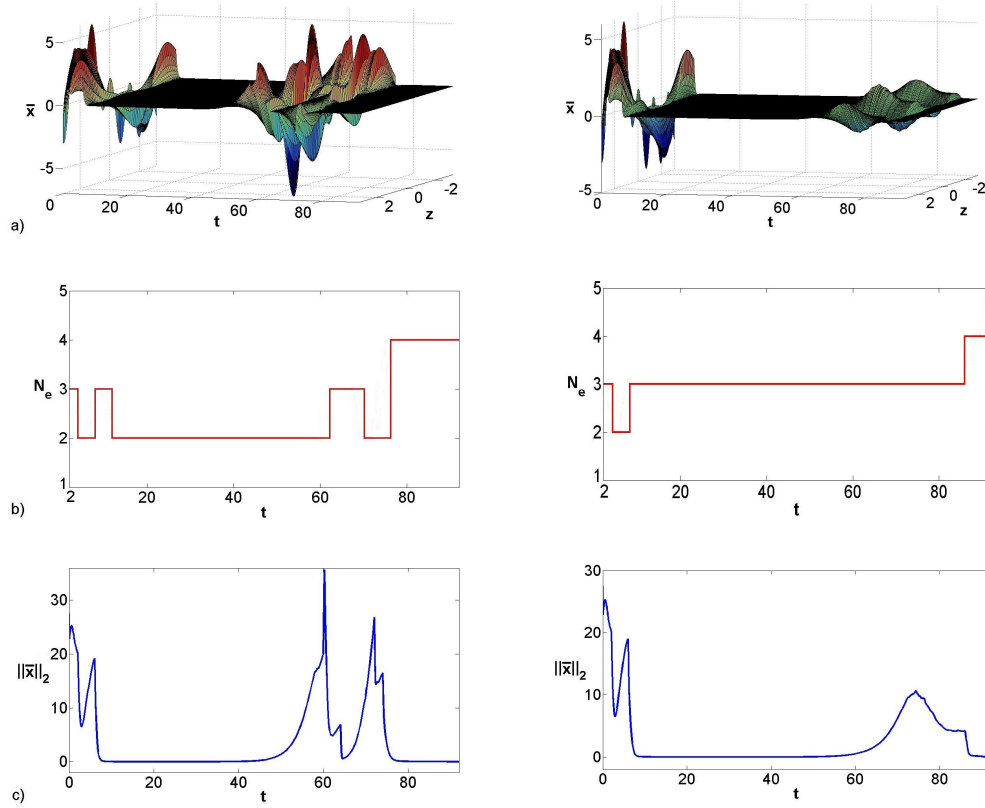
Figure 4.6: Closed-loop temporal profiles of (a) the state spatial profile, (b) number of dominant eigenfunctions and (c) norm of the state in the presence of uncertainty when v changes from 0.4 to 0.23 at $t = 40$. The left figures present results when using original APOD and the right figures present results using entropic APOD (note the scale differences).

zero without any peaking.

Figure 4.7 shows the control actions and the norms of error between the real system and the ROMs. Using both approaches, the control actions and the model errors converge to zero and we do not observer any chattering before the parameter of the system changes. The following indexes indicate that the entropic APOD has better performance compared to the original approach; $INC_{or} = 95.77$, $INC_{mod} = 32.66$, $INE_{or} = 90.73$, $INE_{mod} = 62.30$.
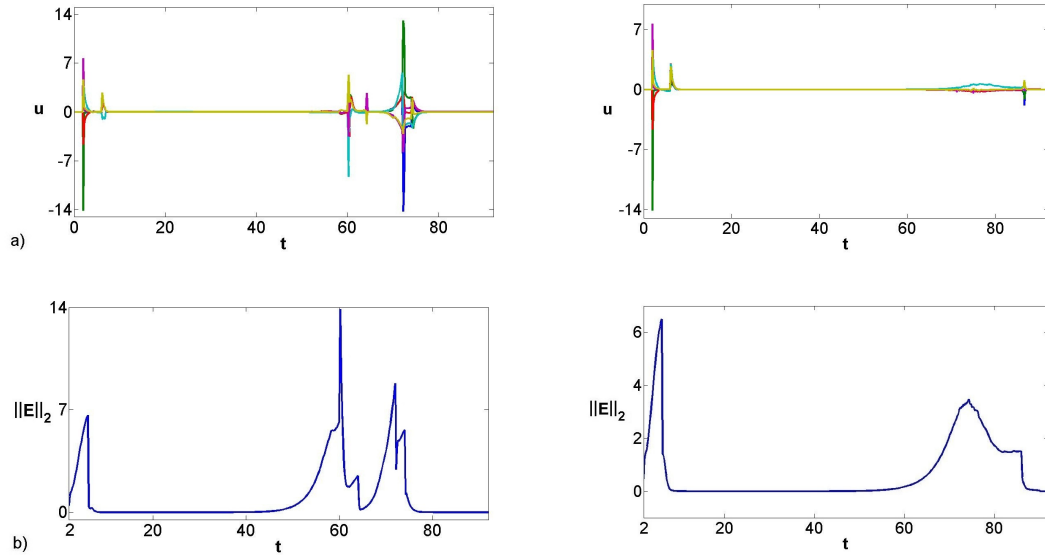
Figure 4.7: Closed-loop temporal profiles of (a) control action and (b) norm of error between the real system and the model in the presence of uncertainty when v changes from 0.4 to 0.23 at $t = 40$. The left figures present results when using original APOD and the right figures present results using entropic APOD (note the scale differences).

Note that the control action using entropic APOD is smoother than the control action using original APOD when the system changes in the absence and presence of uncertainty due to the faster ROM revisions in response to the changed system dynamics. Having less discontinuities in control action leads to less system excitation and reduces the observer/controller computation load. Large peaking or discontinuities in control action causes fast modes excitation. In response the basis functions change and the observer and controller need more revisions which increases the observer/controller computation load.

Figure 4.8 shows the temporal profile of the norm of Shanon entropy in the presence of uncertainty. It presents the information content measurement of the
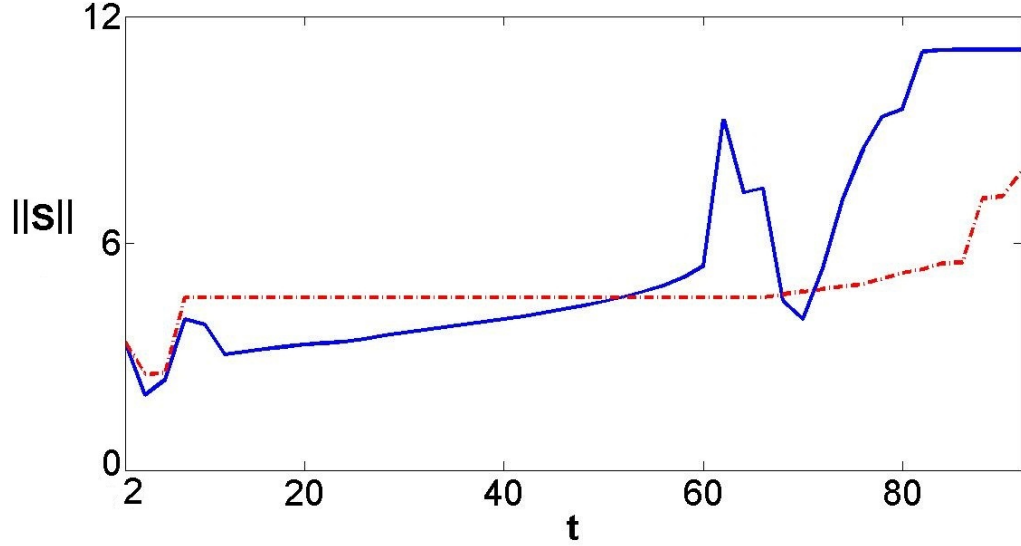
Figure 4.8: Closed-loop temporal profiles of Shanon entropy norm using original APOD (blue line) and entropic APOD (red dashed line) in the presence of uncertainty, when v changes from 0.4 to 0.23 at $t = 40$.

ensembles. During the time period before the change in the system parameter, the system entropy using entropic APOD is more than the system entropy using original APOD that leads to construct more accurate ROM due to retaining the complex trends in the ensemble. When the system changes, the controller based on entropic APOD adapted to the change rejection without any sharp control action due to more accurate ROM. However, the controller based on original APOD further excites the system with its sharp action and causes complex trends to resurface, which in turn increase the system entropy at time $t = 50$.

Figure 4.9 presents the case when the diffusivity parameter, v, changes from 0.4 to 0.15 at $t = 25$ unbeknownst to the control structure. The process dynamics then become very fast making the time interval between snapshots too large for standard
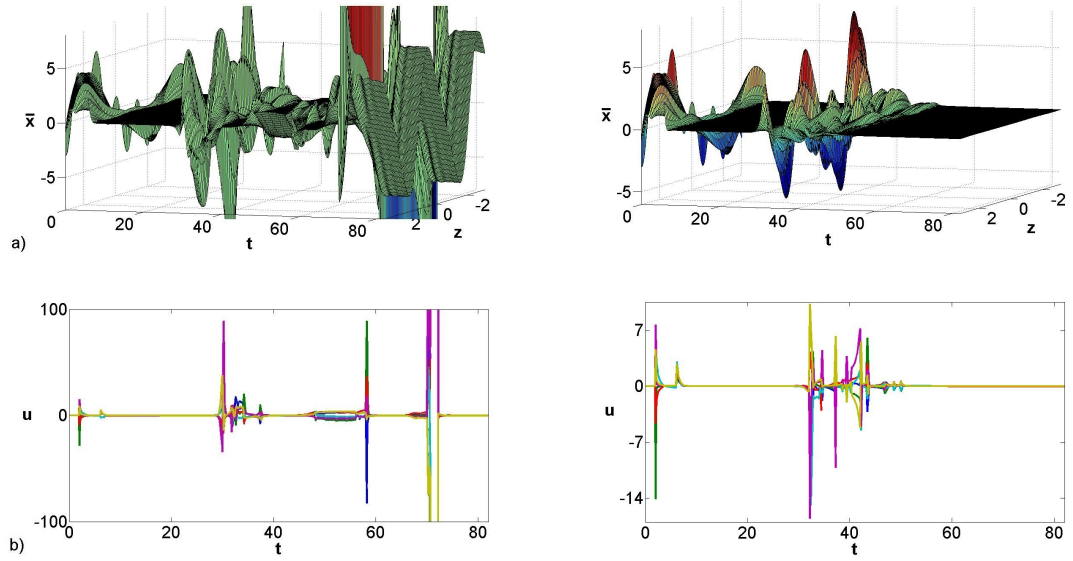
Figure 4.9: Closed-loop temporal profiles of (a) the state spatial profile and (b) control actions in the presence of uncertainty when v changes from 0.4 to 0.15 at $t = 25$. The left figures present results when using original APOD and the right figures present results using entropic APOD.

APOD. The original APOD not only could not regulate the process but it further destabilized the system while the refined approach could still stabilize the closed-loop process at the desired steady state profile using reasonable control action. There is because the controllers based on entropic APOD successfully stabilized the process since the ROM revisions were able to account for the changed dynamics faster.

In the APOD-based control of DPSs using static observers that addressed in [203, 204, 256], the number of available point measurements should be equal to or greater than the dimension of ROM. One of the important advantages of using dynamic observers in this case is using less continuous point measurement sensors.

Obviously, we want to use the minimum number of sensors to reduce costs even only one sensor when able to. The dynamic observer based on original APOD then becomes sensitive to the location and shape of the measurement sensor requiring sensor placement strategies. This limitation can be circumvented using entropic APOD to construct observers that in general are more robust to the sensors locations and near unobservability, as it keeps information from previously traversed regions. Figure 4.10 presents the case when $v = 0.4$ and only one point measurement sensor is used at $-\dfrac{\pi}{2}$. The original APOD could not regulate the process due to the unobservability while the refined approach still could stabilize the closed-loop process at the desired steady state profile using reasonable control action.

Figure 4.11 presents the closed-loop temporal profiles of norm of the state for different availability of snapshots time periods, δt when using one point measurement sensor at $-\dfrac{\pi}{2}$. It shows the relation between system dynamics and sampling time; when δt increases the fluctuations in 2-norm of the state will increase due to the states unobservability. In the first four cases when $\delta t = 0.25$, $\delta t = 0.5$, $\delta t = 1$ and $\delta t = 2$ the observer/controller can stabilize the system but in the final case, $\delta t = 4$, the state 2-norm remains bounded but it does not converge to zero since the model uncertainty is larger than the threshold set during the initial controller design step.

Another important advantage of entropic APOD is its robustness with respect
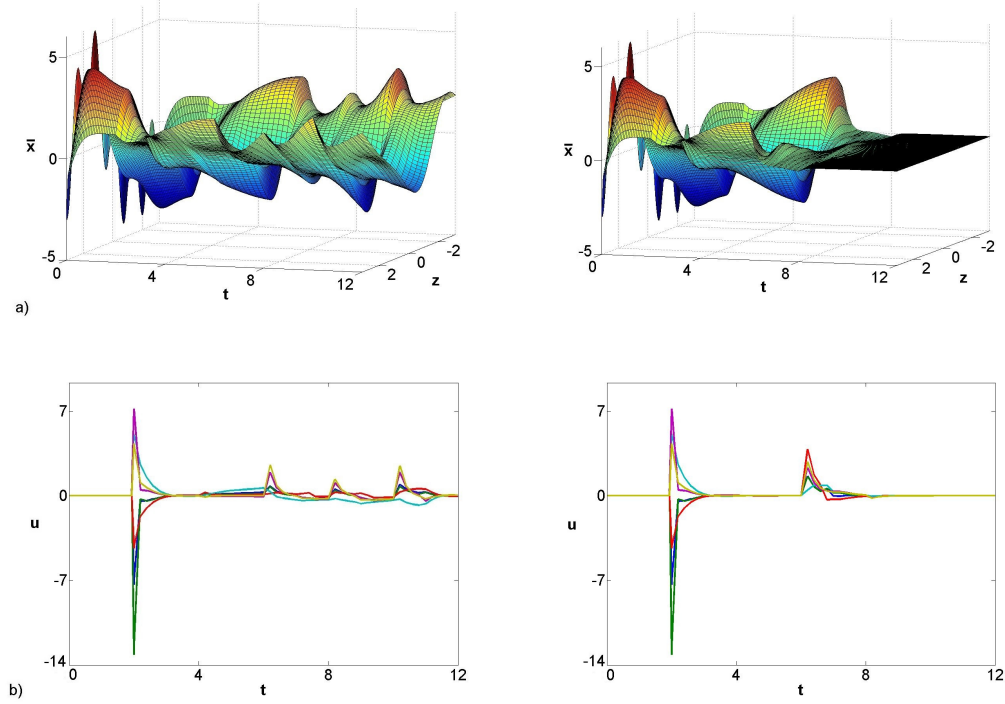
Figure 4.10: Closed-loop temporal profiles of (a) the state spatial profile and (b) control action using one point measurement sensor at $-\dfrac{\pi}{2}$. The left figures present results when using original APOD and the right figures present results using entropic APOD.

to ensemble size to construct accurate ROMs. When using entropic APOD a lower number of snapshots may be kept; this implies low dimensional covariance matrices will be derived that significantly improves the computational needs and memory requirements of the proposed controller/observer. This is illustrated in Figure 4.12 which presents the temporal profiles of the state and control action when $v = 0.4$; only 11 snapshots are retained during the system evolution and only one sensor is used at $-\dfrac{\pi}{2}$, greatly reducing the computational load.
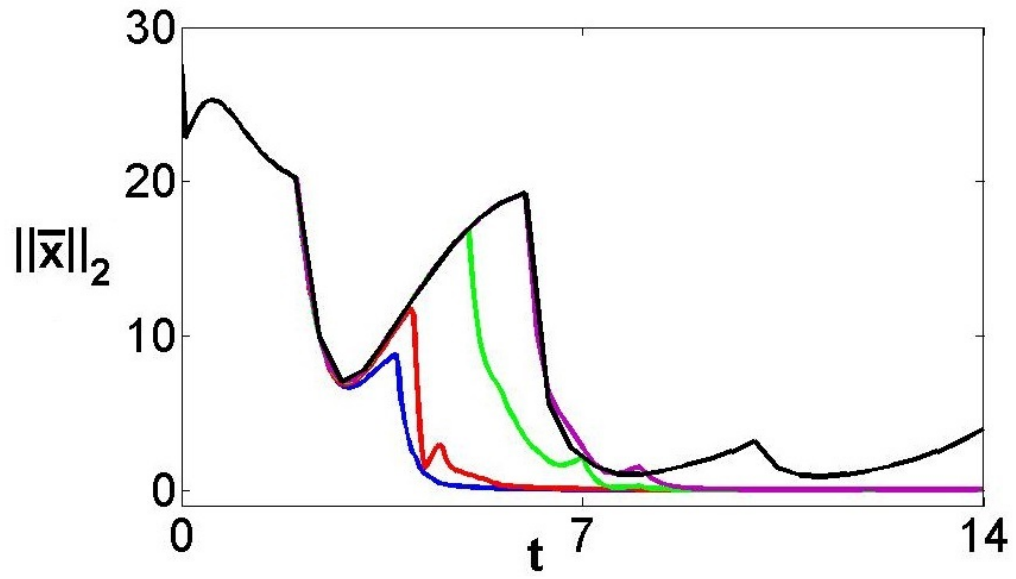
Figure 4.11: Closed-loop temporal profiles of norm of the state using one point measurement sensor at $-\dfrac{\pi}{2}$ for different availability of snapshots time periods, $\delta t = 0.25$ (blue), $\delta t = 0.5$ (red), $\delta t = 1$ (green), $\delta t = 2$ (pink), $\delta t = 4$ (black), under entropic APOD.
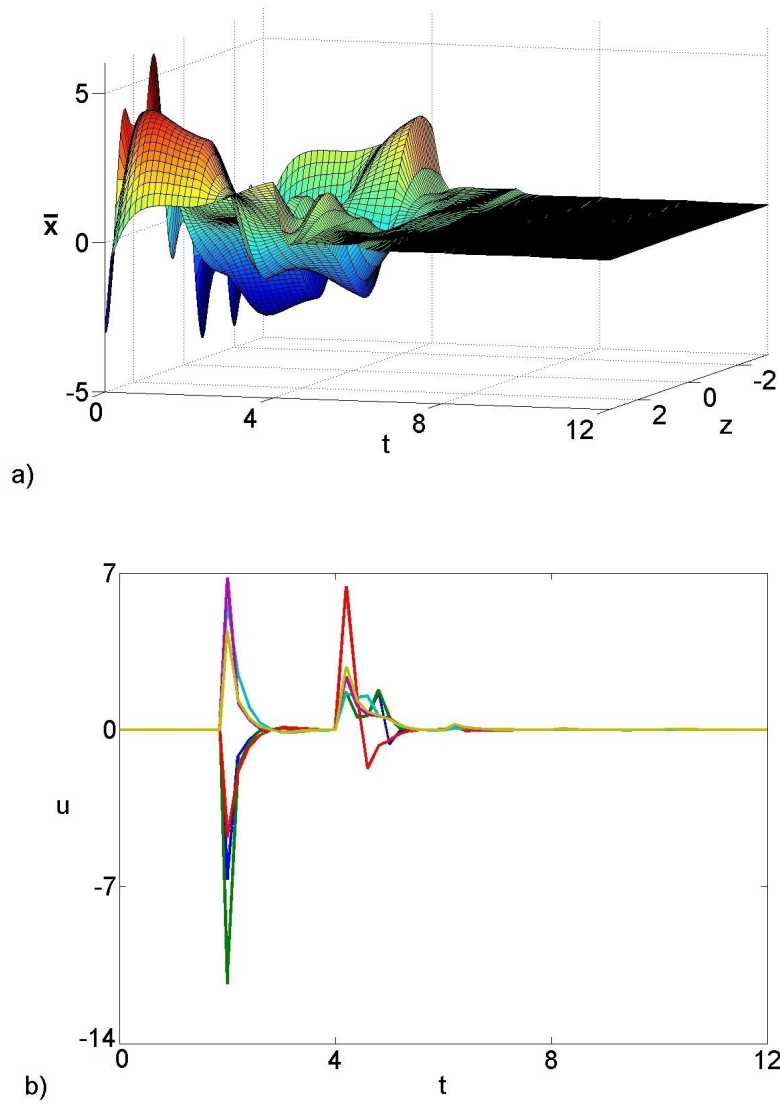
Figure 4.12: Closed-loop temporal profiles of (a) the state spatial profile and (b) control actions using an ensemble of 11 snapshots in entropic APOD and a sensor at $-\frac{\pi}{2}$.

GEOMETRIC OUTPUT FEEDBACK CONTROLLER FOR OUTPUT TRACKING

In this chapter, an adaptive proper orthogonal decomposition (APOD) based geometric output feedback control structure is synthesized for output tracking of nonlinear distributed parameter systems (DPSs) based on continuous point measurements available from limited number of sensors. The control structure is a combination of a nonlinear Luenberger-like geometric dynamic observer and a globally linearizing controller (GLC). The specific structure is employed to compensate model uncertainty due to model reduction procedure. The proposed control struc-

ture is successfully illustrated on a catalytic reactor. The controller considers the

thermal dynamics of the reactor, reduces the hot spot temperature and manages

the thermal energy distribution across the reactor length during process operation.

5.1 Preliminaries

5.1.1 Class of nonlinear dissipative PDE system

In this work, a class of nonlinear dissipative, input-affine partial differential equation (PDE) systems is considered with a state space representation of the following form

$$\frac{\partial}{\partial t}\bar{x}(z,t) = \mathcal{A}(z)\bar{x}(z,t) + \mathcal{F}(z,\bar{x}) + b(z)u(t),$$

$$y_c(t) = \int_{\Omega} c(z)\bar{x}(z,t) \ dz,$$

$$y_m(t) = \int_{\Omega} s(z)\bar{x}(z,t) \ dz, \tag{5.1}$$

$$y_r(z,k) = \int_0^t \delta(t - t_k)\bar{x}(z,t) \ dt,$$

subject to boundary conditions

$$q(\bar{x}, \frac{\partial \bar{x}}{\partial z}, ..., \frac{\partial^{n_0-1}\bar{x}}{\partial z^{n_0-1}}) = 0 \ \ \text{on} \ \ \partial\Omega, \tag{5.2}$$

and initial condition

$$\bar{x}(z,0) = \bar{x}_0(z), \tag{5.3}$$

where $\bar{x}(z,t) \in \mathbb{R}$ denotes the vector of state variables and $u(t) \in \mathbb{R}^l$ is the vector of manipulated inputs. t is the time, $z \in \Omega \subset \mathbb{R}^3$ denotes the spatial coordinate and Ω is the process domain with boundary, $\partial\Omega$. $\mathcal{A}(z)$ and $\mathcal{F}(z,\bar{x})$ are linear and bounded Lipschitz nonlinear parts of spatial differential operator of order n_0, respectively. $b^T(z) \in \mathbb{R}^l$ is a smooth vector function of z that describes how the control action is distributed in the spatial domain, e.g. point actuation is defined using standard Dirac delta. $q(\cdot)$ is a sufficiently smooth nonlinear vector function, $\frac{\partial^i \bar{x}}{\partial z^i}|_{\partial\Omega}$ for $i = 1, \ldots, n_0 - 1$, denotes the spatial derivatives in the direction perpendicular to the boundary and $\bar{x}_0(z)$ is a smooth vector function of z. $y_c \in \mathbb{R}^v$ is the vector of controlled outputs where v is the number of desired outputs. $c(z)$ is a known vector function of z which is determined by the desired performance specifications in the process domain, Ω. We assume that two types of measurement sensors are available during process evolution: periodic distributed snapshot measurements, $y_r(z,k) \in \mathbb{R}$, and continuous measurements, $y_m \in \mathbb{R}^w$, where w is the number of continuous sensors and k is a discrete variable that indicates the sample time counter to taking the snapshots. Note that y_r indicates measured spatial profiles while y_m is a vector variable. $s(z)$ is the sensor shape functions corresponding to y_m and t_k is the time instance for snapshot measurement. In this chapter, the results are presented for $\bar{x} \in \mathbb{R}$, however, it is straightforward to extend them for $\bar{x} \in \mathbb{R}^n$, by treating each state independently [228]. Once each state has been reduced, the interactions between distributed system states can be easily captured

through the inner products of the modal expansions.

5.1.2 Infinite-dimensional representation in Sobolev subspace

To address the control and observation problem we represent the PDE system of (5.1)-(5.3) as an infinite-dimensional system in a relevant Sobolev space

$$\mathbf{W}^{(n_0-1),2}(\Omega, \mathbb{R})$$

where for every $1 \leqslant j < \infty$, $i \in \mathbb{N}$ and $i \geqslant 1$,

$$\mathbf{W}^{i,j} = \{\bar{x} \in L^j(\Omega): \quad \partial^\alpha \bar{x} \in L^j(\Omega), \forall \alpha \in \mathbb{N}, |\alpha| \leqslant i\}.$$

Sobolev spaces are functional spaces that consider functions for which all the distributional derivatives and most of the differential rules can be applied. When distributional derivatives in such spaces belong to the space of square integrable functions, $L_2(\Omega)$, then we also define the inner product and norm in $L_2(\Omega)$ as

$$(\vartheta_1, \vartheta_2) = \int_\Omega r(z)\vartheta_1^T(z)\vartheta_2(z)dz, \quad \|\vartheta_1\|_2 = (\vartheta_1, \vartheta_1)^{1/2}$$

where ϑ^T denotes the transpose and $r(z)$ is the weight function that is assumed to

be equal to 1 in this work. We define the state x on $\mathbb{W}^{(n_0-1),2}(\Omega, \mathbb{R})$ as

$$x(t) = \bar{x}(z, t), \tag{5.4}$$

the differential operators

$$\mathbf{A}x = \mathcal{A}(z)\bar{x}, \quad \mathbf{F}(x) = \mathcal{F}(z, \bar{x}), \tag{5.5}$$

and the manipulating input, measured and controlled output operators as

$$\mathbf{B}u = b(z)u, \ C_c x = \int_\Omega c(z)\bar{x} \, dz, \ S_m x = \int_\Omega s(z)\bar{x} \, dz, \ Rx = \int_0^t \delta(t - t_k)\bar{x} \, dt,$$

where $\mathbb{W}^{(n_0-1),2}(\Omega, \mathbb{R})$ is a Sobolev subspace that satisfies the homogeneous bound-ary conditions of (5.2), i.e.,

$$\mathbb{W}^{(n_0-1),2}(\Omega, \mathbb{R}) = \left\{ f \in \mathbf{W}^{(n_0-1),2}(\Omega, \mathbb{R}) : \ q(f, \frac{\partial f}{\partial z}, ..., \frac{\partial^{n_0-1} f}{\partial z^{n_0-1}}) = 0 \ \text{ on } \ \partial\Omega \right\}.$$

Then the PDE system of (5.1) can be expressed in the following form in the Sobolev subspace

$$\dot{x} = \mathbf{A}x + \mathbf{F}(x) + \mathbf{B}u,$$

$$y_c = C_c x,$$

$$y_m = S_m x, \tag{5.6}$$

$$y_r = Rx,$$

with the initial condition

$$x(0) = x_0, \qquad\qquad (5.7)$$

where y_c, y_m and y_r are representations of the vector of control outputs, the vector of continuous measurements and periodic distributed snapshot measurements in the defined Sobolev subspace, respectively. Considering locally Lipschitz assumption of $\mathcal{F}$, we obtain that $\mathbf{F}$ is a nonlinear smooth vector function that is locally Lipschitz and satisfies $\mathbf{F}(0) = 0$. Note that to simplify the notation we use $\mathbb{W}$ instead of $\mathbb{W}^{(n_0-1),2}(\Omega, \mathbb{R})$ for the rest of the chapter.

Dissipative systems naturally enjoy a property that the model dynamics can be separated in appropriate Sobolev subspaces. This property is formally stated by following assumption.

Assumption 5.1. *The infinite-dimensional modal representation of the system of (5.1)-(5.3) with respect to an appropriate basis of the functional subspace, $\mathbb{W}$, can be decomposed to a finite-dimensional slow and possibly unstable modal subsystem and an infinite-dimensional stable and fast modal subsystem and there is a time scale separation between the dynamic behavior of the two subsystems.*

The set of basis functions for the functional subspace of $\mathbb{W}$ can be identified through the solution of the eigenvalue problem for the operator $\mathbf{A}$, defined as follows

$$\mathbf{A}\phi_i = \lambda_i\phi_i, \quad i = 1, \ldots, \infty \qquad\qquad (5.8)$$

subject to

$$q(\phi_i, \frac{d\phi_i}{dz}, ..., \frac{d^{n_0-1}\phi_i}{dz^{n_0-1}}) = 0 \quad \text{on} \quad \partial\Omega, \tag{5.9}$$

where λ_i and ϕ_i denote the ith eigenvalue and the corresponding basis function, respectively.

Based on Assumption 5.1, the ordered eigenspectrum of $\mathbf{A}$, $\{\lambda_1, \lambda_2, \dots\}$ can be partitioned into a finite-dimensional set of p slow eigenvalues, $\{\lambda_1, \lambda_2, \dots, \lambda_p\}$, and a stable infinite-dimensional complement set of the remaining fast eigenvalues $\{\lambda_{p+1}, \lambda_{p+2}, \dots\}$. There is a large separation between the slow and fast eigenvalues of $\mathbf{A}$. The associated eigenfunctions are defined as $\Phi_s = [\phi_1 \ \phi_2 \ \cdots \phi_p]^T$, $\Phi_f = [\phi_{p+1} \ \phi_{p+2} \ \cdots]^T$.

Subsequently, the Sobolev subspace, $\mathbb{W}$, can be partitioned into two subspaces, one that includes a finite number of slow and possibly unstable modes, $\mathbb{W}_s \triangleq span\{\phi_i\}_{i=1}^p$, and a complement subspace that includes an infinite number of fast and stable modes, $\mathbb{W}_f \triangleq span\{\phi_i\}_{i=p+1}^\infty$. By defining the following orthogonal integral projection operators, the state of system (5.6) can be described as

$$x = x_s + x_f = \mathcal{P}x + \mathcal{Q}x, \tag{5.10}$$

where $x_s = \mathcal{P}x \in \mathbb{W}_s$, $x_f = \mathcal{Q}x \in \mathbb{W}_f$ and $\mathbb{W} = \mathbb{W}_s \oplus \mathbb{W}_f$. The orthogonal integral projection operators are defined as $\mathcal{P} : \mathbb{W} \to \mathbb{W}_s$, $\mathcal{P} = (\cdot, \Phi_s)$ and $\mathcal{Q} : \mathbb{W} \to \mathbb{W}_f$, $\mathcal{Q} = (\cdot, \Phi_f)$.

Using (5.10), the set of basis functions of (5.8) and the method of weighted residuals, the system and the controlled and measurement outputs of (5.6) can be expressed as a partitioned ODE set of vectorized modes in the following form

$$
\begin{aligned}
\dot{x}_s &= A_s x_s + F_s(x_s, x_f) + B_s u, \\
\dot{x}_f &= A_f x_f + F_f(x_s, x_f) + B_f u, \\
y_c &= C_c x_s + C_c x_f, \\
y_m &= S_m x_s + S_m x_f,
\end{aligned}
\tag{5.11}
$$

where $A_s = \mathcal{P}\mathcal{A}$, $A_f = \mathcal{Q}\mathcal{A}$, $F_s = \mathcal{P}\mathbf{F}$, $F_f = \mathcal{Q}\mathbf{F}$, $B_s = \mathcal{P}\mathbf{B}$ and $B_f = \mathcal{Q}\mathbf{B}$. Note that in above modal expansions, $A_s = diag\{\lambda_i\}_{i=1}^{p}$ and $A_f = diag\{\lambda_i\}_{i=p+1}^{\infty}$ are diagonal matrices in principle. There is a time scale separation between the dynamic behavior of the two subsystems. Also there is an order of magnitude difference between $Re(\lambda_1)$ and $Re(\lambda_{p+1})$. The initial condition (5.7) becomes

$$
\begin{aligned}
x_s(0) &= \mathcal{P}x(0) = \mathcal{P}x_0, \\
x_f(0) &= \mathcal{Q}x(0) = \mathcal{Q}x_0.
\end{aligned}
\tag{5.12}
$$

Remark 5.1. *The eigenvalue problem of (5.8)-(5.9) can be solved analytically for neither general nonlinear PDEs nor systems with irregular domains. Then, most of the standard analytical model reduction techniques can not be used for these general nonlinear DPSs. Statistical techniques can be used to circumvent this limitation.*

5.2 Model reduction using method of weighted residuals

The finite-dimensional approximation of the infinite-dimensional representation of (5.1)-(5.3) can be computed using the method of weighted residuals when the set of empirical basis functions are available. Generally, the original state of the PDE system, $\bar{x}(z,t)$, can be described as an infinite weighted summation of a complete vectorized set of basis functions $\Psi(z)$ as follows

$$\bar{x}(z,t) \simeq \sum_{k=1}^{r_m} \psi_k(z)a_k(t) \overset{r_m\to\infty}{\Longrightarrow} \bar{x}(z,t) = \sum_{k=1}^{\infty} \psi_k(z)a_k(t) \tag{5.13}$$

where $a_k(t)$ for $k = 1, \cdots, r_m$ are time varying coefficients known as system modes. The following $r_m{}^{th}$ order system of ODEs is obtained by substituting (5.13) in (5.1)-(5.3), multiplying the PDE with the weighting functions, $\varphi(z)$, and integrating over the entire spatial domain:

$$\sum_{k=1}^{r_m} (\varphi_v(z), \psi_k(z))\dot{a}_k(t) = \sum_{k=1}^{r_m} (\varphi_v(z), \mathcal{A}(z)\psi_k(z))a_k(t)$$
$$+ \left(\varphi_v(z), \mathcal{F}(z, \sum_{k=1}^{r_m} \psi_k(z)a_k(t))\right) + (\varphi_v(z), b(z))u,$$
$$v = 1, ..., r_m, \tag{5.14}$$
$$y_c = \sum_{k=1}^{r_m} (c(z), \psi_k(z))a_k(t),$$
$$y_m = \sum_{k=1}^{r_m} (s(z), \psi_k(z))a_k(t).$$

The type of weighted residual method can be determined by the weighting functions in the above equation. The method reduces to Galerkin projection when the weighting functions, $\varphi(z)$, and the basis functions, $\Psi(z)$, are the same. Then (5.14) can be summarized as

$$\dot{a} = Aa + f(a) + Bu,$$
$$y_c = Ca, \tag{5.15}$$
$$y_m = Sa,$$

where $A^{r_m \times r_m}$, $B^{r_m \times l}$, $C^{v \times r_m}$ and $S^{w \times r_m}$ are constant matrices and f is a nonlinear smooth vector function of the modes that can be described based on the comparison between (5.14) and (5.15). From Lipschitz condition of $\mathcal{F}$, we obtain that f satisfies local Lipschitz condition. Note that this assumption can be concluded from the local Lipschitz property of the nonlinear part of the original system of (5.6) in the Sobolev subspace for special cases.

Assumption 5.2. *The PDE system of (5.1)-(5.3) and as a result, the slow and fast subsystems of (5.11) are assumed to be approximately observable and controllable based on the approximate observability and controllability of infinite-dimensional systems in [84].*

Remark 5.2. *The control performance of the system of (5.1)-(5.3) directly depends on the accuracy of its reduced order model (ROM). Using APOD methodology, the ROM will need to be adaptively revised at certain time instants to remain accurate.*

Then the ROM structure and dimensionality will change during process evolution. As a result, when the ROM switches the observers and controllers will be redesigned as well.

5.3 APOD-based geometric dynamic observer design

The switching ROM needs the periodic availability of the process snapshots. In addition to that the dynamic observer also requires continuous availability of point measurements from a restricted number of sensors. These requirements are quite common in industrial processes. We can define the observation error based on the state of the system of (5.1) as follows

$$E(z,t) = \bar{x}_e(z,t) - \bar{x}_s(z,t), \tag{5.16}$$

where $\bar{x}_e$ and $\bar{x}_s$ are the estimated and original states of the slow subsystem of PDE system in Eqs. (5.1)-(5.3), respectively.

By neglecting the fast and stable part of the process system dynamic behavior and using separation of variables, we obtain the slow part of the original state as

$$\bar{x}_s(z,t) = \Phi_s{}^T(z)\, x_s(t), \tag{5.17}$$

and the estimated state

$$\bar{x}_e(z,t) = \Psi^T(z)\,\hat{a}(t), \qquad (5.18)$$

where $\Psi = [\psi_1\ \psi_2\ \ldots\ \psi_{r_m}]^T$, $\Phi_s = [\phi_1\ \phi_2\ \ldots\ \phi_p]^T$; r_m is the number of empirical basis functions of the system that are computed using APOD and p is the number of unavailable basis functions of the slow subsystem and $\hat{a}$ is the vector of estimated modes of (5.15). The dimension of the vectors of modes, x_s and $\hat{a}$ in Eqs. (5.17) and (5.18), respectively is not necessarily the same because the number of identified slow subsystems basis functions, Φ_s, and APOD-based basis functions, Ψ, may be different; so the observation error can not be defined directly by the simple subtraction, $\hat{a} - x_s$, where $\hat{a}$ is the observer state.

Assumption 5.3. *Consider the local subspace of the slow and unstable modes,* $\mathbb{W}_s \triangleq span\{\phi_i(z_0)\}_{i=1}^p$ *and subspace* $\mathbb{P}$ *defined as* $\mathbb{P} \triangleq span\{\psi_i(z_0)\}_{i=1}^{r_m}$, *where* $\{\phi_i\}_{i=1}^p$ *is the set of unavailable basis functions of the slow subsystem,* $\{\psi_i\}_{i=1}^{r_m}$ *is the set of basis functions computed based on APOD and* z_0 *indicates the equilibrium point. We assume that* $\mathbb{W}_s \subseteq \mathbb{P}$, *locally in some neighborhood of* z_0.

Note that Assumption 5.3 is justified based on the excitation of the higher modes during the closed-loop process evolution. Based on Assumption 5.3, subspace $\mathbb{P}$ includes subspace $\mathbb{W}_s$ and it may include a part of subspace $\mathbb{W}_f$. One solution to bridge slow Sobolev subspace $\mathbb{W}_s$ and subspace $\mathbb{P}$ is by defining a bounded mapping between these two subspaces to find the corresponding states. The map should be defined as a linear transformation that changes at ROM revi-

sions to conserve all of the subspaces' properties during system evolution. Then, from (5.17) we can define a bounded map between two subspaces, $\mathbb{W}_s$ and $\mathbb{P}$ as follows

$$\bar{x}_s = \Phi_s^T x_s = \Psi^T \mathcal{M} x_s = \Psi^T \tilde{a}, \tag{5.19}$$

where $\tilde{a} = \mathcal{M} x_s$, $\mathcal{M} : \mathbb{W}_s \mapsto \mathbb{P}$ and

$$\mathcal{M} = (\Psi^T, \Phi_s^T). \tag{5.20}$$

Note that $\mathcal{M} = (\Psi^T, \Phi_s^T)$, $\mathcal{M} : \mathbb{W}_s \mapsto \mathbb{P}$, is injective due to the fact that subspace $\mathbb{P}$ contains subspace $\mathbb{W}_s$. Then $\tilde{a}_1 = \tilde{a}_2, \forall \tilde{a}_1, \tilde{a}_2 \in \mathbb{P}$ implies that $x_{s,1} = x_{s,2}, \forall x_{s,1}, x_{s,2} \in \mathbb{W}_s$. To complete the analysis, the bounded reverse map can be defined as $\mathcal{M}^\perp = (\Phi_s^T, \Psi^T)$, $\mathcal{M}^\perp : \mathbb{P} \mapsto \mathbb{W}_s$ such that $\mathcal{I} = \mathcal{M}^\perp \mathcal{M} : \mathbb{W}_s \mapsto \mathbb{W}_s$ is a bijective map. Interestingly, $\mathcal{M}^\perp = \mathcal{M}^T$.

Using Assumption 5.3 and the above transformation, the modal slow dynamics in Eq. (5.11) can be expressed within subspace $\mathbb{P}$ in the following form

$$\dot{\tilde{a}} = A\tilde{a} + f(\tilde{a}) + Bu,$$
$$y_c = C\tilde{a}, \tag{5.21}$$
$$y_m = S\tilde{a},$$

where $A = \mathcal{M} A_s \mathcal{M}^\perp$, $B = \mathcal{M} B_s$, $C = C_c \mathcal{M}^\perp$ and $S = S_m \mathcal{M}^\perp$ are constant matrices between ROM revisions and $f = \mathcal{M} F_s$ is a nonlinear function. Using the

definition of the map and its inverse, it can be easily shown that these matrices

and function are the same as used in (5.15). Note that we do not require Φ_s for

the proposed method, we need it just for our analysis.

In addition to previous assumptions, the robust exponential observability of

(5.21) is assumed. The following nonlinear geometric dynamic observer [6, 249] is

used to reconstruct the dynamics of (5.21),

$$
\dot{\hat{a}} = A\hat{a} + f(\hat{a}) + Bu + \Pi_{\hat{a}}^{-1} L(y_m - \hat{y}_m),
$$
$$
\hat{y}_m = C\hat{a}.
$$
(5.22)

In (5.22), $\hat{a}$ is the dynamic observer state which is the vector of estimated modes

and L is the observer gain. There are w integers, $\zeta_1, \zeta_2, \cdots, \zeta_w$, as observability

indexes where $\zeta_i > 0$ for $i = 1, \cdots, w$ and $\zeta_1 + \zeta_2 + \cdots + \zeta_w = r_m$. Note that w

is the number of measurement outputs. $\Pi_{\hat{a}}^{r_m \times r_m}$ is the Jacobian of the map $\Pi^{r_m \times 1}$

with respect to the state of the system. The map $\Pi^{r_m \times 1}(\hat{a}, u)$ defined as follows

$$
\Pi(\hat{a}, u) = [\hat{y}_{m,1} \quad L_F \hat{y}_{m,1} \quad \ldots \quad L_F^{\zeta_1 - 1} \hat{y}_{m,1} \quad \ldots \quad \hat{y}_{m,w} \quad L_F \hat{y}_{m,w} \quad \ldots \quad L_F^{\zeta_w - 1} \hat{y}_{m,w}]^T
$$
(5.23)

is assumed to be continuously differentiable and robustly invertible with respect

to $\hat{a}$ where $L_F(\cdot) = \dfrac{\partial(\cdot)}{\partial \hat{a}} F$ denotes Lie derivatives and $F(\hat{a}) = A\hat{a} + f(\hat{a})$. The

j^{th} order Lie derivative with respect to the same vector argument is defined as

$L_F^j(\cdot) = L_F L_F^{j-1}(\cdot)$. That means there is an inverse map in the form of $\Pi^{-1}(\hat{a}, u)$

where Π and Π^{-1} are both Lipschitz continuous and

$$\Pi^{-1}(\Pi(\hat{a}, u), u) = \hat{a}, \quad t \geq 0.$$

The observer gain, L, is then a block diagonal matrix in the following form

$$L = \begin{bmatrix} L_1 & 0 & \cdots & 0 \\ 0 & L_2 & \cdots & 0 \\ \vdots & \vdots & \ddots & \vdots \\ 0 & 0 & \cdots & L_w \end{bmatrix},$$

$$L_1 = \begin{bmatrix} \zeta_{11} \\ \zeta_{21} \\ \vdots \\ \zeta_{\zeta_1 1} \end{bmatrix}, \quad L_2 = \begin{bmatrix} \zeta_{12} \\ \zeta_{22} \\ \vdots \\ \zeta_{\zeta_2 2} \end{bmatrix}, \quad \cdots, \quad L_w = \begin{bmatrix} \zeta_{1w} \\ \zeta_{2w} \\ \vdots \\ \zeta_{\zeta_w w} \end{bmatrix}$$

(5.24)

where ζ_{ij} for $i = 1, \cdots, \zeta_w$ and $j = 1, \cdots, w$ are the dynamic observer gain parameters. The observer error dynamics become linear and the above parameters are set such that the pole-assignable observer error dynamics are stable [7]. The detailed analysis and stability proof of the observation error can be found in [6, 7].

Thus, based on Assumption 5.1, the observation error with respect to original states can be defined within subspace $\mathbb{P}$ as follows

$$E = \bar{x}_e - \bar{x}_s \simeq \Psi^T e, \tag{5.25}$$

where $e = \hat{a} - \tilde{a}$ is the observer error with respect to modes.

Remark 5.3. *The invertibility assumption of $\Pi_{\hat{a}}^{r_m \times r_m}$ is not a restrictive assumption for DPSs. It requires a preliminary sensor placement step in the controller synthesis that is properly addressed in [87]. It is a unique characteristic of DPSs that sensor placement confers observability.*

5.4 APOD-based geometric controller design

In this section, we focus on the geometric controller structure design to achieve the output tracking objective of the system. We used globally linearizing control (GLC) structure that includes a static geometric state feedback controller combined with a stable dynamic observer in an inner loop and an external linear controller [138, 155]. Assuming the separation principle for the system of (5.21) holds, the following GLC structure can asymptotically stabilize the minimum phase system of (5.21) at the desired output,

$$u = \frac{v - L_F^{r_c}\hat{y}_c - \beta_1 L_F^{r_c - 1}\hat{y}_c - \cdots - \beta_{r_c - 1} L_F \hat{y}_c - \beta_{r_c}\hat{y}_c}{L_B L_F^{r_c - 1}\hat{y}_c} \tag{5.26}$$

where $\hat{y}_c = C\hat{a}$ is the vector of controlled outputs, $F(\hat{a}) = A\hat{a} + f(\hat{a})$, r_c is the relative order of the system. The input-output dynamics of the globally linearized

system can be expressed as follows

$$\frac{d^{r_c}\hat{y}_c}{dt^{r_c}} + \beta_1 \frac{d^{r_c-1}\hat{y}_c}{dt^{r_c-1}} + \cdots + \beta_{r_c-1}\frac{d\hat{y}_c}{dt} + \beta_{r_c}\hat{y}_c = v. \tag{5.27}$$

The inner loop is stable when all of the roots of the characteristic polynomial of

$s^{r_c} + \beta_1 s^{r_c-1} + \cdots + \beta_{r_c-1}s + \beta_{r_c}$ are in the open left-half plane. Then an external

linear controller is designed for the globally linearized system as

$$v = \int_0^t \chi(t - \tau)\Big(y_{sp}(\tau) - \hat{y}_c(\tau)\Big)d\tau, \tag{5.28}$$

where $\chi(t)$ indicates the desired input-output dynamic behavior of the overall

system. Considering a critically damped behavior as the desired input-output

dynamics in the following form,

$$\chi(t) = \mathcal{L}^{-1}\Big\{\frac{s^{r_c} + \beta_1 s^{r_c-1} + \cdots + \beta_{r_c-1}s + \beta_{r_c}}{(\varepsilon s + 1)^{r_c} - 1}\Big\}, \tag{5.29}$$

where $\mathcal{L}^{-1}$ indicates the inverse Laplace transform, the overall closed-loop dynam-

ics will be

$$\Big(\varepsilon\frac{d}{dt} + 1\Big)^{r_c}\hat{y}_c = y_{sp}. \tag{5.30}$$

When $r_c = 1$ the external controller becomes proportional-integral (PI),

$$v(t) = K_c\Big([y_{sp}(t) - \hat{y}_c(t)] + \frac{1}{\tau_I}\int_0^t [y_{sp}(t) - \hat{y}_c(t)]dt\Big), \tag{5.31}$$

where $K_C = \dfrac{1}{\varepsilon}$ and $\tau_I = \dfrac{1}{\beta_1}$ are the proportional and integral coefficients of the external PI controller, respectively. A detailed analysis and stability proof of the closed-loop system can be found in [138, 154, 155].

Theorem 5.1. *Consider the nonlinear dissipative PDE system in (5.1), for which Assumptions 5.1-5.2 always hold, Assumption 5.3 holds for finite periods between revisions and the system of (5.21) is robustly exponentially observable. The geometric control structure of (5.26) and dynamic observer of (5.22) asymptotically stabilizes the system of (5.1) when the time interval between ROM updates, δt, is finite and larger than a critical value, t_b.*

Proof *See Appendix A.3.1 for proof of the theorem.*

In Figure 5.1 the closed-loop process is presented under the proposed control structure in a block diagram form.

Remark 5.4. *When APOD revises the set of empirical basis functions as time evolves the structure and size of the ROM may change. These changes directly affect the dynamic observer and controller components. In this case, the observer/controller pair must be redesigned. For the dynamic observer we employ a Butterworth polynomial and the order of the desired stable poles of the observation error dynamics before closed-loop operation starts [112]. This predetermined supervisory logic chooses the appropriate number of observer poles when the size of ROM changes during process evolution. For the controller component we also use Butterworth procedure to predetermine a set of Hurwitz characteristic polynomials*
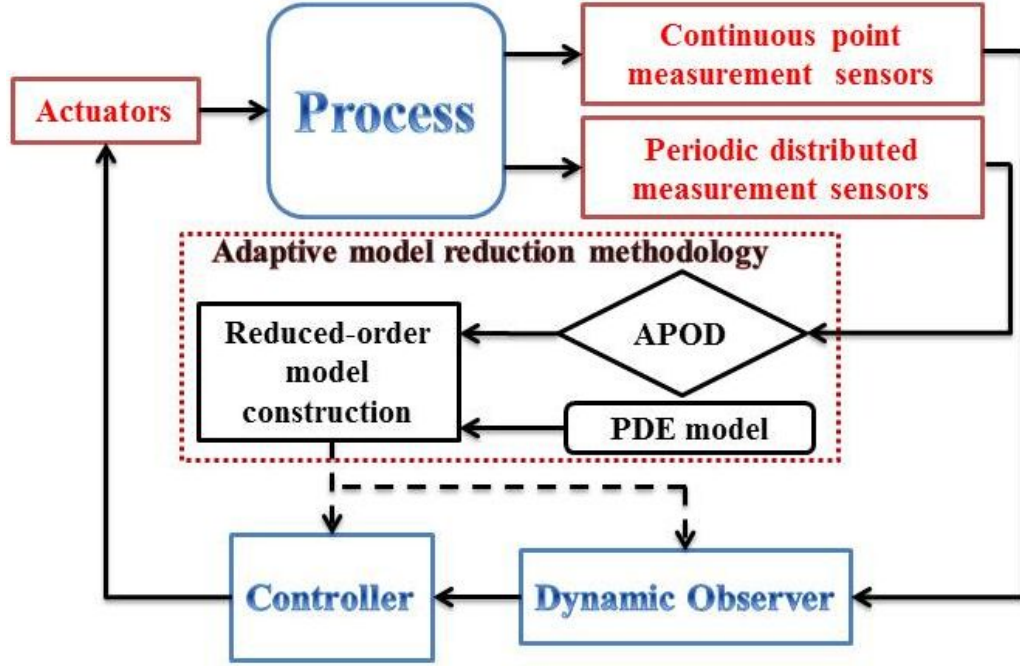
Figure 5.1: Process operation block diagram under proposed controller structure.

before closed-loop operation [112]. When the dimension of the ROM changes as time evolves, the controller component uses the appropriate stable characteristic polynomial to tune the GLC parameters.

Remark 5.5. *The geometric controller of (5.26) is synthesized for single-output systems in this chapter, however it is straightforward to extend the proposed controller structure for multi-output systems; this will be the subject of future work.*

Remark 5.6. *The Butterworth polynomials of the observer and the controller must be designed such that the characteristic times of the polynomials is less than t_b. Based on such design, the controller/observer pair does not violate the time scale separation between the slow and fast subsystems.*

5.5 Application to reduce hot spot temperature

Special attention is paid to the thermal dynamics and their effect on product quality and safety criteria in chemical and petrochemical industries. Due to their importance, thermal dynamic analysis is considered in conceptual and detailed process design and dynamic operation of many processes where thermal distribution plays a key role such as distillation towers, chemical reactors and heat exchanger networks. As an illustrative example we present a hot spot formation issue in tubular chemical reactors due to exothermic reactions that can lead to safety problems, severe catalyst deactivation and its effects on the process selectivity and product quality achieved [55, 145].

The hot spot temperature in many cases is very sensitive to relatively small changes in the process variables such as inlet temperature or concentration and wall temperature. Then even small changes in such conditions can easily result in thermal instabilities. Due to safety considerations the hot spot temperature has to be maintained within given limits, otherwise the temperature may rise uncontrollably and it may lead to thermal runaway [55, 63]. The effectiveness of the proposed APOD-based geometric dynamic observer and controller is illustrated on the output tracking problem of thermal dynamics in a catalytic reactor to reduce the hot spot temperature and manage the thermal energy distribution through reactor length during process evolution.

We consider an elementary exothermic reaction of A $\rightarrow$ B taking place on a

thin catalytic rod where the reactant A is present in excess. The dimensionless temperature of the rod is described by the following dissipative PDE system,

$$\frac{\partial \bar{x}}{\partial t} = \frac{\partial^2 \bar{x}}{\partial z^2} + \beta_T(\mathrm{e}^{-\gamma/(1+\bar{x})} - \mathrm{e}^{-\gamma}) + \beta_U(b(z)u(t) - \bar{x}) \tag{5.32}$$

subject to the boundary conditions

$$\bar{x}(0, t) = 0, \ \bar{x}(\pi, t) = 0, \tag{5.33}$$

and initial conditions of

$$\bar{x}(z, 0) = \bar{x}_0(z). \tag{5.34}$$

In the PDE system of (5.32)-(5.34), $\bar{x}$ denotes the dimensionless temperature of the catalytic rod , $z \in [0, \pi]$ is the spatial coordinate, β_T denotes the dimensionless heat of reaction and γ is the dimensionless activation energy. The parameter β_U denotes the dimensionless heat transfer coefficient, $u(t)$ is the vector of control variables and $b(z)$ accounts for the spatial profile of the actuator. In the above equation we observe that $\mathcal{A}(z) = \dfrac{\partial^2}{\partial z^2}$ and $\mathcal{F}(z, \bar{x}) = \beta_T(\mathrm{e}^{-\gamma/(1+\bar{x})} - \mathrm{e}^{-\gamma}) - \beta_U \bar{x}$.

The nominal values of $\beta_T = 16$, $\gamma = 2$, and $\beta_U = 2$ are set for the system parameters. Due to safety considerations we attempt to avoid severe catalyst deactivation and thermal runaway. Thus, the hot spot temperature reduction is considered as the control objective. This is captured mainly from the first (most important) mode (as shown below). We thus consider the following APOD-based

controlled output of the process

$$y_c = \int_0^\pi \psi_1 \bar{x} dz, \qquad\qquad (5.35)$$

to monitor the thermal energy distribution and the dominant dynamics across the reactor length during process evolution. A sinusoidal state profile with average of 0.5 is set as the initial condition of the system in (5.34). Figure 5.2 presents the open-loop profile of the systems state and its 2-norm when $u = 0$. The hot spot in the middle of the catalytic rod can be observed easily. The initial dominant empirical basis function of the system is illustrated in Figure 5.3. In addition, Figure 5.4 shows the open-loop system output. Only one point actuator is assumed to be available at $L_a = \pi/2$ and the corresponding spatial distribution functions at this location for point actuation is considered as $b(z) = \delta(z - L_a)$, where $\delta(\cdot)$ is the Dirac delta function. The snapshot of the rod temperature is also assumed to be accessible every $\delta t = 0.5s$. Only one continuous point measurement sensor is available placed at $L_s = 0.7\pi$. The continuous sensor shape distribution function, $s(z)$, for all time t, at this respective position is $s(z) = \delta(z - L_s)$.

It is a usual occurrence in chemical process industries that the process objectives dynamically change during operation due to changing product quality requirements and safety reasons. The desired value for controlled output is set to change dynamically from $y_{sp,1} = 1.5$ to $y_{sp,2} = 2$ and $y_{sp,3} = 1.7$ at $t = 10s$ and $t = 20s$, respectively. The objective is to change the hot spot temperature (to
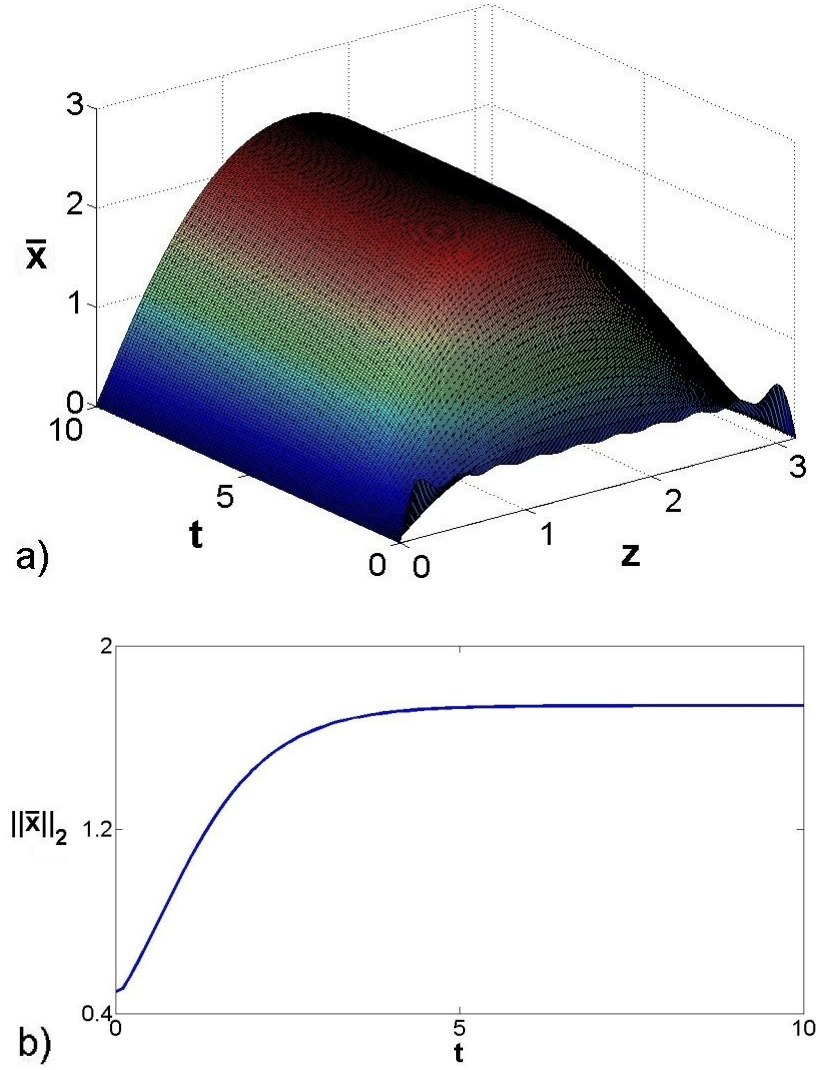
Figure 5.2: Open-loop system temporal profile of (a) the state spatial profile and (b) 2-norm of the state.

reduce the risk of hot spot phenomenon) and manage the thermal energy distribution during process evolution. The proposed control structure can accommodate dynamic set point tracking, however we only present step-changes for simplicity. Since the relative order of the system is equal to 1, we desire the linearized output dynamics to be stable with $\beta_1 = 5$ and the overall output closed-loop characteristic
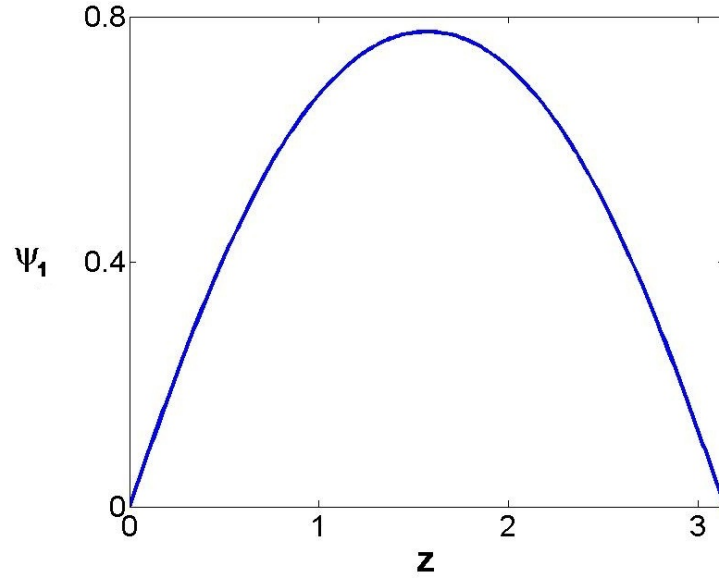
Figure 5.3: The initial dominant empirical basis function.
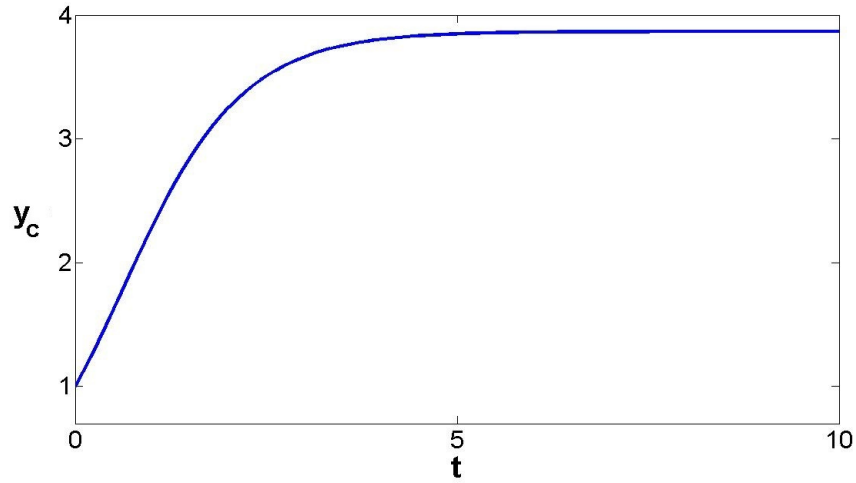
Figure 5.4: The open-loop system output.

time to be $\varepsilon = 0.5$ resulting in the following form for $\chi(t) = \mathcal{L}^{-1}\left\{\dfrac{s+5}{0.5s}\right\}$. As a result, we implement an external PI controller with parameter values $K_C = \dfrac{1}{\varepsilon} = 2$, $\tau_I = \dfrac{1}{\beta_1} = 0.2$, where K_C and τ_I are the proportional gain and integral time of the external PI controller, respectively.

In order to obtain the initial basis functions we "collected" 20 snapshots during the initial time period $t \in [0, 2]$; during this period the process evolves with $u(t) = 0$ (inactive controller). Application of off-line APOD to this ensemble resulted in one empirical basis function for $\bar{x}$ which captured 0.99 of the energy embedded in the ensemble. During closed-loop progression, on-line APOD also obtained only one empirical basis function that shows the effectiveness of the ensemble updating approach. We employed only one measurement output; then according to single empirical basis function we only had to tune ζ_{11} to identify the dynamic observer. We set $\zeta_{11} = 0.032$ to enforce a stable dynamic behavior to the observation error. Figure 5.5 shows the steady state dimensionless temperature profile of the system and temporal profile of the 2-norm of the state. We observe that the controller successfully reduced the hot spot temperature level. Figure 5.6 presents the temporal profile of required control action; it converges to a steady state value without any chattering. We observe also that action peaks due to the step change of the desired set-points. This sharp change in the control action is due to the external controller; these peaks can be reduced by employing a PI controller with a low-pass filter (introduced by an appropriate choice of $\chi(t)$). The temporal profile of the estimated dominant mode of the system is illustrated in Figure 5.7. We observe that it is a linear dynamic behavior and it converges to a constant values, which is expected, since the internal nonlinear controller is designed to enforce this behavior to the first mode.
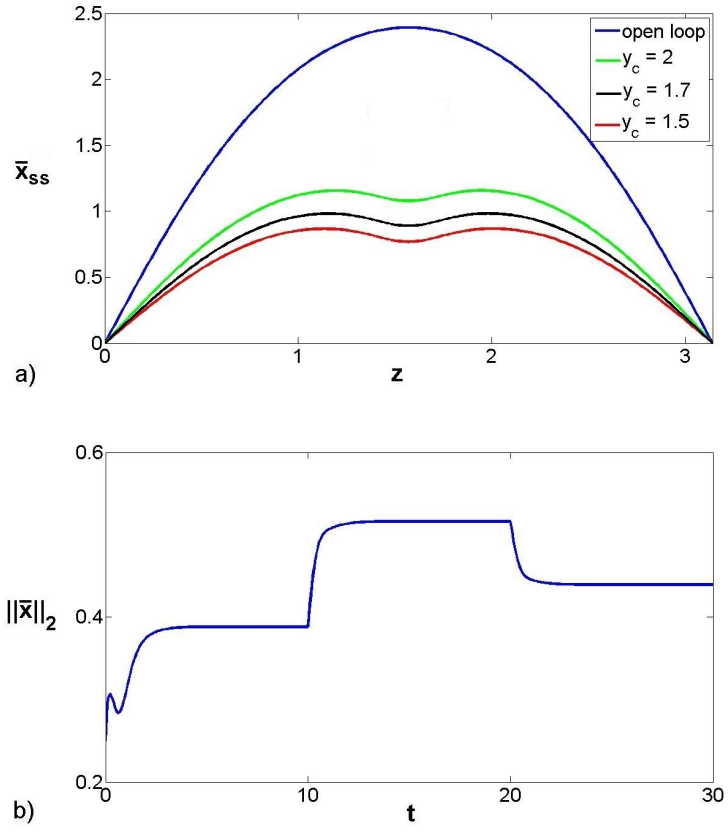
Figure 5.5: (a) Steady state profiles of system state during process evolutions under the proposed controller and (b) temporal profile of 2-norm of the state.
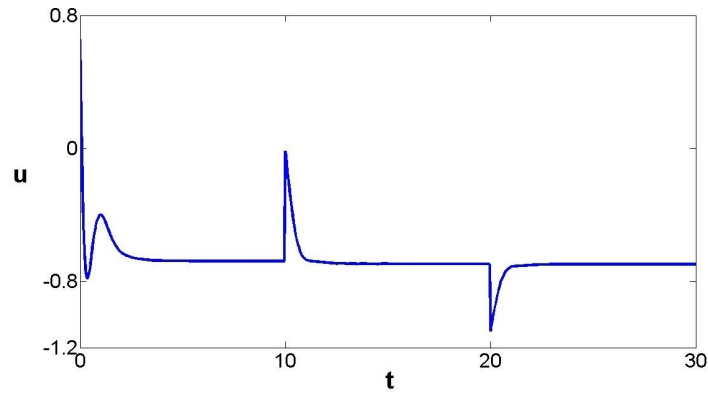
Figure 5.6: Temporal profile of the required control action.
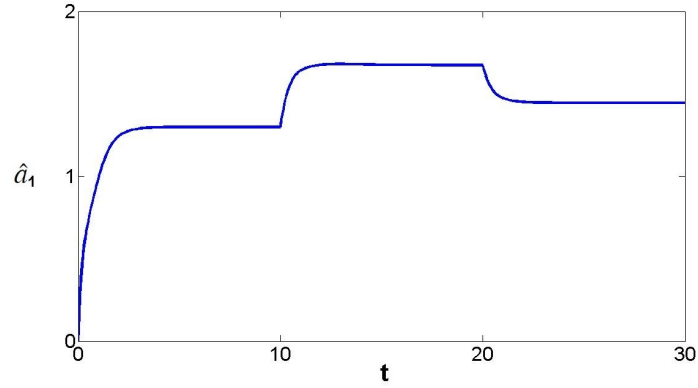
Figure 5.7: Temporal profile of the dominant mode of the system.
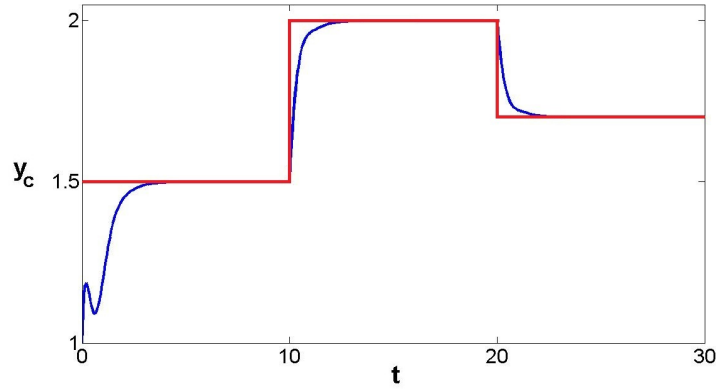
Figure 5.8: Temporal profile of the controlled output of the system.

Figure 5.8 presents the controlled output of the system; it exhibits a linear dynamic behavior in time and converges to the desired setpoint values. The success of the designed output tracking controller is due to the dominant subspace (hence the ROM and the control law) being updated as the process traverses through different regions of the state space during closed-loop operation. During the closed-loop process operation, when new trends appeared the dominant subspace basis was updated to accurately capture the process behavior, appropriately changing the empirical basis function.

APOD-BASED CONTROLLER DESIGNS UNDER SENSOR/CONTROLLER COMMUNICATION BANDWIDTH LIMITATIONS

One of the remaining unanswered questions in adaptive proper orthogonal decomposition (APOD) based control problem of distributed parameter systems (DPSs)

is how one can identify the required frequency for reduced order model (ROM) revisions. The required time interval between the ROM revisions and as a result the frequency of snapshots in the APOD-based control should satisfy closed-loop stability criteria. For DPSs we observe that increasing the time interval between revisions reduces the communication load and the spatially distributed measurement costs but it may inadvertently affect closed-loop system stability as it will be shown in this chapter.

Considering such trade-off between stability and measurement costs, obtaining snapshots at a proper frequency is one of the most important prerequisites of APOD-based controller designs. In the current work, we consider the set of sensors (that acquire information), controller structure (that analyzes process information, revises the ROM and computes the required action) and actuators (that enforce that command) as a small communication network with a limited bandwidth for closed-loop process data transfer. Using such conceptual duality between finding the required revision time intervals for APOD-based control and desired feedback frequency for control of networked systems in the presence of communication constraints can be extremely helpful since communication networks are well studied theoretically and are extensively used in the distributed and networked control of advanced chemical processes for fast dissemination of information between operators. When control system elements communication bandwidth is limited, improved methods are needed for state estimation and controller design to overcome

the communication constraints (see [131] and references therein). Recently, networked model-based control of lumped systems has been studied in detail (see [188] and references therein), while networked controllers that circumvent the sensor-controller communication constrains in DPSs has been investigated [238, 270, 271]. In Section 6.1, we use the concepts behind networked control method to identify criteria that guarantee system closed-loop stability and in this way we address the spatially distributed measurements frequency problem of APOD for linear DPSs. We also address the minimization problem of required ROM revisions for nonlinear DPSs in Section 6.2.

6.1   Linear systems

To achieve our goals in minimizing the frequency of snapshots (minimizing ROM revisions), we apply a similar approach to the networked feedback controller designs for distributed parameter systems [238]. The controller was synthesized for dissipative distributed parameter systems which can be discretized to finite dimensional slow (and possibly unstable) and infinite-dimensional fast subsystems when represented in appropriate Sobolev spaces. The slow subsystem model is included in the control structure to reduce the frequency of sensor measurements over the network when communication is suspended. To compute the smallest frequency at which communication must be reestablished and the ROM must be updated, the concepts of networked control for linear systems has been used. A criterion is then

identified for minimizing communication bandwidth (snapshots transfer rate) from the periodic measurement sensors to the controller considering closed-loop stability. The proposed control structure is successfully illustrated on thermal dynamic regulation in a tubular chemical reactor.

6.1.1   Mathematical Preliminaries

Consider the linear distributed parameter systems modeled by the state space description of dissipative linear PDEs of

$$\frac{\partial}{\partial t}\bar{x}(z,t) = \mathbf{A}(z)\bar{x}(z,t) + b(z)u(t),$$

$$s.t. \quad q(\bar{x}, \frac{\partial \bar{x}}{\partial z}, ..., \frac{\partial^{n-1}\bar{x}}{\partial z^{n-1}}) = 0 \quad \text{on} \quad \partial\Omega, \quad \bar{x}(z,0) = \bar{x}_0(z). \tag{6.1}$$

We define the snapshot measurements as discrete-time full state measurements, mathematically expressed by

$$y(z,t_k) = \int_0^t \delta(\tau - t_k)\bar{x}(z,\tau)d\tau \tag{6.2}$$

In the above system, $z \in \Omega$ is the spatial coordinate, $t \in [0,\infty)$ is time and $\bar{x}(z,t) \in \mathbb{R}$ denotes the state vector of the system. $\Omega \subset \mathbb{R}^3$ is the domain of the process and $\partial\Omega$ is the process boundary, $u \in \mathbb{R}^l$ denotes the manipulated input vector. $\mathbf{A}(z)$ is a linear spatial differential operator of order n, $q(.)$ is a smooth nonlinear vector function and $\bar{x}_0(z)$ is a smooth vector function of z, $b^T(z) \in \mathbb{R}^l$ is

a known smooth vector function of z that describes how manipulated input vector is distributed in the spatial domain Ω, e.g. point actuation can be defined using standard Dirac delta and continuous actuation can be described by step functions. We assume the availability of a periodic distributed snapshot measurement sensor, $y(z, t_k) \in \mathbb{R}$, where y indicates measured spatial profiles and t_k is the occurrence time instant for snapshot measurement. The control objective is to regulate the PDE system of (6.1) at a desired spatial profile, $\bar{x}_d(z)$. Without loss of generality, the spatially uniform steady state $\bar{x}_d(z) = 0$ is considered as the desired profile.

The PDE system of (6.1) can be presented as an infinite-dimensional system in a relevant Sobolev space $\mathbf{W}^{(n-1),2}(\Omega, \mathbb{R})$, $\forall i, j \in \mathbb{N}$, $i \geqslant 1$ and $1 \leqslant j < \infty$,

$$\mathbf{W}^{i,j} = \{x \in L^j(\Omega) : \quad \partial^\alpha x \in L^j(\Omega), \forall \alpha \in \mathbb{N}, |\alpha| \leqslant i\}.$$

where Sobolev spaces are functional subspaces that consider functions for which all the distributional derivatives can be applied. We can define the inner product and norm in $L_2(\Omega)$ as

$$(\vartheta_1, \vartheta_2) = \int_\Omega r(z) \vartheta_1^T(z) \vartheta_2(z) dz, \quad \|\vartheta_1\|_2 = (\vartheta_1, \vartheta_1)^{1/2},$$

where ϑ^T denotes the transpose of ϑ and $r(z)$ is the weight function that is assumed to be 1 in this work.

We define the state $x \in \mathbb{W}^{(n-1),2}$ as

$$x(t) = \bar{x}(z, t), \tag{6.3}$$

the linear differential operator

$$\mathcal{A}x = \mathbf{A}(z)\bar{x}, \tag{6.4}$$

and the manipulated input as $\mathcal{B}u = b(z)u$, where $\mathbb{W}^{(n-1),2}(\Omega, \mathbb{R})$ is a Sobolev subspace that satisfies the homogeneous boundary conditions of (6.1), i.e.,

$$\mathbb{W}^{(n-1),2}(\Omega, \mathbb{R}) = \left\{ f \in \mathbf{W}^{(n-1),2}(\Omega, \mathbb{R}) : \ q(f, \frac{\partial f}{\partial z}, ..., \frac{\partial^{n-1} f}{\partial z^{n-1}}) = 0 \ \text{ on } \ \partial\Omega \right\}.$$

Then the PDE system of (6.1) can be presented in the Sobolev subspace as follows

$$\dot{x} = \mathcal{A}x + \mathcal{B}u,$$
$$x(0) = x_0. \tag{6.5}$$

Note that to simplify the notation we will use $\mathbb{W}$ to denote $\mathbb{W}^{(n-1),2}(\Omega, \mathbb{R})$ in the rest of the chapter.

In the analytical model reduction approaches, the set of basis functions of the system, needed to build ROMs, can be obtained from the solution of the eigenvalue

problem for the linear spatial operator of $\mathcal{A}$, as follows

$$\mathcal{A}\phi_i = \lambda_i\phi_i, \quad \phi_i \in \mathbb{W}, \quad i = 1, \ldots, \infty. \tag{6.6}$$

where λ_i and ϕ_i denote the $i\,th$ eigenvalue and the corresponding basis function, respectively. Note that ϕ_i is a complete basis of $\mathbb{W}$ for self adjoint operators.

Assumption 6.1. *Consider the ordered eigenspectrum of $\mathcal{A}$ as $\sigma_\mathcal{A} = \{\lambda_1, \lambda_2, \ldots\}$ where*

$$Re(\lambda_1) \geq Re(\lambda_2) \geq \cdots$$

and $Re(\lambda)$ denotes real part of λ. We assume that $\sigma_\mathcal{A}$ can be partitioned into a finite dimensional set of α slow eigenvalues, $\sigma_\mathcal{A}^{(s)} = \{\lambda_1, \lambda_2, \ldots, \lambda_\alpha\}$, and a stable infinite dimensional complement set of the remaining fast eigenvalues $\sigma_\mathcal{A}^{(f)} = \{\lambda_{\alpha+1}, \lambda_{\alpha+2}, \ldots\}$. The associated basis functions sets are defined as

$$\Phi_s = [\phi_1 \ \phi_2 \ \cdots \ \phi_\alpha]^T, \qquad \Phi_f = [\phi_{\alpha+1} \ \phi_{\alpha+2} \ \cdots]^T.$$

There is a large separation between the slow and fast eigenvalues of $\mathcal{A}$, i.e.,

$$\frac{|Re(\lambda_1)|}{|Re(\lambda_\alpha)|} = O(1) \quad and \quad \frac{|Re(\lambda_1)|}{|Re(\lambda_{\alpha+1})|} = O(\gamma)$$

where $Re(\lambda_{\alpha+1}) < 0$, $\gamma = \dfrac{|\lambda_1|}{|\lambda_{\alpha+1}|}$ is a small number and $O(\gamma)$ indicates the order of γ.

According to Assumption 6.1, the system Sobolev subspace, $\mathbb{W} \triangleq span\{\phi_i\}_{i=1}^{\infty}$, can be partitioned into two Sobolev subspaces, named slow and fast subspaces, $\mathbb{W}_s$ and $\mathbb{W}_f$, respectively, where $\mathbb{W} = \mathbb{W}_s \oplus \mathbb{W}_f$. The slow subspace includes a finite number of basis functions that correspond to the slow and possibly unstable modes of x, $\mathbb{W}_s \triangleq span\{\phi_i\}_{i=1}^{\alpha}$, and the fast complement subspace contains an infinite number of basis functions that correspond to the fast and stable modes of x, $\mathbb{W}_f \triangleq span\{\phi_i\}_{i=\alpha+1}^{\infty}$. Then the state of the infinite dimensional system of (6.1) can be partitioned into a finite number of slow and possibly unstable modes and an infinite number of stable and fast modes with respect to the basis of the Sobolev subspace, $\mathbb{W}$,

$$x = x_s + x_f, \tag{6.7}$$

where $x_s = \mathcal{P}x \in \mathbb{W}_s$ and $x_f = \mathcal{Q}x \in \mathbb{W}_f$. The orthogonal integral projection operators are defined as $\mathcal{P} : \mathbb{W} \to \mathbb{W}_s$, $\mathcal{P} = (\cdot, \Phi_s)$ and $\mathcal{Q} : \mathbb{W} \to \mathbb{W}_f$, $\mathcal{Q} = (\cdot, \Phi_f)$.

From (6.7) and using the method of weighted residuals based on the set of basis functions, the system of (6.5) can be presented as a partitioned ODE set of vectorized modes in the following form

$$\dot{x}_s = A_s x_s + B_s u, \ x_s(0) = \mathcal{P}x_0,$$
$$\dot{x}_f = A_f x_f + B_f u, \ x_f(0) = \mathcal{Q}x_0, \tag{6.8}$$

where $A_s = \mathcal{P}\mathcal{A}$, $A_f = \mathcal{Q}\mathcal{A}$, $B_s = \mathcal{P}\mathcal{B}$, $B_f = \mathcal{Q}\mathcal{B}$, $\mathcal{P}x(0) = \mathcal{P}x_0$, $\mathcal{Q}x(0) = \mathcal{Q}x_0$, $\bar{x} = \bar{x}_s + \bar{x}_f$, $\bar{x}_s = \Phi_s^T x_s$ and $\bar{x}_f = \Phi_f^T x_f$. Note that in above modal expansions,

$A_s = diag\{\lambda_i\}_{i=1}^{\alpha}$ and $A_f = diag\{\lambda_i\}_{i=\alpha+1}^{\infty}$ are diagonal matrices. Also since there is an order of magnitude difference between $Re(\lambda_1)$ and $Re(\lambda_{\alpha+1})$, then there is a time scale separation between the dynamic behavior of the two subsystems.

On the basis of the above discussion, to implement the analytical model reduction we need to solve the eigenvalue problem of (6.6) and find the set of basis functions. However, generally it is not possible to solve it when we have complex boundary conditions. The interesting fact is that we can not find the analytical solution even for a general class of linear systems over miscellaneous domains. Thus, most of the standard analytical model reduction techniques can not be directly used even for distributed parameter systems described by general linear PDEs. One solution to circumvent this issue is to apply APOD as explained briefly in previous chapters.

Remark 6.1. *The results in this work are presented for $\bar{x} \in \mathbb{R}$, however, it is straightforward to extend the results for $\bar{x} \in \mathbb{R}^m$ by treating each state individually and combining the resulting ODE descriptions. Once each PDE has been reduced, the interactions between distributed system states can be easily captured from their modal expansions [228].*

Remark 6.2. *The assumption of large separation between slow and fast dynamics of the system (Assumption 6.1) is satisfied by wide range of transport-reaction processes (see [75] for heating rod and catalytic packed-bed reactor examples, [1, 178, 248] for chemical vapor deposition process and [172] for plasma discharge reactor).*

Assumption 6.1 is fundamental to the existence of only a few dominant modes that can describe the dominant dynamic behavior of the parabolic PDE system. Based on this assumption we can approximate the distributed parameter system by a finite dimensional ODEs.

6.1.2 Adaptive model reduction

6.1.2.1 Finite dimensional approximation using the method of weighted residuals

The finite-dimensional approximation of the infinite-dimensional PDE system of (6.1) can be presented in the form of an ODE set of slow and possibly unstable modes using the method of weighted residuals if and only if we have a proper set of analytical or empirical basis functions. The state of the original PDE system of (6.1), $\bar{x}(z,t)$, can be recast as an infinite weighted sum of a complete set of basis functions, $\psi_k(z)$, as

$$\bar{x}(z,t) = \sum_{k=1}^{\infty} x_{m,k}(t)\psi_k(z). \tag{6.9}$$

Then the following approximation can be obtained by truncating the series expansion of $\bar{x}(z,t)$ up to order r:

$$\hat{\bar{x}}(z,t) = \sum_{k=1}^{r} x_{m,k}(t)\psi_k(z), \tag{6.10}$$

where r is the number of slow modes and $x_m(t)$ denotes time varying coefficients known as system modes. The following ODE set of order r is obtained by substituting (6.10) in (6.1), multiplying the PDE with the weighting functions, $\varphi(z)$, and integrating over the entire spatial domain:

$$
\begin{aligned}
&\sum_{k=1}^{r} (\varphi_j(z), \psi_k(z)) \dot{x}_{m,k}(t) \\
&= \sum_{k=1}^{r} (\varphi_j(z), \mathcal{A}(z)\psi_k(z)) x_{m,k}(t) + (\varphi_j(z), b(z)) u(t), \quad j = 1, ..., r
\end{aligned}
\tag{6.11}
$$

Note that the type of weighted residual method depends on the type of weighting functions used in the above procedure. It is Galerkin's method when the weighting functions, $\varphi(z)$, and the basis functions, $\psi(z)$, are the same. Galerkin's method leads to accurate finite dimensional ODE models for processes that exhibit strong diffusive phenomena and can thus be described by highly dissipative PDE systems; this is due to the fact that their dominant dynamic behavior can be captured by a finite number of dominant spatial profiles. The reduced order system of (6.11) can be summarized as

$$
\dot{x}_m = A_m x_m + B_m u.
\tag{6.12}
$$

This system is considered for control design purposes in the next section.

6.1.3 Control system

In this section we consider the control problem of general linear distributed parameter systems the spatiotemporal dynamics of which can be described in the form of (6.1). We use the idea of networked control approach to regulate the system and seek appropriate criteria for frequency of periodic spatially distributed measurements considering closed-loop stability. Note that the open-loop spatially distributed process may be stable or unstable; that does not affect the analysis. We assume there is no delay in snapshot communication from the periodic distributed measurement sensors to ROM and controller. The main objective is to find the smallest frequency at which the ROM must be updated based on the availability of the snapshots from the periodic distributed measurement sensors.

Assumption 6.2. *The process slow dynamics and as a result the slow subsystem of (6.8) is assumed to be controllable, and spillover to the fast subsystem is of finite magnitude.*

The partitioned dynamics of the real process, the APOD-based switching model and the state feedback controller equation can be summarized as

$$
\begin{aligned}
Process: \quad & \dot{x}_s = A_s x_s + B_s u, \\
& \dot{x}_f = A_f x_f + B_f u, \\
Model: \quad & \dot{x}_m = A_m x_m + B_m u, \\
Controller: \quad & u = \tilde{K} x_m,
\end{aligned}
\tag{6.13}
$$

where the controller design goal is computing the matrix of $\tilde{K}$ in the state feedback controller equation of $u = \tilde{K}x_m$, such that the eigenvalues of the closed loop system are placed in predetermined positions.

According to Assumption 6.2 the slow dynamics of the system of (6.13) is controllable. Then it is possible to place the closed-loop system poles anywhere in the complex domain, where the poles' locations correspond directly to the eigenvalues of the system [112]. We use the ROM and a pole placement technique, for example Ackermann's formula, to compute a state feedback controller gain matrix, $\tilde{K}$, that places the closed-loop poles of the system in predetermined locations. As the process evolves, when APOD revises the set of empirical basis functions the structure and size of the ROM may change. These changes directly affect the controller structure. In such cases, the controller should be redesigned. We use Butterworth formula to predetermine a set of Hurwitz characteristic polynomials and an ordered set of desired stable poles of closed-loop dynamics before closed-loop operation [112]. When the dimension of ROM changes during process evolution, the controller structure chooses the appropriate number of poles and their predetermined locations.

Remark 6.3. *Assumption 6.2 is not as restrictive as may look, since the controllability of DPSs depends on the actuators' locations. In addition, the controllability of the ROM also depends on the discretization method and discretization points [216]. Using singular perturbation arguments for Galerkin's method we can link*

the controllability of ROM with the controllability of DPS. Most of the spatially distributed processes in the chemical industries are over-designed to be controllable by placing the actuators in appropriate locations with respect to open-loop criteria [21]. The reader may refer to [21, 88] for actuators' placement methods that satisfy controllability of the ROM and DPS and suppress spillover to higher order dynamics.

Remark 6.4. *Alternatively we may assume that the infinite dimensional system of (6.5) is approximately controllable [84]. There is a direct relationship between approximate controllability and exact controllability of the slow subsystem. Assumption 6.2 is less restrictive than this requirement because approximate controllability even though is not enforcing exact controllability to the system, it assumes that the fast subsystem is also controllable which is not the case of the assumption.*

6.1.3.1 Closed-loop system analysis

The slow and dominant part of the state in the original PDE system of (6.1) can be defined as follows

$$\bar{x}_s(z,t) = \Phi_s^T(z) \ x_s(t). \tag{6.14}$$

Also the model state of the PDE system is obtained by

$$\hat{\bar{x}}(z,t) = \Psi^T(z) \ x_m(t), \tag{6.15}$$

where $\Psi = [\psi_1 \ \psi_2 \ \dots \ \psi_r]^T$, $\Phi_s = [\phi_1 \ \phi_2 \ \dots \ \phi_\alpha]^T$; r is the number of empirical basis functions of the slow subsystem that is computed using APOD and α is the number of analytical basis functions of the slow subsystem. Note that we do not require Φ_s for the implementation of the proposed method, we need it just for the stability and performance analysis.

After the fast dynamics have relaxed, i.e. $x_f \to 0$, the model error can not be defined directly by the simple subtraction, $x_s - x_m$ because the dimension of the system slow modes, x_s and APOD-based modes, x_m, in (6.13) is not necessarily the same since the number of identified slow subsystem basis functions Φ_s and Ψ can be different. Thus, we need a transformation to project one subspace to other and define the projected error.

Assumption 6.3. *Consider the local subspace of the slow and unstable modes,* $\mathbb{W}_s \triangleq span\{\phi_i\}_{i=1}^\alpha$ *and subspace* $\mathbb{P}$ *defined as* $\mathbb{P} \triangleq span\{\psi_i\}_{i=1}^r$, *where* $\{\phi_i\}_{i=1}^\alpha$ *is the set of analytical basis functions of the slow subsystem (which are unavailable) and* $\{\psi_i\}_{i=1}^r$ *is the set of empirical basis functions (computed based on APOD). The complement subspace of* $\mathbb{P}$ *can also be defined as* $\mathbb{Q} \triangleq span\{\psi_i\}_{i=r+1}^\infty$. *We assume that* $\mathbb{W}_s \subseteq \mathbb{P}$, *locally.*

Note that Assumption 6.3 is justified based on the excitation of the higher modes and reordering of the modes during the closed-loop process evolution. The problem with linear systems is that due to sub-sampling the empirical basis functions and modes may not be properly ordered. One solution to bridge slow Sobolev

subspace $\mathbb{W}_s$ and subspace $\mathbb{P}$ is by defining a bounded mapping between these two subspaces to find the corresponding states. The map should be defined as a linear transformation that changes at ROM revisions to conserve all of the subspaces' properties during system evolution. Then, from (6.15) we can define a bounded map between two subspaces, $\mathbb{W}_s$ and $\mathbb{P}$ as follows

$$\bar{x}_s = \Phi_s^T x_s = \Psi^T \mathcal{M} x_s = \Psi^T x_p, \tag{6.16}$$

where $x_p = \mathcal{M} x_s$, $\mathcal{M} : \mathbb{W}_s \mapsto \mathbb{P}$ and

$$\mathcal{M} = (\Psi^T, \Phi_s^T). \tag{6.17}$$

Note that $\mathcal{M} : \mathbb{W}_s \mapsto \mathbb{P}$, is injective due to the fact that subspace $\mathbb{P}$ contains subspace $\mathbb{W}_s$. Then $x_{p,1} = x_{p,2}, \forall x_{p,1}, x_{p,2} \in \mathbb{P}$ implies that $x_{s,1} = x_{s,2}, \forall x_{s,1}, x_{s,2} \in \mathbb{W}_s$. To complete the analysis, the bounded reverse map can be defined as $\mathcal{M}^{\perp} = (\Phi_s^T, \Psi^T)$, $\mathcal{M}^{\perp} : \mathbb{P} \mapsto \mathbb{W}_s$ such that $\mathcal{I} = \mathcal{M}^{\perp}\mathcal{M} : \mathbb{W}_s \mapsto \mathbb{W}_s$ is a bijective map. An interesting fact about this transformation is that $\mathcal{M}^{\perp} = \mathcal{M}^T$.

Using the above transformation, the system modes of the process slow dynamics in (6.13) can be expressed using the basis functions of subspace $\mathbb{P}$ in the following form

$$\dot{x}_p = A_p x_p + B_p u, \tag{6.18}$$

where $A_p = \mathcal{M} A_s \mathcal{M}^{\perp}$ and $B_p = \mathcal{M} B_s$.

Now we can define the error based on the difference between states of the process of (6.18) and the model of (6.13) as follows

$$e = x_p - x_m. \tag{6.19}$$

Then the reduced system dynamics can be obtained for $t \in [t_i, t_{i+1}]$ in terms of process and error state

$$\begin{cases} \dot{x}_p = (A_p + B_p \tilde{K})x_p - (B_p \tilde{K})e \\ \dot{e} = (A_e + B_e \tilde{K})x_p + (A_m - B_e \tilde{K})e \end{cases} \tag{6.20}$$

where the model is revised every δ_t seconds based on the state profile information from spatially distributed sensors at t_i , i.e. $e(t_i) = 0$ and we have $\delta_t = t_{i+1} - t_i$. $A_e = A_p - A_m$ and $B_e = B_p - B_m$ are the modeling error matrices that represent the difference between plant and model structures. In linear systems, the only reason for system deviation can be the modeling error due to sampling which causes an erroneous ordering of the empirical basis functions; basically the empirical eigenvalues have significant deviation from the operator eigenvalues. Once the model starts diverging from the system, APOD revises it.

Defining $x = \begin{bmatrix} x_p \\ e \end{bmatrix}$, the system of (6.20) can be summarized as the following networked system

$$\dot{x} = \mathcal{G}x, \tag{6.21}$$

where $\mathcal{G} = \begin{bmatrix} A_p + B_p\tilde{K} & -B_p\tilde{K} \\ A_e + B_e\tilde{K} & A_m - B_e\tilde{K} \end{bmatrix}$ and $x(t_i) = \begin{bmatrix} x_p(t_i) \\ 0 \end{bmatrix}$ for $t \in [t_i, t_{i+1}]$. Now we can derive the criteria for stability of the networked system.

Proposition 6.1. *The system of (6.21) with the initial condition of $x_0 = x(t_0) = \begin{bmatrix} x_p(t_0) \\ 0 \end{bmatrix}$ has the following solution*

$$x(t) = e^{\mathcal{G}(t-t_i)}\mathcal{S}^i x_0, \tag{6.22}$$

where $\mathcal{S} = \begin{bmatrix} I & 0 \\ 0 & 0 \end{bmatrix} e^{\mathcal{G}\delta_t} \begin{bmatrix} I & 0 \\ 0 & 0 \end{bmatrix}$ *and* $t \in [t_i, t_{i+1}]$ *(Proposition 1 in [188]).*

Proof *See Appendix A.4.1 for proof of the proposition.*

To proceed we need to analyze the global exponential stability of the system around the origin. The necessary and sufficient conditions for the system to be stable are identified in the following theorem.

Theorem 6.1. *The solution of the system of (6.21) is globally exponentially stable in the neighborhood of $x = \begin{bmatrix} 0 \\ 0 \end{bmatrix}$ if and only if the eigenvalues of*

$$\mathcal{S} = \begin{bmatrix} I & 0 \\ 0 & 0 \end{bmatrix} e^{\mathcal{G}\delta_t} \begin{bmatrix} I & 0 \\ 0 & 0 \end{bmatrix}$$

are inside the unit circle (Theorem 1 in [188]).

Proof *See Appendix A.4.2 for proof of the theorem.*

By defining the transformation matrix, $M_{tr} = \begin{bmatrix} I & 0 \\ I & -I \end{bmatrix}$, we obtain

$$\mathcal{G}^* = M_{tr}\mathcal{G}M_{tr}^{-1} = \begin{bmatrix} A_p & B_p\tilde{K} \\ 0 & A_m + B_m\tilde{K} \end{bmatrix}. \tag{6.23}$$

Then from (6.23) and the definition of matrix $\mathcal{S}$ we conclude

$$\mathcal{S} = \begin{bmatrix} I & 0 \\ 0 & 0 \end{bmatrix} e^{\mathcal{G}\delta_t} \begin{bmatrix} I & 0 \\ 0 & 0 \end{bmatrix} = \begin{bmatrix} I & 0 \\ 0 & 0 \end{bmatrix} M_{tr}^{-1} e^{\mathcal{G}^*\delta_t} M_{tr} \begin{bmatrix} I & 0 \\ 0 & 0 \end{bmatrix}$$

$$= \begin{bmatrix} I & 0 \\ 0 & 0 \end{bmatrix} e^{\mathcal{G}^*\delta_t} \begin{bmatrix} I & 0 \\ I & 0 \end{bmatrix}. \tag{6.24}$$

If we consider the Laplace transformation of matrix $\mathcal{S}$ we obtain

$$\mathcal{L}\{\mathcal{S}\} = \begin{bmatrix} I & 0 \\ 0 & 0 \end{bmatrix} \mathcal{L}\{e^{\mathcal{G}^*\delta_t}\} \begin{bmatrix} I & 0 \\ I & 0 \end{bmatrix}$$

$$= \begin{bmatrix} (sI - A_p)^{-1} + (sI - A_p)^{-1}B_p\tilde{K}(sI - A_m - B_m\tilde{K})^{-1} & 0 \\ 0 & 0 \end{bmatrix}, \tag{6.25}$$

and only the element of $(sI - A_p)^{-1} + (sI - A_p)^{-1}B_p\tilde{K}(sI - A_m - B_m\tilde{K})^{-1}$ has

non-zero eigenvalues. By inverse Laplace transformation we obtain

$$\mathcal{L}^{-1}\big\{(sI - A_p)^{-1} + (sI - A_p)^{-1}B_p\tilde{K}(sI - A_m - B_m\tilde{K})^{-1}\big\}$$

$$= \mathcal{L}^{-1}\big\{(sI - A_p)^{-1}(sI - A_m - B_m\tilde{K} + B_p\tilde{K})(sI - A_m - B_m\tilde{K})^{-1}\big\}$$

$$= \mathcal{L}^{-1}\big\{(sI - A_p)^{-1}(sI - A_p + A_e + B_e\tilde{K})(sI - A_m - B_m\tilde{K})^{-1}\big\}$$

$$= \mathcal{L}^{-1}\big\{\big(I + (sI - A_p)^{-1}(A_e + B_e\tilde{K})\big)(sI - A_m - B_m\tilde{K})^{-1}\big\}$$

$$= \mathcal{L}^{-1}\big\{(sI - A_m - B_m\tilde{K})^{-1} + (sI - A_p)^{-1}(A_e + B_e\tilde{K})(sI - A_m - B_m\tilde{K})^{-1}\big\}$$

$$= e^{(A_m + B_m\tilde{K})\delta_t} + e^{A_p\delta_t}\int_0^{\delta_t} e^{-A_p t}(A_e + B_e\tilde{K})e^{(A_m + B_m\tilde{K})t}dt.$$

Then the nonzero eigenvalues of matrix $\mathcal{S}$ are the eigenvalues of matrix [188]

$$\mathcal{N} = e^{(A_m + B_m\tilde{K})\delta_t} + e^{A_p\delta_t}\int_0^{\delta_t} e^{-A_p t}(A_e + B_e\tilde{K})e^{(A_m + B_m\tilde{K})t}dt, \qquad (6.26)$$

where $\mathcal{N}$ consists of two parts; the major term, $\mathcal{N}_m = e^{(A_m + B_m\tilde{K})\delta_t}$, and the perturbation term, $\mathcal{N}_e = e^{A_p\delta_t}\int_0^{\delta_t} e^{-A_p t}(A_e + B_e\tilde{K})e^{(A_m + B_m\tilde{K})t}dt$. The eigenvalues of $\mathcal{N}$ should be placed in a unit circle to satisfy the closed-loop stability requirement. The perturbation term depends on the updating period for snapshots (time interval between ROM revisions), δ_t, and the model mismatch. Also based on (6.26) we conclude that δ_t for a process depends on the controller gain, locations of the actuators and the model mismatch. Then we can ensure $\mathcal{N}_e \ll \mathcal{N}_m$ by choosing small values for δ_t or using more accurate models.

One way to find a criteria for δ_t based on closed-loop stability is by assuming an upper bound for the uncertain term as follows

$$\left\|\lambda^{max}\{\mathcal{N}_e\}\right\|_2 \leq \sigma, \tag{6.27}$$

where $\lambda^{max}(\cdot)$ denotes the maximum eigenvalue of matrix $(\cdot)$ and σ is a small positive number. From Theorem 6.1, Eqs. (6.24)-(6.26) and triangular inequality we obtain

$$\left\|\lambda^{max}\{\mathcal{N}_m + \mathcal{N}_e\}\right\|_2 \leq \left\|\lambda^{max}\{\mathcal{N}_m\}\right\|_2 + \left\|\lambda^{max}\{\mathcal{N}_e\}\right\|_2 < 1. \tag{6.28}$$

Using (6.27), we have

$$\left\|\lambda^{max}\{\mathcal{N}_m\}\right\|_2 = \left\|\lambda^{max}\{e^{(A_m+B_m\tilde{K})\delta_t}\}\right\|_2 < 1 - \sigma. \tag{6.29}$$

Finally, the above inequality can be presented as follows,

$$\log_{10}\left(\left\|\lambda^{max}\{e^{(A_m+B_m\tilde{K})\delta_t}\}\right\|_2\right) < \log_{10}(1 - \sigma) < 0. \tag{6.30}$$

Then by tracking λ^{max} for different values of δ_t, the δ_t values can be found that satisfy the system closed-loop stability. Note that considering $\log_{10}\left(\left\|\lambda^{max}\{\mathcal{N}_m\}\right\|_2\right) < 0$ gives us an idea of δ_t values for the error-free case.

Another approach to identify an upper bound for δ_t considering closed-loop

stability can be presented by setting upper bounds for open-loop and closed-loop

model uncertainty. We know that for matrix $\mathcal{N}$,

$$\left\| \lambda^{max}\{\mathcal{N}\} \right\|_2 \leq \sigma^{max}\{\mathcal{N}\} = \left\| \mathcal{N} \right\|_2, \tag{6.31}$$

where $\sigma^{max}(\cdot)$ denotes the maximum singular value of matrix $(\cdot)$. Then using (6.26)

we obtain

$$
\begin{aligned}
\left\| \mathcal{N} \right\|_2 &= \left\| e^{(A_m + B_m \tilde{K})\delta_t} + e^{A_p \delta_t} \int_0^{\delta_t} e^{-A_p t}(A_e + B_e \tilde{K})e^{(A_m + B_m \tilde{K})t} dt \right\|_2 \\
&\leq \left\| e^{(A_m + B_m \tilde{K})\delta_t} \right\|_2 + \left\| e^{A_p \delta_t} \int_0^{\delta_t} e^{-A_p t}(A_e + B_e \tilde{K})e^{(A_m + B_m \tilde{K})t} dt \right\|_2.
\end{aligned}
\tag{6.32}
$$

From this point we consider two cases based on the stability or instability of the

open-loop process:

Case I. open-loop process is unstable.

$$
\begin{aligned}
&\left\| e^{(A_m + B_m \tilde{K})\delta_t} \right\|_2 + \left\| e^{A_p \delta_t} \int_0^{\delta_t} e^{-A_p t}(A_e + B_e \tilde{K})e^{(A_m + B_m \tilde{K})t} dt \right\|_2 \\
&\leq \left(\left\| e^{A_m^{cl}} \right\|_2 \right)^{\delta_t} + e^{\tilde{\sigma}_1 \delta_t} \left\| \int_0^{\delta_t} e^{-A_p t} \| A_e + B_e \tilde{K} \|_2 e^{(A_m + B_m \tilde{K})t} dt \right\|_2 \\
&\leq \left(\left\| e^{A_m^{cl}} \right\|_2 \right)^{\delta_t} + e^{\tilde{\sigma}_1 \delta_t} \left(\tilde{\sigma}_1 + \| A_m \|_2 + (\tilde{\sigma}_2 + \| B_m \|_2) \| \tilde{K} \|_2 \right) \left\| \int_0^{\delta_t} e^{(A_m^{cl} - A_p)t} dt \right\|_2 \\
&= \left(\left\| e^{A_m^{cl}} \right\|_2 \right)^{\delta_t} + \Sigma \frac{e^{\tilde{\sigma}_1 \delta_t}}{\| A_m + B_m \tilde{K} - A_p \|_2} \left\| e^{(A_m^{cl} - A_p)\delta_t} - 1 \right\|_2 \\
&\leq \left(\left\| e^{A_m^{cl}} \right\|_2 \right)^{\delta_t} + \Sigma \frac{e^{\tilde{\sigma}_1 \delta_t}}{\left| \| A_m^{cl} \|_2 - \tilde{\sigma}_1 \right|} \left\| e^{(A_m^{cl} - A_p)\delta_t} - 1 \right\|_2 < 1
\end{aligned}
\tag{6.33}
$$

where $A_m^{cl} = A_m + B_m\tilde{K}$, $\|A_p\|_2 \leq \tilde{\sigma}_1$, $\|B_p\|_2 \leq \tilde{\sigma}_2$ and $\Sigma = \tilde{\sigma}_1 + \|A_m\|_2 + (\tilde{\sigma}_2 + \|B_m\|_2)\|\tilde{K}\|_2$. If we assume that $e^{(A_m^{cl}-A_p)\delta_t} \approx 0$ (from the fact that the open-loop process is unstable and by designing the controller gain), we obtain

$$\left(\left\|e^{A_m^{cl}}\right\|_2\right)^{\delta_t} + \Sigma\frac{e^{\tilde{\sigma}_1\delta_t}}{\left|\|A_m^{cl}\|_2 - \tilde{\sigma}_1\right|} < 1$$

$$\Rightarrow \delta_t\left[\ln\left(\left\|e^{A_m^{cl}}\right\|_2\right) + \tilde{\sigma}_1\right] + \ln(\Sigma) - \ln\left(\left|\|A_m^{cl}\|_2 - \tilde{\sigma}_1\right|\right) < 0 \qquad (6.34)$$

$$\Rightarrow \delta_t < \frac{\ln\left(\left|\|A_m^{cl}\|_2 - \tilde{\sigma}_1\right|/\Sigma\right)}{\ln\left(\left\|e^{A_m^{cl}}\right\|_2\right) + \tilde{\sigma}_1} = \delta_t^*$$

Case II. open-loop process is stable.

$$\left\|e^{(A_m^{cl})\delta_t}\right\|_2 + \left\|e^{A_p\delta_t}\int_0^{\delta_t} e^{-A_pt}(A_e + B_e\tilde{K})e^{(A_m+B_m\tilde{K})t}dt\right\|_2$$

$$\leq \left(\left\|e^{A_m^{cl}}\right\|_2\right)^{\delta_t} + \tilde{\sigma}_3\left\|\int_0^{\delta_t} e^{-A_pt}\|A_e + B_e\tilde{K}\|_2 e^{(A_m^{cl})t}dt\right\|_2 \qquad (6.35)$$

$$\leq \left(\left\|e^{A_m^{cl}}\right\|_2\right)^{\delta_t} + \Sigma\frac{\tilde{\sigma}_3}{\left|\|A_m^{cl}\|_2 - \tilde{\sigma}_1\right|}\left\|e^{(A_m^{cl}-A_p)\delta_t} - 1\right\|_2 < 1$$

where $\left\|e^{A_p\delta_t}\right\|_2 \leq \tilde{\sigma}_3$. If we assume that $e^{(A_m^{cl}-A_p)\delta_t} \approx 0$ (by designing the controller

gain), we obtain

$$
\left(\left\|e^{A_m^{cl}}\right\|_2\right)^{\delta_t} + \frac{\Sigma\tilde{\sigma}_3}{\left|\|A_m^{cl}\|_2 - \tilde{\sigma}_1\right|} < 1
$$

$$
\Rightarrow \delta_t \ln\left(\left\|e^{A_m^{cl}}\right\|_2\right) + \ln(\Sigma\tilde{\sigma}_3) - \ln\left(\left|\|A_m^{cl}\|_2 - \tilde{\sigma}_1\right|\right) < 0 \tag{6.36}
$$

$$
\Rightarrow \delta_t < \frac{\ln\left(\left|\|A_m^{cl}\|_2 - \tilde{\sigma}_1\right|/(\Sigma\tilde{\sigma}_3)\right)}{\ln\left(\left\|e^{A_m^{cl}}\right\|_2\right)} = \delta_t^{**}
$$

Theorem 6.2. *Consider the dissipative, input-affine, linear PDE system of (6.1) for which Assumptions 6.1-6.2 always hold and Assumption 6.3 holds for finite periods between revisions. Also consider the infinite dimensional representation of (6.5) and finite dimensional approximation of (6.12) in subspace $\mathbb{P}$ with APOD-based empirical basis functions. Under Assumptions of 6.1-6.3, the networked control strategy asymptotically stabilizes the system of (6.1) when the time interval between ROM updates, δ_t, is finite and larger than a critical value, t_b.*

Proof *See Appendix A.4.3 for proof of the theorem.*

In Figure 6.1 the closed-loop process is presented under the proposed control structure in a block diagram form.

Remark 6.5. *Using the concept of settling time for linear systems we can relax the assumption of absence of $O(\frac{1}{\gamma})$ in the controller term and obtain a conservative estimate of t_b without considering singular perturbations arguments. The solution*
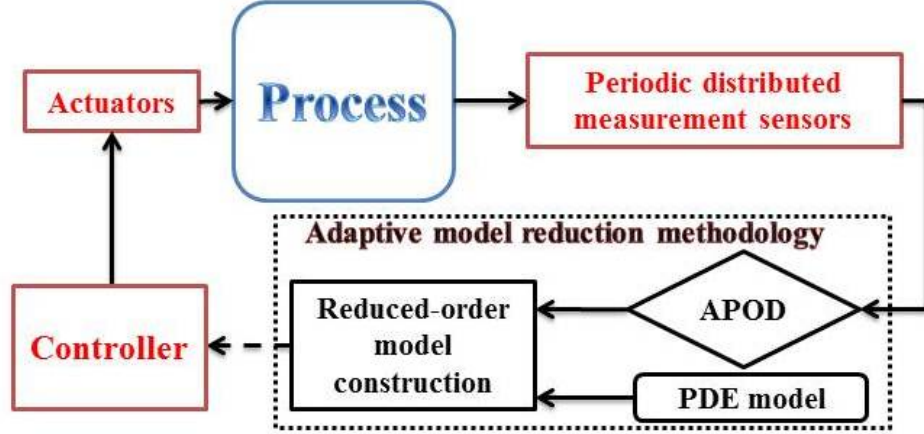
Figure 6.1: Process operation block diagram under proposed controller structure. Red signifies the controller system.

of fast mode dynamics of the system can be presented as,

$$\dot{x}_f = A_f x_f + B_f \tilde{K} x_m \Rightarrow x_f(t) = e^{A_f t} x_f(0) + \int_0^t e^{A_f(t-s)} B_f \tilde{K} x_m ds.$$

We can find the final value of the fast modes as follows,

$$\lim_{t \to \infty} x_f = x_{f,ss} = -A_f^{-1} B_f \tilde{K} x_m.$$

Considering the settling time when the fast modes of the system reach within a 1% region of their final value, we obtain

$$\left| \frac{\|x_f(t_b)\|_2 - \|x_{f,ss}\|_2}{\|x_{f,ss}\|_2} \right| \le 0.01.$$

Using triangular inequality we can simplify the inequality as follows,

$$\left| \frac{\|x_f(t_b)\|_2 - \|x_{f,ss}\|_2}{\|x_{f,ss}\|_2} \right| \leq \frac{\|x_f(t_b) - x_{f,ss}\|_2}{\|x_{f,ss}\|_2} \leq 0.01.$$

From the above inequality we obtain,

$$\frac{\left\| e^{A_f t_b} x_f(0) + \int_0^{t_b} e^{A_f(t_b - T)} B_f \tilde{K} x_m dT + A_f^{-1} B_f \tilde{K} x_m \right\|_2}{\|A_f^{-1} B_f \tilde{K} x_m\|_2} \leq 0.01.$$

If we assume that x_m does not change sharply during the time period of $[0, t_b]$ then by using Cauchy-Schwarz and triangular inequalities we can simplify the problem as follows,

$$\frac{\left\| e^{A_f t_b} x_f(0) + \int_0^{t_b} e^{A_f(t_b - T)} B_f \tilde{K} x_m dT + A_f^{-1} B_f \tilde{K} x_m \right\|_2}{\|A_f^{-1} B_f \tilde{K} x_m\|_2}$$

$$= \frac{\left\| e^{A_f t_b} x_f(0) + \left(\int_0^{t_b} e^{A_f(t_b - T)} dT \right) B_f \tilde{K} x_m + A_f^{-1} B_f \tilde{K} x_m \right\|_2}{\|A_f^{-1} B_f \tilde{K} x_m\|_2}$$

$$= \frac{\left\| e^{A_f t_b} \left(x_f(0) + A_f^{-1} B_f \tilde{K} x_m \right) \right\|_2}{\|A_f^{-1} B_f \tilde{K} x_m\|_2}$$

$$\leq \frac{\|e^{A_f t_b}\|_2 \left(\|x_f(0)\|_2 + \|A_f^{-1} B_f \tilde{K} x_m\|_2 \right)}{\|A_f^{-1} B_f \tilde{K} x_m\|_2} \leq 0.01.$$

Now we can solve the above inequality for t_b,

$$\|e^{A_f t_b}\|_2 \left(\frac{\|x_f(0)\|_2}{\|A_f^{-1} B_f \tilde{K} x_m\|_2} + 1 \right) \leq 0.01 \Rightarrow \|e^{A_f t_b}\|_2 \leq \frac{0.01}{\frac{\|x_f(0)\|_2}{\|A_f^{-1} B_f \tilde{K} x_m\|_2} + 1}$$

$$\Rightarrow e^{-\|\lambda_{\alpha+1}\|_2 t_b} \leq \frac{0.01}{\frac{\|x_f(0)\|_2}{\|A_f^{-1} B_f \tilde{K} x_m\|_2} + 1}$$

$$\Rightarrow t_b \geq \frac{1}{\|\lambda_{\alpha+1}\|_2} \left[4.605 + \ln \left(\frac{\|x_f(0)\|_2}{\|A_f^{-1} B_f \tilde{K} x_m\|_2} + 1 \right) \right].$$

Remark 6.6. *The maximum allowable time interval between snapshots being communicated from the periodic spatially distributed measurement sensors to the model reduction and control structure is less than*

(a) the minimum time interval from (6.30) and δ_t^* for unstable open-loop process,

(b) the minimum time interval from (6.30) and δ_t^{**} for stable open-loop process.

Remark 6.7. *To identify the criterion presented in (6.30), (6.34) and (6.36), we have to find an upper bound for process operators, A_p and B_p, otherwise we can not determine criteria for δ_t. Considering $A_p = A_e + A_m$ and $B_p = B_e + B_m$ we obtain that $\|A_p\|_2 \leq \|A_e\|_2 + \|A_m\|_2$ and $\|B_p\|_2 \leq \|B_e\|_2 + \|B_m\|_2$. Note that the upper bounds of modeling error operators, $\|A_e\|_2$ and $\|B_e\|_2$, always converge to small neighborhood around zero by using recursive POD methods (like APOD) during process evolution as more dynamical modes of the system are excited. Thus, an approximate upper bound of $\|A_e\|_2$ and $\|B_e\|_2$ can be obtained via subspace $\mathbb{Q}$. Then we may implement the summation of upper bounds of the empirical and*

modeling error operators in (6.30), (6.34) and (6.36), specifically for diffusion-reaction processes when the fast modes of the system converges to zero after a short period of time.

Remark 6.8. *Based on the presented analysis one may encounter cases when $t_b > \delta_t^*$ which implies that the proposed procedure can not be used to regulate the system. This hurdle is surpassed by increasing ξ in APOD [203] which increases the dimensionality of the slow system and thus considers faster settling times, t_b.*

Remark 6.9. *For finite periods longer than the critical period of t_b, basis functions of the slow subsystem belong in $\mathbb{P} \oplus \mathbb{Q}$. The relative significance of the empirical eigenvalues is a strong indicator that the slow subsystem is included in $\mathbb{P} \oplus \mathbb{Q}$. Assumption 6.3 has two restrictions; the snapshot frequency is considered to be of the same order as magnitude of the dominant dynamics frequency and the slow dynamics are sufficiently excited [256]. The appearance of new trends in the system dynamics during process evolution is the main reason that Assumption 6.3 conditions are violated because they make the empirical basis functions and ROM inaccurate. When the conditions of this assumption are violated the APOD algorithm revises the set of empirical basis functions and modifies the ROM. Furthermore, the controller is redesigned to retain relevancy. Such "corrections" will always be repeated at revision times to enforce closed-loop stability.*
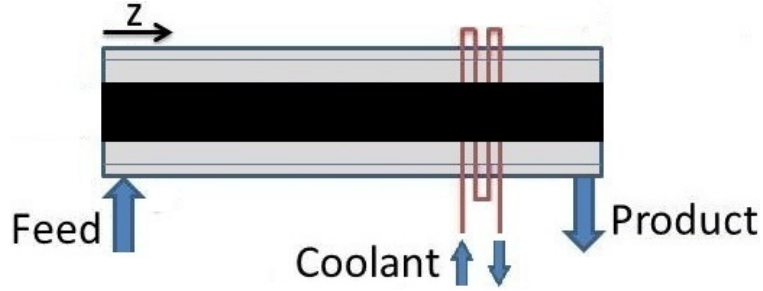
Figure 6.2: Tubular chemical reactor with cooling spiral at $z = 0.75L$.

6.1.4 Simulation results

In this section, the proposed method is illustrated on temperature regulation of a tubular reactor. We considered a tubular chemical reactor shown in Figure 6.2, where an irreversible exothermic reaction of zeroth order with reaction rate, R, took place and a cooling jacket was used to remove heat from the reactor. We assumed constant physical properties and considered only the temperature. We studied two cases; (1) constant reaction rate and (2) Arrhenius dependence of the reaction rate to temperature.

6.1.4.1 Constant reaction rate

We considered an energy balance along the reactor length where the reaction rate was constant, $R = R_0$, as follows

$$\frac{\partial T}{\partial t} = \frac{k}{\rho c_p} \frac{\partial^2 T}{\partial z^2} - \nu \frac{\partial T}{\partial z} + \frac{(-\Delta H)}{\rho c_p} R_0 - \frac{hA_s}{\rho c_p}\left(T - b(z)T_c\right), \tag{6.37}$$

with boundary conditions

$$z = 0 : \qquad \frac{\partial T}{\partial z} = \frac{\rho c_p \nu}{k}(T - T_f),$$

$$z = L : \qquad \frac{\partial T}{\partial z} = 0, \tag{6.38}$$

and initial condition

$$t = 0 : \qquad T = T_f. \tag{6.39}$$

In Eqs. (6.37)-(6.39), T is the reactor temperature, t is time and $z \in [0, L]$ is the spatial domain. k, ρ and c_p denote the thermal conductivity, density and heat capacity of the fluid inside the reactor, respectively. ν is the axial fluid velocity, h is heat transfer coefficient between the reactor and the cooling jacket and A_s is the surface area of the reactor walls. Also $b(z)$ describes the location of the cooling jacket and $(-\Delta H)$ denotes the heat of the reaction.

By considering the steady state temperature

$$\frac{k}{\rho c_p} \frac{\partial^2 T_{ss}}{\partial z^2} - \nu \frac{\partial T_{ss}}{\partial z} + \frac{(-\Delta H)}{\rho c_p} R_0 - \frac{h A_s}{\rho c_p}\left(T_{ss} - b(z)T_{c,ss}\right) = 0, \tag{6.40}$$

subject to the following boundary conditions

$$z = 0 : \qquad \frac{dT_{ss}}{dz} = \frac{\rho c_p \nu}{k}(T_{ss} - T_f),$$

$$z = L : \qquad \frac{dT_{ss}}{dz} = 0, \tag{6.41}$$

the following equations can be obtained from the system of (6.37)-(6.39)

$$\frac{\partial \bar{T}}{\partial \bar{t}} = \frac{1}{Pe} \frac{\partial^2 \bar{T}}{\partial \bar{z}^2} - \frac{\partial \bar{T}}{\partial \bar{z}} - \beta \bar{T} + \beta b(\bar{z}) u \tag{6.42}$$

$$\bar{z} = 0: \qquad \frac{\partial \bar{T}}{\partial \bar{z}} = Pe \bar{T},$$
$$\bar{z} = 1: \qquad \frac{\partial \bar{T}}{\partial \bar{z}} = 0, \tag{6.43}$$

$$\bar{t} = 0: \qquad \bar{T} = \bar{T}_f, \tag{6.44}$$

where the dimensionless variables and parameters are defined as follows

$$\bar{T} = \frac{T - T_{ss}}{T_{ss}}, \quad \bar{T}_f = \frac{T_f - T_{ss}}{T_{ss}}, \quad u = \frac{T_c - T_{c,ss}}{T_{ss}}, \quad \bar{z} = \frac{z}{L},$$
$$Pe = \frac{\rho c_p \nu L}{k}, \quad \beta = \frac{h A_s L}{\rho c_p \nu}, \quad \bar{t} = \frac{t\nu}{L}. \tag{6.45}$$

We considered $Pe = 7$, $\bar{T}_f = -0.3$ and $\beta = 2$ for the parameters in process system of (6.42)-(6.44). One control actuator was assumed to be available at $\mathcal{L}_a = 0.75$ in the spatial domain $\bar{z} = [0, 1]$ and the corresponding spatial distribution function at the actuator location was $b(\bar{z}) = \delta(\bar{z} - \mathcal{L}_a)$ that indicates point actuation ($\delta(\cdot)$ denotes the standard Dirac delta function). Figure 6.3 presents the steady state temperature where $T_f = 17^oC$, $T_{c,ss} = 27^oC$ and $\gamma = \frac{(-\Delta H)}{\rho c_p \nu} R_0 L = 15$. This temperature profile is the desired basis for the regulation problem.

As the availability of snapshots of the process is usually limited, in order to obtain δ_t, we initially simulated the open-loop process for the time period of $\bar{t} = [0, 2]$.
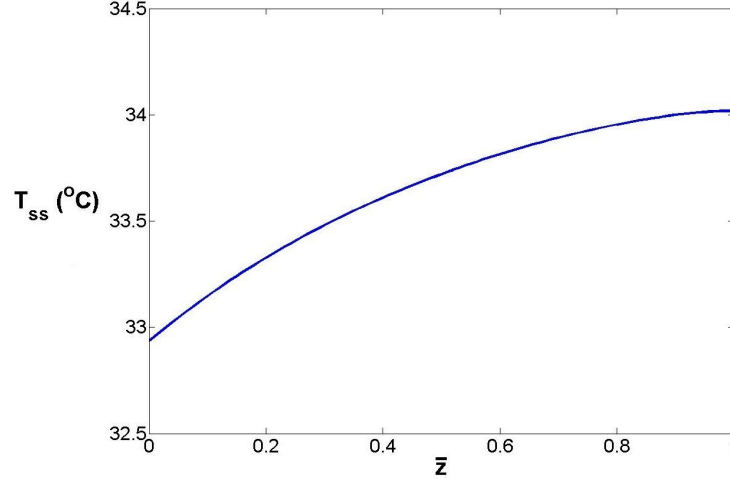
Figure 6.3: The desired spatial profile of steady state temperature.

We obtained 20 snapshots during this open-loop period, then we computed the initial basis functions by applying the off-line APOD to the ensemble of snapshots. This off-line procedure resulted in 2 empirical basis functions for $\bar{T}$ which captured 0.99 of the energy embedded in the ensemble. The APOD model was derived using the empirical basis functions and Galerkin's projection, i.e. A_m and B_m were obtained. Then we computed $t_b = 0.2$ from (A.57) and the open-loop simulation results. Note that t_b must be considered as a lower bound for δ_t. Considering $\sigma = 0.05$, the initial upper bound of δ_t was computed based on (6.30) where $\tilde{K} = 0$ ($\delta_t \leq 0.67$). We chose the initial value of δ_t using such lower and upper bounds.

During the closed-loop process evolution assuming $\|A_p\|_2 \approx \|A_m\|_2$ and $\|B_p\|_2 \approx \|B_m\|_2$, we set $\tilde{\sigma}_1 = \|A_m\|_2$ and $\tilde{\sigma}_2 = \|B_m\|_2$. Then we computed $\Sigma = \tilde{\sigma}_1 + \|A_m\|_2 + (\tilde{\sigma}_2 + \|B_m\|_2)\|\tilde{K}\|_2$. The parameter $\tilde{\sigma}_3$ was also adjusted at the value of 1 considering $\delta_t > 0$ and $\lambda(A_p) < 0$. The value of δ_t^{**} was computed from (6.36) (where the

smallest value of δ_t^{**} was equal to 0.63 as time evolved). The final value of δ_t at each revision was identified based on Remark 6 considering t_b as the lower bound.

Considering the above discussion we adjusted the sampling frequency of snapshots of the process at every $\delta_t = 0.5$ units of time during closed loop operation. This value satisfied all criteria. We can change δ_t during process evolution, however we only considered a constant value in this example for simplicity reasons. Figure 6.4 presents the temporal profile of closed-loop process and its 2-norm, respectively. We observe that the controller successfully stabilized the system of (6.42)-(6.44) at $\bar{T}(\bar{z}, \bar{t}) = 0$, since the process profile and its norm converged to zero without any peaking.

Figure 6.5 shows the temporal profile of required control action, the dominant mode estimated using APOD and the norm of error between the process and the ROM. To compute the controller gain we placed the first closed-loop pole at -5 (for $r = 1, 2$) and the second closed-loop pole at -7 (for $r = 2$). The control action converged to zero and we did not observe any chattering. The mode of the system converged to zero which illustrates the effectiveness of the proposed controller structure to stabilize the system. The success of the designed controller in regulating the process was due to the dominant subspace (hence the ROM and the control law) being updated as the process traverses through different regions of the state space during closed-loop operation. Figure 6.6 presents the change of number of basis functions. During the closed-loop process operation,
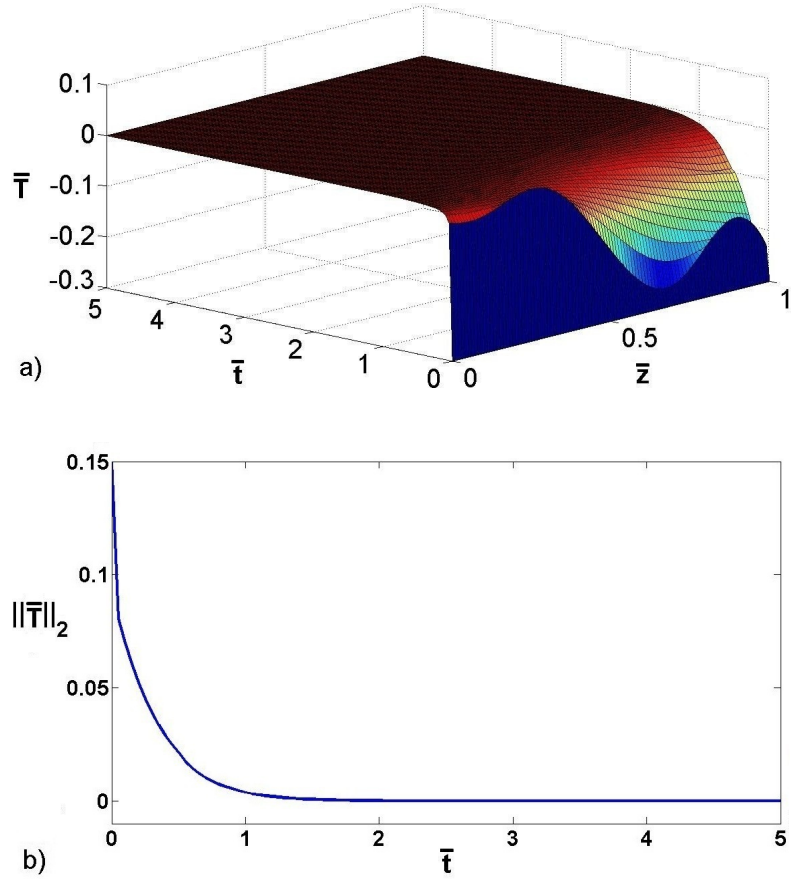
Figure 6.4: Closed-loop system temporal profile of (a) the deviation state spatial profile and (b) norm of the deviation state.

when new trends appeared the dominant subspace basis was updated to accurately capture the process behavior, appropriately changing the number of empirical basis functions. Note that the system is linear and there are no basic dynamic behavior changes; the only reason for changes in the ROM dynamics as time evolved was the erroneous ordering of the empirical basis functions since the specific modes can be locally close to zero during initial sampling. Figure 6.7 presents the temporal profile of the dominant empirical basis functions. Note that the second empirical
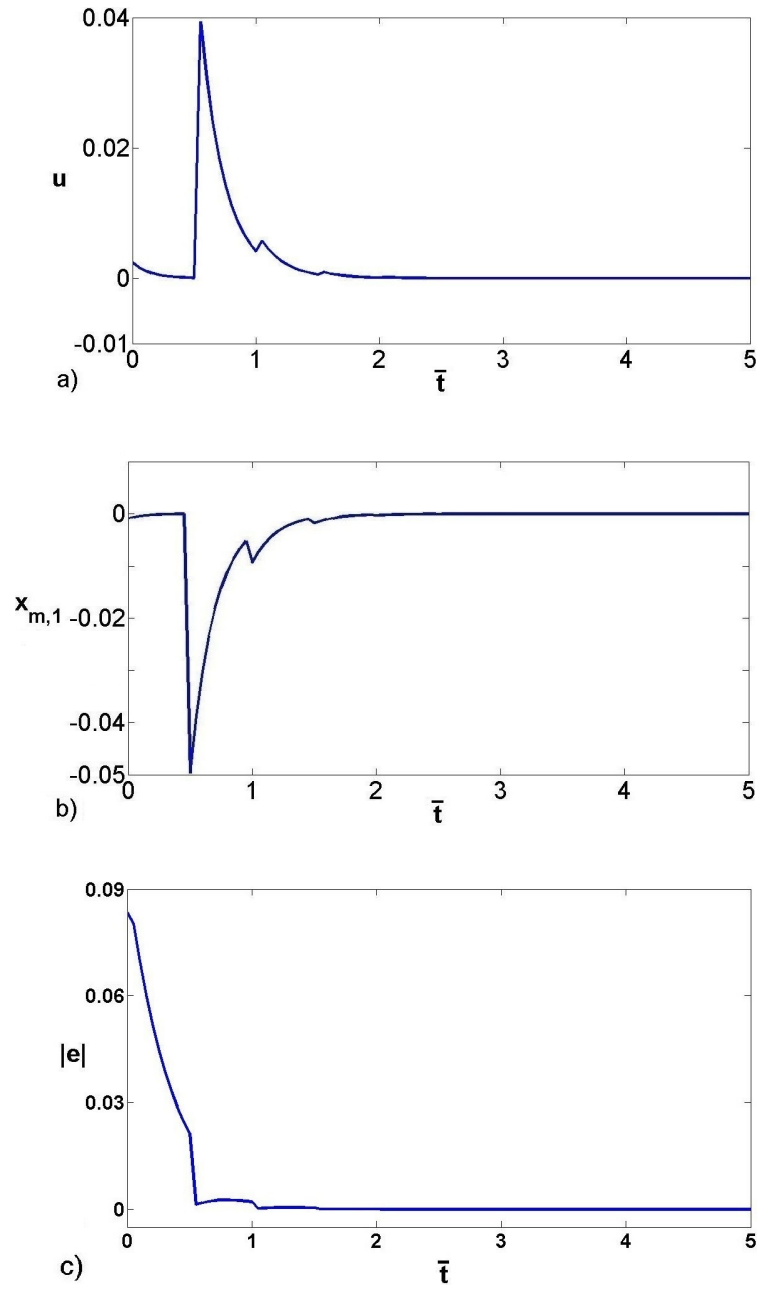
Figure 6.5: Temporal profile of (a) control action, (b) dominant estimated mode and (c) norm of error between the process and the ROM.
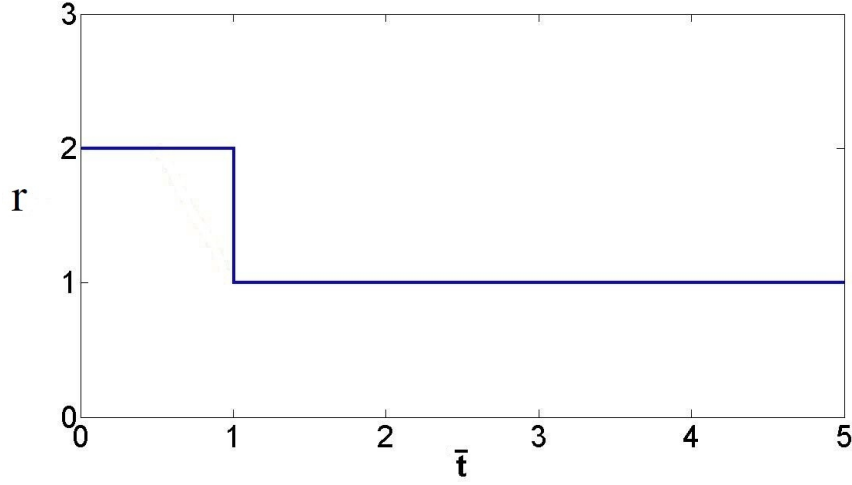
Figure 6.6: Number of basis functions.

basis function only existed during the time period of $[0, 1]$. It was observed that the basis function was adapting itself with the system during the process evolution.

There is always a trade-off between stability satisfaction and ROM revision load based on the value of δ_t. Larger values of δ_t reduce the computation load for ROM updates but lead to loss of closed-loop stability. Figure 6.8 compares the logarithmic temporal profiles of $\|\lambda^{max}\{\mathcal{N}_m\}\|_2$ for different values of δ_t. Based on the criteria of (6.29) for $\sigma = 0.05$ the value of δ_t that satisfies $\log_{10}\left(\|\lambda^{max}\{\mathcal{N}_m\}\|_2\right) \leq -0.02$ at steady state had to been chosen; this means the previously chosen value of δ_t satisfied the system closed-loop stability requirements.
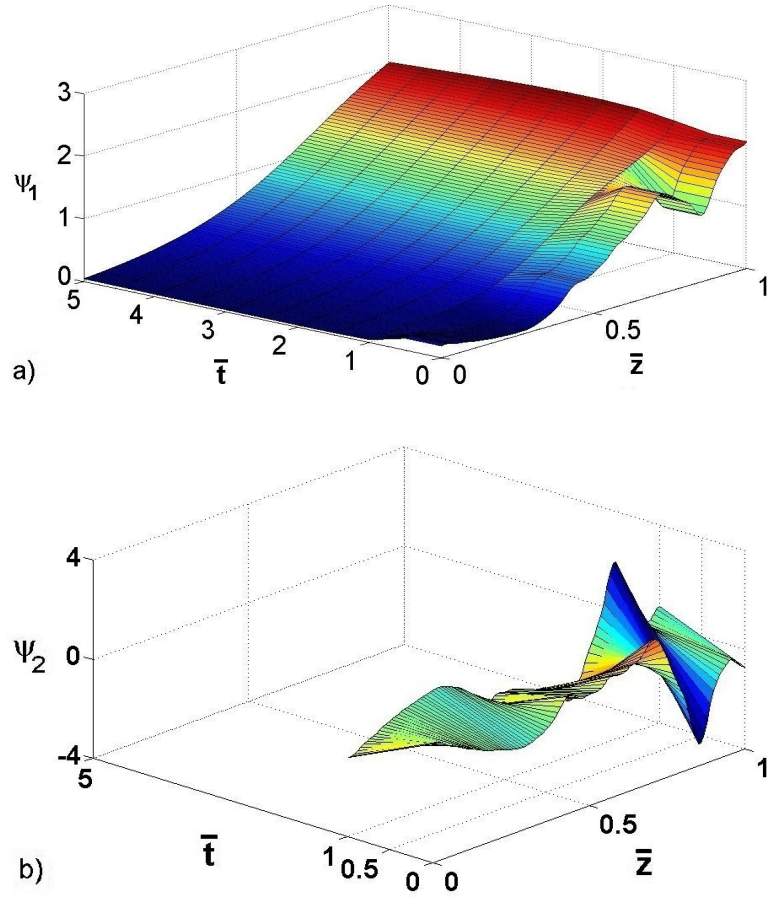
Figure 6.7: Temporal profile of the (a) first and (b) second empirical basis functions.
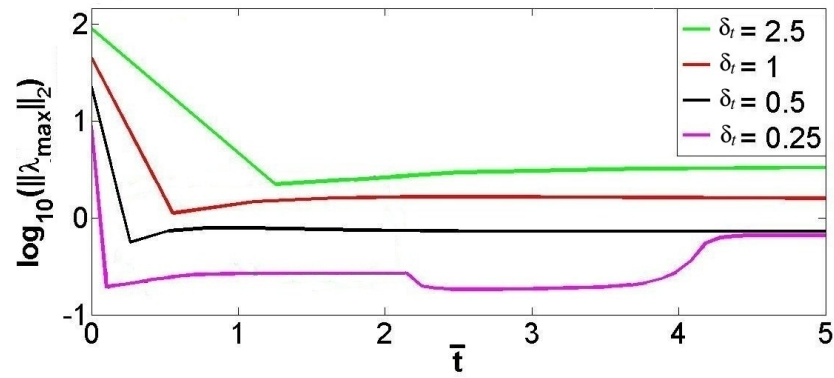
Figure 6.8: Temporal profile of absolute value of maximum characteristic eigenvalue for different ROM updating period times.

6.1.4.2 Temperature dependent reaction rate

To illustrate the importance of choosing the correct time interval for ROM revisions of open-loop unstable linearized DPSs we now focus on regulating the thermal dynamics in the same tubular reactor of the previous section when an irreversible exothermic reaction of zeroth order with Arrhenius temperature dependent reaction rate of $\tilde{R}_0 e^{-\frac{E}{RT}}$ takes place. The energy balance can then be presented in the following form,

$$\frac{\partial T}{\partial t} = \frac{k}{\rho c_p}\frac{\partial^2 T}{\partial z^2} - \nu\frac{\partial T}{\partial z} + \frac{(-\Delta H)}{\rho c_p}\tilde{R}_0 e^{-\frac{E}{RT}} - \frac{hA_s}{\rho c_p}\left(T - b(z)T_c\right), \qquad (6.46)$$

with the same boundary and initial conditions of (6.38)-(6.39), where E denotes the reaction activation energy and R is the universal gas constant. Considering the Taylor expansion of the nonlinear term, $e^{-\frac{E}{RT}}$, around an unstable steady state, T_{ss}, as

$$e^{-\frac{E}{RT}} \approx e^{-\frac{E}{RT_{ss}}}\left(1 + \frac{E}{RT_{ss}^2}(T - T_{ss})\right),$$

we obtained the linearized PDE system of

$$\begin{aligned}\frac{\partial T}{\partial t} &= \frac{k}{\rho c_p}\frac{\partial^2 T}{\partial z^2} - \nu\frac{\partial T}{\partial z} + \frac{(-\Delta H)}{\rho c_p}\tilde{R}_0 e^{-\frac{E}{RT_{ss}}}\left(1 + \frac{E}{RT_{ss}^2}(T - T_{ss})\right) \\ &\quad - \frac{hA_s}{\rho c_p}\left(T - b(z)T_c\right)\end{aligned} \qquad (6.47)$$

Accordingly, the spatial profile of the unstable steady state temperature took the following form

$$\frac{k}{\rho c_p}\frac{\partial^2 T_{ss}}{\partial z^2} - \nu\frac{\partial T_{ss}}{\partial z} + \frac{(-\Delta H)}{\rho c_p}\tilde{R}_0 e^{-\frac{E}{RT_{ss}}} - \frac{hA_s}{\rho c_p}\left(T_{ss} - b(z)T_{c,ss}\right) = 0, \qquad (6.48)$$

with respect to the same boundary conditions of (6.41). Then we derived the following dimensionless PDE from (6.47)-(6.48),

$$\begin{aligned}
\frac{\partial \bar{T}}{\partial \bar{t}} &= \frac{1}{Pe}\frac{\partial^2 \bar{T}}{\partial \bar{z}^2} - \frac{\partial \bar{T}}{\partial \bar{z}} + \hat{\beta}\bar{T} + \beta b(\bar{z})u \\
\bar{z} = 0: &\qquad \frac{\partial \bar{T}}{\partial \bar{z}} = Pe\bar{T}, \\
\bar{z} = 1: &\qquad \frac{\partial \bar{T}}{\partial \bar{z}} = 0, \\
\bar{t} = 0: &\qquad \bar{T} = \bar{T}_f,
\end{aligned} \qquad (6.49)$$

where

$$\hat{\beta} = \frac{(-\Delta H)}{\rho c_p \nu}\tilde{R}_0 L\frac{E}{RT_{ss}^2}e^{-\frac{E}{RT_{ss}}} - \beta$$

subject to the dimensionless variables and parameters of (6.45).

We considered the same set of operation parameters as in the previous section ($Pe = 7$, $\bar{T}_f = -0.3$ and $\beta = 2$). The reaction thermal source parameter was also considered as $\hat{\beta} = 1.5$ in the simulation. An analysis of the open-loop process behavior showed that the spatially uniform steady state was now unstable. As a result the control objective became to regulate the process at the spatially uniform

steady state of $\bar{T} = 0$.

A single actuator was assumed to be available at $\mathcal{L}_a = 0.75$ and the control and model order reduction (MOR) strategy was the same as previous section. In order to obtain δ_t, we initially simulated the open-loop process and computed the initial basis functions by applying the off-line APOD to the ensemble of snapshots. Then we obtained A_m and B_m from the APOD model. We thus computed the value of $t_b = 0.1$ from the open-loop simulation results. The initial upper bound of δ_t was computed based on (6.30) ($\delta_t \leq 0.52$). We chose the initial value of δ_t using such lower and upper bounds. During the closed-loop process evolution by assuming $\|A_p\|_2 \approx \|A_m\|_2$ and $\|B_p\|_2 \approx \|B_m\|_2$, we set $\tilde{\sigma}_1 = \|A_m\|_2$ and $\tilde{\sigma}_2 = \|B_m\|_2$. Then we computed $\Sigma = \tilde{\sigma}_1 + \|A_m\|_2 + (\tilde{\sigma}_2 + \|B_m\|_2)\|\tilde{K}\|_2$. The value of δ_t^* was computed from (6.34) (where the smallest value of δ_t^* was equal to 0.5 as time evolved). The final value of δ_t at each revision was identified based on Remark 6 considering t_b as the lower bound. We applied $\delta_t = 1$ as the initial time interval between sampling snapshots and we compared it to $\delta_t = 0.4$, that had been identified based on the criterion of (6.30) and (6.34). The controller structure performance for two different values of δ_t are presented in the figures 6.9-6.11. Figure 6.9 compares the closed-loop spatiotemporal behavior of the dimensionless temperature for the two applied time intervals. The temporal profiles of the closed-loop system 2-norm are presented in Figure 6.10, and Figure 6.11 shows the required control actions. We observe that the controller successfully stabilized the system of (6.49)
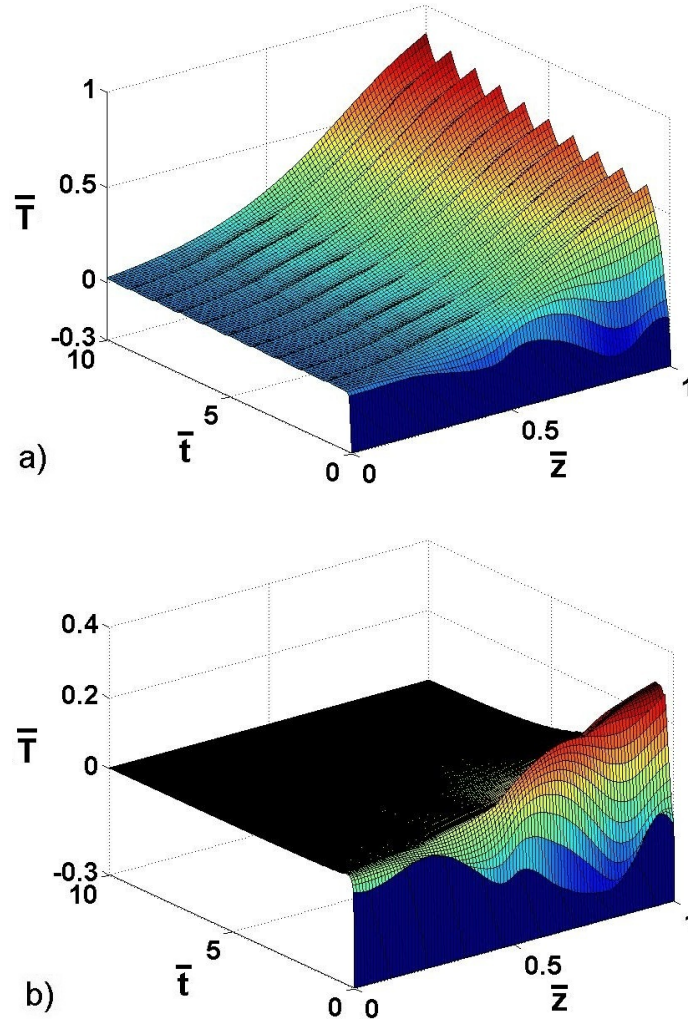
Figure 6.9: Closed-loop spatiotemporal profile of the system for (a) $\delta_t = 1$ and (b) $\delta_t = 0.4$.

at $\bar{T}(\bar{z}, \bar{t}) = 0$ when $\delta_t = 0.4$. We also observe that the sampling frequency of $\delta_t = 1$ was insufficient to stabilize the plan, and the process exhibited an oscillatory behavior far away from the desired steady state (shown in Figs. 6.9a and 6.10a). This was due to the control action (shown in Figure 6.11a) which was insufficient to drive the closed-loop system due to ROM inaccuracy.

The effectiveness of the proposed APOD-based control structure in stabilizing
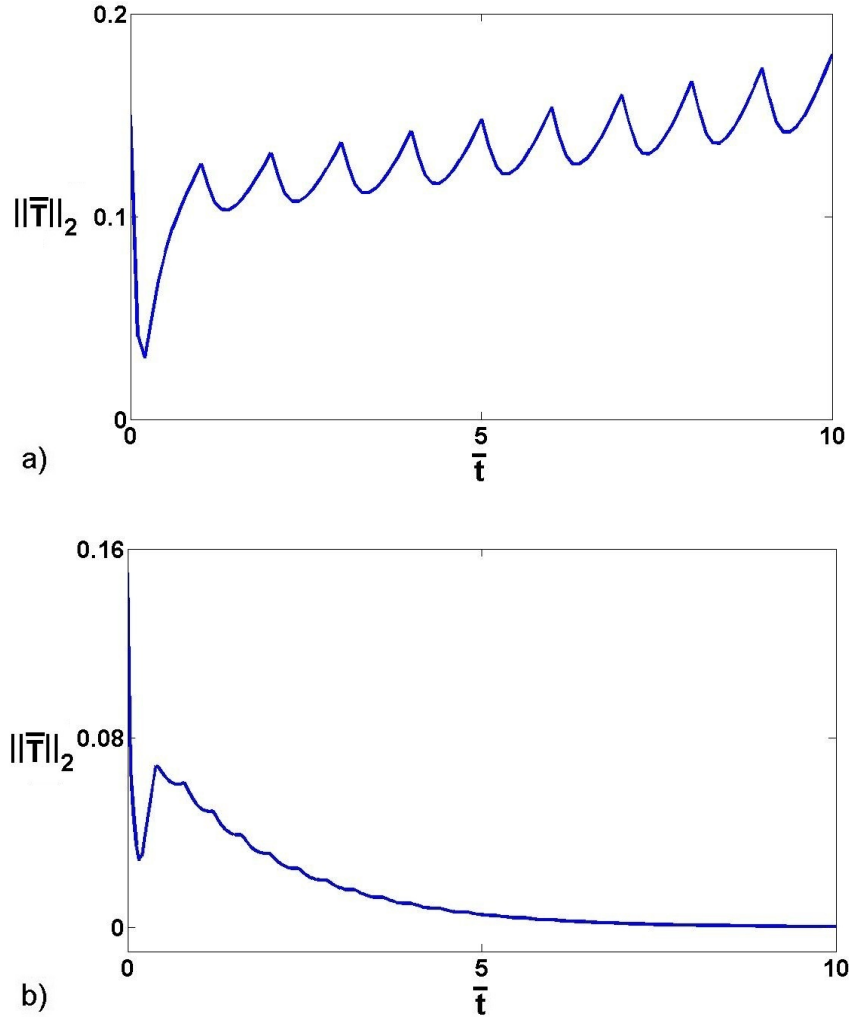
Figure 6.10: Closed-loop temporal profile of the system 2-norm for (a) $\delta_t = 1$ and (b) $\delta_t = 0.4$.

the linear process lies on the ROM revisions as the process passes through different regions of the state space domain. As we discussed in this chapter, such revisions had to be quite frequent to accurately capture the process behavior when new trends appeared during closed-loop operation.
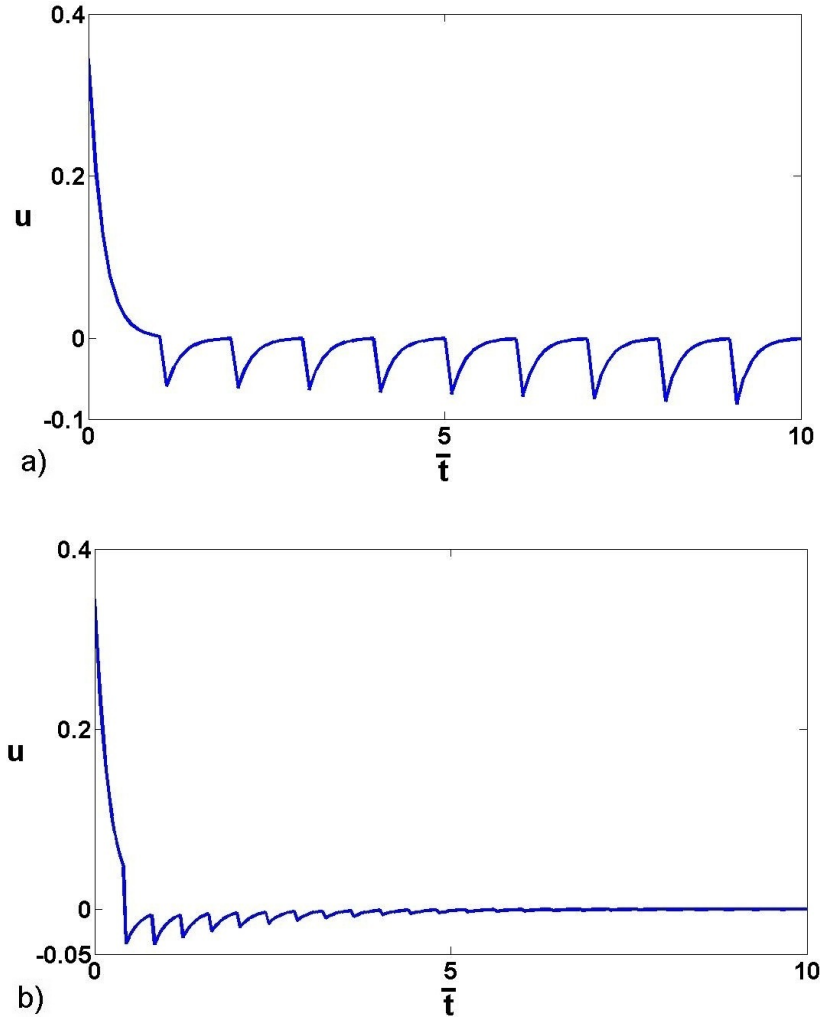
Figure 6.11: Temporal profile of required control action for (a) $\delta_t = 1$ and (b) $\delta_t = 0.4$.

6.2 Nonlinear systems

In this section we focus on algorithmic aspects of APOD-based output feedback control of highly dissipative DPS using Lyapunov direct method. To identify the minimum ROM revisions we monitor the value of a control Lyapunov function (CLF) as the process evolves. CLF is a quadratic function of system modes esti-

mated by a static observer. The static observer is applied due to unavailability of system modes direct measurements during the closed-loop process evolution. The Lyapunov stability theorem states that for the closed-loop system to be asymptotically stable, the CLF has to decrease during process evolution. We synthesize the controller based on the ROM to force the CLF to decrease; the positive time derivative of the CLF at any time then indicates that the ROM is inaccurate. Accordingly, by tracking the time derivative of CLF we can identify the time instances when the ROM must be revised using APOD. The revision procedure continues until the value of Lyapunov function satisfies the stability criteria and performance. The effectiveness of the proposed output feedback control approach is illustrated on the regulation problem of a physico-chemical system described by the Kuramoto-Sivashinsky equation (KSE).

6.2.1 System description

We consider one-dimensional highly dissipative DPSs which can be described by the following general form of input-affine PDE,

$$
\frac{\partial}{\partial t}\bar{x}(z,t) = \mathcal{F}_n(z,\bar{x}) + H(z,\bar{x}) + B(z)u(t),
$$
$$
\Gamma(\bar{x}, \frac{\partial}{\partial z}\bar{x}, \ldots, \frac{\partial^{n-1}}{\partial z^{n-1}}\bar{x})\Big|_{\partial\Omega} = 0, \tag{6.50}
$$
$$
\bar{x}(z,0) = \bar{x}_0(z),
$$

where $\bar{x}$ denotes the spatially distributed state of the system, $z \in \Omega \subset \mathbb{R}$ is the spatial coordinate, Ω is the process domain and t indicates the time. The term $\mathcal{F}_n$ presents the nonlinear differential operator of orders n, H denotes an algebraic smooth nonlinear Lipschitz function and $u \in \mathbb{R}^l$ is the vector of manipulated inputs where l denotes the number of inputs. The vector function of $B^T(z)$ describes the spatial distribution of the manipulated inputs. The vector of $\Gamma(\cdot)$ presents the n homogeneous boundary conditions defined over the process boundary of $\partial\Omega$, and $\bar{x}_0$ is a smooth function that describes the initial spatial profile.

In the general PDE system of (6.50), limited continuous point measurement sensors are considered to be available at predefined locations in the process domain. The vector of measurement outputs of such sensors can then be presented in the following form during the process evolution,

$$y(t) = \int_\Omega \delta(z - L_s)\bar{x}(z,t) \ dz, \qquad (6.51)$$

where $\delta(\cdot)$ is the standard Dirac function and L_s denotes the vector of point measurement sensors' locations. We also consider a periodic spatially distributed sensor to take the system snapshots as needed,

$$Y(z, t_k) = \int_0^t \delta(t - t_k)\bar{x}(z,t) \ dt, \qquad (6.52)$$

where t_k for $k = 1, 2, \ldots$, indicates the time instances when the snapshot of the

system state must be available. Such system profiles can be obtained by periodic fixed or moving spatially distributed sensors [88] or computed by a parallel high fidelity simulator. The required snapshots at each revisions in the presence of partial sensor information can be reconstructed from previous spatially distributed profiles [204]. The snapshot construction problem can also be addressed by spatially distributed dynamic observers in the form of PDEs which only use a limited number of fixed point measurement sensors. Our intention is to reduce the number of such revisions in the presence of bounded manipulated inputs and measured outputs.

Assumption 6.4. *We assume the approximate observability and controllability [81, 84] of the DPS described by the PDE system of (6.50)-(6.51).*

By defining the infinite-dimensional system state,

$$x(t) = \bar{x}(\cdot, t),$$

the nonlinear differential, nonlinear algebraic and the manipulated input operators,

$$\mathbf{F}(x) = \mathcal{F}_n(z, \bar{x}),$$

$$\mathbf{H}(x) = H(z, \bar{x}),$$

$$\mathbf{B}u = B(z)u,$$

and the measurement output operators,

$$\mathbf{S}x = \int_\Omega \delta(z - L_s)\bar{x}(\cdot, t) \ dz,$$

$$\mathbf{R}x = \int_0^t \delta(t - t_k)\bar{x}(\cdot, t) \ dt,$$

in an appropriate functional Sobolev subspace of $\mathbb{W}$, the PDE system of (6.50) and its measurement outputs, (6.51)-(6.52), can be represented in the following infinite-dimensional functional form

$$\dot{x} = \mathbf{F}(x) + \mathbf{H}(x) + \mathbf{B}u, \quad x(0) = x_0,$$

$$y = \mathbf{S}x, \tag{6.53}$$

$$Y = \mathbf{R}x,$$

where $x \in \mathbb{W}$ and

$$\mathbb{W}(\Omega) = \Big\{ \mathcal{G} \in L_2(\Omega) : \ \forall \alpha \in \mathbb{N}, \ |\alpha| \leqslant n - 1, \ \partial^\alpha \mathcal{G} \in L_2(\Omega),$$

$$\Gamma(\mathcal{G}, \frac{\partial \mathcal{G}}{\partial z}, \dots, \frac{\partial^{n-1}\mathcal{G}}{\partial z^{n-1}})\Big|_{\partial\Omega} = 0 \Big\}.$$

To present the infinite-dimensional functional form of (6.53) in a normal form and present the idea that is the basis for the proposed work, we have to find the basis functions needed to discretize the system. Such basis functions must be computed

from the eigenproblem of the nonlinear operator of $\mathbf{F}$ as

$$
\begin{aligned}
&\mathbf{F}(\psi_i) - \lambda_i \psi_i = 0, \\
&\Gamma(\psi_i, \frac{\partial \psi_i}{\partial z}, \dots, \frac{\partial^{n-1} \psi_i}{\partial z^{n-1}})\Big|_{\partial \Omega} = 0, \\
&i = 1, \dots, \infty,
\end{aligned}
\tag{6.54}
$$

where ψ_i denote the ith basis function corresponds to the eigenvalue of λ_i.

6.2.2 Finite-dimensional approximation using Galerkin projection

In this section, we employ Galerkin projection to accurately reproduce the dominant dynamics of the nonlinear highly dissipative PDE system of (6.50) by a low-dimensional nonlinear ODEs. A complete set of global orthonormal basis functions are assumed to be available which span the entire spatial domain of the process operation and satisfy the process boundary conditions. In practice, such basis function may be computed using POD-type approaches. For such approximation we need a time scale separation between the slow and fast dynamics of the system which is officially stated in the following assumption.

Assumption 6.5. *The dynamics of highly dissipative DPS described by the nonlinear PDE of (6.50) with infinite-dimensional representation of (6.53) can be decomposed to two subsystem dynamics; (1) the finite slow subsystem that includes*

the slow and possibly unstable modes of the system, and (2) the infinite complement

fast subsystem that contains the remaining fast and stable modes of the system. We

also assume that there is a time scale separation between the slow and fast subsys-

tems which can be in practice identified by the sets of slow and fast basis functions

computed based on analytical or statistical methods.

Based on Assumption 6.5, which is satisfied by the majority of transport-reaction processes [76], the Sobolev subspace of

$$\mathbb{W} \triangleq span\{\psi_i\}_{i=1}^{\infty},$$

can be decomposed to a slow subspace,

$$\mathbb{W}_s \triangleq span\{\psi_i\}_{i=1}^{m},$$

and its complement fast subspace,

$$\mathbb{W}_f \triangleq span\{\psi_i\}_{i=m+1}^{\infty}.$$

The projection operator of $\mathcal{P} : \mathbb{W} \to \mathbb{W}_s$ and its complement operator, $\mathcal{Q} : \mathbb{W} \to \mathbb{W}_f$, can be defined as

$$
\begin{aligned}
\mathcal{P}(\cdot) &= (\cdot, \Psi_s), \\
\mathcal{Q}(\cdot) &= (\cdot, \Psi_f),
\end{aligned}
\tag{6.55}
$$

to decompose the infinite-dimensional system of (6.53) to the following modal vectorized slow and fast forms,

$$
\begin{aligned}
\dot{x}_s &= F_s(x_s, x_f) + H_s(x_s, x_f) + B_s u, \quad x_s(0) = \mathcal{P} x_0, \\
\dot{x}_f &= F_f(x_s, x_f) + H_f(x_s, x_f) + B_f u, \quad x_f(0) = \mathcal{Q} x_0, \\
y &= S_s x_s + S_f x_f, \\
Y &= R_s x_s + R_f x_f,
\end{aligned}
\tag{6.56}
$$

where $x = x_s \oplus x_f$, $x_s = \mathcal{P} x \in \mathbb{W}_s$, $x_f = \mathcal{Q} x \in \mathbb{W}_f$, $F_s = \mathcal{P} \mathbf{F}$, $F_f = \mathcal{Q} \mathbf{F}$, $H_s = \mathcal{P} \mathbf{H}$, $H_f = \mathcal{Q} \mathbf{H}$, $B_s = \mathcal{P} \mathbf{B}$, $B_f = \mathcal{Q} \mathbf{B}$, $S_s = \mathcal{P} \mathbf{S}$, $S_f = \mathcal{Q} \mathbf{S}$, $R_s = \mathcal{P} \mathbf{R}$, $R_f = \mathcal{Q} \mathbf{R}$, $\Psi_s = [\psi_1 \quad \psi_2 \quad \cdots \quad \psi_m]^T$ and $\Psi_f = [\psi_{m+1} \quad \psi_{m+2} \quad \cdots]^T$. In the modal infinite-dimensional system of (6.56), F_s is a nonlinear bounded and F_f is a nonlinear unbounded differential operator, and H_s and H_f are nonlinear Lipschitz vector functions according to the properties of the nonlinear operator and function in the PDE system of (6.50). In addition according to Assumption 6.5, the unbounded operator of F_f is exponentially stable and generates a strongly continuous exponentially stable semigroup. The terms $S_s x_s$, $R_s x_s$ and $S_f x_f$, $R_f x_f$ denote system outputs associated with the slow and fast subsystems, respectively. We can compute locally accurate empirical eigenvalues and corresponding empirical basis functions required to discretize the infinite-dimensional system of (6.53) in the form of partitioned set of ODEs of (6.56).

Neglecting the fast dynamics of (6.56) we can approximate the infinite-dimensional

system by the slow subsystem of

$$\dot{x}_s = F_s(x_s, 0) + H_s(x_s, 0) + B_s u, \quad x_s(0) = \mathcal{P}x_0, \qquad (6.57)$$

which can be directly used to design a low-dimensional controller employing standard control methods for ODEs [76]. To employ such finite-dimensional approximation as the basis for the controller synthesis we must show that if the finite-dimensional slow subsystem of (6.57) is exponentially stable, then the infinite-dimensional system of (6.56) is also exponentially stable. The following theorem is officially addresses the required conditions which guarantee the accuracy of the finite-dimensional approximations in presenting the full infinite-dimensional system dynamics.

Theorem 6.3. *Consider the infinite-dimensional representation of the dissipative PDE system of (6.50) in the form of (6.53) for which Assumptions 6.4-6.5 hold. If the finite-dimensional system approximation of (6.57) is exponentially stable, then the infinite-dimensional system of (6.56) is also exponentially stable.*

Proof *See Appendix A.4.4 for proof of the theorem.*

6.2.3   Output feedback control

We focus on output feedback control structure synthesis that is a combination of a Lyapunov-based controller and a static observer to estimate the modes of the

system that are not available directly from the process measurements. The control objective is defined as the spatiotemporal dynamic regulation of the system state at the desired uniform profile of $\bar{x}_d(z) = 0$. The block diagram of the closed-loop process operation under proposed output feedback control structure is presented in Figure 6.12. The sensors and actuators physically attached to the process are shown by red blocks. The MOR structure is denoted by black blocks while green blocks are used to present the output feedback control architecture. In the closed-loop system, the supervisory controller checks the ROM consistency and orders ROM revisions as required during the closed-loop process evolution. Note that even through the process is continuous the control structure is a switching one, since at certain time-instants the ROM will be switched (by the supervisor) and as a result the controller will be switched as well.

6.2.3.1 Implementation of MOR methodology for controller synthesis

The spatiotemporal state of the system can be mathematically presented by the following infinite series

$$\bar{x}(z, t) = \sum_{k=1}^{\infty} \psi_k(z) a_k(t),$$

where $\psi_k(z)$ and $a_k(t)$ denote the spatially distributed basis functions and time-varying system modes for $k = 1, \ldots, \infty$. Practically, a finite number of states in the above series are required to capture the dominant spatiotemporal dynamic of
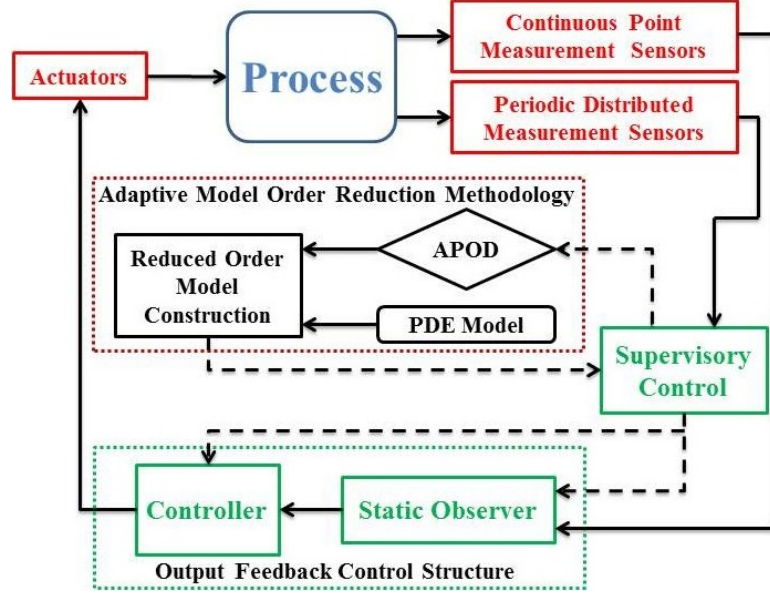
Figure 6.12: Closed-loop process operation under proposed output feedback control structure.

the system states as follows,

$$\bar{x}(z,t) \approx \sum_{k=1}^{m} \psi_k(z)a_k(t), \qquad (6.58)$$

where m, the optimal number of required empirical orthonormal basis functions, can be obtained using APOD algorithm during closed-loop process evolution.

Then by substituting (6.58) in the PDE system of (6.50) and applying Galerkin projection we obtain m ODEs that describe the dominant dynamics of the system,

$$\dot{a}_v(t) = \big(\psi_v(z), \mathcal{F}_n(z, \sum_{k=1}^{m} \psi_k(z)a_k(t))\big) + \big(\psi_v(z), \mathcal{B}(z)\big)u, \qquad (6.59)$$

for $v = 1, ..., m$. The inner product appearing in the above ODEs is defined by

$$(\varphi_1, \varphi_2) = \int_\Omega \varphi_1^T(z)\varphi_2(z)dz,$$

where φ^T presents the transpose of φ.

The ODE system of (6.59) can be summarized in the following compact form

$$\dot{a} = f(a) + gu, \tag{6.60}$$

which can be used as the basis for controller design. In (6.60), $f^{m \times 1}$ is a nonlinear vector and $g^{m \times l}$ is a matrix where their components are defined by

$$f_v = \left(\psi_v(z), \mathcal{F}(z, \sum_{k=1}^{m} \psi_k(z)a_k(t))) \right),$$

$$g_{v,i} = \left(\psi_v(z), b_i(z) \right).$$

Note that the form and dimension of the above ODE system may change as needed during the process evolution due to the required APOD-based modifications of the number and shape of empirical orthonormal basis functions.

6.2.3.2 Lyapunov-based controller design

In this section, we synthesize a Lyapunov-based controller to regulate the ROM of (6.60). The CLF is considered as the following quadratic form of system modes

$$V_c = \frac{1}{2}a^T a, \tag{6.61}$$

where $V_c(0) = 0$ and $V_c(a) > 0 \in \mathbb{R}^m - \{0\}$. To asymptotically stabilize the ROM we employ the Sontag formula [235],

$$u(t) = -k(a, c_o)(L_g V_c), \tag{6.62}$$

where

$$k(a, c_o) = \begin{cases} c_o + \dfrac{L_f V_c + \sqrt{\left(L_f V_c\right)^2 + \left(\left\|L_g V_c\right\|_2\right)^4}}{\left(\left\|L_g V_c\right\|_2\right)^2}, & L_g V_c \neq 0 \\ \\ c_o, & L_g V_c = 0 \end{cases}$$

In the above controller design, $c_o > 0$ denotes the adjustable control parameter and $L_h V_c = \dfrac{\partial V_c}{\partial a}h$ presents the Lie derivative. From (6.60)-(6.62) we obtain

$$\dot{V}_c = L_f V_c + L_g V_c u = -c_o \left(\left\|L_B V_c\right\|_2\right)^2 - \sqrt{\left(L_f V_c\right)^2 + \left(\left\|L_g V_c\right\|_2\right)^4} < 0.$$

Thus, according to the Lyapunov's stability theorem [148] the closed-loop system of (6.60) is locally asymptotically stable under the proposed controller of (6.62).

6.2.3.3 Static observer design

The system modes needed by the output feedback control structure in (6.61)-(6.62) to compute the control actions can not be directly accessible from the process measurements. To bypass the unavailability issues of such full state direct measurements we employ a static observer design to estimate the states of (6.60) using a limited number of continuous point measurement sensors as follows,

$$\hat{a} = \left(\Psi(L_s) \Psi^T(L_s) \right)^{-1} \Psi(L_s) y, \tag{6.63}$$

where $\Psi = [\psi_1 \ \psi_2 \ \cdots \ \psi_m]^T$.

Remark 6.10. *To circumvent the possible control action chattering near the manifold of $L_g V_c = 0$, we may add a sufficiently small positive value, η in the denominator of $k(\cdot)$ in (6.62). We can also adjust the closed-loop system stabilization speed by changing the value of c_o.*

Remark 6.11. *For the system modes to be accurately estimated by the static observer design of (6.63), the number of required continuous point measurement sensors in the output measurement vector of (6.51) have to be supernumerary to the number of modes at all times and for all ROM revisions.*

6.2.3.4 ROM revisions minimization

To update the set of empirical orthonormal basis functions the APOD algorithm requires the spatially distributed profile of the system state at the time of revisions. Such profiles must be obtained by spatially distributed measurement sensors or must be computed using a high fidelity numerical simulator which works in parallel with the process operation. In addition, the output feedback control structure must be revised based on the updated ROM which obtained by reapplying Galerkin's method to PDE model using the new set of empirical basis functions. To minimize the required measuring, communication and computation costs we need to reduce the frequency of ROM revisions as much as possible.

According to the Lyapunov-based controller design in Section 6.2.3.2 the CLF,

$$V_c = \frac{1}{2}\hat{a}^T\hat{a}, \tag{6.64}$$

which is computed based on the estimated modes, has to decrease as time evolves for the closed-loop process to be stable. A possible increase in the CLF at a specific time instant indicates that the ROM has become inaccurate. To implement such idea we design the supervisory control.

6.2.3.5 Supervisory control

We monitor the time derivative of the CLF as

$$\dot{V}_c = L_f V_c + L_g V_c u = \hat{a}^T[f(\hat{a}) + gu], \tag{6.65}$$

during the process evolution. When the time derivative of the CLF becomes positive we activate the adaptive MOR super block. It employs APOD to revise the set of empirical basis functions based on new snapshots and update the ROM. These revisions continue until the sign of the time derivative of CLF changes to negative which enforces the closed-loop stability. Following the ROM revisions, the controller is redesigned to retain relevancy. At that time the supervisory controller deactivates the adaptive MOR super block. Such supervisory strategy also forces the resulting closed-loop system to satisfy the stability criteria of switching systems [79, 86] at revisions.

6.2.4 Simulation Results

In this section we focus on illustrating the capability of the proposed Lyapunov-based feedback control strategy in stabilizing a class of physico-chemical DPSs that can be described in the form of the Kuramoto-Sivashinsky equation (KSE). Such systems can be exemplified by wave motions of falling liquid thin films, instabilities in the interface of two viscous fluids and phase turbulence in transport-reaction

processes [71, 93, 146].

The KSE can be described by

$$\frac{\partial}{\partial t}\bar{x}(z,t) = -v\frac{\partial^4}{\partial z^4}\bar{x}(z,t) - \frac{\partial^2}{\partial z^2}\bar{x}(z,t) - \bar{x}(z,t)\frac{\partial}{\partial z}\bar{x}(z,t) + b(z)u(t),$$

$$\frac{\partial^j}{\partial z^j}\bar{x}(-\pi,t) = \frac{\partial^j}{\partial z^j}\bar{x}(\pi,t), \quad j = 0, ..., 3, \tag{6.66}$$

$$\bar{x}(z,0) = \bar{x}_0(z),$$

where $\bar{x}(z,t)$ denotes the spatially distributed system state, $z \in [-\pi, \pi]$, $u(t) \in \mathbb{R}^l$ presents the manipulated inputs and $b(z)$ describes their distributions in the process domain. In the PDE of (6.66), v is the system diffusion parameter which is a function of the physico-chemical properties of the system. Figure 6.13 shows the spatiotemporal profile of the system state and its spatial norm in the absence of controller. We see that the system stabilizes at a spatially nonuniform shape, where the system parameter was assumed to be constant, $v = 0.32$, and the process started at the nonuniform spatial profile of

$$\bar{x}_0(z) = -\sin(z) + 0.5\cos(2z) - 0.5\sin(5z) + \cos(5z).$$

We employed four point actuators placed at

$$L_a = [-2\pi/3, \; -\pi/4, \; \pi/2, \; 3\pi/4],$$
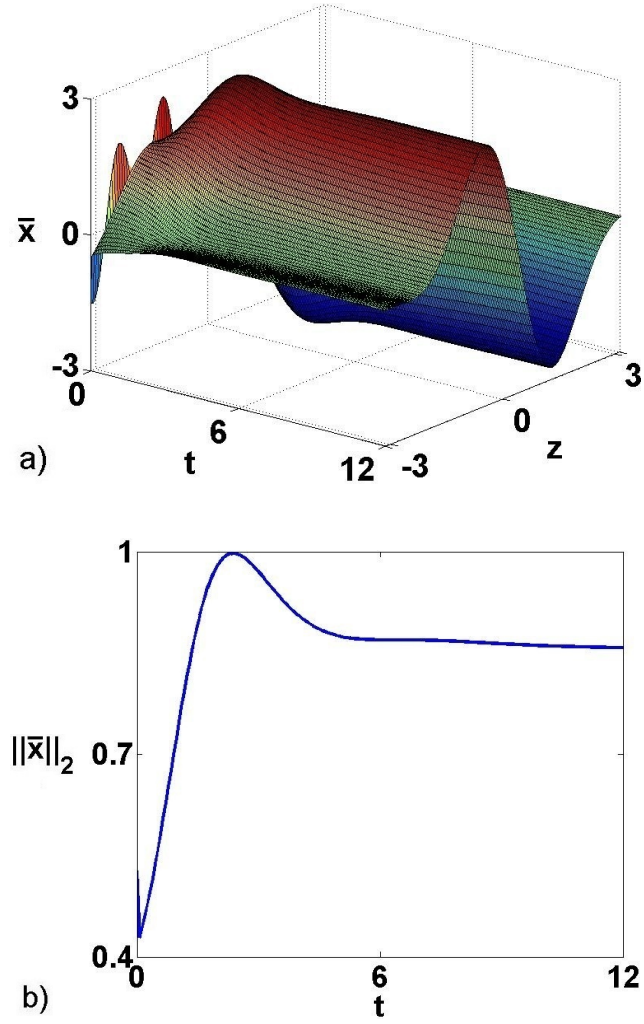
Figure 6.13: (a) Spatiotemporal profile and (b) its spatial norm of the system state in the absence of controller.

to stabilize the spatiotemporal dynamics of the system at the desired spatially uniform desired profile of $\bar{x}_d(z) = 0$ by setting the actuator distribution function as $b_i(z) = \delta(z - L_{a,i})$ for $i = 1, ..., 4$. We also considered five point measurement sensors placed at

$$L_s = [-3\pi/4, \ -\pi/3, \ -\pi/5, \ \pi/4, \ 2\pi/3],$$
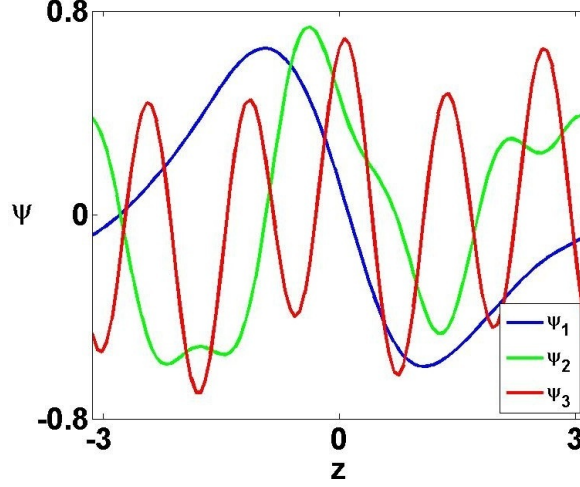
Figure 6.14: The initial empirical basis functions.

with $s(z) = \delta(z - L_s)$. The process operation included two parts; (1) open-loop operation in $t_o = [0, \ 2]$ when the controller was inactivate $(u = 0)$, and (2) closed-loop operation in $t_c = [2, \ 12]$. We collected 20 snapshots of the system state profile during the open-loop time period of t_o and applied off-line APOD to obtain an initial set of empirical basis functions and procure the ROM via Galerkin's method. We obtained 3 dominant empirical basis functions which captured 0.99 of the energy of the snapshots ensemble. These initial empirical basis functions are presented in Figure 6.14.

We employed $\eta = 0.005$ and $c_o = 1$ to implement the Lyapunov-based feedback controller structure of (6.62). In Figure 6.15, the spatiotemporal profile and its spatial norm are presented during process operation under the proposed feedback control, where the controller successfully stabilized the spatiotemporal dynamics of the system at the desired uniform profile of $\bar{x}_d(z) = 0$. The temporal profiles
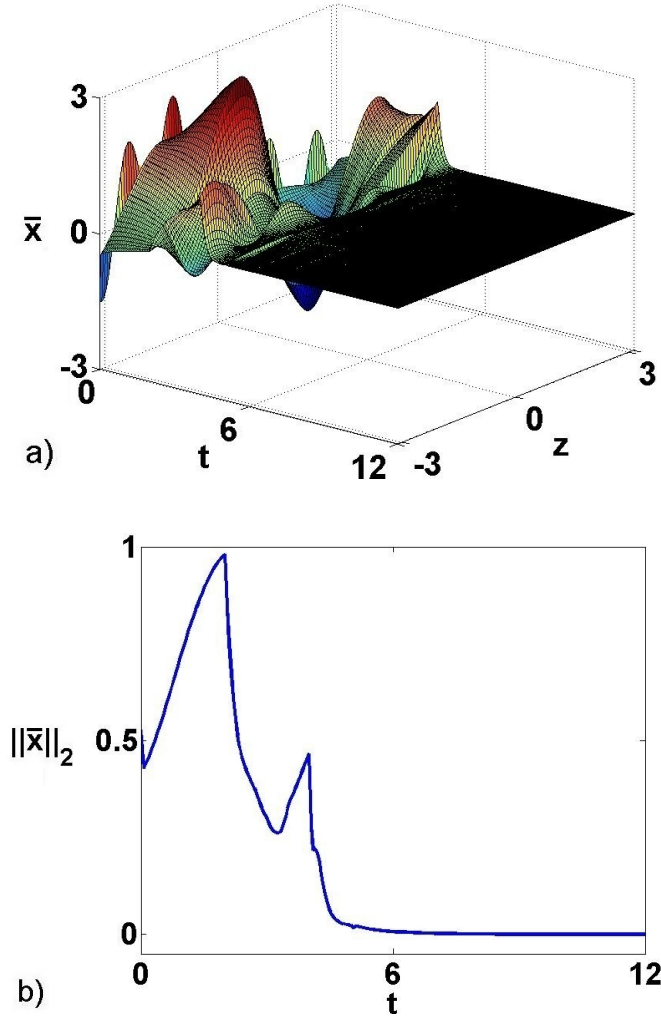
Figure 6.15: Closed-loop (a) spatiotemporal profile and (b) its spatial norm of the system state during process operation.

of the control actions and the CLF are presented in Figure 6.16. The controller was inactive in the open-loop process operation period of t_o. We observe that the control actions converged to zero as time evolved with some relatively large values at specific time instances. The first large control actions corresponds to the initial controller response to the system dynamics when the controller became active at the beginning of the closed-loop process operation period of t_c and the remainder
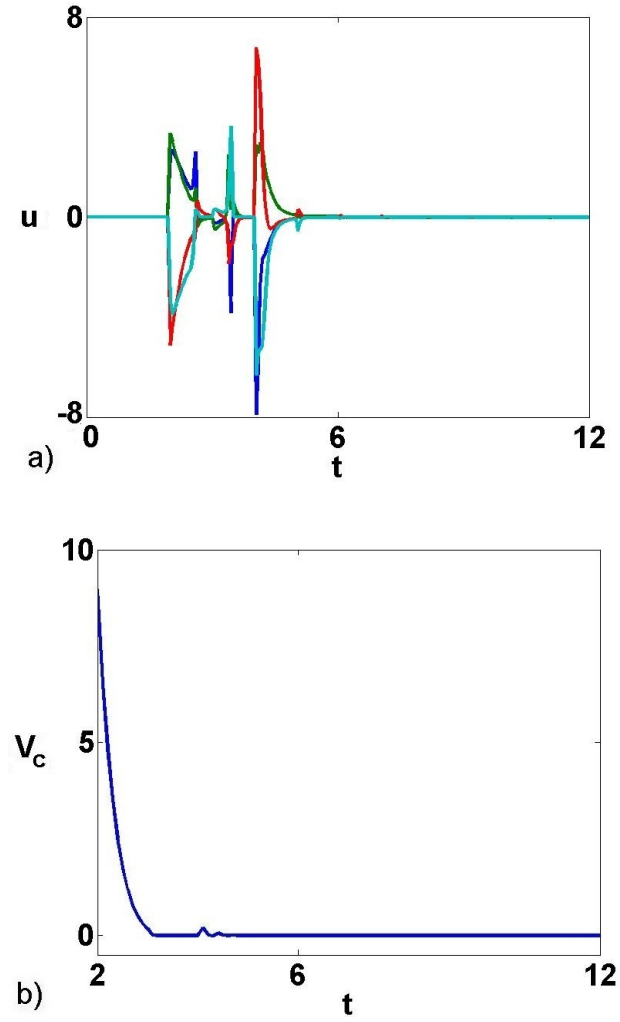
Figure 6.16: Temporal profiles of (a) the control actions and (b) the CLF.

of the peaking in the control actions corresponds to the ROM revisions due to the shape and dimension changes in the empirical basis functions. The overall decrease in the CLF also indicates the stability of the proposed model reduction and control approach. Figure 6.17 shows the number of basis functions obtained by APOD that shows the ROM dimension during closed-loop time period of t_c.

The time instances when the ROM had to be revised based on the CLF time
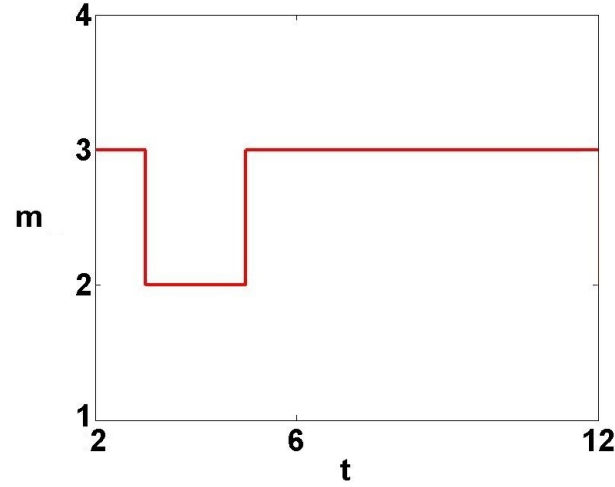
Figure 6.17: Number of empirical basis functions.

derivative monitoring are presented in Figure 6.18. In this figure, index 0 indicates that there was no need to revise the ROM and index 1 shows the times when the APOD algorithm revised the set of empirical basis functions and reconstructed output feedback control structure based on the updated ROMs. The strategy allowed us to minimize the number of required ROM revisions and reduced the spatially distributed sensing costs and computational loads. It shows that in the specific simulation only four ROM revisions were required during the closed-loop process evolution to guarantee the accuracy of the ROM used as a basis for Lyapunov-based output feedback controller design.

The first, second, third and fourth revised sets of empirical basis functions are also presented in Figure 6.19. We observe that the number and spatial distribution of the basis functions reordered and changed as needed to capture the dominant spatiotemporal behavior of the system. The second empirical basis function in
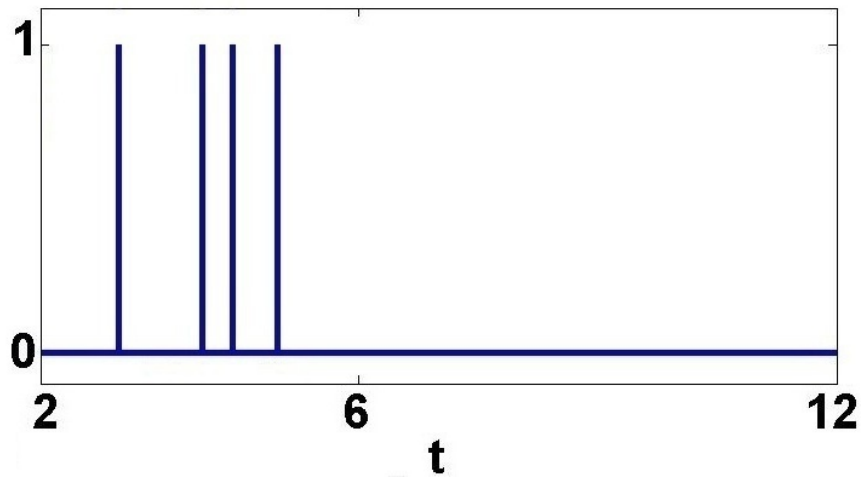
Figure 6.18: ROM revision times.

Figure 6.19(c) became the third in Figure 6.19(d), while the second empirical basis function in Figure 6.19(a) disappeared in Figure 6.19(c) which shows how that trend was briefly suppressed by the controller during process evolution.
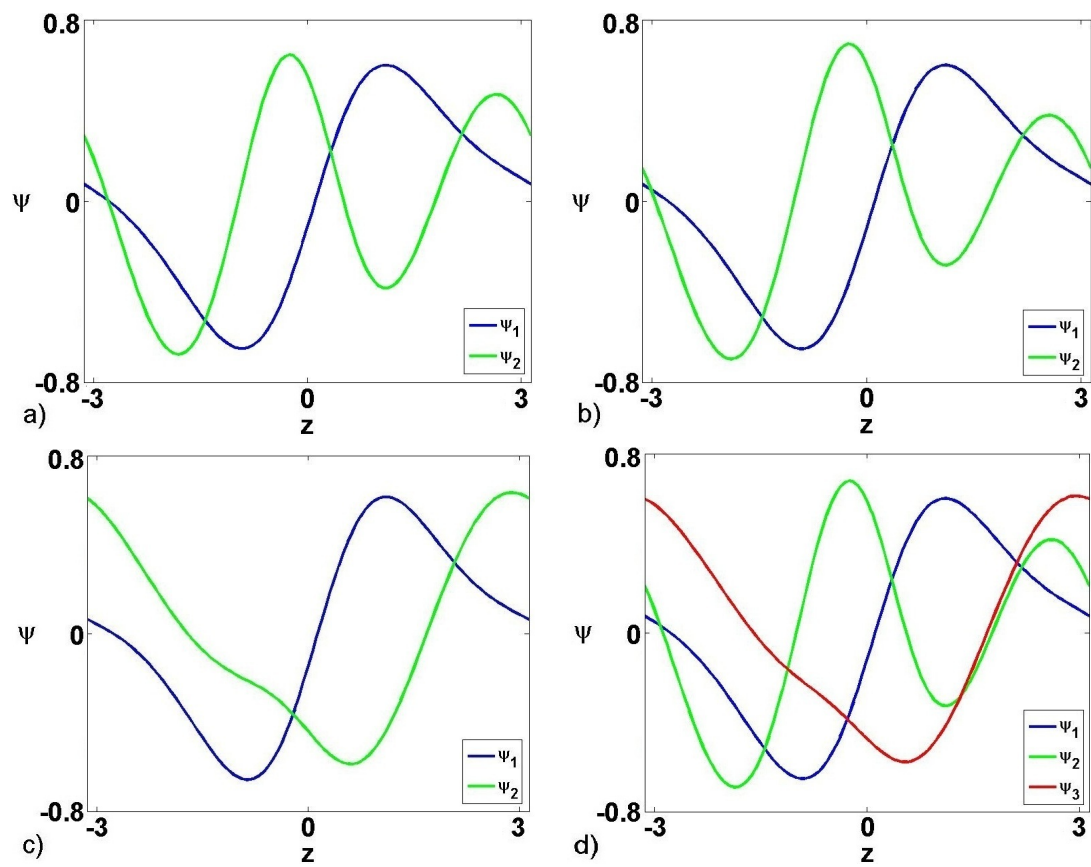
Figure 6.19: (a) First, (b) second, (c) third and (d) fourth set of revised empirical orthonormal basis functions.

SLIDING MODE

SPATIOTEMPORAL DYNAMIC

SHAPING OF DISTRIBUTED

PARAMETER SYSTEMS VIA

MODEL ORDER REDUCTION

Sliding mode control is a variable structure nonlinear control method which changes

the nonlinear system dynamics by applying a discontinuous control signal [148,

230]. The sliding mode controller forces the system dynamics to slide along the boundaries of the system normal behavior called "sliding surface" [96, 253]. The discontinuous nature of the controller structure causes insensitivity to parameter variations and complete disturbance rejection [53]. Sliding mode optimization and controller designs have been applied in a wide range of chemical, mechanical and electrical systems [56, 57, 111, 186].

In this chapter we consider the spatiotemporal dynamic shaping of transport-reaction processes via model order reduction (MOR). The dynamic shaping problem is addressed by regulating the error dynamics between the governing partial differential equation (PDE) and a desired spatiotemporal dynamics which are described by a target PDE with the same spatial differential operator. The governing target PDEs are discretized by applying Galerkin's method to obtain reduced order models (ROMs) in the form of low-dimensional modal ordinary differential equations (ODEs) when the required dominant basis functions are computed analytically by solving the eigenproblem of the linear part of the spatial differential operator. The error dynamics between the governing and target systems is derived by subtracting the ROMs in the form of low-dimensional ODEs which describe the spatiotemporal error dynamics. Then an output feedback control structure is synthesized to stabilize the error dynamics. The control structure is considered as a combination of a Lyapunov-based sliding mode controller [148, 230] and a Luenberger-type dynamic observer to estimate the system modes. The proposed

dynamic shaping method is successfully illustrated on thermal dynamic shaping inside a tubular chemical reactor described by a semi-linear PDE.

7.1 Preliminaries

7.1.1 Problem formulation

To formulate the spatiotemporal dynamic shaping problem we consider a 1D transport-reaction process which can be described by a semi-linear PDE,

$$
\begin{aligned}
&\frac{\partial}{\partial t}\bar{x}(z,t) = \mathcal{A}_n(z)\bar{x}(z,t) + F\big(z,\,\bar{x}(z,t)\big) + B(z)u(t), \\
&y(t) = \int_\Omega s(z)\,\bar{x}(z,t)\,dz, \\
&q\big(\bar{x}, \frac{\partial \bar{x}}{\partial z}, \ldots, \frac{\partial^{n-1}\bar{x}}{\partial z^{n-1}}\big) = 0 \quad \text{on} \quad \partial\Omega, \\
&\bar{x}(z,0) = \bar{x}_0(z),
\end{aligned}
\tag{7.1}
$$

where

$\bar{x}(z,t) \in \mathbb{R}$: *spatiotemporal state of the system,*

$z \in \Omega$: *1D spatial coordinate,*

t : *time,*

Ω : *process domain,*

$\partial\Omega$: *process boundaries,*

$\mathcal{A}_n(z)$: *linear spatial differential operator of order n,*

$F\big(z,\,\bar{x}(z,t)\big)$: *smooth Lipschitz nonlinear function,*

$u(t) \in \mathbb{R}^l$: *vector of manipulated inputs,*

$B(z)$: *spatial distribution of manipulated inputs,*

$y(t) \in \mathbb{R}^p$: *vector of contentious measurements,*

$s(z)$: *vector of measurements' spatial distribution,*

$q\big(\bar{x}, \dfrac{\partial \bar{x}}{\partial z}, \ldots, \dfrac{\partial^{n-1} \bar{x}}{\partial z^{n-1}}\big)$: *vector of linear homogeneous boundary conditions,*

$\bar{x}_0(z)$: *initial spatial profile of the system state.*

The dissipative PDE of (7.1) is linearly dominant, i.e., the spatial differential operator is purely linear and the nonlinearity only appears as a Lipschitz function in the system dynamics. Such equation arises in the majority of transport-reaction processes in the chemical process industries [76, 212], where the linear term of $\mathcal{A}_n(z)\bar{x}(z,t)$ indicates the transport (diffusion, dispersion and convection) component and the nonlinear term of $F\big(z, \bar{x}(z,t)\big)$ expresses the reaction dynamics.

Remark 7.1. *According to the Lipschitz property of the nonlinear function of* $F\big(z, \bar{x}(z,t)\big)$ *which makes it to be sufficiently smooth, the Picard-Lindelöf theorem can be applied to guarantee the existence and uniqueness of the solution [245].*

7.1.2 System representation

The studied DPS which is described by PDE of (7.1), can be represented in the abstract infinite-dimensional form of

$$\dot{x}(t) = Ax(t) + f\big(x(t)\big) + bu(t), \quad x(0) = x_0,$$

$$y(t) = Sx(t),$$

(7.2)

by defining the functional state of $x(t) \in \mathbb{W}$,

$$x(t) = \bar{x}(\cdot, t),$$

the linear differential operator,

$$Ax(t) = \mathcal{A}(z)\bar{x}(\cdot, t),$$

the nonlinear function,

$$f\big(x(t)\big) = F\big(z, \bar{x}(\cdot, t)\big),$$

and the manipulated input operator,

$$bu(t) = B(z)u(t),$$

in an appropriate Sobolev subspace of $\mathbb{W}$,

$$\mathbb{W}(\Omega) = \left\{ \mathcal{H}, \frac{\partial \mathcal{H}}{\partial z}, \ldots, \frac{\partial^{n-1}\mathcal{H}}{\partial z^{n-1}} \in \mathcal{L}_2(\Omega) : q\big(\mathcal{H}, \frac{\partial \mathcal{H}}{\partial z}, \ldots, \frac{\partial^{n-1}\mathcal{H}}{\partial z^{n-1}}\big) = 0 \right\},$$

equipped with following inner product and norm,

$$\big(\mathcal{H}, \mathcal{G}\big) = \int_\Omega r(z)\mathcal{H}^T\mathcal{G}\,dz,$$

$$\big\|\mathcal{H}\big\|_2 = \big(\mathcal{H}, \mathcal{H}\big)^{1/2},$$

where $\mathcal{H}$ and $\mathcal{G}$ are the elements of $\mathbb{W}$, and $\mathcal{H}^T$ denotes the transpose. Note that the inner product weighting function, $r(z)$, is considered to be 1 to simplify the analysis.

Assumption 7.1. *We assume that the DPS described by the PDE of (7.1) and its infinite-dimensional representation, (7.2), is approximately observable and controllable [84].*

Remark 7.2. *We may replace the approximate observability and controllability assumption of the infinite-dimensional system of (7.2) formally addressed in Assumption 7.1, by observability and controllability of the system approximation (slow subsystem) of (7.7) [84].*

7.2 Model order reduction via Galerkin's method

The infinite-dimensional functional representation of (7.2) can be projected into an infinite set of ODEs of the system vectorized eigenmodes using standard Galerkin's method. The required eigenfunctions to discretize the states of the Sobolev sub-

space are the solution of the following eigenproblem,

$$A\phi_i = \lambda_i\phi_i,$$

$$q\Big(\phi_i, \frac{d\phi_i}{dz}, \dots, \frac{d^{n-1}\phi_i}{dz^{n-1}}\Big)_{\partial\Omega} = 0,$$

(7.3)

for $i = 1, \dots, \infty$, where λ_i and ϕ_i denote the ith eigenvalue and its corresponding orthogonal eigenfunction, respectively. Note that the resulting countable set of eigenfunctions is a strong generator of the defined Sobolev subspace, i.e., $\mathbb{W} \triangleq span\{\phi_i\}_{i=1}^\infty$. To apply Galerkin's method we also require defining the adjoint eigenfunctions which satisfy the orthonormal property,

$$\big(\phi_i, \phi_j^*\big) = \delta_{ij},$$

(7.4)

where $\phi_i^* \in \mathbb{W}$ indicates the ith adjoint eigenfunction and δ_{ij} the Kronecker delta.

For the majority of transport-reaction processes where diffusion and dispersion play an important role we can assume a time-scale separation in the eigenspectrum of the linear operator of A. This assumption is formally stated as:

Assumption 7.2. *Assume the eigenspectrum of linear operator of A denoted by* $\Lambda(A) \triangleq \{\lambda_1, \lambda_2, \dots\}$, *where* $Re(\lambda_1) \geq Re(\lambda_2) \geq \cdots \geq Re(\lambda_m) \geq Re(\lambda_{m+1}) \geq \cdots$, *satisfies* $Re(\lambda_{m+1}) < 0$, $\sigma = \dfrac{|Re(\lambda_1)|}{|Re(\lambda_{m+1})|}$, *where* $Re(\cdot)$ *denotes the real part and* σ *is a small positive number. According to such separation the eigenspectrum and corresponding Sobolev subspace,* $\mathbb{W} \triangleq span\{\phi_i\}_{i=1}^\infty$, *can be partitioned into the*

following subsets and subspaces;

1. *finite subset of first m eigenvalues,*

$$\Lambda_s(A) \triangleq \{\lambda_1, \lambda_2, \ldots, \lambda_m\},$$

   which are slow and possibly unstable, and its corresponding slow Sobolev subspace, $\mathbb{W}_s \triangleq span\{\phi_i\}_{i=1}^m$,

2. *complement infinite subset of the remainder eigenvalues,*

$$\Lambda_f(A) \triangleq \{\lambda_{m+1}, \lambda_{m+2}, \ldots\},$$

   which are fast and stable, and its corresponding fast Sobolev subspace, $\mathbb{W}_f \triangleq span\{\phi_i\}_{i=m+1}^\infty$,

where $\mathbb{W} = \mathbb{W}_s \cup \mathbb{W}_f$.

Taking advantage of Assumption 7.1, the Galerkin integral projectors can be defined,

$$
\begin{aligned}
\mathcal{P} : \mathbb{W} \to \mathbb{W}_s, \quad \mathcal{P}(\cdot) = (\cdot, \Phi_s), \quad \Phi_s = [\phi_1 \; \phi_2 \; \cdots \; \phi_m]^T, \\
\mathcal{Q} : \mathbb{W} \to \mathbb{W}_f, \quad \mathcal{Q}(\cdot) = (\cdot, \Phi_f), \quad \Phi_f = [\phi_{m+1} \; \phi_{m+2} \; \cdots]^T,
\end{aligned}
\tag{7.5}
$$

to project the infinite-dimensional system representation of (7.2) to partitioned

sets of ODEs of the vectorized slow and fast eigenmodes,

$$\dot{x}_s(t) = A_s x_s(t) + f_s\big(x_s(t), x_f(t)\big) + b_s u(t), \quad x_s(0) = \mathcal{P}x_0,$$
$$\dot{x}_f(t) = A_f x_f(t) + f_f\big(x_s(t), x_f(t)\big) + b_f u(t), \quad x_f(0) = \mathcal{Q}x_0,$$
$$(7.6)$$

where $x(t) = x_s(t) \oplus x_f(t)$, $A_s = \mathcal{P}A = diag\{\lambda_i\}_{i=1}^m$, $A_f = \mathcal{Q}A = diag\{\lambda_i\}_{i=m+1}^\infty$, $f_s = \mathcal{P}f$, $f_f = \mathcal{Q}f$, $b_s = \mathcal{P}b$, $b_f = \mathcal{Q}b$ and $diag\{\cdot\}$ denotes the diagonal matrix with diagonal elements. Then the partitioned infinite dimensional ODEs of (7.6) can be approximated by

$$\dot{x}_s(t) = A_s x_s(t) + f_s\big(x_s(t), 0\big) + b_s u(t), \quad x_s(0) = \mathcal{P}x_0, \qquad (7.7)$$

after a short period of time, t_b, when $x_f \to 0$, by applying singular perturbation analysis [29, 31, 76] and considering Tykhonov's theorem for solution convergence of systems that consist of slow and fast subsystems [175].

Remark 7.3. *The time-scale separation between slow and fast dynamics of the DPS modeled by PDEs ensures that a controller which exponentially stabilizes the closed-loop finite dimensional approximation also exponentially stabilizes the closed-loop infinite-dimensional system [76].*

Remark 7.4. *A lower bound for the relaxation time, t_b, required by the fast dynamics of the system to relax, can be identified by singular perturbation analysis [29, 35, 76].*

7.3 Spatiotemporal dynamic shaping using sliding mode controller designs

7.3.1 Dynamic shaping error formulation

To address the spatiotemporal dynamic shaping problem of the DPSs described by PDE system of (7.1), we consider a desired spatiotemporal dynamics described by a target PDE with the same spatial differential operator,

$$
\begin{aligned}
&\frac{\partial}{\partial t}\bar{x}_d(z,t) = \mathcal{A}_n(z)\bar{x}_d(z,t) + F'\big(z,\,\bar{x}_d(z,t)\big), \\
&q\big(\bar{x}_d, \frac{\partial \bar{x}_d}{\partial z}, \ldots, \frac{\partial^{n-1}\bar{x}_d}{\partial z^{n-1}}\big) = 0 \quad \text{on} \quad \partial\Omega, \\
&\bar{x}_d(z,0) = \bar{x}_{d0}(z).
\end{aligned}
\tag{7.8}
$$

According to same spatial differential operator and boundary conditions, both the system and target PDEs have the same set of dominant eigenfunctions which can be applied to approximate the spatiotemporal states as follows,

$$
\begin{aligned}
\bar{x}(z,t) &\approx x_s^T(t)\Phi_s(z), \\
\bar{x}_d(z,t) &\approx x_{ds}^T(t)\Phi_s(z).
\end{aligned}
\tag{7.9}
$$

Note that such approximations are quite accurate after a short relaxation time when the fast dynamics stabilize. Then the spatiotemporal dynamic shaping error

with respect to slow system dynamics can be formulated by

$$E(z,t) = \bar{x}(z,t) - \bar{x}_d(z,t) \approx \left(x_s^T(t) - x_{ds}^T(t) \right) \Phi_s(z) = e^T(t)\, \Phi_s(z). \qquad (7.10)$$

where $e(t) = x_s(t) - x_{ds}(t)$ indicates the vector of modal errors.

By applying MOR via Galerkin projection as it was discussed in Section 7.2, we can discretize the target PDE to the following set of ODEs,

$$\dot{x}_{ds}(t) = A_s x_{ds}(t) + f_s'\big(x_{ds}(t)\big), \quad x_{ds}(0) = \mathcal{P}x_{d0}, \qquad (7.11)$$

which describes the slow modal dynamics of the desired spatiotemporal behavior. The modal tracking error dynamics can then be derived by subtracting the ODEs of (7.7) and (7.11),

$$\dot{e}(t) = A_s e(t) + f_s\big(e(t), x_{ds}(t)\big) - f_s'\big(x_{ds}(t)\big) + b_s u(t), \quad e(0) = \mathcal{P}e_0, \qquad (7.12)$$

where $e_0 = x_0 - x_{d0}$. Thus the spatiotemporal dynamic shaping problem of the transport-reaction processes described by (7.1) can be addressed via error dynamics regulation of the low-dimensional ODEs of (7.12).

Remark 7.5. *Note that the fast dynamics must be exponentially stable for the specific method to be applicable even for the unstable target PDEs.*

Remark 7.6. *We may directly apply the proposed MOR to the PDE of the spatiotemporal dynamic shaping error which formulated by subtracting the governing PDE of (7.1) from the target of (7.8). Such alternative approach results to the same modal tracking error dynamics as (7.12).*

7.3.2 Sliding mode controller design

Consider the nonlinear dynamical modal error system of (7.12),

$$\dot{e} = A_s e + f_s(e, x_{ds}) - f_s'(x_{ds}) + b_s u,$$

where $e = [e_1, e_2, \ldots, e_m]^T \in \mathbb{R}^m$ and $u = [u_1, u_2, \ldots, u_l]^T \in \mathbb{R}^l$. The objective is designing an output-feedback control law, $u(t)$, which regulates the error dynamics at the origin. By stabilizing the error, such regulator enforces the system dominant eigenmodes to follow the target eigenmodes. According to the dynamical modal error system dimension, we require at least m manipulated inputs (i.e. $l \geq m$) to stabilize the tracking error and force the system spatiotemporal dynamics to follow target dynamics with a general nonlinear part [112, 126].

To reach such objective a sliding mode control approach is applied. The controller synthesis includes two steps: (1) Choosing a manifold (reduced-order subspace), also known as sliding surface, which describes the desired dynamic behavior. (2) Designing the feedback control law which forces the tracking error trajectory to confine to the sliding surface and slides along it [96, 253]. Thus the problem

of dynamic modal response shaping $a \to \tilde{a}$ is equivalent to "approaching to the sliding surface and remaining on it". The time-varying sliding surface, $S(t)$, is defined by the scalar equation of $s(e) = 0$ which must guarantee the system control objective in regulating the tracking error dynamics,

$$S = \{e \in \mathbb{R}^m : \quad s(e) = 0\}. \tag{7.13}$$

The switching function of $s(e)$ is a distance measurement which indicates how far the system eigenmodes are from the target eigenmodes. It can be simply defined as the following proportional-integral form,

$$s(e) = e + \Pi \int e \, dt, \tag{7.14}$$

where $\Pi = diag\{\pi_i\}_{i=1}^m$. To assure the stability of sliding mode dynamic, the diagonal components of Π must have negative real parts, i.e, $Re(\lambda_i) < 0$ for $i = 1, \ldots, m$. The places of such components in the left half-plane determine the performance of the sliding mode controller in stabilizing the tracking error dynamics.

Due to the discontinuous nature of the resulting sliding mode control action, the existence and uniqueness of the closed-loop system solution can not be verified by the Picard-Lindelöf theorem [245]. Such switching discontinuous closed-loop dynamics must be analyzed using Filippov theorem [106, 281] which states the resulting closed-loop system that slides along $s(e) = 0$, can be approximated by a

smooth dynamics which is described using

$$\dot{s}(e) = 0$$

under a continuous control design [148, 230]. To formulate the sliding mode controller design we consider the Lyapunov function in the quadratic form of

$$V(s) = \frac{1}{2}s^T s. \tag{7.15}$$

By considering the above Lyapunov function, the asymptotic stability can be obtained by

$$\dot{V}(s) = s^T \dot{s} \le 0. \tag{7.16}$$

Then using Filippov's construction of the equivalent dynamics, the control action can be computed by considering the smooth dynamics of $\dot{s} = 0$, which

$$\dot{s} = \dot{e} + \Pi e = A_s e + f_s(e, x_{ds}) - f'_s(x_{ds}) + b_s u_{eq} + \Pi e = 0. \tag{7.17}$$

As a result the equivalent control law takes the following form

$$u_{eq} = -b_s^{\perp}\Big((A_s + \Pi)e + f_s(e, x_{ds}) - f'_s(x_{ds})\Big), \tag{7.18}$$

where $b_s^{\perp} = b_s^T(b_s b_s^T)^{-1}$ identifies the Moore-Penrose pseudo-inverse [202]. Note

that $b_s^{\perp} = b_s^{-1}$ for $m = l$. In order to satisfy the sliding condition we consider the control law as

$$u = u_{eq} - b_s^{\perp} \, \eta \, sign(s), \tag{7.19}$$

where $\eta > 0$ and $sign(\cdot)$ denotes the sign function. Then we obtain

$$\dot{V}(s) = s^T \dot{s} = -\eta \, s^T \, sign(s), \tag{7.20}$$

where $\dot{V}(s) < 0$ and $\dot{V}(0) = 0$, thus the closed-loop system is locally asymptotically stable in the Lyapunov sense [148, 230].

7.3.3 Dynamic observer design

For the desired spatiotemporal dynamics which is described by (7.8) and approximated by the slow dynamics of (7.11) we have access to the dominant eigenmodes, x_{ds}. However, to compute the tracking error vectors, e, and implement the control law of (7.19), we need to estimate the values of the system dominant eigenmodes of x_s. For such estimation purpose, a Luenberger-type dynamic observer is synthesized based on the system ROM,

$$\begin{aligned} \dot{\hat{x}}_s &= A_s \hat{x}_s + f_s(\hat{x}_s) + b_s u + \Theta(y - C\hat{x}_s), \\ y &= Cx_s, \end{aligned} \tag{7.21}$$

where

$$C = \begin{bmatrix} \phi_1(\omega_1) & \phi_2(\omega_1) & \cdots & \phi_m(\omega_1) \\ \phi_1(\omega_2) & \phi_2(\omega_2) & \cdots & \phi_m(\omega_2) \\ \vdots & \vdots & \ddots & \vdots \\ \phi_1(\omega_p) & \phi_2(\omega_p) & \cdots & \phi_m(\omega_p) \end{bmatrix},$$

and $\hat{x}_s$ denotes the estimated dominant eigenmodes of the system, Θ presents the dynamic observer gain matrix and $\omega = [\omega_1 \ \omega_2 \ \cdots \ \omega_p]^T$ is the vector of locations of continuous measurements, y. The modal observation error dynamics can then be formulated as follows

$$\dot{e}_o = (A_s - \Theta C)e_o + f_s(e_o + \hat{x}_s) - f_s(\hat{x}_s), \tag{7.22}$$

where the vector of observation error is defined by $e_o = x_s - \hat{x}_s$. Assuming the principle of separation between control and observation holds [26, 68], we consider the observation Lyapunov function (OLF) in the standard quadratic form

$$V_o = \frac{1}{2}e_o^T P e_o, \tag{7.23}$$

where P is a symmetric positive definite matrix with a bounded norm, $\|P\| \leq K_1$. The time derivative of the OLF is obtained as follows

$$\dot{V_o} = \frac{1}{2}\left(\dot{e}_o^T P\, e_o + e_o^T P\, \dot{e}_o\right)$$

$$= \frac{1}{2}\Big([(A_s - \Theta C)e_o + f_s(e_o + \hat{x}_s) - f_s(\hat{x}_s)]^T P\, e_o$$

$$+ e_o^T P\left[(A_s - \Theta C)e_o + f_s(e_o + \hat{x}_s) - f_s(\hat{x}_s)\right]\Big)$$

$$= \frac{1}{2}\Big([e_o^T (A_s - \Theta C)^T + \left(f_s(e_o + \hat{x}_s) - f_s(\hat{x}_s)\right)^T]P\, e_o \qquad (7.24)$$

$$+ e_o^T P\left[(A_s - \Theta C)e_o + f_s(e_o + \hat{x}_s) - f_s(\hat{x}_s)\right]\Big)$$

$$= \frac{1}{2}\Big(e_o^T[(A_s - \Theta C)^T P + P(A_s - \Theta C)]e_o$$

$$+ e_o^T P\big[f_s(e_o + \hat{x}_s) - f_s(\hat{x}_s)\big] + \left(e_o^T P\big[f_s(e_o + \hat{x}_s) - f_s(\hat{x}_s)\big]\right)^T\Big)$$

Then the dynamic observer gain matrix, Θ, must be identified subject to $\dot{V_o} < 0$ which indicates the observation stability. Due to the Lipschitz property of the nonlinear function of F in the DPS of (7.1) and bounded nature of the eigenfunctions and their adjoints, the nonlinear function of f_s in the system approximation of (7.7) is also Lipschitz continuous,

$$\left\|f_s(e_o + \hat{x}_s) - f_s(\hat{x}_s)\right\| \le K_2 \|e_o\|, \qquad (7.25)$$

where K_2 denotes the Lipschitz upper bound gain. From (7.24) and (7.25) and using Cauchy-Schwarz inequality we obtain that

$$e_o^T P\big[f_s(e_o + \hat{x}_s) - f_s(\hat{x}_s)\big] + \Big(e_o^T P\big[f_s(e_o + \hat{x}_s) - f_s(\hat{x}_s)\big]\Big)^T$$

$$\leq 2\big\|e_o^T P\big[f_s(e_o + \hat{x}_s) - f_s(\hat{x}_s)\big]\big\| \leq 2\big\|e_o^T\big\|\|P\|\big\|f_s(e_o + \hat{x}_s) - f_s(\hat{x}_s)\big\|$$

$$\leq 2K_1 K_2 \big\|e_o^T\big\|\,\big\|e_o\big\|$$

$$= K\big\|e_o\big\|^2 = K e_o^T e_o, \tag{7.26}$$

where $K = K_1 K_2$.

By applying the inequality of (7.26), we conclude that if

$$e_o^T\big[(A_s - \Theta C)^T P + P(A_s - \Theta C)\big]e_o + K e_o^T e_o < 0. \tag{7.27}$$

then $\dot{V}_o < 0$ and $\dot{V}(0) = 0$. Thus

$$e_o^T\big[(A_s - \Theta C)^T P + P(A_s - \Theta C) + KI\big]e_o < 0, \tag{7.28}$$

where $(A_s - \Theta C)^T P + P(A_s - \Theta C) + KI < 0$ guarantees the asymptotic stability of the observation error dynamics. We can then address the dynamic observer synthesis problem via a standard linear matrix inequality (LMI) problem

$$(A_s - \Theta C)^T P + P(A_s - \Theta C) + KI < -PYP - P\Theta Z\Theta^T P, \tag{7.29}$$

where Y and Z are the symmetric positive definite weighting matrices. From the inequality of (7.29) we obtain

$$(A_s^T - C^T \Theta^T)P + P(A_s - \Theta C) + KI + PYP + P\Theta Z\Theta^T P < 0$$

$$\Rightarrow A_s^T P + PA_s - (P\Theta C)^T - P\Theta C + PYP + P\Theta Z\Theta^T P + KI < 0$$

$$\Rightarrow A_s^T P + PA_s - (UC)^T - UC + PYP + UZU^T + KI < 0$$

$$\Rightarrow A_s^T P + PA_s + (U^T - Z^{-1}C)^T Z(U^T - Z^{-1}C) - C^T Z^{-1}C + PYP + KI < 0,$$

$$(7.30)$$

where $U = P\Theta$. Then we reduce the degrees of freedom in the inequality by setting $U = C^T Z^{-T}$,

$$A_s^T P + PA_s - C^T Z^{-1}C + PYP + KI < 0. \tag{7.31}$$

Using the Schur Complement Lemma we represent the inequality of (7.31) in the following standard form [64],

$$\begin{bmatrix} PA_s + A_s^T P - C^T Z^{-1}C + KI & P \\ P & -Y^{-1} \end{bmatrix} < 0. \tag{7.32}$$

The observer gain matrix can be computed by minimizing the trace of P^{-1} subject to the LMI constraint of (7.32),

$$\Theta = P^{-1}C^T Z^{-1}. \tag{7.33}$$

A detailed discussion on the LMI-constrained optimization problem can be found in [219].

7.4 Application to thermal dynamic shaping in a tubular reactor

In this section, we illustrate the effectiveness of the proposed output feedback sliding mode control on spatiotemporal dynamic shaping of a typical transport-reaction process example. In the first part we present the mathematical model of the thermal dynamics in a tubular chemical reactor. The desired spatiotemporal behavior is described in the second part. Then the tailored MOR and control structure are presented for the specific dynamic shaping problem in the third part of this section. Finally, the closed-loop simulation results are provided to assess the system performance under the proposed output feedback sliding mode control structure.

7.4.1 System description

We consider a tubular chemical flow reactor [76] where an irreversible exothermic reaction of the zero-th order takes place. As presented in Figure 7.1, a limited set of l cooling jackets are employed as the manipulated inputs to remove the heat from the reactor and manage the thermal energy along the reactor length as time
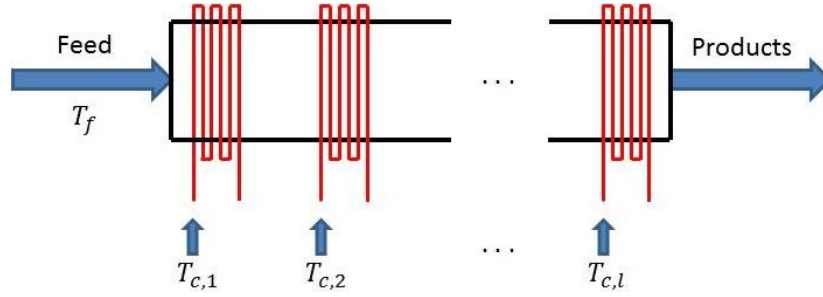
Figure 7.1: Tubular flow reactor with l independent cooling jackets.

evolves. The spatiotemporal thermal dynamics in the presence of temperature-dependent reaction rate is derived from the energy balance which takes the form of the following dissipative PDE,

$$\frac{\partial T}{\partial t} = \frac{k}{\rho C_p} \frac{\partial^2 T}{\partial z^2} - v \frac{\partial T}{\partial z} + \frac{(-\Delta H)}{\rho C_p} r_o \exp\left(\frac{-E}{RT}\right) - \sum_{j=1}^{l} \mathcal{B}_j(z) \frac{hA_c}{\rho C_p} (T - T_{c,j}),$$

$$z = 0: \qquad \frac{\partial T}{\partial z} = \frac{\rho C_p v}{k} (T - T_f),$$

$$z = L: \qquad \frac{\partial T}{\partial z} = 0,$$

$$t = 0: \qquad T = T_0, \tag{7.34}$$

where

T : temperature of the fluid inside the reactor,

t : time,

$z \in [0, L]$: spatial coordinate,

L : reactor length,

k : thermal conductivity,

ρ : density,

C_p : *heat capacity,*

v : *axial velocity,*

$(-\Delta H)$: *heat of reaction,*

r_0 : *pre-exponential reaction constant,*

E : *activation energy,*

h : *heat transfer coefficient between reactor and cooling jacket,*

A_c : *cooling surface area,*

$T_{c,j}$: *cooling jackets temperatures,*

T_f : *feed temperature,*

l : *number of cooling jackets,*

$\mathcal{B}_j(z)$: *spatial distribution of the jth cooling jacket,*

T_0 : *initial temperature profile.*

We reformulate the PDE set of (7.34) in the dimensionless form and homogenize the left boundary condition to employ the proposed MOR. To homogenize the boundary condition we induce the non-homogeneous part in the PDE by standard Dirac function. The resulting dimensionless PDE takes the following form,

$$\frac{\partial \bar{T}}{\partial \bar{t}} = \frac{1}{Pe}\frac{\partial^2 \bar{T}}{\partial \bar{z}^2} - \frac{\partial \bar{T}}{\partial \bar{z}} + B_t \exp\left(\frac{\gamma \bar{T}}{1+\bar{T}}\right) + B_c \sum_{j=1}^{l} \mathcal{B}_j(\bar{z})(\bar{u}_i - \bar{T}) + \delta(\bar{z}-0)\bar{T}_f$$

$$\bar{z} = 0 : \qquad \frac{\partial \bar{T}}{\partial \bar{z}} = Pe\bar{T},$$

$$\bar{z} = 1 : \qquad \frac{\partial \bar{T}}{\partial \bar{z}} = 0,$$

$$\bar{t} = 0 : \qquad \bar{T} = 0,$$

$$(7.35)$$

where

$$\bar{t} = \frac{tv}{L}, \quad \bar{z} = \frac{z}{L}, \quad \bar{T} = \frac{T - T_0}{T_0}, \quad Pe = \frac{\rho C_p v L}{k},$$

$$\gamma = \frac{E}{RT_0}, \quad \bar{u}_j = \frac{T_{c,j} - T_0}{T_0}, \quad \bar{T}_f = \frac{T_f - T_0}{T_0},$$

$$B_t = \frac{(-\Delta H) r_o \exp(-\frac{E}{RT_0}) L}{\rho C_p T_0 v}, \quad B_c = \frac{h A_c L}{\rho C_p v}.$$

A typical diffusion-convection-reaction process with the same spatial differential operator is considered as the target PDE which describes the desired spatiotemporal dynamics,

$$\frac{\partial \bar{T}_d}{\partial \bar{t}} = \frac{1}{Pe} \frac{\partial^2 \bar{T}_d}{\partial \bar{z}^2} - \frac{\partial \bar{T}_d}{\partial \bar{z}} + \alpha_3 \bar{T}_d^3 + \alpha_2 \bar{T}_d^2 + \alpha_1 \bar{T}_d + \alpha_0$$

$$+ \beta_2 \cos(0.5\pi\,\bar{t}) + \beta_1 \sin(0.5\pi\,\bar{t}),$$

$$\bar{z} = 0: \qquad \frac{\partial \bar{T}_d}{\partial \bar{z}} = Pe \bar{T}_d, \tag{7.36}$$

$$\bar{z} = 1: \qquad \frac{\partial \bar{T}_d}{\partial \bar{z}} = 0,$$

$$\bar{t} = 0: \qquad \bar{T}_d = 0.$$

7.4.2 Model order reduction and output feedback control structure

For MOR of the system and target PDEs we require the eigenfunctions which must be computed by solving the following eigenproblem of the system and target spatial differential operator,

$$\frac{1}{Pe}\frac{d^2\phi_i}{d\bar{z}^2} - \frac{d\phi_i}{d\bar{z}} = \lambda_i\phi_i,$$

$$\bar{z} = 0 : \quad \frac{d\phi_i}{d\bar{z}} = Pe\phi_i, \qquad (7.37)$$

$$\bar{z} = 1 : \quad \frac{d\phi_i}{d\bar{z}} = 0.$$

where $i = 1, 2, \ldots, \infty$. The solution of above eigenvalue-eigenfunction problem takes the following form [76, 166, 174],

$$\lambda_i = -\left(\frac{\alpha_i^2}{Pe} + \frac{Pe}{4}\right), \qquad \tan(\alpha_i) = \frac{Pe\alpha_i}{\alpha_i^2 - \left(\frac{Pe}{2}\right)^2},$$

$$\phi_i(\bar{z}) = \xi_i \exp\left(\frac{Pe\bar{z}}{2}\right)\left[\cos(\alpha_i\bar{z}) + \frac{Pe}{2\alpha_i}\sin(\alpha_i\bar{z})\right], \qquad (7.38)$$

$$\xi_i = \left(\int_0^1 \left[\cos(\alpha_i\bar{z}) + \frac{Pe}{2\alpha_i\bar{z}}\sin(\alpha_i\bar{z})\right]^2 d\bar{z}\right)^{-\frac{1}{2}}.$$

The resulting eigenfunctions are not self-adjoint because the spatial differential operator of $\frac{1}{Pe}\frac{\partial^2}{\partial\bar{z}^2} - \frac{\partial}{\partial\bar{z}}$ is non-self-adjoint; then to apply the Galerkin projection we must define the adjoint eigenfunctions

$$\phi_i^*(\bar{z}) = exp(-Pe\bar{z})\phi_i(\bar{z}), \qquad (7.39)$$

which satisfy the orthonormal property of (7.4). By considering the set of m dominant eigenfunctions of $\Phi_s = [\phi_1 \ \phi_2 \ \cdots \ \phi_m]^T$, we approximate the system and

desired dimensionless temperatures

$$\bar{T}(\bar{z},\bar{t}) \approx \sum_{i=1}^{m} a_i(\bar{t})\phi_i(\bar{z}), \qquad \bar{T}_d(\bar{z},\bar{t}) \approx \sum_{i=1}^{m} \tilde{a}_i(\bar{t})\phi_i(\bar{z}), \qquad (7.40)$$

where $\sigma = \dfrac{|\lambda_1|}{|\lambda_{m+1}|}$ has a small positive value. Then by employing Galerkin's method, the ROMs of the system and target PDEs take the following modal forms,

$$\dot{a}_k = \lambda_k a_k + B_t \int_0^1 \phi_k^* \exp\Big(\frac{\gamma \sum_{i=1}^m a_i\phi_i}{1 + \sum_{i=1}^m a_i\phi_i}\Big)d\bar{z} + \phi_k^*(0)\bar{T}_f$$

$$-B_c \sum_{j=1}^{l}\Big(\int_0^1 \mathcal{B}_j\phi_k^* \sum_{i=1}^m a_i\phi_i\,d\bar{z}\Big) + B_c \sum_{j=1}^{l}\Big(\int_0^1 \mathcal{B}_j\phi_k^*\,d\bar{z}\Big)\bar{u}_j,$$

$$\dot{\tilde{a}}_k = \lambda_k \tilde{a}_k + \int_0^1 \Big(\alpha_3\Big(\sum_{i=1}^m \tilde{a}_i\phi_i\Big)^3 + \alpha_2\Big(\sum_{i=1}^m \tilde{a}_i\phi_i\Big)^2 + \alpha_0 \qquad\qquad (7.41)$$

$$+\beta_2 \cos(0.5\pi\,\bar{t}) + \beta_1 \sin(0.5\pi\,\bar{t})\Big)\phi_k^* d\bar{z} + \alpha_1 \tilde{a}_k,$$

for $k = 1, 2, \ldots, m$. Then the above ROMs can be summarized in the following abstract forms

$$\dot{a} = Aa + f(a) + Bu,$$
$$\qquad\qquad (7.42)$$
$$\dot{\tilde{a}} = A\tilde{a} + f'(\tilde{a}),$$

where

$$a = \begin{bmatrix} a_1 \\ a_2 \\ \vdots \\ a_m \end{bmatrix}, \qquad \tilde{a} = \begin{bmatrix} \tilde{a}_1 \\ \tilde{a}_2 \\ \vdots \\ \tilde{a}_m \end{bmatrix}, \qquad A = \begin{bmatrix} \lambda_1 & 0 & \cdots & 0 \\ 0 & \lambda_2 & \cdots & 0 \\ \vdots & \vdots & \ddots & \vdots \\ 0 & 0 & \cdots & \lambda_m \end{bmatrix}, \qquad u = \begin{bmatrix} \bar{u}_1 \\ \bar{u}_2 \\ \vdots \\ \bar{u}_l \end{bmatrix},$$

$$f(a) = \begin{bmatrix} B_t \int_0^1 \phi_1^* \exp\Big(\dfrac{\gamma \sum_{i=1}^m a_i\phi_i}{1+\sum_{i=1}^m a_i\phi_i}\Big)d\bar{z} + \phi_1^*(0)\bar{T}_f - B_c \sum_{j=1}^l \Big(\int_0^1 \mathcal{B}_j\phi_1^* \sum_{i=1}^m a_i\phi_i\, d\bar{z}\Big) \\[2ex] B_t \int_0^1 \phi_2^* \exp\Big(\dfrac{\gamma \sum_{i=1}^m a_i\phi_i}{1+\sum_{i=1}^m a_i\phi_i}\Big)d\bar{z} + \phi_2^*(0)\bar{T}_f - B_c \sum_{j=1}^l \Big(\int_0^1 \mathcal{B}_j\phi_2^* \sum_{i=1}^m a_i\phi_i\, d\bar{z}\Big) \\[2ex] \vdots \\[2ex] B_t \int_0^1 \phi_m^* \exp\Big(\dfrac{\gamma \sum_{i=1}^m a_i\phi_i}{1+\sum_{i=1}^m a_i\phi_i}\Big)d\bar{z} + \phi_m^*(0)\bar{T}_f - B_c \sum_{j=1}^l \Big(\int_0^1 \mathcal{B}_j\phi_m^* \sum_{i=1}^m a_i\phi_i\, d\bar{z}\Big) \end{bmatrix},$$

$$B = \begin{bmatrix} B_c \int_0^1 \mathcal{B}_1\phi_1^*\, d\bar{z} & B_c \int_0^1 \mathcal{B}_2\phi_1^*\, d\bar{z} & \cdots & B_c \int_0^1 \mathcal{B}_l\phi_1^*\, d\bar{z} \\[2ex] B_c \int_0^1 \mathcal{B}_1\phi_2^*\, d\bar{z} & B_c \int_0^1 \mathcal{B}_2\phi_2^*\, d\bar{z} & \cdots & B_c \int_0^1 \mathcal{B}_l\phi_2^*\, d\bar{z} \\[2ex] \vdots & \vdots & \ddots & \vdots \\[2ex] B_c \int_0^1 \mathcal{B}_1\phi_m^*\, d\bar{z} & B_c \int_0^1 \mathcal{B}_2\phi_m^*\, d\bar{z} & \cdots & B_c \int_0^1 \mathcal{B}_l\phi_m^*\, d\bar{z} \end{bmatrix},$$

$$f'(\tilde{a}) = \begin{bmatrix} \int_0^1 \Big(\alpha_3\Big(\sum_{i=1}^m \tilde{a}_i\phi_i\Big)^3 + \alpha_2\Big(\sum_{i=1}^m \tilde{a}_i\phi_i\Big)^2 + \alpha_0 \\ \qquad +\beta_2 \cos(0.5\pi\,\bar{t}) + \beta_1 \sin(0.5\pi\,\bar{t})\Big)\phi_1^* d\bar{z} + \alpha_1\tilde{a}_1 \\[3ex] \int_0^1 \Big(\alpha_3\Big(\sum_{i=1}^m \tilde{a}_i\phi_i\Big)^3 + \alpha_2\Big(\sum_{i=1}^m \tilde{a}_i\phi_i\Big)^2 + \alpha_0 \\ \qquad +\beta_2 \cos(0.5\pi\,\bar{t}) + \beta_1 \sin(0.5\pi\,\bar{t})\Big)\phi_2^* d\bar{z} + \alpha_1\tilde{a}_2 \\[3ex] \vdots \\[3ex] \int_0^1 \Big(\alpha_3\Big(\sum_{i=1}^m \tilde{a}_i\phi_i\Big)^3 + \alpha_2\Big(\sum_{i=1}^m \tilde{a}_i\phi_i\Big)^2 + \alpha_0 \\ \qquad +\beta_2 \cos(0.5\pi\,\bar{t}) + \beta_1 \sin(0.5\pi\,\bar{t})\Big)\phi_m^* d\bar{z} + \alpha_1\tilde{a}_m \end{bmatrix}.$$

By considering the modal error as $e = a - \tilde{a}$, the error dynamics can be formulated by

$$\dot{e} = Ae + f(e, \tilde{a}) - f'(\tilde{a}) + Bu. \tag{7.43}$$

Then the sliding mode controller and dynamics observer structures take the following form

$$
\begin{aligned}
u &= -B^{\perp}\left((A + \Pi)\hat{e} + f(\hat{e}, \tilde{a}) - f'(\tilde{a}) + \eta \, sign\left(\hat{e} + \Pi \int_0^t \hat{e} \, dt \right) \right), \\
\dot{\hat{a}} &= A\hat{a} + f(\hat{a}) + Bu + \Theta(y - C\hat{a}), \\
\hat{e} &= \hat{a} - \tilde{a},
\end{aligned} \tag{7.44}
$$

where the dynamic observer gain matrix, Θ, can be computed using the LMI-constrained optimization problem described in Section 7.3.3.

7.4.3 Simulation results

To simulate the system we set the following typical values for the process parameters: $Pe = 5$, $\gamma = 3$, $B_t = 0.4$, $B_c = 0.5$ and $\bar{T}_f = 0$. The dominant eigenvalues of the system are presented in Table 7.1. We can easily recognize an

Table 7.1: Dominant eigenvalues

Eigenvalues	$i = 1$	$i = 2$	$i = 3$	$i = 4$	$i = 5$	$i = 6$
λ_i	-1.94	-4.80	-10.97	-20.93	-34.78	-52.56
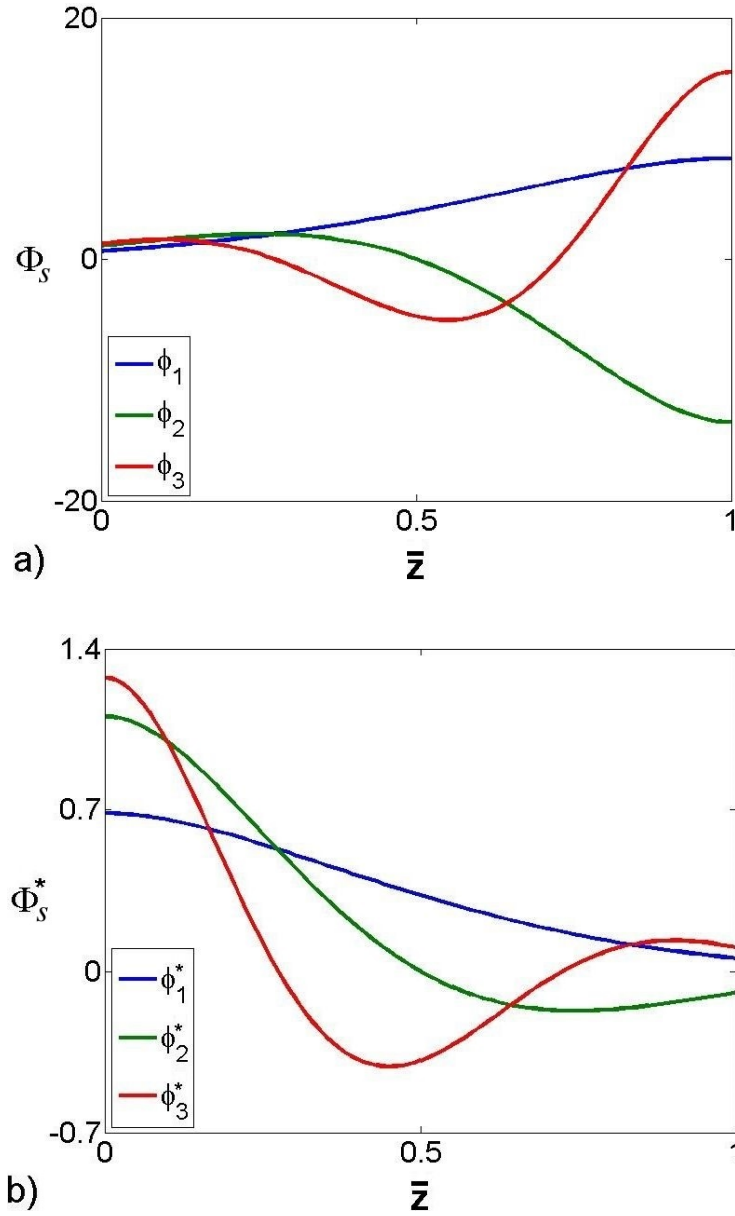
Figure 7.2: (a) Temperature dominant eigenfunctions and (b) their adjoints.

order of magnitude separation between the 3 dominant eigenvalues and the remainder, $\sigma = \dfrac{Re(|\lambda_1|)}{Re(|\lambda_4|)} = O(0.1)$, where $O(\cdot)$ denotes the order of magnitude. The corresponding dominant eigenfunctions and their adjoints are presented in Figure 7.2.

When considering the first three dominant eigenfunctions to discretize the system and desired PDEs, the resulting system and target approximations are of dimension 3 ($m = 3$). We set $l = 3$ cooling jackets along the reactor length to shape the spatiotemporal temperature dynamics of the system. The spatial distributions of the control actuators are also described by $\mathcal{B}_1(\bar{z}) = H(\bar{z} - 0.1) - H(\bar{z} - 0.2)$, $\mathcal{B}_2(\bar{z}) = H(\bar{z} - 0.4) - H(\bar{z} - 0.5)$ and $\mathcal{B}_3(\bar{z}) = H(\bar{z} - 0.7) - H(\bar{z} - 0.9)$, where $H(\cdot)$ indicates the standard Heaviside step function. We also consider two point sensors to measure the reactor temperature at $\omega = [0.3 \ \ 0.6]^T$ which can be employed by the dynamic observer to estimate the dominant eigenmodes of the system.

The entire system operation was partitioned into two time periods: (1) open-loop process operation, $\bar{t}_o = [0, 8]$ when the controller was inactive, and (2) closed-loop process operation, $\bar{t}_c = (8, 12]$ under the proposed controller design. The open-loop spatiotemporal profile of the dimensionless temperature and the temporal profile of its spatial L_2-norm while the controller was inactive ($\bar{u}_i = 0$ for $i = 1, 2, 3$) are presented in Figure 7.3.

It is observed that the dimensionless temperature converges to a nonuniform steady state profile. Figure 7.4 also shows the desired spatiotemporal profile and its L_2-norm where $\alpha_0 = 0.15$, $\alpha_1 = 0.05$, $\alpha_2 = -0.1$, $\alpha_3 = 0.15$, $\beta_1 = 0.2$ and $\beta_2 = -0.05$. We observe a permanent oscillatory behavior in the desired temperature spatiotemporal dynamics.

The open-loop spatiotemporal profile of the shaping error and its spatial L_2-

norm are presented in Figure 7.5.

The dynamic observer gain matrix was computed as follows,

$$\Theta = \begin{bmatrix} 0.20 & 0.64 \\ 0.31 & -0.48 \\ -0.27 & -2.12 \end{bmatrix},$$

by solving the LMI-constrained optimization problem. Figure 7.6 presents the open-loop temporal profiles of the estimated dominant eigenmodes of the system, the desired dominant eigenmodes and the open-loop modal errors where the non-dominant system and desired eigenmodes were negligible.

To implement the proposed sliding mode controller we set $\eta = 0.5$ for the controller parameter. The spatiotemporal profile of the dimensionless reactor temperature and the temporal profile of its spatial L_2-norm is illustrated in Figure 7.7 for the entire process operation.

The spatiotemporal profile of the shaping error and its L_2-norm are also presented in Figure 7.8. Note that the controller was only active during the closed-loop process operation of $\bar{t}_c = (8, 12]$. We observe that the shaping error converges to zero and the system follows the desired spatiotemporal behavior under the proposed control approach.

The required control actions to stabilize the shaping error are shown in Figure 7.9. The zero control actions in the period of $\bar{t}_o = (0, 8)$ illustrate the open-loop

process operation. An oscillatory behavior is observed in the controller signals due to the permanent oscillatory behavior of the target spatiotemporal dynamics.

Finally, the temporal profile of the estimated dominant eigenmodes and the modal errors are presented in Figure 7.10 which illustrates the effectiveness of the sliding mode controller in regulating the shaping error and tracking the desired spatiotemporal dynamics.
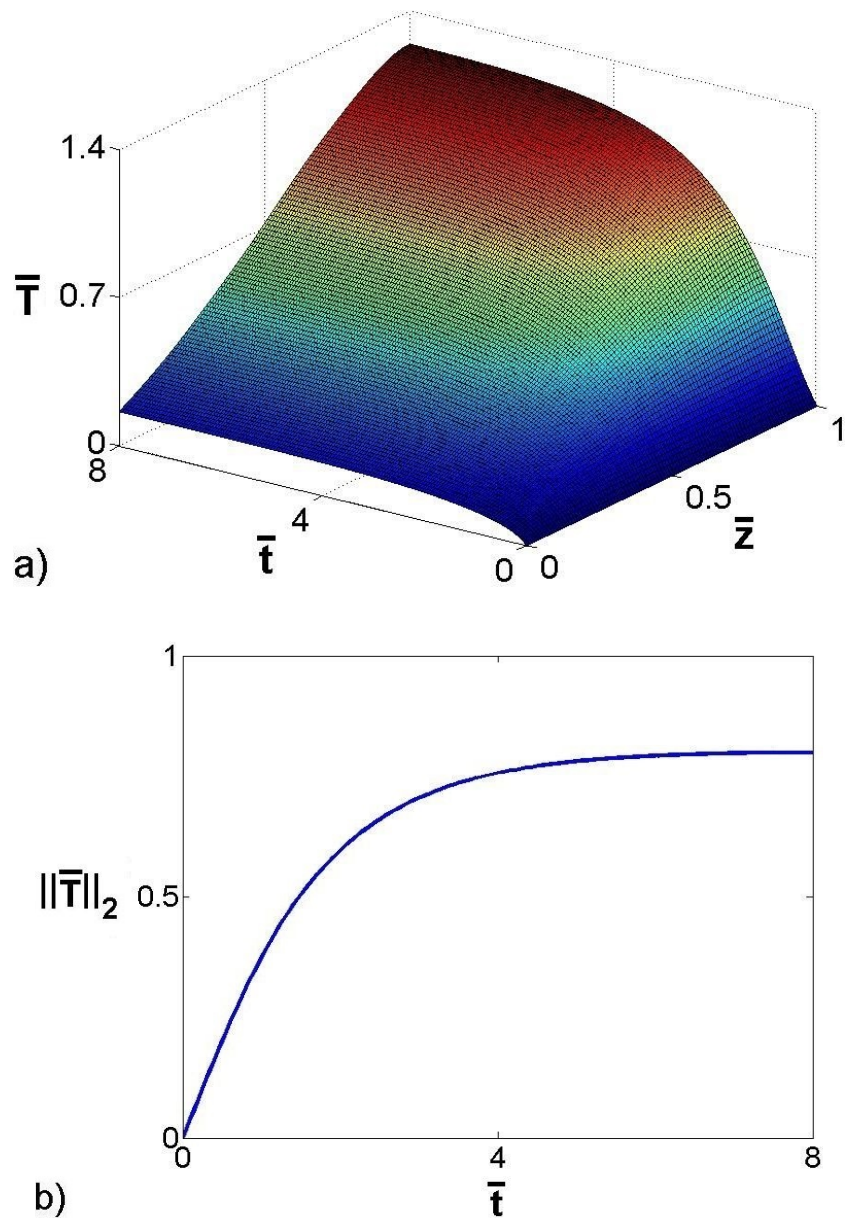
Figure 7.3: Open-loop (a) spatiotemporal profile of the dimensionless temperature and (b) temporal profile of temperature L_2-norm.
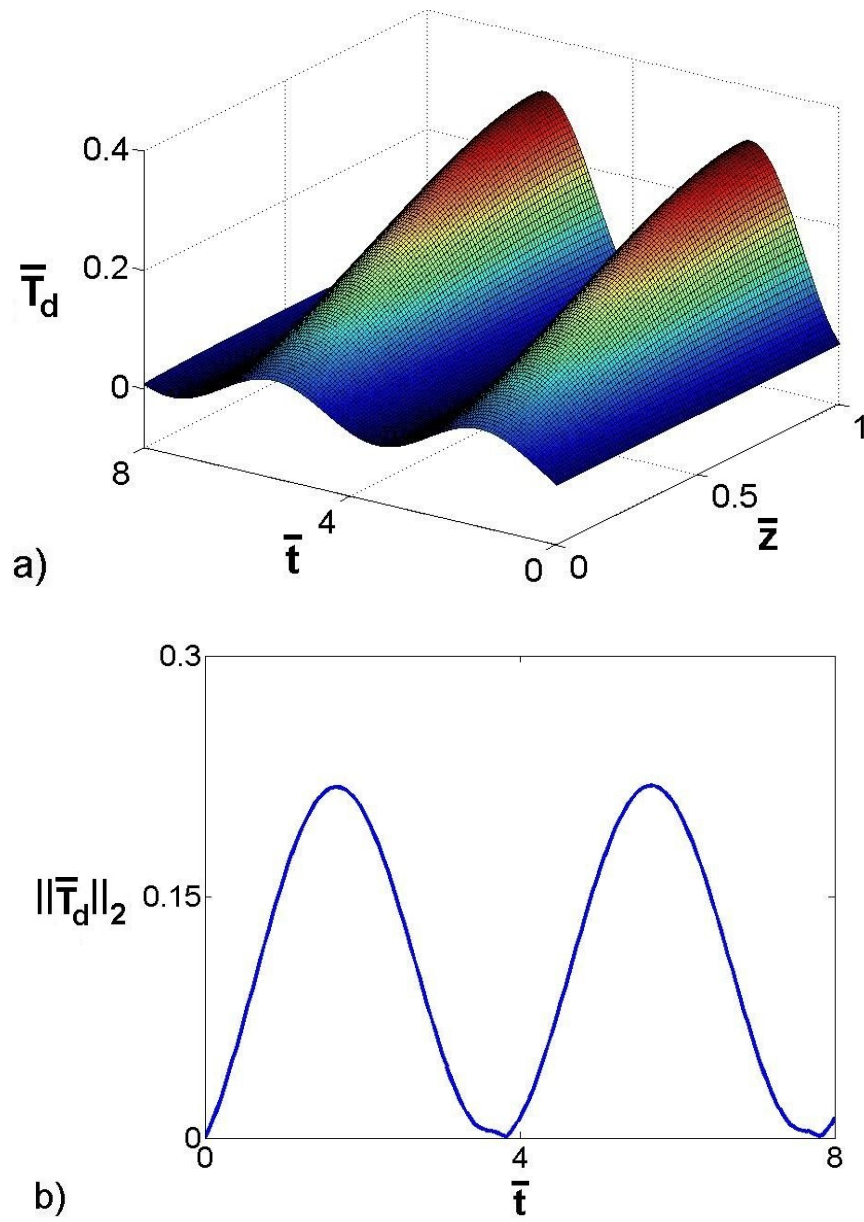
Figure 7.4: (a) Spatiotemporal profile of the desired dimensionless temperature and (b) temporal profile of its L_2-norm.
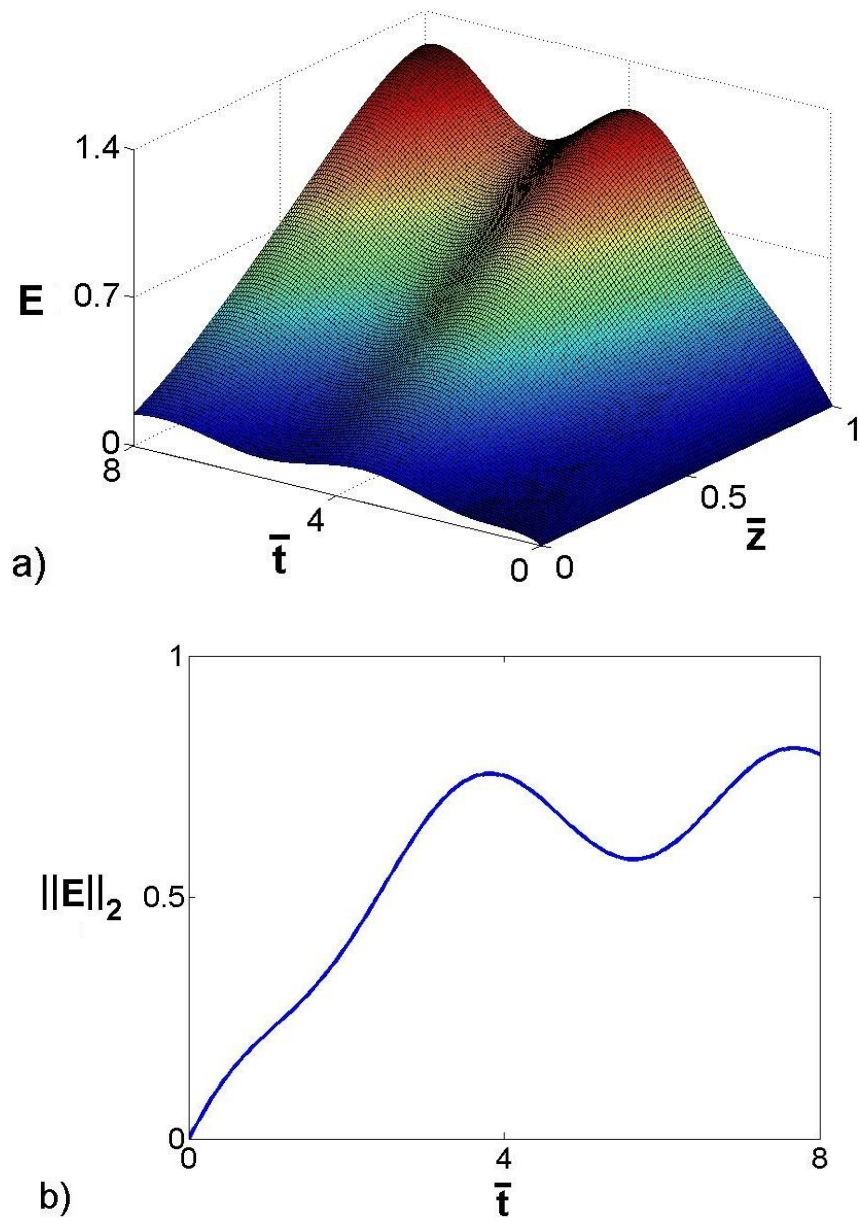
Figure 7.5: Open-loop (a) spatiotemporal profile of the shaping error and (b) temporal profile of its L_2-norm.
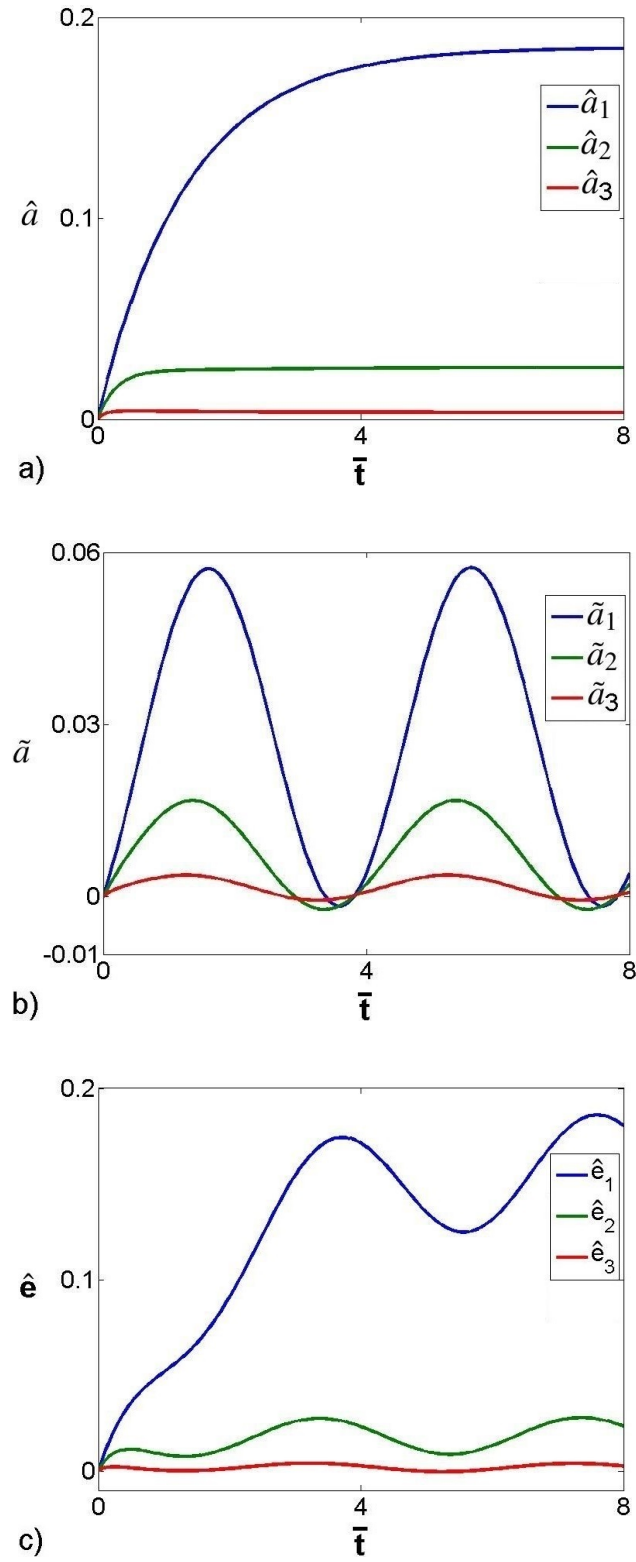
Figure 7.6: Temporal profiles of (a) dominant eigenmodes of the system, (b) desired dominant eigenmodes and (c) modal errors during the open-loop period.
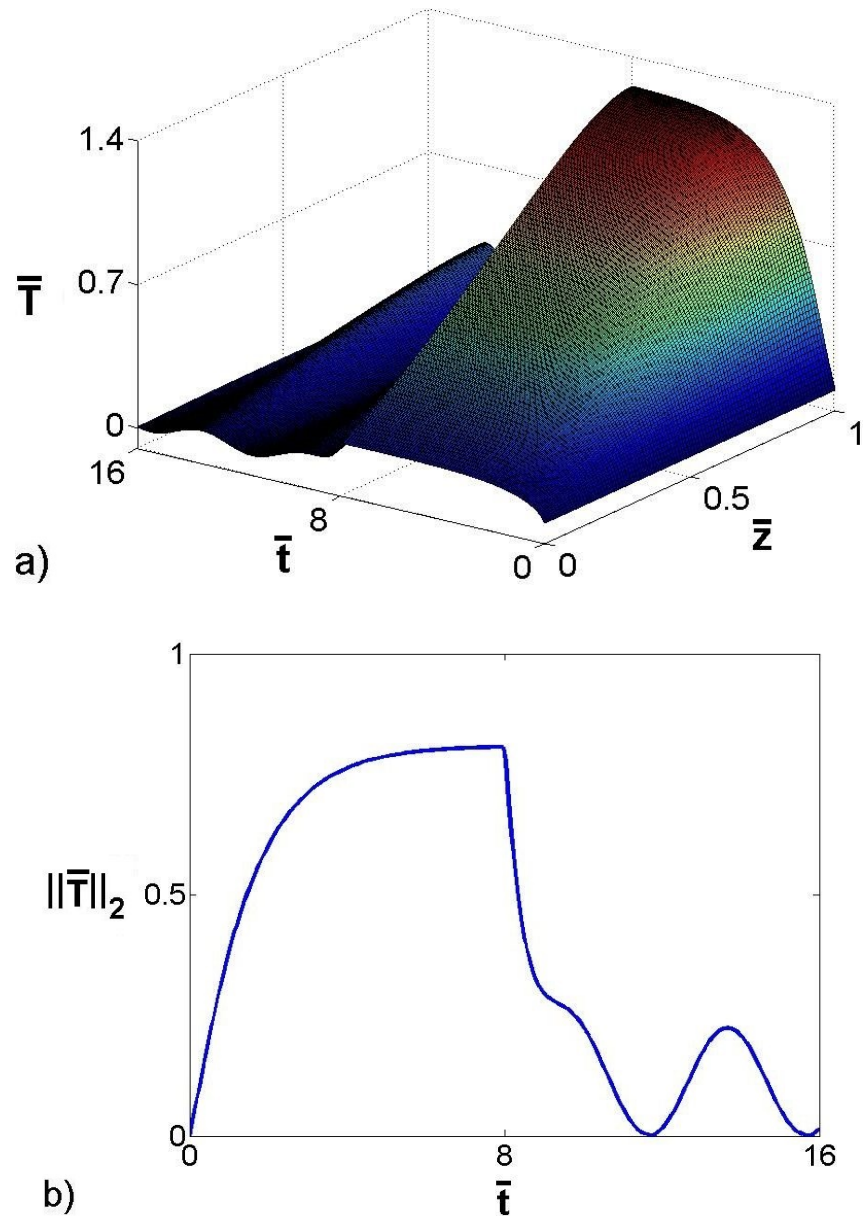
Figure 7.7: (a) Spatiotemporal profile of the dimensionless temperature and (b) temporal profile of its L_2-norm for the entire process operation.
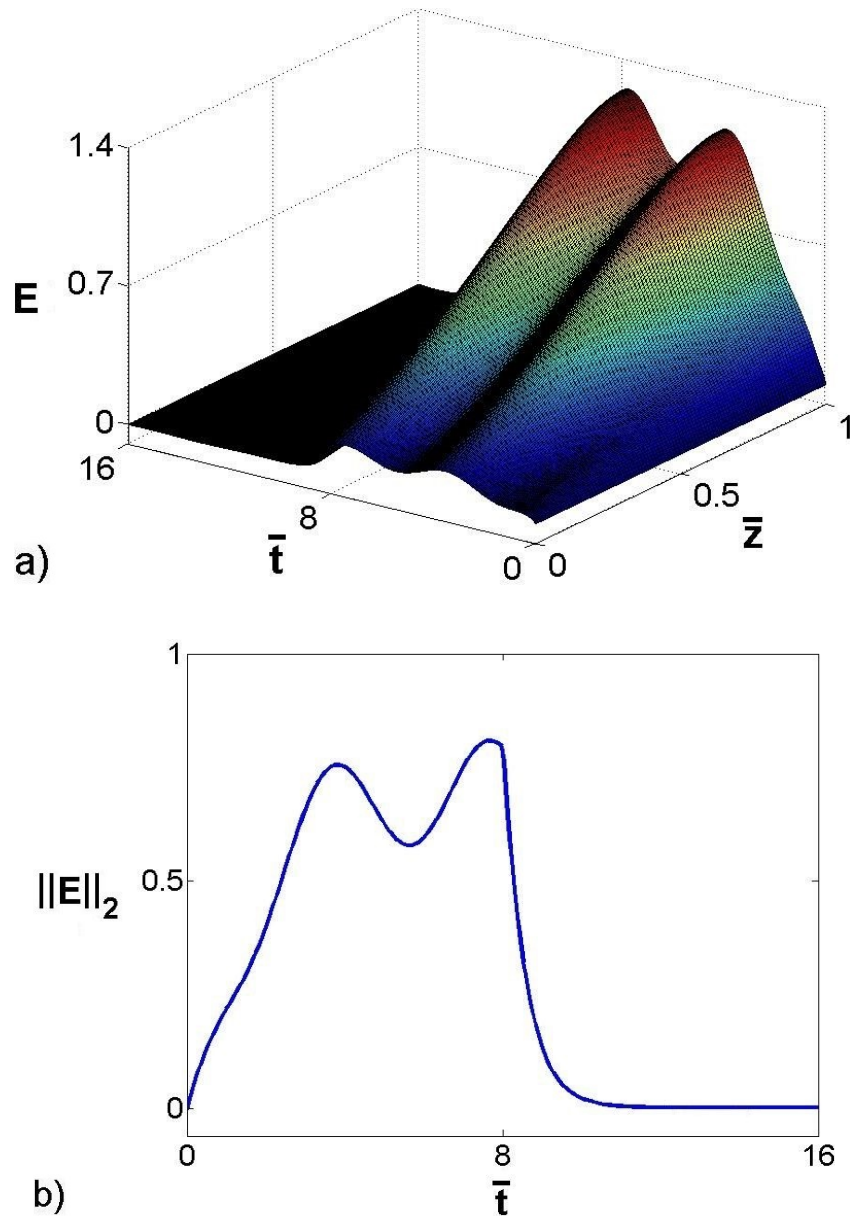
Figure 7.8: (a) Spatiotemporal profile of the shaping error and (b) temporal profile of its L_2-norm for the entire process operation.
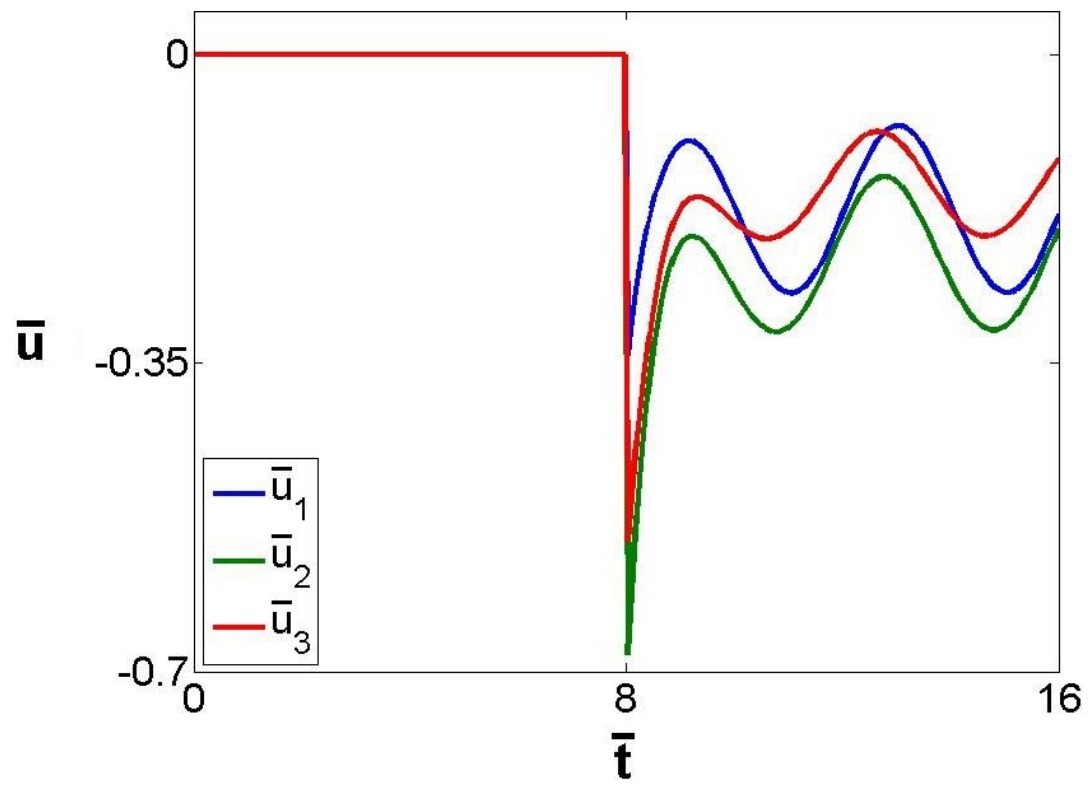
Figure 7.9: Required control actions for the entire process operation. The zero in $[0, 8]$ denotes the open-loop period.
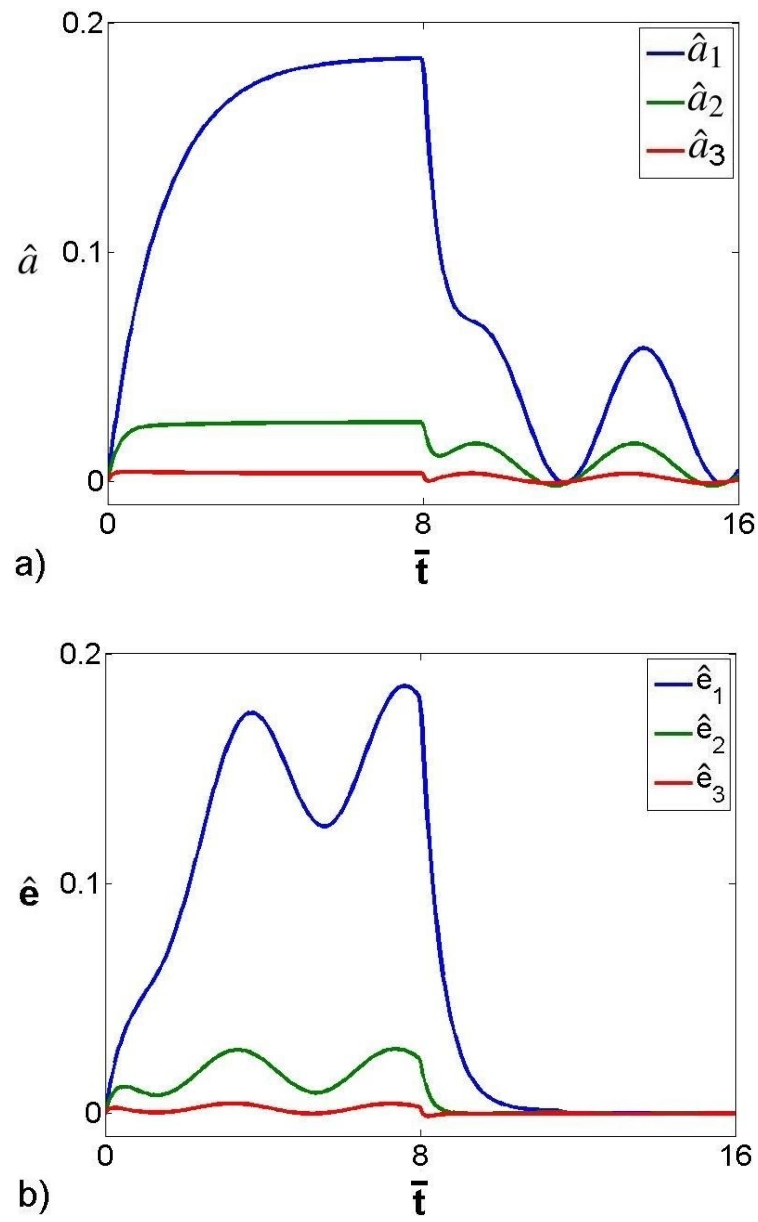
Figure 7.10: Temporal profiles of (a) dominant eigenmodes of the system and (b) modal errors for the entire process operation.

ADAPTIVE CONTROL OF DISTRIBUTED PARAMETER SYSTEMS VIA MODEL ORDER REDUCTION

8.1 introduction

The early pioneering research which introduced the importance of adaptation in control theory and applications may be traced back to sixty years ago [23, 58, 143, 250, 264]. The first model reference Lyapunov-based adaptive law design was

presented in [201]. Study of globally stable continuous adaptive control systems [98, 105, 121, 187, 190, 194, 195], discrete deterministic and stochastic adaptive systems [119–121], robust adaptive control [136] and other practical issues of adaptive control brought to light new problems and solutions.

While the adaptive control is a very broad subject in the control engineering field presented in the wide range of topics from stochastic adaptive control and adaptive variable structure control to adaptive model predictive control, the unified theme of adaptive control is the use of a certainty equivalence principle. This essential principle indicates that the adaptive parameter estimates can be used in the feedback controller design as if they are the true parameters for a plant with uncertainty. The immediate problem is the convergence of the identified parameters to their true values. In adaptive estimation, the parameter estimates converge to their true values under the following conditions:

- the plant model does not have zero-pole cancellation,

- the plant estimate model has the same plant order,

- the adaptive system is persistently exciting, ensured by previous conditions and by a sufficiently rich input.

The certainty equivalence principle relies on the basis of two technical foundations; maximal plant uncertainty parametrization and stable controller parameter adaptation. The concept of persistence excitation and its effects on param-

eter convergence in lumped and distributed parameter system was addressed in [90, 159, 170]. The early study of adaptive control in the absence of persistence excitation was also introduced in [10, 176].

The important research results in the field of adaptive control in recent years can be summarized as follows; the concept of parameter convergence in adaptive control of continuous and discrete systems [41, 65, 66, 239, 268], robust performance of adaptive systems in the presence of uncertainty [85, 137, 199, 276], stability of adaptive control systems [102, 114, 129], adaptive control of distributed parameter systems [63], stochastic adaptive control [95, 128, 277], model reference adaptive control [105, 141, 223, 237], nonlinear adaptive output feedback control [147, 246], adaptive control via feedback linearization [144], adaptive control of non-minimum phase systems [132, 173], adaptive backstepping control [160], adaptive control of nonlinearly parameterized systems [150, 171], hybrid adaptive control [191, 193], improving adaptive control systems performance [152, 184, 185, 200, 240, 267], adaptive dynamics programming optimal control [259], robust adaptive control [206, 236, 260, 262, 263, 277] and adaptive control considering input bounds [275]. A brief description of recent results in adaptive control theory and application can be found in [241].

Compare to the control problem of Lumped parameter systems (LPSs) described by ordinary differential equations (ODEs) which has been well studied in the chemical process industries for more than 50 years, the control of chemical

distributed parameter systems (DPSs) modeled by partial differential equations (PDEs) is a much more difficult task that needs more powerful mathematical tools [76]. Such types of systems frequently arise in many industrial chemical processes which can be exemplified by packed and fluidized bed reactors, crystallization and polymerization processes, chemical vapor deposition systems, microelectronic fabrication and plasma etching processes, where spatial distribution and nonlinearity take the essential roles due to the importance of transport phenomena and reaction mechanisms [1, 76, 172, 198, 212].

While direct approaches for control of PDE systems are limited to simple processes operate over regular domains [84, 233], one of the practically effective methods to address the control problem of DPSs is via model order reduction (MOR) [47, 76]. In MOR-based approaches, an approximation of the system in the form of low-dimensional ODEs is applied as the basis for controller design. Then most of the control techniques tailored for LPSs can be indirectly applied to DPSs through such approximations [28, 31, 37, 47, 99, 166]. Weighted residual techniques like Galerkin projection is one of the methods that has been widely employed to discretize the governing PDEs to finite number of ODEs. The shape and efficient number of basis functions required by such spatial discretization methods to approximate the distributed systems can be computed analytically or using statistical techniques [29, 30, 32, 35, 76, 94, 166].

In governing PDEs described the chemical DPSs, the chemical reaction term

is the source of nonlinearity that usually contains unknown parameters due to the temperature dependency and possible lack of knowledge about the reaction passes. Thus, applying system identification and adaptation strategies are unavoidable to address the control problem of such systems. Direct adaptive controller and observer designs for describing PDEs has been widely used for DPSs [54, 60, 91, 135, 161, 233], however it is limited to linear PDEs subject to simple boundary conditions. The adaptive control synthesis for more general class of DPSs can be motivated by applying adaptive control designed which tailored for LPSs [25, 147, 218] taking advantageous of MOR, when we employ the ODE approximations to model the dominant behavior of DPSs.

In this chapter we focus on modal adaptive output feedback control structure designs for transport-reaction processes in the presence of unknown parameters. Galerkin projection is employed to approximate the infinite-dimensional representation of the governing PDEs by low-dimensional ODEs. The studied systems are divided to three categories: (1) when the required basis functions can be analytically computed, (2) when the required empirical basis functions can be computed using POD and (3) when the required empirical basis functions must be computed and updated using APOD during process evolution. Then a Lyapunov-based adaptive controller is designed to stabilize the system at the desired point. An observer is applied to estimate the system modes based on limited number of continuous point measurement sensors. The effectiveness of the proposed adaptive control ap-

proach is illustrated on temperature regulation in a tubular chemical reactor which can be described by semi-linear parabolic PDEs and wave motion suppression in a thin film described by Korteweg-de Vries-Burgers (KdVB) equation.

8.2 Adaptive control of DPSs via analytical model order reduction

8.2.1 Preliminaries

8.2.1.1 A class of semi-linear distributed parameter systems

We focus on transport-reaction processes in the presence of unknown reaction parameters which can be modeled by the following PDEs,

$$
\frac{\partial \bar{x}(z,t)}{\partial t} = \mathcal{A}(z)\bar{x}(z,t) + \mathcal{F}\big(z, \bar{x}(z,t)\big) + \mathcal{G}\big(z, \bar{x}(z,t)\big)\theta + \mathcal{B}(z)u(t),
$$

$$
y(t) = \int_{\Omega} \delta(z - L_s)\bar{x}(z,t) \ dz, \tag{8.1}
$$

$$
\Gamma\left(t, \bar{x}(z,t), \frac{\partial \bar{x}(z,t)}{\partial z}\right)_{\partial\Omega} = 0, \qquad \bar{x}(z,0) = \bar{x}_0(z),
$$

where $\bar{x} \in \mathbb{R}^n$ is the vector of spatiotemporal states, $z \in \Omega$ denotes the spatial coordinate and t is time. The process domain is denoted by $\Omega \subset \mathbb{R}$ with the boundary of $\partial\Omega$. The terms $\mathcal{A}^{n \times n}$, $\mathcal{F}^{n \times 1}$ and $\mathcal{G}^{n \times q}$ present the second order linear spatial differential operator, nonlinear vector and matrix functions, respectively. The vector of unknown parameters is denoted by $\theta \in \mathbb{R}^q$ and the vector of $u \in \mathbb{R}^l$

presents manipulated inputs where their spatial distributions is described by $\mathcal{B}^{n \times l}$. The vector of $y \in \mathbb{R}^r$ presents the continuous point measurement outputs of the process where L_s is the vector of locations of the measurement sensors and δ denotes the standard Dirac function. The general homogeneous boundary conditions are presented by the smooth nonlinear vector of equations of $\Gamma^{2n \times 1}(\cdot) = 0$ and $\bar{x}_0$ is the initial spatial profile of the system state.

In above PDEs, $\mathcal{A}(z)\bar{x}$ describes diffusion, dispersion and convection phenomena, $\mathcal{F}(z, \bar{x})$ presents the known reaction dynamics of the system and the possible non-homogeneous part of the boundary conditions that can be induced in the governing PDEs. The term $\mathcal{G}(z, \bar{x})\theta$, also shows the unknown reaction dynamics of the process. Note that even multiple reactions take place in a system, the mathematical model can still be described in the above form where $\mathcal{F}(z, \bar{x})$ and $\mathcal{G}(z, \bar{x})\theta$ indicate the known and unknown dynamics of the multiple reactions, respectively.

8.2.1.2 Infinite-dimensional representation

By defining an appropriate Sobolev subspace of $\mathbb{W}$ as

$$\mathbb{W}(\Omega) = \left\{ \mathcal{H}, \ \frac{\partial \mathcal{H}}{\partial z} \in L_2(\Omega) : \ \Gamma\left(\mathcal{H}, \frac{\partial \mathcal{H}}{\partial z}\right)_{\partial \Omega} = 0 \right\},$$

the functional state of $x(t) \in \mathbb{W}$, $x(t) = \bar{x}(z, t)$, the linear operator of

$$\mathbf{A}x(t) = \mathcal{A}(z)\bar{x}(z, t),$$

the nonlinear functions of

$$\mathbf{F}\big(x(t)\big) = \mathcal{F}\big(z, \bar{x}(z,t)\big), \qquad \mathbf{G}\big(x(t)\big)\theta = \mathcal{G}\big(z, \bar{x}(z,t)\big)\theta$$

and the input operator of $\mathbf{B}u(t) = \mathcal{B}(z)u(t)$, we can represent the PDEs of (8.1) in the following semi-linear infinite-dimensional form,

$$\dot{x}(t) = \mathbf{A}x(t) + \mathbf{F}\big(x(t)\big) + \mathbf{G}\big(x(t)\big)\theta + \mathbf{B}u(t), \ x(0) = x_0, \tag{8.2}$$

The set of basis functions required to discretize the dynamics of (8.2) can be found by solving the eigenproblem of the linear operator which takes the following form

$$\mathbf{A}\phi_i = \lambda_i \phi_i, \qquad i = 1, \ldots, \infty \tag{8.3}$$

subject to the boundary conditions

$$\Gamma\left(\phi_i, \frac{d\phi_i}{dz}\right)_{\partial\Omega} = 0,$$

where ϕ_i denotes the basis function corresponds to the eigenvalue of λ_i. The adjoint basis function of ϕ_i^* can also be defined subject to the orthonormal property of the basis functions as

$$\big(\phi_i(z), \phi_i(z)\big) = \int_\Omega \phi_i(z)\phi_i^*(z) \, dz = 1.$$

Note that the linear operator is a strong generator of the defined Sobolev subspace, i.e., $\mathbb{W} \triangleq span\{\phi_i\}_{i=1}^{\infty}$.

For the majority of transport-reaction processes we can assume that the eigenspectrum of the linear operator, $\{\lambda_1, \lambda_2, \dots\}$, can be partitioned into the following subsets;

1. finite subset of first m eigenvalues, $\{\lambda_1, \lambda_2, \dots, \lambda_m\}$, which are slow and possibly unstable,

2. complement infinite subset of the remainder eigenvalues, $\{\lambda_{m+1}, \lambda_{m+2}, \dots\}$, which are fast and stable,

where $Re(\lambda_1) \geq Re(\lambda_2) \geq \cdots \geq Re(\lambda_m) \geq Re(\lambda_{m+1}) \geq \cdots$, $Re(\lambda_{m+1}) < 0$ and $Re(\cdot)$ denotes the real part. In addition to such partitioning, a time scale separation can also be identified between the subsets by $\sigma = \dfrac{|Re(\lambda_1)|}{|Re(\lambda_{m+1})|}$, where σ is a small positive number.

Then the corresponding Sobolev subspaces for such subsets can be defined as follows;

1. slow subspace, $\mathbb{W}_s \triangleq span\{\phi_i\}_{i=1}^{m}$,

2. complement fast subspace, $\mathbb{W}_f \triangleq span\{\phi_i\}_{i=m+1}^{\infty}$,

where $\mathbb{W} = \mathbb{W}_s \cup \mathbb{W}_f$.

8.2.2 Model order reduction

By defining the appropriate slow and fast integral projections

$$\mathcal{P} : \mathbb{W} \to \mathbb{W}_s, \quad \mathcal{P}(\cdot) = (\cdot, \Phi_s),$$
$$\mathcal{Q} : \mathbb{W} \to \mathbb{W}_f, \quad \mathcal{Q}(\cdot) = (\cdot, \Phi_f),$$

(8.4)

where $\Phi_s = [\phi_1 \ \phi_2 \ \cdots \ \phi_m]^T$, $\Phi_f = [\phi_{m+1} \ \phi_{m+2} \ \cdots]^T$, and φ^T denotes the transpose of φ, and using Galerkin's method we can derive two sets of modal ODEs as follows

$$\dot{x}_s = A_s x_s(t) + F_s\big(x_s(t), x_f(t)\big) + G_s\big(x_s(t), x_f(t)\big)\theta + B_s u(t),$$
$$x_s(0) = \mathcal{P}x_0,$$
$$\dot{x}_f = A_f x_f(t) + F_f\big(x_s(t), x_f(t)\big) + G_f\big(x_s(t), x_f(t)\big)\theta + B_f u(t),$$
$$x_f(0) = \mathcal{Q}x_0,$$

(8.5)

where $x = x_s \oplus x_f$, $A_s = \mathcal{P}\mathbf{A} = diag\{\lambda_i\}_{i=1}^{m}$, $A_f = \mathcal{Q}\mathbf{A} = diag\{\lambda_i\}_{i=m+1}^{\infty}$, $F_s = \mathcal{P}\mathbf{F}$, $F_f = \mathcal{Q}\mathbf{F}$, $G_s = \mathcal{P}\mathbf{G}$, $G_f = \mathcal{Q}\mathbf{G}$, $B_s = \mathcal{P}\mathbf{B}$, $B_f = \mathcal{Q}\mathbf{B}$ and $diag$ denotes the diagonal matrix.

By applying singular perturbation analysis [76] and considering Tykhonov's theorem for solution convergence of systems include slow and fast subsystems [175], after a short period of time, the infinite-dimensional system of (8.5) can be reduced

to

$$\dot{x}_s = A_s x_s(t) + F_s\big(x_s(t), 0\big) + G_s\big(x_s(t), 0\big)\theta + B_s u(t),$$

$$x_s(0) = \mathcal{P}x_0,$$

(8.6)

when $x_f \to 0$. Note that the required relaxation time can be identified using singular perturbation arguments [37, 76].

8.2.3 Adaptive output feedback control

Taking advantageous of MOR explained in the previous sections, we synthesize a low-dimensional adaptive output feedback controller based on the following ROM,

$$\dot{x}_s = A_s x_s + F_s(x_s) + G_s(x_s)\theta + B_s u,$$

(8.7)

obtained by applying Galerkin method to the PDEs of (8.1) using the first m dominant basis functions where $x_s \in \mathbb{R}^m$, $\theta \in \mathbb{R}^q$, $A_s \in \mathbb{R}^{m \times m}$, $F_s : \mathbb{R}^m \to \mathbb{R}^m$, $G_s : \mathbb{R}^m \to \mathbb{R}^{m \times q}$, $B_s \in \mathbb{R}^{m \times l}$ and $u \in \mathbb{R}^l$. We assume that the identification error, $e_\theta = \theta - \hat{\theta}$, remains bounded under the proposed stable adaptive output feedback controller synthesis, $\|e_\theta\| < \Theta$, where $\hat{\theta}$ denotes the vector of estimated values for unknown parameters and Θ is the identification error upper bound. We also assume that the vector of unknown parameters does not change rapidly during closed-loop process operation however it may change step-wise, thus $\dot{e}_\theta = \dot{\theta} - \dot{\hat{\theta}} = -\dot{\hat{\theta}}$.

For the controller synthesis we consider a control Lyapunov function (CLF) in

the following standard quadratic form,

$$V_c(x_s) = \frac{1}{2} x_s^T x_s, \tag{8.8}$$

where V_c is a positive definite function (i.e., $V_c(x_s) > 0$ and $V_c = 0$ only for $x_s = 0$). The time derivative of the CLF can then be derived as

$$\dot{V}_c = x_s^T \dot{x}_s = x_s^T \left(A_s x_s + F_s(x_s) + G_s(x_s)\theta + B_s u \right). \tag{8.9}$$

By considering

$$A_s x_s + F_s(x_s) + G_s(x_s)\theta + B_s u = -C_o x_s - \|G_s(x_s)\| \Theta \, sign(x_s), \tag{8.10}$$

where $C_o > 0$ and $sign(\cdot)$ shows the sign function, we obtain

$$\dot{V}_c = -C_o x_s^T x_s - \|G_s(x_s)\| \Theta \, x_s^T \, sign(x_s) \le 0.$$

Therefore V_c is a decreasing positive definite function that shows the closed-loop stability of the controller in the Lyapunov sense [148]. The controller formula can be derived from (8.10) as

$$u = -B_s^{\perp} \left(C_o x_s + A_s x_s + F_s(x_s) + G_s(x_s)\theta + \|G_s(x_s)\| \Theta \, sign(x_s) \right), \tag{8.11}$$

in the presence of unknown parameters, where $B_s^{\perp} = B_s^T(B_s B_s^T)^{-1}$ is the Moore-Penrose pseudo-inverse [202]. Note that $B_s^{\perp} = B_s^{-1}$ for $m = l$.

Then using certainty equivalence principle [25] we obtain the controller formula by replacing the unknown variable with the estimated one,

$$u = -B_s^{\perp}\Big(C_o x_s + A_s x_s + F_s(x_s) + G_s(x_s)\hat{\theta} + \|G_s(x_s)\|\Theta\, sign(x_s)\Big), \tag{8.12}$$

By defining a refined closed-loop Lyapunov function that contains the CLF and the identification Lyapunov function (ILF),

$$V = V_c(x_s) + V_i(e_\theta) = \frac{1}{2}x_s^T x_s + \frac{1}{2}e_\theta^T Z^{-1} e_\theta, \tag{8.13}$$

where $Z^{q \times q}$ is a symmetric positive definite matrix, we conclude $\dot{V} = \dot{V}_c + \dot{V}_i = x_s^T \dot{x}_s + \dot{e}_\theta^T Z^{-1} e_\theta$, then from $\dot{e}_\theta = -\dot{\hat{\theta}}$ and considering the following adaptation law to estimate the vector of unknown parameters,

$$\dot{\hat{\theta}} = Z\, G_s^T(x_s)\, x_s, \tag{8.14}$$

we obtain

$$\dot{V} = x_s^T\Big(A_s x_s + F_s(x_s) + G_s(x_s)\theta - C_o x_s$$
$$\qquad\qquad - A_s x_s - F_s(x_s) - G_s(x_s)\hat{\theta} - \|G_s(x_s)\|\Theta\, sign(x_s)\Big)$$
$$\qquad - \big(Z\, G_s^T(x_s)\, x_s\big)^T Z^{-1} e_\theta$$
$$\quad = x_s^T\big(G_s(x_s)\theta - C_o x_s - G_s(x_s)\hat{\theta} - \|G_s(x_s)\|\Theta\, sign(x_s)\big) - x_s^T G_s(x_s)e_\theta$$
$$\quad = -C_o x_s^T x_s - \|G_s(x_s)\|\Theta\, x_s^T\, sign(x_s) \le 0.$$
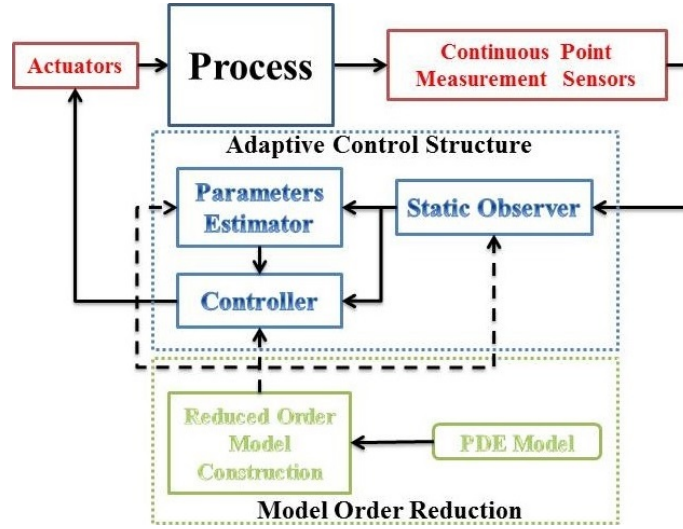
Figure 8.1: Closed-loop process block diagram.

Therefore $V = V_c + V_i$ is a decreasing positive definite function that shows the system closed-loop stability [148].

To estimate the vector of unknown parameters and compute the control action from (8.14) and (8.12), respectively, we must access to the full measurements of the system slow modes, x_s. We employ the following static observer structure to estimate the slow modes,

$$\hat{x}_s(t) = \left(\Phi_s(L_s)\Phi_s^T(L_s)\right)^{-1}\Phi_s(L_s)y(t), \tag{8.15}$$

where the number of required sensors has to be supernumerary to the number of slow modes, i.e., $r \geq m$.

The block diagram of the closed-loop process under the proposed adaptive output feedback controller design is presented in Figure 8.1.

8.2.4 Application to transport-reaction processes

In this section we focus on application of the proposed low-dimensional adaptive output feedback controller design to a tubular whose temperature and concentration spatiotemporal dynamics can be modeled by two semi-linear parabolic PDEs.

8.2.4.1 Process description

We consider a tubular reactor with a cooling jacket (Figure 8.2), where an irreversible exothermic second order chemical reaction in the form of $A \rightarrow B$ takes place. The cooling jacket and feed temperature are selected as the system manipulated inputs for control purposes. The spatiotemporal dynamics of the stream temperature and concentration of component A can be derived from heat and component mass balance considering constant physico-chemical properties as follows [166, 212],

$$\frac{\partial T}{\partial t} = \frac{k}{\rho C_p}\frac{\partial^2 T}{\partial z^2} - v\frac{\partial T}{\partial z} + \frac{-\Delta H}{\rho C_p}r_o \exp\left(\frac{-E}{RT}\right)C_A^2 - \frac{hA_c}{\rho C_p}(T - T_c),$$

$$\frac{\partial C_A}{\partial t} = D_A\frac{\partial^2 C_A}{\partial z^2} - v\frac{\partial C_A}{\partial z} - r_o \exp\left(\frac{-E}{RT}\right)C_A^2,$$

$$z = 0: \quad \frac{\partial T}{\partial z} = \frac{\rho C_p v}{k}(T - T_f), \quad \frac{\partial C_A}{\partial z} = \frac{v}{D_A}(C_A - C_{Af}), \qquad (8.16)$$

$$z = L: \quad \frac{\partial T}{\partial z} = 0, \quad \frac{\partial C_A}{\partial z} = 0,$$

$$t = 0: \quad T = T_0, \quad C_A = C_{A0},$$
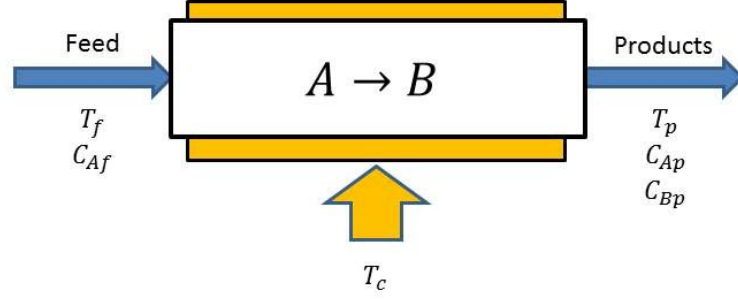
Figure 8.2: Tubular reactor with a cooling jacket.

where T is the reactor temperature, C_A denotes the concentration of component A, t is time $z \in [0, L]$ presents the spatial coordinate and L is the reactor length. The terms k, ρ, C_p, v, $-\Delta H$, r_0, E and h present thermal conductivity, density, heat capacity, axial velocity, heat of reaction, pre-exponential reaction constant (reaction amplitude), activation energy and heat transfer coefficient between reactor and cooling jackets, respectively. The cooling surface area is denoted by A_c and T_c is cooling jacket temperature. The term D_A is the diffusivity coefficient, T_f presents the feed temperature and C_{Af} is the component A concentration in feed stream. The temperature and concentration initial profiles are denoted by T_0 and C_{A0}, respectively. We consider $-\Delta H$ and r_0 as unknown reaction parameters of the system.

To simplify the equation forms and basis functions' computation, we reformulated (8.16) using dimensionless parameters and variables, and homogenized the boundary conditions by inducing the non-homogeneous parts in the governing PDEs using Dirac function. The resulting dimensionless equations with respect to

initial temperature, T_0 and concentration, C_{A0}, take the following form,

$$\frac{\partial \hat{T}}{\partial \bar{t}} = \frac{1}{Pe_1} \frac{\partial^2 \hat{T}}{\partial \bar{z}^2} - \frac{\partial \hat{T}}{\partial \bar{z}} + B_T B_C \exp\left(\frac{\gamma \hat{T}}{1 + \hat{T}}\right)(1 + \hat{C}_A)^2$$

$$+ \beta_T(\hat{u}_1 - \hat{T}) + \delta(\bar{z} - 0)\hat{u}_2,$$

$$\frac{\partial \hat{C}_A}{\partial \bar{t}} = \frac{1}{Pe_2} \frac{\partial^2 \hat{C}_A}{\partial \bar{z}^2} - \frac{\partial \hat{C}_A}{\partial \bar{z}} - B_C \exp\left(\frac{\gamma \hat{T}}{1 + \hat{T}}\right)(1 + \hat{C}_A)^2$$

$$+ \delta(\bar{z} - 0)\hat{C}_{Af}, \tag{8.17}$$

$$\bar{z} = 0: \quad \frac{\partial \hat{T}}{\partial \bar{z}} = Pe_1 \hat{T}, \quad \frac{\partial \hat{C}_A}{\partial \bar{z}} = Pe_2 \hat{C}_A,$$

$$\bar{z} = 1: \quad \frac{\partial \hat{T}}{\partial \bar{z}} = 0, \quad \frac{\partial \hat{C}_A}{\partial \bar{z}} = 0,$$

$$\bar{t} = 0: \quad \hat{T} = 0, \quad \hat{C}_A = 0,$$

where

$$\bar{t} = \frac{tv}{L}, \quad \bar{z} = \frac{z}{L}, \quad Pe_1 = \frac{\rho C_p v L}{k}, \quad Pe_2 = \frac{vL}{D_A},$$

$$\hat{T} = \frac{T - T_0}{T_0}, \quad \hat{C}_A = \frac{C_A - C_{A0}}{C_{A0}}, \quad \gamma = \frac{E}{RT_0},$$

$$\hat{u}_1 = \frac{T_c - T_0}{T_0}, \quad \hat{u}_2 = \frac{T_f - T_0}{T_0}, \quad \hat{C}_{Af} = \frac{C_{Af} - C_{A0}}{C_{A0}},$$

$$\beta_T = \frac{hA_c L}{\rho C_p v}, \quad B_T = \frac{(-\Delta H)C_{A0}}{\rho C_p T_0},$$

$$B_C = \frac{r_o C_{A0} \exp(-\frac{E}{RT_0})L}{v}.$$

By defining the new state variables of $\bar{T} = \hat{T} - \hat{T}_{ss}$ and $\bar{C}_A = \hat{C}_A - \hat{C}_{A,ss}$, and manipulated variables of $\bar{u}_1 = \hat{u}_1 - \hat{u}_{1,ss}$ and $\bar{u}_2 = \hat{u}_2 - \hat{u}_{2,ss}$ where $\hat{T}_{ss}$, $\hat{C}_{A,ss}$, $\hat{u}_{1,ss}$ and $\hat{u}_{2,ss}$ denote the variables at the steady state values, we can reformulated the

PDEs in the following deviation form,

$$
\frac{\partial \bar{T}}{\partial \bar{t}} = \frac{1}{Pe_1} \frac{\partial^2 \bar{T}}{\partial \bar{z}^2} - \frac{\partial \bar{T}}{\partial \bar{z}} + \theta_1 \Big[\exp\Big(\frac{\gamma \bar{T}}{1+\bar{T}}\Big)(1+\bar{C}_A)^2
$$
$$
- \exp\Big(\frac{\gamma \hat{T}_{ss}}{1+\hat{T}_{ss}}\Big)(1+\hat{C}_{A,ss})^2 \Big] + \beta_T(\bar{u}_1 - \bar{T}) + \delta(\bar{z} - 0)\bar{u}_2,
$$
$$
\frac{\partial \bar{C}_A}{\partial \bar{t}} = \frac{1}{Pe_2} \frac{\partial^2 \bar{C}_A}{\partial \bar{z}^2} - \frac{\partial \bar{C}_A}{\partial \bar{z}} - \theta_2 \Big[\exp\Big(\frac{\gamma \bar{T}}{1+\bar{T}}\Big)(1+\bar{C}_A)^2
$$
$$
- \exp\Big(\frac{\gamma \hat{T}_{ss}}{1+\hat{T}_{ss}}\Big)(1+\hat{C}_{A,ss})^2 \Big], \tag{8.18}
$$
$$
\bar{z} = 0: \quad \frac{\partial \bar{T}}{\partial \bar{z}} = Pe_1 \bar{T}, \quad \frac{\partial \bar{C}_A}{\partial \bar{z}} = Pe_2 \bar{C}_A,
$$
$$
\bar{z} = 1: \quad \frac{\partial \bar{T}}{\partial \bar{z}} = 0, \quad \frac{\partial \bar{C}_A}{\partial \bar{z}} = 0,
$$
$$
\bar{t} = 0: \quad \bar{T} = 0, \quad \bar{C}_A = 0,
$$

where $\theta_1 = B_T B_C$ and $\theta_2 = B_C$ are the unknown parameters of the system due to unavailability of heat of reaction and reaction amplitude.

8.2.4.2 Open-loop simulation results

To simulate the system we set parameters of the process at the following practical values, $Pe_1 = 5$, $Pe_2 = 7$, $\hat{C}_{Af} = 0.1$, $\gamma = 10$, $\hat{u}_{1,ss} = 0.15$, $\hat{u}_{2,ss} = 0.2$, $\beta_T = 2$, we also considered the following the nominal values of $\theta_1 = 0.25$, $\theta_2 = 0.1$, for unknown parameters of the system while the controller structure does not access to these values. The open-loop spatiotemporal profiles of the system dimensionless deviation states and the temporal profile of their second norm are presented in Figure 8.3-8.4. The steady state profiles are unstable, the deviation states' dy-

Figure 8.3: Open-loop dimensionless temperature deviation (a) spatiotemporal profile and (b) its second norm temporal profile.
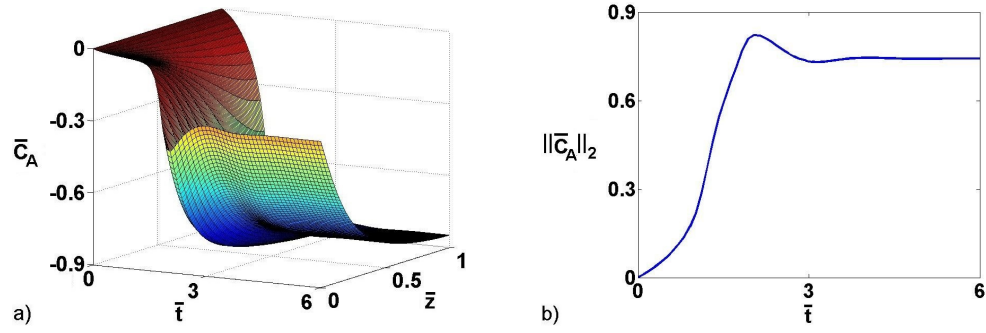
Figure 8.4: Open-loop dimensionless concentration deviation (a) spatiotemporal profile and (b) its second norm temporal profile.

namics start at zero uniform profiles and they converge to different nonuniform profiles. The adaptive controller design objective is the dimensionless temperature regulation at the uniform unstable steady state of zero in the presence of unknown heat of reaction and reaction amplitude.

8.2.4.3   Model order reduction using Galerkin's method

To compute the set of basis functions required by the Galerkin's method to construct the ROM, the following eigenproblem must be considered,

$$\frac{1}{Pe_i}\frac{d^2\phi_{ij}}{d\bar{z}^2} - \frac{d\phi_{ij}}{d\bar{z}} = \lambda_{ij}\phi_{ij},$$

$$\frac{d\phi_{ij}}{d\bar{z}}(0) = Pe_i\phi_{ij}(0), \quad \frac{d\phi_{ij}}{d\bar{z}}(1) = 0,$$

(8.19)

for $i = 1, 2$ and $j = 1, 2, \ldots, \infty$. By solving (8.19), we obtain

$$\lambda_{ij} = -\left(\frac{\alpha_{ij}^2}{Pe_i} + \frac{Pe_i}{4}\right), \qquad \tan(\alpha_{ij}) = \frac{Pe_i\alpha_{ij}}{\alpha_{ij}^2 - \left(\frac{Pe_i}{2}\right)^2},$$

$$\phi_{ij}(\bar{z}) = \xi_{ij}\exp\left(\frac{Pe_i\bar{z}}{2}\right)\left[\cos(\alpha_{ij}\bar{z}) + \frac{Pe_i}{2\alpha_{ij}}\sin(\alpha_{ij}\bar{z})\right].$$

(8.20)

The basis functions are non-self-adjoint because the linear operator of

$$\mathbf{A} = \begin{bmatrix} \dfrac{1}{Pe_1}\dfrac{\partial^2}{\partial\bar{z}^2} - \dfrac{\partial}{\partial\bar{z}} & 0 \\ 0 & \dfrac{1}{Pe_2}\dfrac{\partial^2}{\partial\bar{z}^2} - \dfrac{\partial}{\partial\bar{z}} \end{bmatrix},$$

is non-self-adjoint, then by considering the orthonormal property of basis functions we obtain

$$\phi_{ij}^*(\bar{z}) = exp(-Pe_i\bar{z})\phi_{ij}(\bar{z}),$$

$$\xi_{ij} = \left(\int_0^1 \left[\cos(\alpha_{ij}\bar{z}) + \frac{Pe_i}{2\alpha_{ij\bar{z}}}\sin(\alpha_{ij}\bar{z})\right]^2 d\bar{z}\right)^{-\frac{1}{2}}.$$

(8.21)

The dominant eigenvalues of the systems is presented in Table 8.1, where we

Table 8.1: Dominant eigenvalues

Eigenvalues	Values for $j = 1, \ldots, 6$					
λ_{1j}	-1.9	-4.8	-11.0	-20.9	-34.8	-52.6
λ_{2j}	-2.4	-4.6	-9.1	-16.3	-26.2	-38.9

observe a separation in the magnitudes of the first 3 eigenvalues from the re-

mainder eigenvalues for temperature dynamics, $\sigma_1 = \dfrac{Re|\lambda_{11}|}{Re|\lambda_{14}|} = O(0.1)$, and the first 4 eigenvalues from the remainder eigenvalues for concentration dynamics, $\sigma_2 = \dfrac{Re|\lambda_{21}|}{Re|\lambda_{25}|} = O(0.1)$, where $O(\cdot)$ denotes the order of magnitude. Then by considering $m_1 = 3$ and $m_2 = 4$,

$$\bar{T}(\bar{z},\bar{t}) = \sum_{k=1}^{m_1} a_k(\bar{t})\phi_{1k}(\bar{z}), \quad \bar{C}_A(\bar{z},\bar{t}) = \sum_{p=1}^{m_2} b_p(\bar{t})\phi_{2p}(\bar{z}), \tag{8.22}$$

and applying the Galerkin's projection, the ROM of the DPSs of (8.18) takes the following modal form,

$$
\begin{aligned}
\dot{a}_k = {}& (\lambda_{1k} - \beta_T)a_k + \theta_1\left(\int_0^1 \phi_{1k}^*\left[\exp\left(\frac{\gamma\bar{T}}{1+\bar{T}}\right)(1+\bar{C}_A)^2 \right.\right. \\
& \left.\left. - \exp\left(\frac{\gamma\hat{T}_{ss}}{1+\hat{T}_{ss}}\right)(1+\hat{C}_{A,ss})^2\right]d\bar{z} \right) \\
& + \beta_T\left(\int_0^1 \phi_{1k}^* d\bar{z} \right)\bar{u}_1 + \phi_{1k}^*(0)\,\bar{u}_2, \\
\dot{b}_p = {}& \lambda_{1p}b_p - \theta_2\left(\int_0^1 \phi_{2p}^*\left[\exp\left(\frac{\gamma\bar{T}}{1+\bar{T}}\right)(1+\bar{C}_A)^2 \right.\right. \\
& \left.\left. - \exp\left(\frac{\gamma\hat{T}_{ss}}{1+\hat{T}_{ss}}\right)(1+\hat{C}_{A,ss})^2\right]d\bar{z} \right),
\end{aligned}
\tag{8.23}
$$

for $k = 1,\ldots,3$ and $p = 1,\ldots,4$. The dominant basis functions and their adjoints for temperature and concentration are presented in Figures 8.5-8.6, respectively.
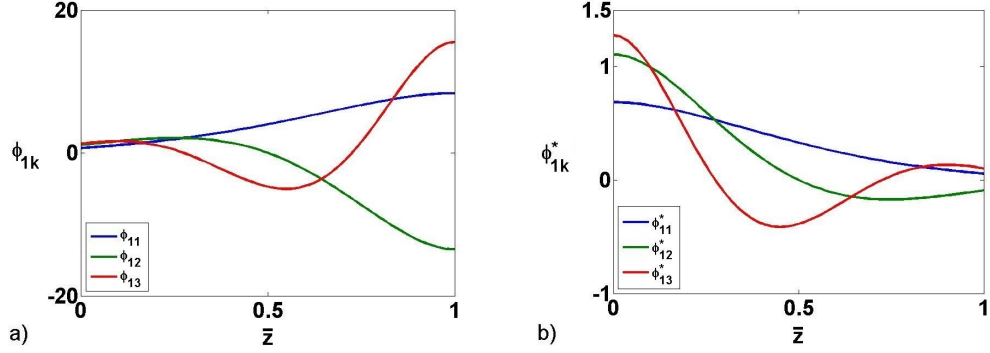
Figure 8.5: Temperature dominant (a) basis functions and (b) their adjoints.
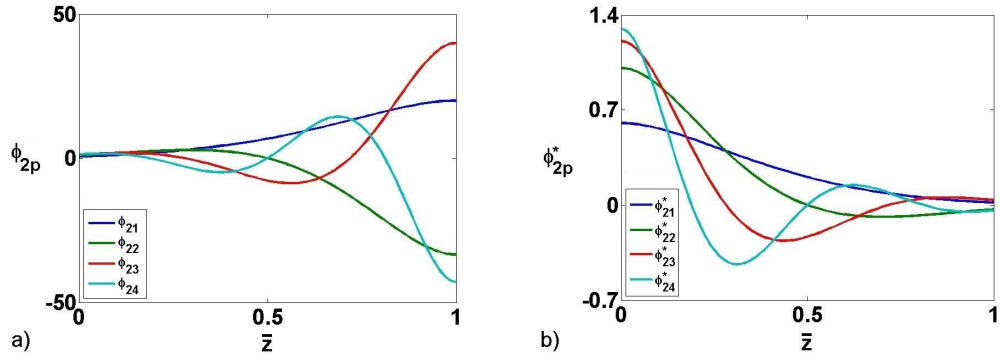
Figure 8.6: Concentration dominant (a) basis functions and (b) their adjoints.

8.2.4.4 Controller parameters and Closed-loop simulation results

To estimate the system modes, $a = [a_1 \quad a_2 \quad a_3]^T$, $b = [b_1 \quad b_2 \quad b_3 \quad b_4]^T$, we consider $r_1 = 5$ temperature continuous point measurements at

$$L_{s1} = [0.05 \quad 0.25 \quad 0.45 \quad 0.65 \quad 0.85]^T$$

, and $r_2 = 5$ concentration continuous point measurements at

$$L_{s2} = [0.15 \quad 0.35 \quad 0.55 \quad 0.75 \quad 0.95]^T.$$

We consider the thermal dynamics regulation as the control objective. In such case we still require to find the basis functions and ROMs for both temperature and concentration because their dynamics are interconnected in reaction terms. Even due to the strong relationship between concentration of the reactant component and temperature, the concentration also regulates at a certain level. To design the adaptive output feedback controller that regulates the temperature dynamics and identifies both of unknown parameters we consider the controller and identification parameters as $C_o = 2$, $\Theta = 0.5$, $z = I_2$ and the Lyapunov function as

$$V = \frac{1}{2}a^T a + \frac{1}{2}\theta_1^T \theta_1, \tag{8.24}$$

where I_2 denotes the identity matrix of size 2.

To show the effective performance of the proposed control approach even far from steady state, we allowed the system to operate open-loop while the controller was inactive $(\bar{u}_1 = \bar{u}_2 = 0)$ for $t_{open} \in [0 \quad 1.5]$. After such period we activated the controller to stabilize the thermal dynamics, $t_{closed} \in [1.5 \quad 6]$. The closed-loop spatiotemporal profile of dimensionless temperature deviation and its second norm temporal profile is illustrated in Figure 8.7. The controller successfully stabilized the dimensionless temperature deviation dynamics at the steady state profile. Due to the strong nonlinear interconnections between temperature and concentration, the dimensionless concentration deviation was also converges to an acceptable neighborhood of the desired unstable steady state even it was not the objective of
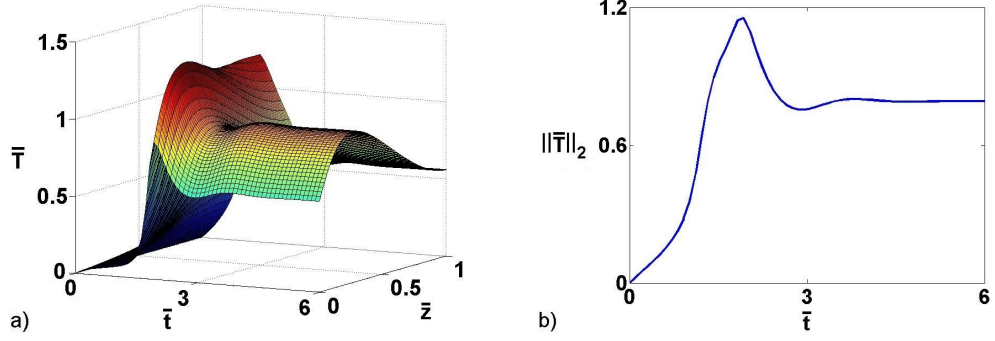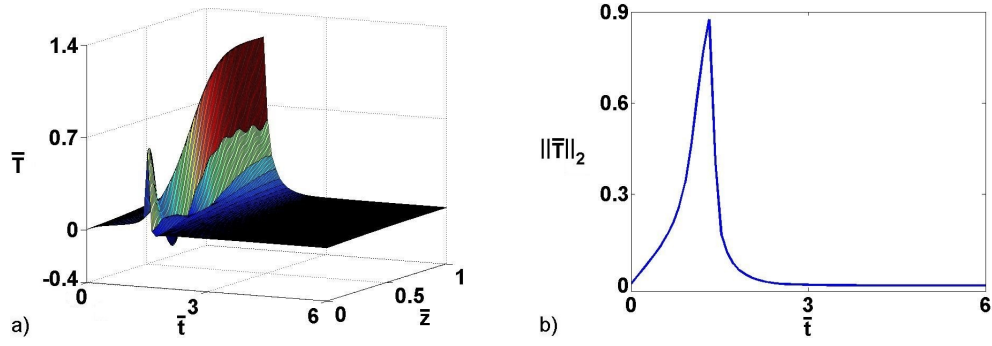
Figure 8.7: Closed-loop dimensionless temperature deviation (a) spatiotemporal profile and (b) its second norm temporal profile.
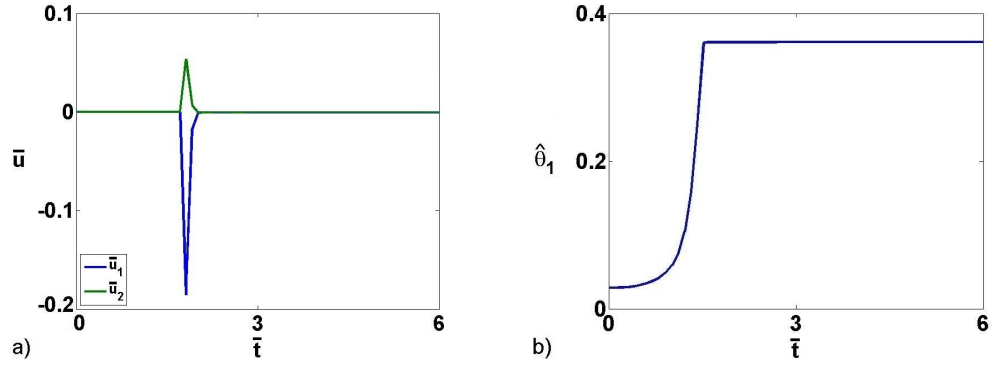
Figure 8.8: Temporal profiles of (a) required control actions and (b) estimated parameter.

the controller design.

Figure 8.8 shows the temporal profiles of required control actions' deviations to regulate the thermal dynamics and the estimated unknown parameter. We observe that the controller action converge to the steady state values without any chattering. The estimated parameter converge to the final value of $\hat{\theta}_{1,final} = 0.36$ which indicates the adaptation law did not correctly identify the parameters due to the lack of required condition of persistent excitation.

8.3 POD-based model order reduction

8.3.1 Semi-linear distributed parameter systems and their properties

We consider chemical distributed parameter systems with unknown transport-reaction parameters which can be described by the following set of semi-linear PDEs,

$$
\begin{aligned}
\frac{\partial \bar{x}(z,t)}{\partial t} &= \mathcal{A}(z,\vartheta)\,\bar{x}(z,t) + \mathcal{F}\big(z,\,\bar{x}(z,t)\big) + \mathcal{G}\big(z,\,\bar{x}(z,t)\big)\,\Theta + \mathcal{B}(z)\,u(t), \\
y(t) &= \int_\Omega \delta(z - L_s)\,\bar{x}(z,t)\,dz, \\
\Gamma\Big(t,\,\bar{x}(z,t),\,\frac{\partial \bar{x}(z,t)}{\partial z}\Big)_{\partial\Omega} &= 0, \qquad \bar{x}(z,0) = \bar{x}_0(z),
\end{aligned}
\tag{8.25}
$$

where $\bar{x} \in \mathbb{R}^n$ denotes the vector of spatiotemporal states, t is time and $z \in \Omega$ is the vector of spatial coordinates. The process domain is presented by $\Omega \subset \mathbb{R}^3$ with the process boundary of $\partial\Omega$ and $\mathcal{A}$ denotes the second order linear spatial differential operator. The terms $\mathcal{F}^{n\times1}$ and $\mathcal{G}^{n\times q}$ present the smooth nonlinear vector and matrix functions, respectively. We also consider $\vartheta \in \mathbb{R}^p$ and $\Theta \in \mathbb{R}^q$ as the vectors of unknown transport and reaction parameters, respectively. The vector of manipulated inputs is denoted by $u \in \mathbb{R}^l$ where $\mathcal{B} \in \mathbb{R}^{n\times l}$ describes their spatial distributions, $y \in \mathbb{R}^r$ is the vector of point measurements where the vector of L_s presents location of the sensors and δ is standard Dirac function. The initial spatial profile of the system state is denoted by $\bar{x}_0$ and Γ is the vector of

homogeneous boundary conditions.

In the PDE system of (8.25), the term $\mathcal{A}(z, \vartheta) \, \bar{x}(z, t)$ presents transport phenomena where the diffusion, dispersion and convection parameters may be unknown. $\mathcal{F}\big(z, \, \bar{x}(z, t)\big)$ describes the known part of nonlinear reaction dynamics and $\mathcal{G}\big(z, \, \bar{x}(z, t)\big)\Theta$ presents the unknown-affine (linear in terms of unknown parameters) dynamics of the reaction. Note that the boundary conditions don't have to be homogeneous necessarily. To homogenize the non-homogeneous boundary conditions, we can include the non-homogeneous parts in the PDEs using standard Dirac functions.

We can represent the above PDE system as the following infinite-dimensional system [84]

$$\dot{x}(t) = \mathbf{A}(\vartheta)x(t) + \mathbf{F}\big(x(t)\big) + \mathbf{G}\big(x(t)\big)\Theta + \mathbf{B}u(t),$$

$$x(0) = x_0,$$

$$(8.26)$$

in the Sobolev subspace of $\mathbb{W}$,

$$\mathbb{W}(\Omega) = \left\{ \mathcal{H}, \, \frac{\partial \mathcal{H}}{\partial z} \in L_2(\Omega) : \, \Gamma\Big(\mathcal{H}, \frac{\partial \mathcal{H}}{\partial z}\Big)_{\partial\Omega} = 0 \right\},$$

endowed with inner product

$$(\mathcal{H}_1, \mathcal{H}_2) = \int_\Omega \mathcal{H}_1(z)^* \mathcal{H}_2(z) \, dz$$

by defining the infinite-dimensional state of $x(t) \in \mathbb{W}$,

$$x(t) = \bar{x}(z, t),$$

the linear operator with unknown parameters,

$$\mathbf{A}(\vartheta)x(t) = \mathcal{A}(z, \vartheta)\,\bar{x}(z, t),$$

the nonlinear vector and matrix functions,

$$\mathbf{F}\big(x(t)\big) = \mathcal{F}\big(z,\,\bar{x}(z, t)\big), \quad \mathbf{G}\big(x(t)\big)\Theta = \mathcal{G}\big(z,\,\bar{x}(z, t)\big)\Theta,$$

and the manipulated input operator,

$$\mathbf{B}u(t) = \mathcal{B}(z)u(t).$$

We can discretize the infinite-dimensional system of (8.26) to infinite and countable modal set of ODEs by applying Galerkin projection to individual PDEs of the components of the spatiotemporal state vector while we also capture the interactions between the PDEs of such components. To employ such discretization we need the system basis functions which are the solution of the eigenproblem of

the linear differential operator,

$$\mathbf{A}(\vartheta)\phi_i = \lambda_i\phi_i, \qquad \forall i = 1, \dots, \infty \tag{8.27}$$

subject to

$$\Gamma\left(\phi_i, \frac{d\phi_i}{dz}\right)_{\partial\Omega} = 0,$$

where ϕ_i and λ_i denote the $i\,th$ basis function and eigenvalue, respectively, and $\mathbb{W} \triangleq span\{\phi_i\}_{i=1}^{\infty}$, i.e., the linear operator is a strong generator of the defined Sobolev subspace.

For the majority of chemical DPSs, specifically the transport-reaction processes, we can assume that the eigenspectrum of the linear operator, $\{\lambda_1, \lambda_2, \dots\}$, can be decomposed to the following subsets;

1. finite subset of first m eigenvalues, $\{\lambda_1, \lambda_2, \dots, \lambda_m\}$, which indicate the slow and possibly unstable dynamics of the infinite-dimensional system,

2. complement countable subset of the remainder eigenvalues, $\{\lambda_{m+1}, \lambda_{m+2}, \dots\}$, which indicate the fast and stable dynamics of the infinite-dimensional system,

when we order $Re(\lambda_1) \geq Re(\lambda_2) \geq \cdots \geq Re(\lambda_m) \geq Re(\lambda_{m+1}) \geq \cdots$, and require $Re(\lambda_{m+1}) < 0$; here $Re(\cdot)$ denotes the real part. In addition, a time scale separation can also be recognized between the subsets by $\sigma = \dfrac{|Re(\lambda_1)|}{|Re(\lambda_{m+1})|}$, where σ is a small positive number.

Note that the eigenproblem of (8.27) can not be solved due to the unavailability of the unknown parameters vector of ϑ, that clearly shows the limitation of the analytical approach even for the system with linear dominant operator defined over simple domains. To bypass the solution of such problem we can apply POD that will be briefly discussed in the next section. However, to continue the analysis and illustrate the system properties let's assume the basis functions are available for the remainder of this section. This assumption will be lifted when the proposed method will be presented.

By considering the set of basis functions, $\{\phi_i\}_{i=1}^{\infty}$, and eigenspectrum decomposition, the Sobolev subspaces for the subsets can be defined as follows;

1. slow subspace, $\mathbb{W}_s \triangleq span\{\phi_i\}_{i=1}^{m}$,

2. complement fast subspace, $\mathbb{W}_f \triangleq span\{\phi_i\}_{i=m+1}^{\infty}$,

where $\mathbb{W} = \mathbb{W}_s \cup \mathbb{W}_f$. Then by considering the vector of slow and fast basis functions as

$$\Phi_s = [\phi_1 \ \phi_2 \ \cdots \ \phi_m]^T, \quad \Phi_f = [\phi_{m+1} \ \phi_{m+2} \ \cdots]^T,$$

and the corresponding integral Galerkin projectors of

$$\begin{aligned}
\mathcal{P} : \mathbb{W} \to \mathbb{W}_s, \quad \mathcal{P}(\cdot) = \int_{\Omega} (\cdot) \, \Phi_s^* \, dz, \\
\mathcal{Q} : \mathbb{W} \to \mathbb{W}_f, \quad \mathcal{Q}(\cdot) = \int_{\Omega} (\cdot) \, \Phi_f^* \, dz,
\end{aligned} \tag{8.28}$$

where φ^T and φ^* denote the transpose and adjoint of φ, we can derive the modal

representation of the system as partitioned sets of ODEs,

$$
\begin{aligned}
\dot{x}_s &= A_s x_s(t) + F_s\big(x_s(t), x_f(t)\big) + G_s\big(x_s(t), x_f(t)\big)\Theta + B_s u(t), \\
x_s(0) &= \mathcal{P}x_0, \\
\dot{x}_f &= A_f x_f(t) + F_f\big(x_s(t), x_f(t)\big) + G_f\big(x_s(t), x_f(t)\big)\Theta + B_f u(t), \\
x_f(0) &= \mathcal{Q}x_0,
\end{aligned}
\tag{8.29}
$$

where $x = x_s \oplus x_f$, $A_s = \mathcal{P}\mathbf{A}$, $A_f = \mathcal{Q}\mathbf{A}$, $F_s = \mathcal{P}\mathbf{F}$, $F_f = \mathcal{Q}\mathbf{F}$, $G_s = \mathcal{P}\mathbf{G}$,

$G_f = \mathcal{Q}\mathbf{G}$, $B_s = \mathcal{P}\mathbf{B}$, $B_f = \mathcal{Q}\mathbf{B}$.

According to singular perturbation analysis [76] and considering Tykhonov's

theorem for solution convergence of systems include slow and fast subsystems [175],

the partitioned infinite-dimensional system of (8.29) can be reduced to

$$
\begin{aligned}
\dot{x}_s &= A_s x_s(t) + F_s\big(x_s(t), 0\big) + G_s\big(x_s(t), 0\big)\Theta + B_s u(t), \\
x_s(0) &= \mathcal{P}x_0,
\end{aligned}
\tag{8.30}
$$

when $x_f \to 0$ after a short period of time, t_b. Such required relaxation time, t_b,

can be identified form singular perturbation arguments [29, 35, 76].

8.3.2 Model order reduction

In this section, we derive the finite-dimensional approximation of the PDE system

of (8.25) by applying Galerkin's projection while the optimal required empirical

basis functions are computed by employing POD to the ensemble of snapshots captured from spatially distributed measurement sensors during the open-loop process evolution. We consider a general form of a one-dimensional ($z \in \Omega \subset \mathbb{R}$) transport-reaction process with a single state ($n = 1$) described by the following semi-linear PDE that is abstractly represented by (8.25),

$$\frac{\partial \bar{x}(z,t)}{\partial t} = \vartheta_2 \frac{\partial^2 \bar{x}(z,t)}{\partial z^2} + \vartheta_1 \frac{\partial \bar{x}(z,t)}{\partial z} + \mathcal{F}\big(z, \, \bar{x}(z,t)\big) + \theta \mathcal{G}\big(z, \, \bar{x}(z,t)\big) + \mathcal{B}(z)\, u(t),$$

$$(8.31)$$

in the presence of unknown convection, diffusion and reaction parameters which are denoted by ϑ_1, ϑ_2 and θ, respectively (i.e., $p = 2$ and $q = 1$).

By employing the set of empirical basis functions from POD algorithm described in previous section, we can approximate the spatiotemporal state as

$$\bar{x}(z,t) \approx \sum_{i=1}^{m} x_{s,i}(t)\phi_i(z). \tag{8.32}$$

Then by substituting such state approximation in the PDE system of (8.31), we obtain

$$\sum_{i=1}^{m} \dot{x}_{s,i}\phi_i = \vartheta_2 \sum_{i=1}^{m} x_{s,i}\frac{d^2\phi_i}{dz^2} + \vartheta_1 \sum_{i=1}^{m} x_{s,i}\frac{d\phi_i}{dz} + \mathcal{F}\big(z, \sum_{i=1}^{m} x_{s,i}\phi_i\big)$$
$$+ \theta\mathcal{G}\big(z, \sum_{i=1}^{m} x_{s,i}\phi_i\big) + \mathcal{B}(z)\, u(t), \tag{8.33}$$

Then we can obtain the ROM by employing Galerkin projection to equation (8.33)

as

$$\dot{x}_s = \big(\vartheta_1 A_{s,1} + \vartheta_2 A_{s,2}\big)x_s + F_s(x_s) + \theta G_s(x_s) + B_s u, \tag{8.34}$$

where

$$[A_{s,1}]_{j,i} = \int_\Omega \phi_j(z)\frac{d\phi_i(z)}{dz}dz, \quad [A_{s,2}]_{j,i} = \int_\Omega \phi_j(z)\frac{d^2\phi_i(z)}{dz^2}dz,$$

$$[F_s]_j = \int_\Omega \phi_j(z)\mathcal{F}\big(z, \textstyle\sum_{i=1}^m x_{s,i}\phi_i\big)dz,$$

$$[G_s]_j = \int_\Omega \phi_j(z)\mathcal{G}\big(z, \sum_{i=1}^m x_{s,i}\phi_i\big)dz, \quad [B_s]_{j,k} = \int_\Omega \phi_j(z)\mathcal{B}_k(z)dz$$

Note that $x_s \in \mathbb{R}^m$, $A_{s,1}, A_{s,2} \in \mathbb{R}^{m\times m}$, $F_s, G_s : \mathbb{R}^m \to \mathbb{R}^m$, $B_s \in \mathbb{R}^{m\times l}$, $u \in \mathbb{R}^l$ and $\vartheta_1, \vartheta_2, \theta \in \mathbb{R}$. Such ROM can be used as the basis for the adaptive output feedback controller design.

8.3.3 Adaptive output feedback control

In this section we address the synthesis of the low-dimensional adaptive output feedback controller structure which is a combination of a Lyapunov-based adaptive controller and a static observer.

8.3.3.1 Controller design

We assume that the identification errors remain bounded under the proposed adaptive controller design,

$$\begin{aligned}
e_{\vartheta_1} &= \vartheta_1 - \hat{\vartheta}_1, \quad |e_{\vartheta_1}| < \alpha_1 \\
e_{\vartheta_2} &= \vartheta_2 - \hat{\vartheta}_2, \quad |e_{\vartheta_2}| < \alpha_2 \\
e_\theta &= \theta - \hat{\theta}, \qquad |e_\theta| < \beta
\end{aligned} \tag{8.35}$$

where $\hat{\vartheta}_1$, $\hat{\vartheta}_2$ and $\hat{\theta}$ denote the estimated values for unknown transport and reaction parameters. To synthesize the controller we consider the following standard quadratic control Lyapunov function (CLF),

$$V_c(x_s) = \frac{1}{2}x_s^T x_s, \tag{8.36}$$

where $V_c(x_s) > 0$ and $V_c = 0$ only for $x_s = 0$. Then we can obtain the time derivative of the CLF as

$$\dot{V}_c = x_s^T \dot{x}_s = x_s^T \left(\vartheta_1 A_{s,1} x_s + \vartheta_2 A_{s,2} x_s + F_s(x_s) + \theta G_s(x_s) + B_s u\right).$$

Then by considering

$$\vartheta_1 A_{s,1} x_s + \vartheta_2 A_{s,2} x_s + F_s(x_s) + \theta G_s(x_s) + B_s u$$
$$= -C_o x_s - \left(\alpha_1 \|A_{s,1}\|_2 + \alpha_2 \|A_{s,2}\|_2\right)x_s - \beta \|G_s(x_s)\|_2 \, sign(x_s), \tag{8.37}$$

where $C_o > 0$ and $sign$ denotes the sign function, we conclude

$$u = -B_s^\perp \Big[\left(C_o + \vartheta_1 A_{s,1} + \vartheta_2 A_{s,2} + \alpha_1 \|A_{s,1}\|_2 + \alpha_2 \|A_{s,2}\|_2\right)x_s$$
$$+ F_s(x_s) + \theta G_s(x_s) + \beta \|G_s(x_s)\|_2 \, sign(x_s)\Big], \tag{8.38}$$

where $B_s^\perp = B_s^T(B_s B_s^T)^{-1}$ is the Moore-Penrose pseudo-inverse [202]. Note that $B_s^\perp = B_s^{-1}$ for $m = l$ and the controller of (8.38) is implementable when the

parameters are known. Then the time derivative of the CLF can be derived by

$$\dot{V}_c = -\big(C_o + \alpha_1\|A_{s,1}\|_2 + \alpha_2\|A_{s,2}\|_2\big)x_s^T x_s - \beta\|G_s(x_s)\|_2\, x_s^T\, sign(x_s) \le 0,$$

(8.39)

which shows the closed-loop stability of the controller in the Lyapunov sense [148].

We obtain the controller formula in the presence of unknown parameters by the applying certainty equivalence principle [25],

$$u = -B_s^\perp\Big[\big(C_o + \hat{\vartheta}_1 A_{s,1} + \hat{\vartheta}_2 A_{s,2} + \alpha_1\|A_{s,1}\|_2 + \alpha_2\|A_{s,2}\|_2\big)x_s$$
$$+F_s(x_s) + \hat{\theta}G_s(x_s) + \beta\|G_s(x_s)\|_2\, sign(x_s)\Big].$$

(8.40)

By considering the closed-loop Lyapunov function as a combination of the CLF and the identification Lyapunov function (ILF),

$$V = V_c(x_s) + V_i(e_{\vartheta_1}, e_{\vartheta_2}, e_\theta) = \frac{1}{2}x_s^T x_s + \frac{1}{2P_1}e_{\vartheta_1}^2 + \frac{1}{2P_2}e_{\vartheta_2}^2 + \frac{1}{2Z}e_\theta^2, \qquad (8.41)$$

where $P_1, P_2, Z > 0$, we conclude

$$\dot{V} = \dot{V}_c + \dot{V}_i = x_s^T \dot{x}_s + \frac{1}{P_1}e_{\vartheta_1}\dot{e}_{\vartheta_1} + \frac{1}{P_2}e_{\vartheta_2}\dot{e}_{\vartheta_2} + \frac{1}{Z}e_\theta\dot{e}_\theta. \qquad (8.42)$$

We assume that the unknown parameters of ϑ_1, ϑ_2 and θ do not change sharply as process evolves however it may change step-wise. According to such assumption,

$$\dot{e}_{\vartheta_1} = \dot{\vartheta}_1 - \dot{\hat{\vartheta}}_1 = -\dot{\hat{\vartheta}}_1, \quad \dot{e}_{\vartheta_2} = \dot{\vartheta}_2 - \dot{\hat{\vartheta}}_2 = -\dot{\hat{\vartheta}}_2, \quad \dot{e}_\theta = \dot{\theta} - \dot{\hat{\theta}} = -\dot{\hat{\theta}}. \qquad (8.43)$$

If we employ the following identification laws to estimate the unknown parameters,

$$\dot{\hat{\vartheta}}_1 = P_1\, x_s^T A_{s,1} x_s, \quad \dot{\hat{\vartheta}}_2 = P_2\, x_s^T A_{s,2} x_s, \quad \dot{\hat{\theta}} = Z\, x_s^T G_s(x_s), \qquad (8.44)$$

we obtain

$$\dot{V} = -\left(C_0 + \alpha_1\|A_{s,1}\|_2 + \alpha_2\|A_{s,2}\|_2\right) x_s^T x_s - \beta\|G_S(x_s)\|_2 x_s^T\, sign(x_s) \leq 0.$$
$$(8.45)$$

Therefore $V = V_c + V_i$ is a decreasing positive definite Lyapunov function which indicates the closed-loop system stability in the Lyapunov sense [148].

8.3.3.2 State estimation

To implement the proposed adaptive control structure we must have access to full measurements of the system slow modes, x_s, to compute the control action of (8.40) and estimate the parameters from (8.44). We employ the following static observer design to estimate the slow modes based on continuous point measurements from limited number of sensors,

$$\hat{x}_s(t) = \left(\Phi_s(L_s)\Phi_s^T(L_s)\right)^{-1}\Phi_s(L_s)\, y(t), \qquad (8.46)$$

where $\Phi_s = [\phi_1\ \phi_2\ \cdots\ \phi_m]^T$, $y \in \mathbb{R}^r$. Note that the number of required continuous measurement sensors has to be supernumerary to the number of slow modes, i.e. $r \geq m$. Such requirement can be circumvented using dynamic observer design
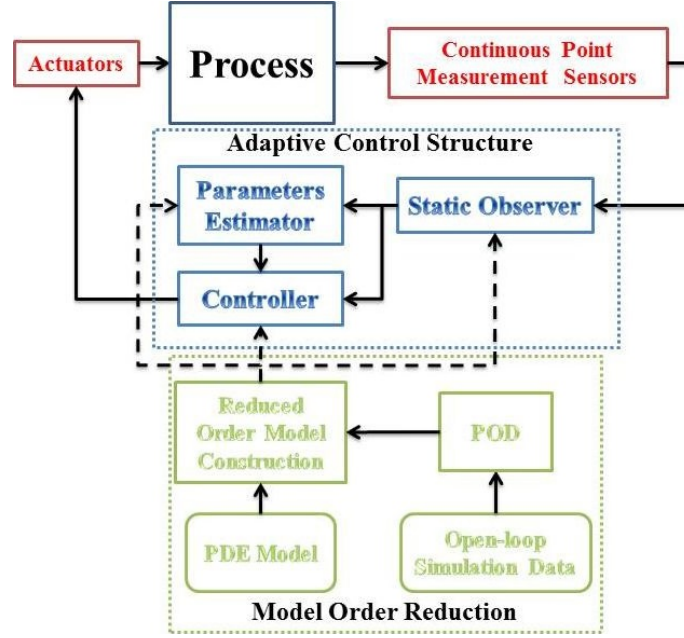
Figure 8.9: Closed-loop process.

which conceptually needs only one measurement output [28, 31, 37].

Figure 8.9 presents the block diagram of the closed-loop process operation under the proposed adaptive output feedback controller structure.

8.3.4 Application to thermal dynamics regulation

8.3.4.1 Process description

We consider a tubular flow reactor with a cooling jacket where an irreversible exothermic zero-th order reaction takes place (Figure 8.10). The reaction rate is considered to be temperature dependent, then it varies with time and location of the reactor. The cooling jacket and feed temperatures are chosen as the manipulated variables for control purposes. The thermal spatiotemporal dynamics can

be derived from the energy balance inside the reactor and can be presented as the following PDE with initial and boundary conditions,

$$\frac{\partial T}{\partial t} = \frac{k}{\rho C_p} \frac{\partial^2 T}{\partial z^2} - v \frac{\partial T}{\partial z} + \frac{(-\Delta H)}{\rho C_p} r_o \exp\left(\frac{-E}{RT}\right) - \frac{hA_c}{\rho C_p}(T - T_c),$$

$$\frac{\partial T}{\partial z}(0, t) = \frac{\rho C_p v}{k}(T(0, t) - T_f), \quad \frac{\partial T}{\partial z}(L, t) = 0, \tag{8.47}$$

$$T(z, 0) = T_0(z),$$

where T is the stream temperature inside the reactor, t is time and $z \in [0, L]$ denotes spatial coordinate where L is the reactor length. The terms k, ρ, C_p, v, $(-\Delta H)$, r_0, E and h are used for thermal conductivity, density, heat capacity, axial velocity, heat of reaction, pre-exponential reaction constant, activation energy, and heat transfer coefficient between reactor and cooling jacket, respectively. The cooling surface area is denoted by A_c and T_c, T_f and T_0 present the cooling jacket temperature, feed temperature and initial temperature profile, respectively. In above PDE system, k, $(-\Delta H)$ and r_0 are considered as unknown transport-reaction parameters of the system.

To generalize the governing equation we reformulate (8.47) using dimensionless variables and parameters, and homogenize the first boundary condition by inducing the non-homogeneous part in the governing PDE using standard Dirac function. The dimensionless form of the PDE with respect to initial temperature, T_0, takes
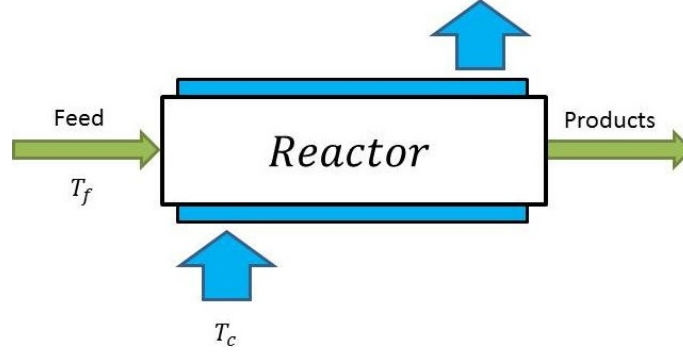
Figure 8.10: Tubular flow reactor with a cooling jacket.

the following form,

$$
\frac{\partial \bar{T}}{\partial \bar{t}} = \vartheta \frac{\partial^2 \bar{T}}{\partial \bar{z}^2} - \frac{\partial \bar{T}}{\partial \bar{z}} + \theta \exp\left(\frac{\gamma \bar{T}}{1 + \bar{T}}\right)
$$

$$
+ B_C(\bar{u}_1 - \bar{T}) + \delta(\bar{z} - 0)\bar{u}_2, \tag{8.48}
$$

$$
\frac{\partial \bar{T}}{\partial \bar{z}}(0, \bar{t}) = \frac{1}{\vartheta} \bar{T}(0, \bar{t}), \quad \frac{\partial \bar{T}}{\partial \bar{z}}(1, \bar{t}) = 0, \quad \bar{T}(\bar{z}, 0) = 0,
$$

where

$$
\bar{t} = \frac{tv}{L}, \quad \bar{z} = \frac{z}{L}, \quad \bar{T} = \frac{T - T_0}{T_0}, \quad \vartheta = \frac{k}{\rho C_p v L},
$$

$$
\gamma = \frac{E}{RT_0}, \quad \bar{u}_1 = \frac{T_c - T_0}{T_0}, \quad \bar{u}_2 = \frac{T_f - T_0}{T_0},
$$

$$
B_C = \frac{hA_c L}{\rho C_p v}, \quad \theta = \frac{(-\Delta H)r_o \exp(-\frac{E}{RT_0})L}{\rho C_p T_0 v},
$$

where ϑ and θ are the unknown parameters of the system due to unavailability of thermal conductivity, heat of reaction and pre-exponential reaction constant. We consider the jacket and feed stream temperatures as the manipulated inputs for control purposes.
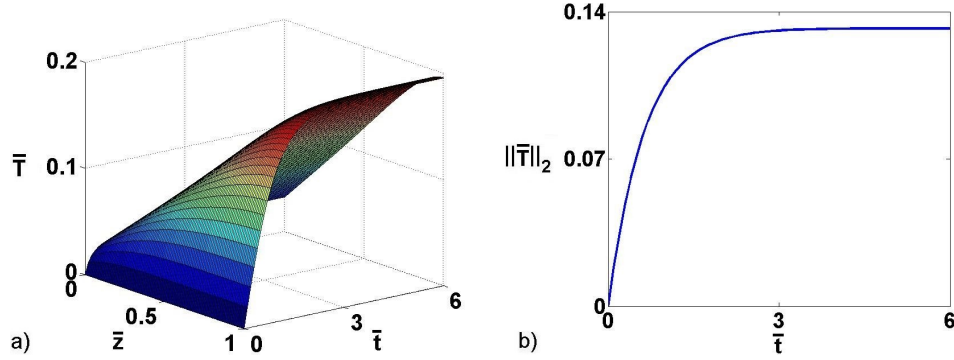
Figure 8.11: Open-loop dimensionless temperature (a) spatiotemporal profile and (b) spatial second norm temporal profile.

8.3.4.2 Simulation results

The known parameters of the system are set at the following practical values, $\gamma = 7$ and $B_C = 2$, we also consider the following nominal values for unknown transport-reaction parameters of the system, $\vartheta = 0.18$ and $\theta = 0.25$. Note that the controller structure does not have access to such nominal values. Figure 8.11 presents the open-loop spatiotemporal profile of the stream dimensionless temperature and the temporal profile of its spatial second norm. We can observe that the dimensionless temperature converges to a nonuniform steady state profile. The controller objective is to regulate the dimensionless temperature profile at the origin, i.e., keeping the stream temperature at the uniform reference profile of T_0. To construct the ROM required by the adaptive control structure we collect the snapshots of the system state profile from spatially distributed measurement sensors during the open-loop process operation, $t_{ol} = [0 \ \ 3]$, while the controllers are inactivated ($\bar{u}_1 = \bar{u}_2 = 0$). By applying the POD to the ensemble of open-loop
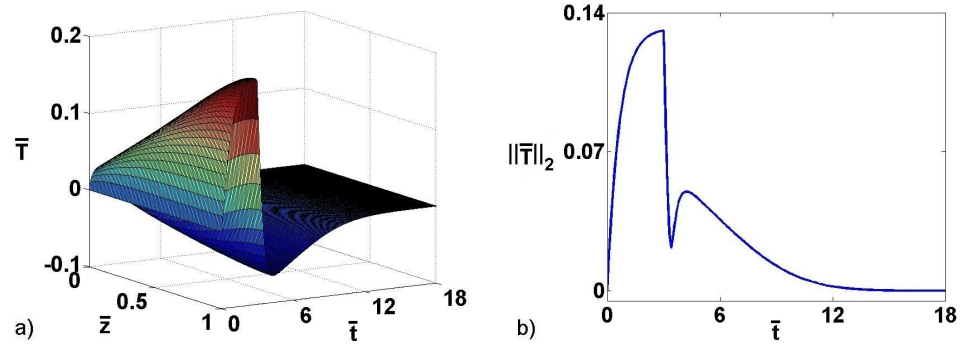
Figure 8.12: Closed-loop dimensionless temperature (a) spatiotemporal profile and (b) spatial second norm temporal profile.
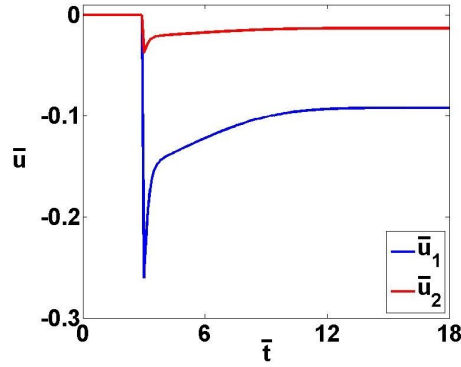
Figure 8.13: Required control actions.

snapshots, we obtain only 1 basis function. The controller actions ($\bar{u}_1$ and $\bar{u}_2 = 0$) and identification laws ($\dot{\hat{\vartheta}}$ and $\dot{\hat{\theta}}$) were derived based on adaptive output feedback control approach which presented in details in Section 8.3.3. Note that in this case study we have one unknown reaction parameter and only one unknown transport parameter. To design the control structure we considered the system tuning parameters as follows, $C_o = 2$, $\alpha = 0.5$, $\beta = 0.2$ and $P = Z = 1$. To estimate the system dominant mode using the static observer of (8.46), we consider $r = 2$ temperature continuous point measurements at $L_s = [0.3 \quad 0.7]^T$. After the open-

loop process operation time period, $t_{ol} = [0 \; 3]$, we activated the controller and identifiers to regulate the system for $t_{cl} > 3$. Figure 8.12 illustrates the closed-loop spatiotemporal profile of dimensionless temperature and its spatial second norm temporal profile. We observe that the controller successfully stabilizes the dimensionless temperature at the uniform zero profile. The temporal profiles of required control actions are shown in Figure 8.13. The controller actions converge to the steady state values corresponded to the desired zero dimensionless temperature profile without any chattering. Figure 8.14 presents the temporal profiles of the estimated unknown transport-reaction parameters. It can be observed that the estimated parameters converge to the final values of $\hat{\vartheta} = 0.485$ and $\hat{\theta} = 0.09$ which indicate the adaptation strategy did not correctly identify the parameters since for that the required condition of persistent excitation [25] was not satisfied and also because the initial guesses were poor. Note that the objective of the proposed output feedback adaptive control strategy was only regulation not system identification. The open-loop process operation, $t_{ol} = [0 \; 3]$, can be easily identified in Figures 8.13-8.14 while during such time period the controllers and identifiers were inactivated.
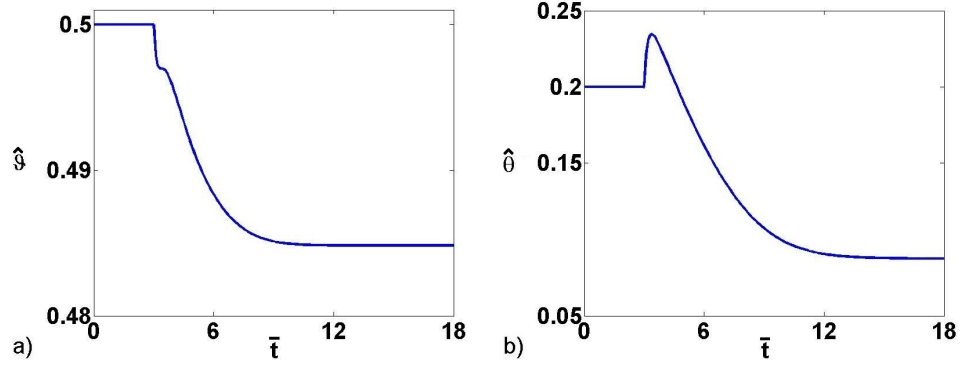
Figure 8.14: Estimated (a) transport and (b) reaction parameters.

8.4 APOD-based model order reduction

8.4.1 Adaptive control through system linearization

8.4.1.1 Preliminaries

8.4.1.1.1 A class of semi-linear parabolic PDE system   We consider processes modeled by semi-linear parabolic PDE systems in the following state space form

$$\frac{\partial}{\partial t}\bar{x}(z,t) = \mathbf{A}\frac{\partial^2}{\partial z^2}\bar{x}(z,t) + \mathbf{f}\Big(\bar{x}(z,t),\theta(t)\Big) + b(z)u(t), \tag{8.49}$$

subject to boundary and initial conditions

$$q(\bar{x}, \frac{\partial \bar{x}}{\partial z}) = 0 \quad \text{on} \quad \partial\Omega, \quad \bar{x}(z,0) = \bar{x}_0(z). \tag{8.50}$$

In the PDE system of (8.49)-(8.50), $z \in \Omega \subset \mathbb{R}^3$ denotes the spatial coordinate, t is the time, Ω is the process domain with boundary $\partial\Omega$. $\bar{x}(z,t) \in \mathbb{R}$ stands for

the state variable and $u(t) \in \mathbb{R}^l$ is the manipulated inputs vector. $\mathbf{A}$ is a positive constant and $\mathbf{f}(\cdot)$ is a sufficiently smooth nonlinear vector function. $\theta(t)$ is the vector of unknown parameters and $b^T(z) \in \mathbb{R}^l$ is a smooth matrix function which describes the control action distribution in the spatial domain, e.g. point actuation is described by a standard Dirac delta. $q(\cdot)$ is a nonlinear vector function and $\bar{x}_0(z)$ is a smooth vector function.

The availability of two types of measurement sensors is assumed; periodic distributed snapshot measurements, $y_r(z, t_k) \in \mathbb{R}$ that indicates measured spatial profiles, and continuous measurements, $y_m \in \mathbb{R}^r$ that is a vector variable,

$$
\begin{aligned}
y_m(t) &= \int_\Omega s(z)\bar{x}(z, t)\ dz, \\
y_r(z, t_k) &= \int_0^t \delta(\tau - t_k)\bar{x}(z, \tau)\ d\tau,
\end{aligned}
\tag{8.51}
$$

where r is the number of continuous sensors, t_k is the time instance for snapshot measurement and $k = 1, 2, \ldots$. The function $s(z)$ denotes the continuous point sensors distribution in the process domain, Ω, and $\delta(\cdot)$ indicate standard Dirac delta function.

Remark 8.1. *The results of this manuscript are presented for $\bar{x} \in \mathbb{R}$, however, we may extend the results for $\bar{x}(z, t) = [\bar{x}_1(z, t) \ \cdots \ \bar{x}_n(z, t)]^T \in \mathbb{R}^n$ by treating each state individually. The interactions between distributed system states is then captured through the spatial integration of the respective basis functions with $\mathbf{f}(\bar{x}, \theta)$ to give appropriate nonlinear functions [228].*

8.4.1.1.2 System representation in Sobolev subspace The semi-linear parabolic PDE system of (8.49)-(8.51) can be presented as an infinite-dimensional system in a relevant Sobolev subspace of $\mathbb{W}^{1,2}(\Omega, \mathbb{R})$, that satisfies the homogeneous boundary conditions of (8.50), i.e.,

$$\mathbb{W}^{1,2}(\Omega, \mathbb{R}) = \left\{ F \in \mathbf{W}^{1,2}(\Omega, \mathbb{R}) : q(F, \frac{\partial F}{\partial z}) = 0 \ \text{ on } \ \partial\Omega \right\},$$

where $\forall i, j \in \mathbb{N}$, $i \geqslant 1$ and $1 \leqslant j < \infty$, Sobolev space of

$$\mathbf{W}^{i,j}(\Omega, \mathbb{R}) = \left\{ \bar{x} \in L_j(\Omega) : \ \partial^\alpha \bar{x} \in L_j(\Omega), \forall \alpha \in \mathbb{N}, |\alpha| \leqslant i \right\},$$

is a functional space that includes all of the α-order differentiable functions with respect to all of spatial coordinates of the process domain. We can define the inner product and norm in subspaces that belong to the space of square integrable functions, $L_2(\Omega)$, in the following form

$$(\vartheta_1, \vartheta_2) = \int_\Omega r(z) \vartheta_1^T(z) \vartheta_2(z) dz, \quad \|\vartheta_1\|_2 = (\vartheta_1, \vartheta_1)^{1/2},$$

where ϑ^T denotes the transpose of ϑ and $r(z)$ is the weight function that is assumed to be 1 in this work. To simplify the notation we will use $\mathbb{W}$ to denote $\mathbb{W}^{1,2}(\Omega, \mathbb{R})$ for the remainder of the paper.

On the basis of the above, we define within $\mathbb{W}$ the state

$$x(t) = \bar{x}(\cdot, t), \quad x \in \mathbb{W}^{1,2} \tag{8.52}$$

the linear and nonlinear differential operators

$$\mathcal{A}x(t) = \mathbf{A}\frac{\partial^2}{\partial z^2}\bar{x}(\cdot, t), \quad \mathcal{F}\Big(x(t), \theta(t)\Big) = \mathbf{f}\Big(\bar{x}(\cdot, t), \theta(t)\Big), \tag{8.53}$$

the manipulated input operator

$$\mathcal{B}u(t) = b(z)u(t), \tag{8.54}$$

and measured outputs' operators

$$\mathcal{S}x(t) = (s^T(z), \bar{x}(\cdot, t)), \quad \mathcal{R}x(t) = \int_0^t \delta(\tau - t_k)\bar{x}(\cdot, \tau) \, d\tau. \tag{8.55}$$

Then the PDE system of (8.49)-(8.51) can be presented in the Sobolev subspace as follows

$$\dot{x}(t) = \mathcal{A}x(t) + \mathcal{F}\Big(x(t), \theta(t)\Big) + \mathcal{B}u(t), \quad x(0) = x_0,$$

$$y_m(t) = \mathcal{S}x(t), \tag{8.56}$$

$$y_r(t_k) = \mathcal{R}x(t_k),$$

where $k = 1, 2, \ldots$, for equations (8.55) and (8.56). The set of analytical basis functions of the system, needed to build the ROM, can in principle be obtained

from the solution of the eigenvalue problem for the linear spatial operator of the system as follows

$$\mathcal{A}\phi_i = \lambda_i\phi_i, \quad i = 1, \ldots, \infty \tag{8.57}$$

subject to the boundary conditions

$$q(\phi_i, \frac{d\phi_i}{dz}) = 0 \quad \text{on} \quad \partial\Omega, \tag{8.58}$$

where λ_i and ϕ_i denote the ith eigenvalue and the corresponding basis function, respectively.

Assumption 8.1. *We assume that the ordered eigenspectrum of $\mathcal{A}$,*

$$\sigma_{\mathcal{A}} = \{\lambda_1, \lambda_2, \ldots\},$$

can be partitioned into a finite set of r_s slow eigenvalues,

$$\sigma_{\mathcal{A}}^{(s)} = \{\lambda_1, \lambda_2, \ldots, \lambda_{r_s}\},$$

and a countable complement set of the remaining fast eigenvalues

$$\sigma_{\mathcal{A}}^{(f)} = \{\lambda_{r_s+1}, \lambda_{r_s+2}, \ldots\}.$$

The associated basis functions sets are defined as $\Phi_s = [\phi_1 \ \phi_2 \ \cdots \ \phi_{r_s}]^T$, $\Phi_f = [\phi_{r_s+1} \ \phi_{r_s+2} \ \cdots]^T$. There is a large separation between the slow and fast eigenvalues of $\mathcal{A}$, i.e., $|Re(\lambda_1)|/|Re(\lambda_{r_s})| = O(1)$ and $|Re(\lambda_1)|/|Re(\lambda_{r_s+1})| = O(\epsilon)$ where $Re(\lambda_{r_s+1}) < 0$, $\epsilon = |\lambda_1|/|\lambda_{r_s+1}|$ is a small number. We also assume that $\mathbb{W} \triangleq span\{\phi_i\}_{i=1}^{\infty}$, i.e., operator $\mathcal{A}$ is a strong generator of the Sobolev subspace of $\mathbb{W}$.

Note that $Re(\epsilon)$ denotes the real part and $O(\epsilon)$ the order of magnitude of ϵ.

From Assumption 8.1, we obtain that the Sobolev subspace defined for the infinite dimensional representation of the system, $\mathbb{W} \triangleq span\{\phi_i\}_{i=1}^{\infty}$, can be partitioned into two other Sobolev subspaces; a slow and a fast one. The slow subspace contains a finite number of basis functions that correspond to slow and possibly unstable modes of x, $\mathbb{W}_s \triangleq span\{\phi_i\}_{i=1}^{r_s}$. The fast complement subspace contains an infinite number of basis functions that correspond to fast and stable modes of x, $\mathbb{W}_f \triangleq span\{\phi_i\}_{i=r_s+1}^{\infty}$. Note that there is a time scale separation between the dynamics of the two subsystems; the state of the infinite dimensional system of (8.56) can be partitioned into a finite dimensional subspace of slow and possibly unstable modes and an infinite dimensional subsystem of stable and fast modes,

$$x = x_s + x_f, \tag{8.59}$$

where $x_s = \mathcal{P}x \in \mathbb{W}_s$, $x_f = \mathcal{Q}x \in \mathbb{W}_f$ and $\mathbb{W} = \mathbb{W}_s \oplus \mathbb{W}_f$. The orthogonal integral projection operators are defined as $\mathcal{P} : \mathbb{W} \to \mathbb{W}_s$, $\mathcal{P} = (\cdot, \Phi_s)$ and $\mathcal{Q} : \mathbb{W} \to \mathbb{W}_f$, $\mathcal{Q} = (\cdot, \Phi_f)$.

Then using the method of weighted residuals based on the set of basis functions, the system of (8.56) can be presented as an ODE set of vectorized modes in the following form

$$\begin{aligned} \dot{x}_s &= A_s x_s + f_s(x_s, x_f, \theta) + B_s u, \quad x_s(0) = \mathcal{P}x_0, \\ \dot{x}_f &= A_f x_f + f_f(x_s, x_f, \theta) + B_f u, \quad x_f(0) = \mathcal{Q}x_0, \end{aligned} \tag{8.60}$$

where $A_s = \mathcal{P}\mathcal{A} = diag\{\lambda_i\}_{i=1}^{r_s}$, $A_f = \mathcal{Q}\mathcal{A} = diag\{\lambda_i\}_{i=r_s+1}^{\infty}$, $f_s = \mathcal{P}\mathcal{F}$, $f_f = \mathcal{Q}\mathcal{F}$, $B_s = \mathcal{P}\mathcal{B}$, $B_f = \mathcal{Q}\mathcal{B}$, $\mathcal{P}x(0) = \mathcal{P}x_0$, $\mathcal{Q}x(0) = \mathcal{Q}x_0$.

The fast dynamics of (8.60) can be represented in the following singular perturbation form,

$$\epsilon \dot{x}_f = \epsilon A_f x_f + \epsilon \big(f_f(x_s, x_f, \theta) + B_f u\big), \tag{8.61}$$

where due to Assumption 8.1, $\epsilon = |\lambda_1|/|\lambda_{r_s+1}|$ is a small number that indicates the time scale separation between the slow and fast dynamics [76].

Assumption 8.2. *The control action is assumed to be bounded and the nonlinear dynamics of the fast and stable subsystem satisfies the Lipschitz condition [76].*

By assuming bounded control action and Lipschitz condition for $f_f(x_s, x_f, \theta)$, we obtain that $f_f(x_s, x_f, \theta) + B_f u$ does not include a term of $O(\frac{1}{\epsilon})$. Considering that A_f has negative eigenvalues of $O(1)$ and by setting $\epsilon = 0$, the fast dynamics can be presented as the following locally exponentially stable form

$$\frac{\partial x_f}{\partial \tau} = A_{f\epsilon} x_f, \tag{8.62}$$

where $\tau = \dfrac{t}{\epsilon}$ and $A_{f\epsilon} = \epsilon A_f$. Note that $A_{f\epsilon}$ is of order $O(1)$ in the fast time scale. After a period of time, x_f converges to a ball of radius $O(\epsilon)$ around zero. Thus, the fast dynamics of x_f can be ignored compared to the slow dynamics of

x_s. Accordingly, the process dynamics can be approximated as follows

$$\dot{x}_s = A_s x_s + f_s(x_s, 0, \theta) + B_s u, \quad x_s(0) = \mathcal{P} x_0. \tag{8.63}$$

Assumption 8.3. *The PDE system of (8.49)-(8.51) and as a result, the slow and fast subsystems of (8.60) are assumed to be approximately observable and controllable [84].*

On the basis of the above expositions, we need to solve the eigenvalue problem of (8.57) and find the set of basis functions to reduce the infinite dimensional system. However, generally it is not possible to solve it when we have complex boundary conditions. The interesting fact is that we can not find the analytical solution even for a general class of linear systems over miscellaneous domains. On the other hand, even if we can compute them analytically, we are not able to directly identify how many of them are enough to capture the dominant dynamic behavior of the system. Note that using large number of basis functions increases the dimensionality of ROM and the controller computational demand. Thus, most of the standard analytical MOR techniques can not be directly used even for distributed parameter systems described by general linear PDEs. One solution to circumvent this issue is to apply APOD as explained briefly in the next section.

Remark 8.2. *Assumption 8.1 is always satisfied when the system is linear. It is also automatically satisfied for semi-linear systems when we have bounded Lipschitz*

nonlinearity. The reader may refer to [103] for semi-linear PDE definition.

Remark 8.3. *The proposed method is not only applicable to parabolic systems but also to higher order semi-linear systems that satisfy Assumption 8.1, such as physico-chemical systems described by Kuramoto-Sivashinsky equation (KSE) [77, 93, 118] and Korteweg de Vries-Burgers (KdVB) equation [48].*

8.4.1.2   Adaptive model order reduction

The finite-dimensional approximation of the infinite-dimensional representation of (8.49)-(8.51) can be computed using the method of weighted residuals when the set of empirical basis functions are available. Generally, the original state of the PDE system, $\bar{x}(z,t)$, can be described as an infinite weighted summation of a complete vectorized set of basis functions $\Psi(z)$ as follows

$$\bar{x}(z,t) \approx \sum_{k=1}^{r_m} \psi_k(z)a_k(t) \xrightarrow{r_m \to \infty} \bar{x}(z,t) = \sum_{k=1}^{\infty} \psi_k(z)a_k(t) \tag{8.64}$$

where $a_k(t)$ for $k = 1, \ldots, r_m$ are time varying coefficients known as system modes. The following $r_m{}^{th}$ order system of ODEs is obtained by substituting (8.64) in (8.49)-(8.51), multiplying the PDE with the weighting functions, $\varphi(z)$, and integrating over the entire spatial domain:

$$\sum_{k=1}^{r_m} (\varphi_v(z), \psi_k(z))\dot{a}_k(t) = \sum_{k=1}^{r_m} (\varphi_v(z), \mathcal{A}\psi_k(z))a_k(t)$$
$$+ \Big(\varphi_v(z), \mathcal{F}(z, \sum_{k=1}^{r_m} \psi_k(z)a_k(t)), \theta\Big) + (\varphi_v(z), b(z))u,$$
$$y_m = \sum_{k=1}^{r_m} (s(z), \psi_k(z))a_k(t), \quad v = 1, \ldots, r_m. \tag{8.65}$$

The type of weighted residual method can be determined by the weighting functions in the above equation. The method reduces to Galerkin projection when the weighting functions, $\varphi(z)$, and the basis functions, $\Psi(z)$, are the same. Then (8.65) can be summarized as

$$\dot{a} = Aa + f(a, \theta) + Bu,$$
$$y_m = Sa,$$
(8.66)

where $A^{r_m \times r_m}$, $B^{r_m \times l}$ and $S^{w \times r_m}$ are constant matrices and f is a nonlinear smooth vector function of the modes that can be described based on the comparison between (8.65) and (8.66). From Lipschitz condition of $\mathbf{f}$, we obtain that f satisfies a local Lipschitz condition. Note that this assumption can be concluded from the local Lipschitz property of the nonlinear part of the original system of (8.56) in the Sobolev subspace for special cases.

Remark 8.4. *The main reason for applying APOD to recursively revise the set of empirical basis functions is the appearance of new trends in the process dynamics during process evolution. Such new trends make the empirical basis functions and ROM inaccurate. In that case APOD algorithm revises the basis functions and modifies the ROM. Then following the ROM revisions, the output feedback control structure is redesigned to retain relevancy. Such "corrections" will always be repeated at revision times to construct an accurate basis for controller design and enforce closed-loop stability [29, 256].*

Remark 8.5. *Since the empirical basis functions of the system are periodically revised, the ROM of (8.66) we obtain is a switching system, i.e., the structure and dimensionality of the system approximation changes as process evolves. Furthermore, the designed adaptation and controller laws will also be revised as well at each switching [29, 35].*

8.4.1.3 Application to thermal regulation in a catalytic chemical reactor

In this section, the adaptive model order reduction (AMOR) and control design is applied to a $1\,D$ diffusion-reaction process. First, we describe the model of thermal dynamics in a catalytic chemical reactor. Then we apply APOD and Galerkin's method to construct the ROM that is the basis for controller synthesis. Finally, we design an adaptive controller to regulate the temperature dynamics of the catalytic reactor and present the results.

Note that the main contribution of this paper is towards the adaptive model order reduction component which facilitates the implementation of adaptive control approaches to distributed systems with unknown parameters. Adaptive control is a well-known control approach as we discussed in the "introduction" section. We are using a Lyapunov-based adaptive method to design the controller. For brevity reasons we do not present the basics and theory of adaptive control approach which can be found in [25, 63, 147, 218].
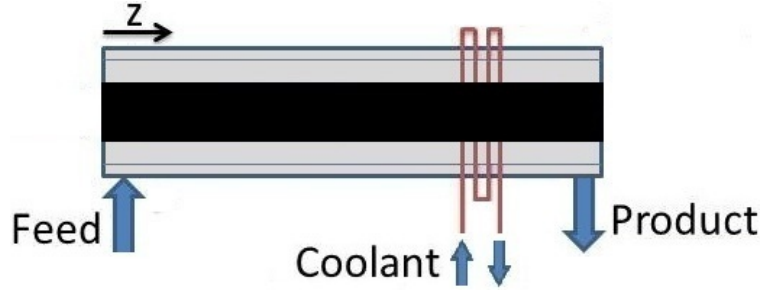
Figure 8.15: Catalytic chemical reactor.

8.4.1.3.1 Reactor description Consider an elementary exothermic reaction $A \to B$ taking place on a long, thin rod in a catalytic chemical reactor that is presented in Figure 8.15. Since the reaction is exothermic, a coolant is used to remove heat from the reactor. To model temperature dynamics inside the catalytic rod we assume constant density, heat capacity and constant conductivity of the rod, and constant temperature at both ends of the rod. We also assume that the reactant A is present in excess and thus can assume constant reactant concentration. The mathematical model that describes the spatiotemporal thermal dynamics inside the catalytic rod is presented by the following semi-linear parabolic PDE,

$$\frac{\partial \bar{x}}{\partial t} = D\frac{\partial^2 \bar{x}}{\partial z^2} + \beta_T \left(e^{-\epsilon/(1+\bar{x})} - e^{-\epsilon} \right) + \beta_U \left(b(z)u(t) - \bar{x} \right) \tag{8.67}$$

subject to boundary and initial conditions

$$\bar{x}(0,t) = 0, \ \bar{x}(\pi,t) = 0, \quad \bar{x}(z,0) = \bar{x}_0(z), \tag{8.68}$$

where $\bar{x}$ denotes the dimensionless temperature of the catalytic rod that is defined over the spatial domain of $[0, \pi]$ and $z \in [0, \pi]$ is the spatial coordinate, D is the dimensionless diffusion coefficient and β_T denotes the dimensionless heat of reaction; γ stands for the dimensionless activation energy and the parameter β_U denotes the dimensionless heat transfer coefficient. The vector of control variables is denoted by $u(t)$ and $b(z)$ describes the spatial distribution of the actuator, e.g., point actuation could be defined using standard Dirac delta. Figure 8.16 presents the open-loop spatiotemporal profile of the system state and temporal profile of its 2-norm when the nominal values of the system unknown parameters are $D = 1$, $\beta_T = 16$ and $\gamma = 2$ and the dimensionless heat transfer coefficient of the system is $\beta_U = 2$. The initial dimensionless temperature of the catalytic rod is considered as a periodic profile with the average value of $\bar{x}_{0,avg} = 0.5$. The hot spot can be observed easily at the middle point of the catalytic rod. The control problem thus becomes regulating the catalyst temperature at a uniform temperature of $\bar{x} = 0$.

To address the control problem we consider the linearization of the PDE system of (8.67) around the spatially uniform unstable steady state of $\bar{x}(z, t) = 0$. It has the following form,

$$\frac{\partial \bar{x}}{\partial t} = D\frac{\partial^2 \bar{x}}{\partial z^2} + \left(\beta_T e^{-\gamma}\gamma - \beta_U\right)x + \beta_U b(z)u(t). \tag{8.69}$$

We assume that we do not know the reaction and diffusion parameters inside the reactor, i.e., the parameters β_T, γ and D that indicate heat of reaction, activation
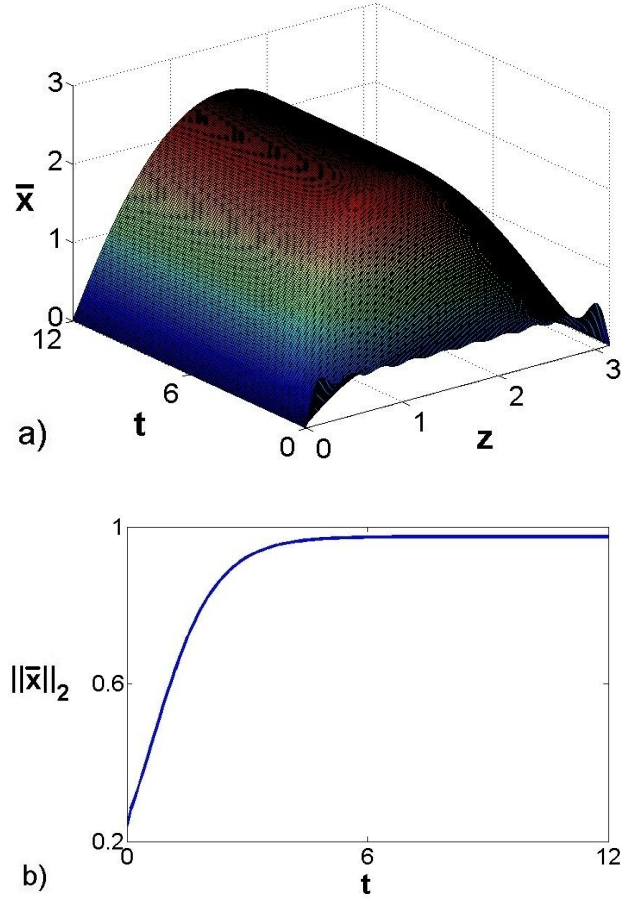
Figure 8.16: Open-loop (a) spatiotemporal profile of the system state and (b) temporal profile of its 2-norm.

energy and diffusion coefficient, respectively, are unknown. The only parameter of the system that is known is the dimensionless heat transfer coefficient, $\beta_U = 2$. The linearized PDE system of (8.69) can be represent in the form of reaction and diffusion uncertainty as follows,

$$\frac{\partial \bar{x}}{\partial t} = \theta_1 \frac{\partial^2 \bar{x}}{\partial z^2} + \theta_2 x + \beta_U b(z) u(t), \tag{8.70}$$

where $[\theta_1 \ \theta_2]^T = [D \ \ \beta_T \mathrm{e}^{-\gamma}\gamma - \beta_U]^T$.

Four continuous point measurement sensors are assumed to be placed uniformly across the domain of the process, $L_s = [\pi/5, 2\pi/5, 3\pi/5, 4\pi/5]$, where $y_m(L_s) = \Psi^T(L_s)a$ and $\Psi = [\psi_1 \ \psi_2 \ \cdots \ \psi_{r_m}]^T$, and we consider the availability of only one point actuator at $L_a = 3\pi/4$, where the corresponding spatial distribution functions at the location for point measurements and actuation is considered as the Dirac delta function, $\delta(z - L)$. The profiles of the rod temperature is also assumed to be accessible every $\delta t = 1s$. The control objective is the regulation of the temperature dynamics in the presence of unknown reaction and diffusion parameters at the unstable steady state of $\bar{x}(z, t) = 0$ based on AMOR.

Remark 8.6. *Considering the local linearization as the basis to design the adaptive control structure for governing nonlinear systems is a promising approach that has been widely applied in the literature [25, 147, 218]. We consider this approach to simplify the adaptation law and adaptive controller derivations.*

Remark 8.7. *Note that the linearization error between model and nonlinear process is also circumvented using a linear model-based controller design whose parameters adaptively change during process evolution.*

8.4.1.3.2   Adaptive model order reduction   Even for the specific process we can not compute the dominant basis functions analytically due to the unknown diffusivity coefficient. We used 20 snapshots and the off-line step of APOD to find
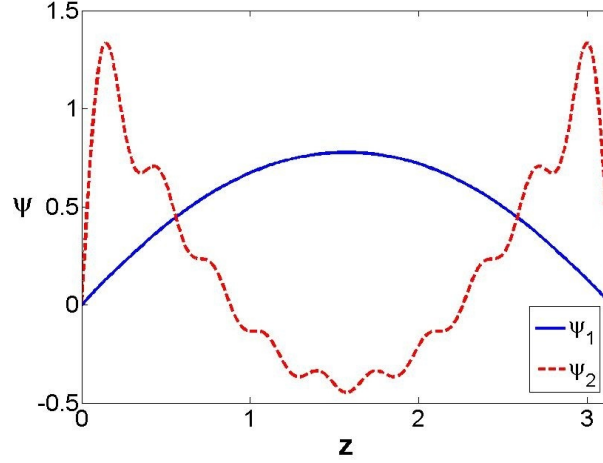
Figure 8.17: The initial dominant empirical basis function (obtained from off-line APOD part).

an initial set of empirical basis functions. These snapshots are generated during the time period of $t \in [0, 2]$ for open-loop process, $u(t) = 0$. Using off-line APOD to compute the basis of the initial ensemble of snapshots we obtain two empirical basis function for $\bar{x}$ which captures 0.999 of the total energy of the ensemble. The initial dominant empirical basis function is presented in Figure 8.17. The first dominant basis function identify the dominant dynamics of the open-loop system and the second one is an artifact of the specific initial single trajectory in the absence of control action.

The on-line APOD adaptively revises the empirical basis functions every $\delta t = 1s$ to keep them accurate. Note that the snapshots needed in Galerkin's method to construct the linear ROMs are obtained from the original nonlinear process. If we consider $\{\psi_i\}_{i=1}^{r_m}$ is the set of empirical basis functions between the revisions, we can approximate the state of the PDE system of (8.70) as $\bar{x}(z,t) \approx \sum_{i=1}^{r_m} a_i(t)\psi_i(z)$.

By substituting this approximation in the PDE of (8.70) we obtain,

$$\sum_{i=1}^{r_m} \dot{a}_i \psi_i = \theta_1 \sum_{i=1}^{r_m} a_i \frac{d^2 \psi_i}{dz^2} + \theta_2 \sum_{i=1}^{r_m} a_i \psi_i + \beta_U b(z) u. \tag{8.71}$$

Then the ROM can be constructed using Galerkin's method as follows,

$$\dot{a}_j = \theta_1 \sum_{i=1}^{r_m} a_i \int_0^\pi \frac{d^2 \psi_i}{dz^2} \psi_j dz + \theta_2 a_j + \beta_U \left(\int_0^\pi b(z) \psi_j dz \right) u,$$
$$j = 1, \ldots, r_m. \tag{8.72}$$

The above equation can be summarized as the following vectorized form,

$$\dot{a} = (\theta_1 A + \theta_2 I) a + Bu, \tag{8.73}$$

where $[A]_{j,i} = \left(\psi_j(z), \frac{d^2 \psi_i(z)}{dz^2} \right)$, $[Bu]_j = \left(\psi_j(z), b(z) \right) u$. The ODE system of (8.73) is the basis to synthesize the controller. Note that the resulting system approximation of (8.73) is a switching system due to the form and dimensionality changes during process evolution. Thus, the stability of the switching system under the control actions must be proven via Lyapunov and hybrid system stability arguments [79, 86].

8.4.1.3.3   Derivation of APOD-based adaptive control structure   In this section, we utilize the ROM of (8.73) in designing adaptive output feedback controllers for the semi-linear parabolic PDE system of (8.67). The controller is syn-

thesized based on continuous point measurements available from restricted number of sensors (4 sensors). We use a static observer of the following form,

$$\tilde{a} = \left(\Psi(L_s)\Psi^T(L_s) \right)^{-1} \Psi(L_s) y_m(L_s), \qquad (8.74)$$

to estimate the state of the ODE system of (8.73) due to the unavailability of full state measurements assuming that the number of point measurement sensors is equal to or greater than r_m.

We consider the following control Lyapunov function (CLF),

$$V_c = \frac{\zeta}{2} a^T a, \qquad (8.75)$$

where $\zeta > 0$ is a adjusting parameter which modifies the CLF at the revisions. By substituting (8.73) in the time derivative of the CLF we obtain

$$\dot{V}_c = \zeta a^T \dot{a} = \zeta a^T \left((\theta_1 A + \theta_2 I)a + Bu \right). \qquad (8.76)$$

Then by considering

$$\dot{V}_c = -\rho a^T a < 0, \qquad (8.77)$$

the control structure is derived as a function of unknown system parameters as follows

$$u = -B^{-1} \left(\frac{\rho}{\zeta} a + (\theta_1 A + \theta_2 I)a \right), \qquad (8.78)$$

where ρ is a positive number that indicates the regulation rate.

We define the closed-loop Lyapunov function as a combination of the CLF and the identification Lyapunov function,

$$V = \frac{\zeta}{2}a^T a + \frac{1}{2}\tilde{\theta}_1^2 + \frac{1}{2}\tilde{\theta}_2^2, \tag{8.79}$$

where $\tilde{\theta}_1 = \hat{\theta}_1 - \theta_1$, $\tilde{\theta}_2 = \hat{\theta}_2 - \theta_2$, and $\hat{\theta}_1$, $\hat{\theta}_2$ are the estimations of the unknown parameters of θ_1 and θ_2, respectively.

By substituting (8.73) in the time derivative of the close-loop Lyapunov function and assuming that θ_1 and θ_2 do not vary continuously, we conclude

$$\dot{V} = \zeta a^T \dot{a} + \tilde{\theta}_1 \dot{\hat{\theta}}_1 + \tilde{\theta}_2 \dot{\hat{\theta}}_2 = \zeta a^T \Big((\theta_1 A + \theta_2 I)a + Bu \Big) + \tilde{\theta}_1 \dot{\hat{\theta}}_1 + \tilde{\theta}_2 \dot{\hat{\theta}}_2. \tag{8.80}$$

The controller formula in the presence of unknown parameters is obtained by the applying certainty equivalence principle [25] to the control structure of (8.78),

$$u = -B^{-1}\Big(\frac{\rho}{\zeta}a + (\hat{\theta}_1 A + \hat{\theta}_2 I)a\Big). \tag{8.81}$$

Then by considering (8.80) and (8.81) we can obtain the adaptation laws

$$\dot{\hat{\theta}}_1 = a^T A a,$$
$$\tag{8.82}$$
$$\dot{\hat{\theta}}_2 = a^T a,$$

where

$$\dot{V} = -\rho a^T a < 0, \tag{8.83}$$

thus the closed-loop system is locally asymptotically stable in the Lyapunov sense.

The control and adaptation laws of (8.81) and (8.82) are redesigned when the ROM is revised by APOD. Stability theorems of hybrid systems are then required to prove that the resulting switching controlled system remains stable at revisions. For switching system stability analysis the multiple CLFs in the form of (8.75) must be considered. The negative time derivative of the multiple CLFs, described in (8.84), guarantees stability of the switching system (Theorem 3.2 in [86]) when the following condition is also satisfied [79, 86]

$$V_c\big(\tilde{a}(t_k)\big) < V_c\big(\tilde{a}(t_{k-1})\big), \tag{8.84}$$

where $k > 1$ and $V_c\big(\tilde{a}(t_k)\big)$ corresponds to the value of CLF at the beginning of time interval $[t_k, t_{k+1}]$. The CLF may possibly increase during dimensionality changes of the ROM, furthermore, the value of ζ must be chosen appropriately in the closed-loop process. The following equation is applied to update the value of ζ as needed

$$\zeta = \eta \frac{\tilde{a}^T(t_{k-1})\,\tilde{a}(t_{k-1})}{\tilde{a}^T(t_k)\,\tilde{a}(t_k)}, \tag{8.85}$$

where $\eta < 1$. Alternatively, we initialize ζ at value $\zeta_0 = 1$, and reevaluate it using (8.85) only when the criteria of (8.84) is violated.
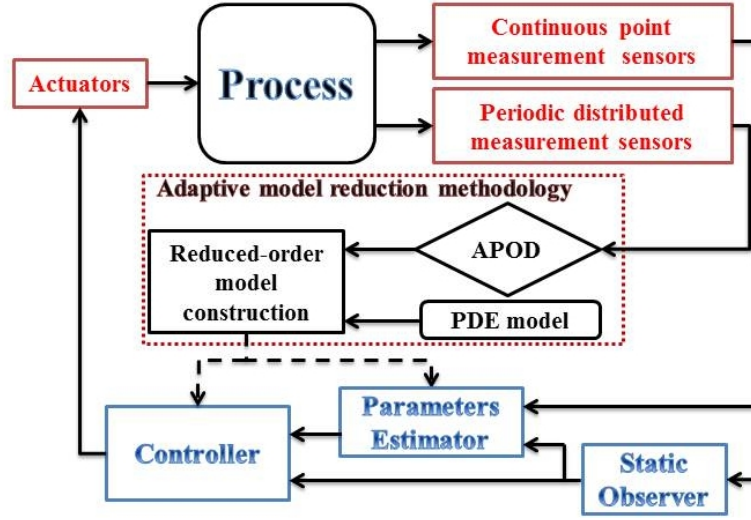
Figure 8.18: Process operation block diagram under proposed control structure.

Figure 8.18 shows the block diagram of closed-loop process under the proposed control structure. The control performance of the system of (8.49)-(8.51) directly depends on the accuracy of its ROM. Using APOD methodology, the ROM will be adaptively revised at certain time instants to remain accurate. Then the ROM structure and dimensionality change during process evolution. As a result, when the ROM switches the controller will be redesigned as well.

Remark 8.8. *The static observer requirements of available number of continuous point measurement sensors being supernumerary to the dimension of the ROM can be circumvented using dynamic observer synthesis which conceptually requires only one measurement output [28, 31, 82].*

Remark 8.9. *To design the controller in the form of (8.81) we assume that the number of control actuators is equal to r_m and the inverse of B exists. To sat-*

isfy such conditions the number of actuators may be decreased or increased during the process evolution if the dimensionality of the ROM changes. We may avoid activating and deactivating actuators during such changes by using more than r_m actuators and employing the right pseudo-inverse of B, $B^\perp = B^T(BB^T)^{-1}$ in (8.81), instead of B^{-1}.

Remark 8.10. *The adaptive control of nonlinear distributed parameter systems in the presence of time-varying unknown parameters using dynamic observer designs is the current subject of authors' research and will be presented in future publications.*

8.4.1.3.4 Closed-loop analysis We present the closed-loop simulation results for the catalytic chemical reactor in the presence of unknown diffusion and reaction parameters. We studied two cases with the same controller structure and parameters; (1) constant diffusion-reaction parameters and (2) time-varying the diffusion-reaction parameters as process evolves. In both cases, we use $\rho = 2$ to adjust the rate of asymptotic decrease in the Lyapunov function.

8.4.1.3.4.1 Constant diffusion-reaction parameters In this section, the closed-loop simulation results are presented for thermal dynamic regulation of the catalytic reactor when the unknown diffusion-reaction parameters are constant and do not change during the process evolution. Figure 8.19 illustrates the closed-loop process profile and its 2-norm. We can easily observe that the adaptive
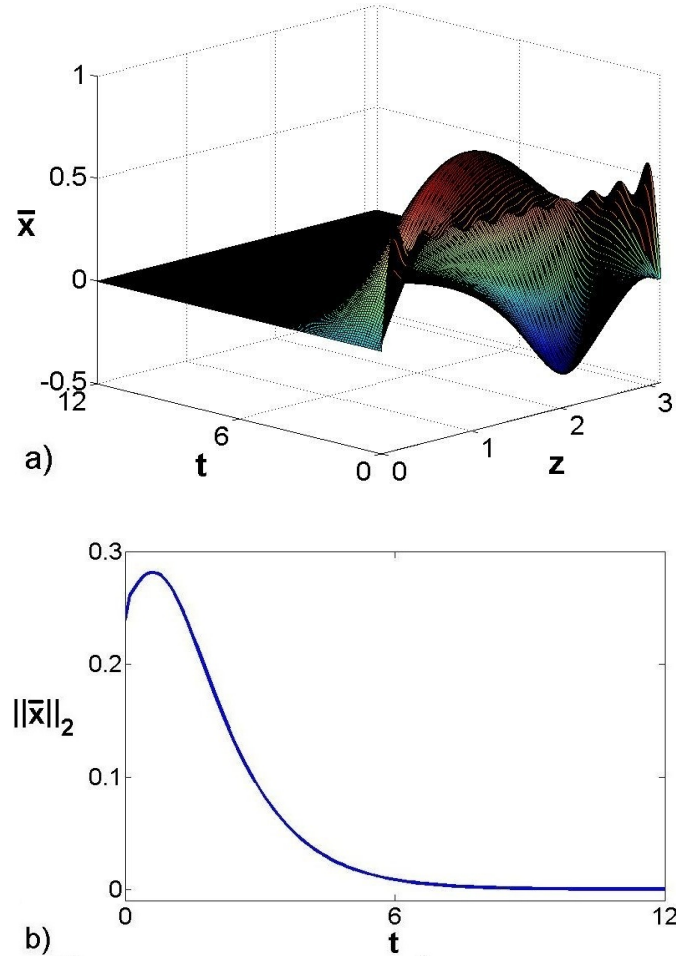
Figure 8.19: Closed-loop (a) spatiotemporal profile of the system state and (b) temporal profile of its 2-norm.

controller successfully regulates the system of (8.67)-(8.68) at the unstable steady state of $\bar{x}(z, t) = 0$.

Figure 8.20 shows the change in the number of empirical basis functions required to capture the dominant dynamics of the system during the process evolution. The number of initial empirical basis functions was two and it increased to three as the process evolved. Figure 8.21 shows the temporal profiles of the first,
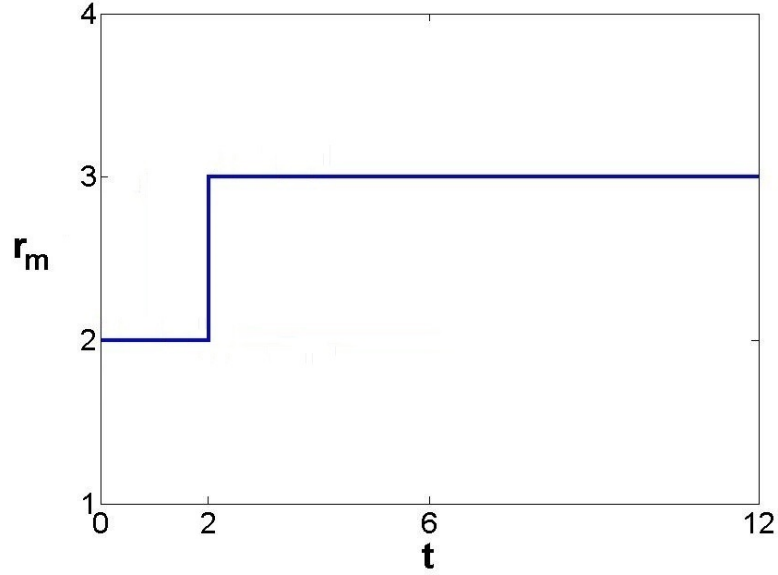
Figure 8.20: Number of empirical basis functions.

second and third empirical basis functions. The dominant empirical basis functions were updated to accurately capture the process behavior when new trends appeared. The temporal profiles of the estimated dominant mode of the system and the required control action is presented in Figure 8.22. The system dominant mode and the control action converged to the steady state value of zero without chattering and any sharp changes. The effects of changes in the unknown parameters of the system can be observed in the temporal profiles of the 2-norm, dominant estimated mode and control action at $t = 5s$. When the actuator is activated, the process behavior significantly changes and the effect of the actuator on the DPS are now captured by the second basis function which has a maximum at $z = 3\pi/4$ where the actuator is located. We see that APOD adapts to this change and a new basis is captured where the closed-loop dynamics.
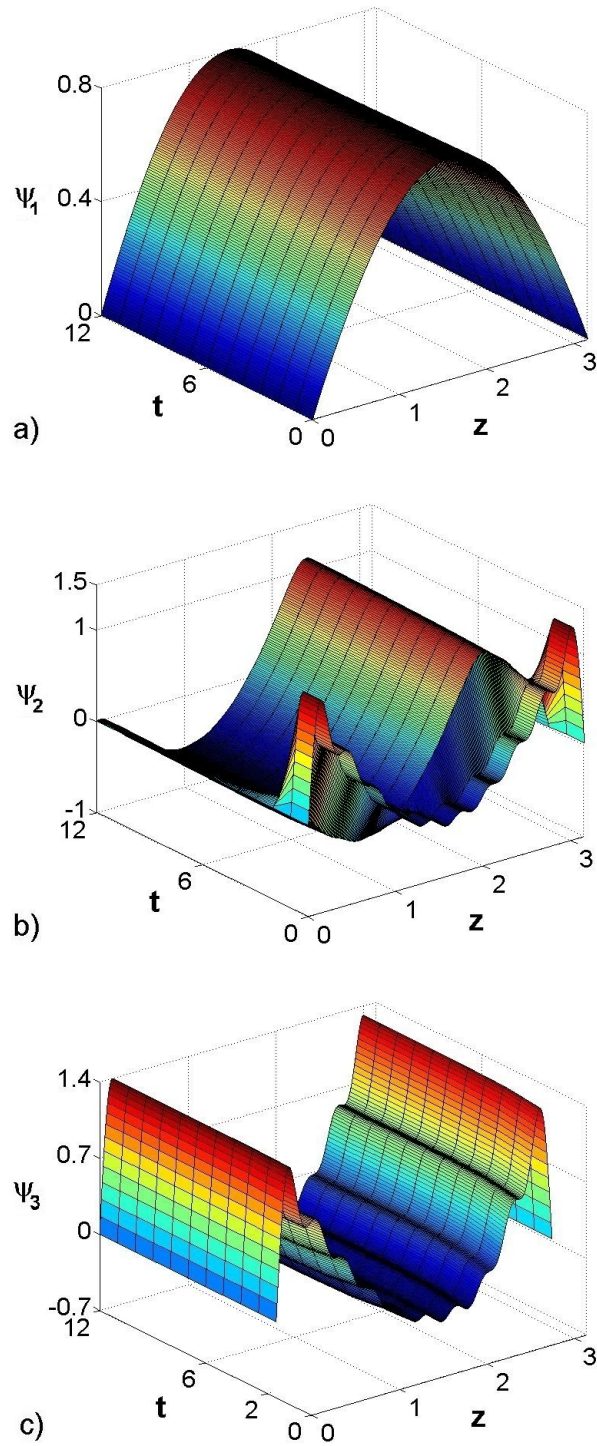
Figure 8.21: Temporal profile of the (a) first, (b) second and (c) third empirical basis functions.
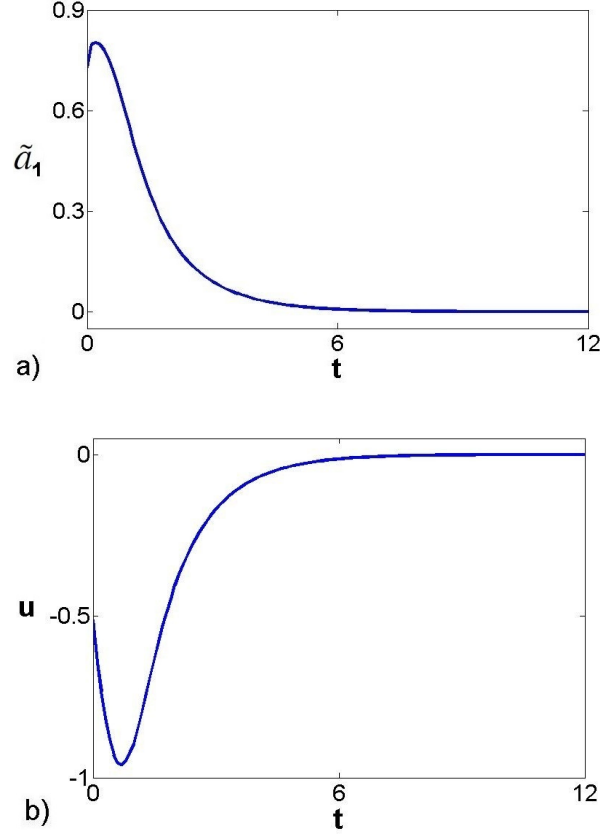
Figure 8.22: Temporal profile of (a) the estimated dominant mode of the system and (b) the required control action.

Figure 8.23 presents the temporal profile of the CLF for $\zeta = \zeta_0 = 1$. The black circles indicates the CLF values at the revisions. We observe that the CLF values at the revisions decreased as time evolves which guarantees the switching system stability. In such case, we did not need to reevaluate the ζ because the criteria of (8.84) was always valid during process evolution. Figure 8.24 presents the dynamics of the estimated unknown parameters from the adaptation law. We observe that the estimated parameters converged the steady state values of $\hat{\theta}_1 = 2.8$ and $\hat{\theta}_2 = 3$ when the nominal values of the system unknown parameters are $\theta_1 = 1$
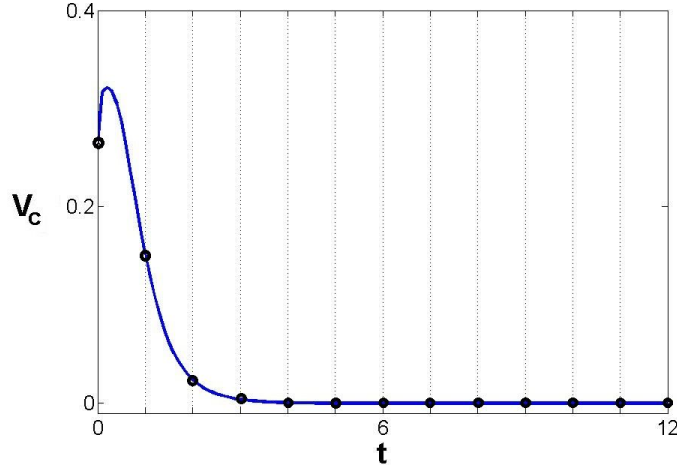
Figure 8.23: Temporal profile of the CLF. The black circles show the CLF values at the ROM revisions.

and $\theta_2 = 2.33$. We may observe that the adaptation law can not estimate the unknown parameters due to the lack of persistent excitation needed for complete system identification. Note that the system identification is not the objective of the proposed control method.

8.4.1.3.4.2 Time-varying diffusion-reaction parameters In this section we present the simulation results in the presence of unknown diffusion and reaction parameters that change from $D = 1$, $\beta_T = 16$ and $\gamma = 2$ to $D = 3$, $\beta_T = 30$ and $\gamma = 3$ at $t = 4s$. Figure 8.25 shows the open-loop process spatiotemporal profile and the temporal profile of its 2-norm, when the controller was inactive. We observe a significant change in the system dynamics due to the parametric change.

The closed-loop system profile and its 2-norm under the impact of the proposed
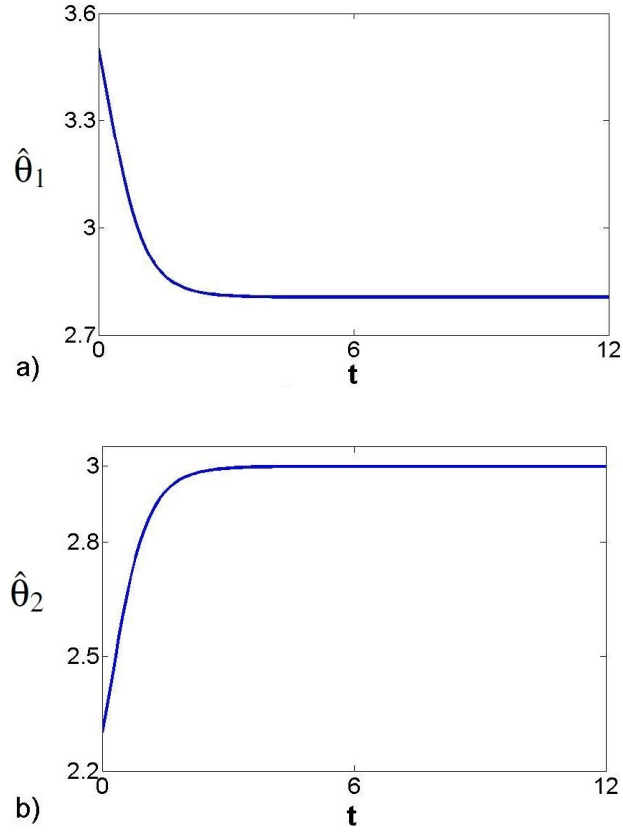
Figure 8.24: Temporal profile of (a) $\hat{\theta}_1$ and (b) $\hat{\theta}_2$.

control structure is presented in Figure 8.26, where the adaptive controller stabilized the process at the unstable steady state of $\bar{x}(z,t) = 0$. Finally, we illustrate the temporal profiles of the estimated dominant mode and the control action in Figure 8.27. The convergence of the dominant mode and control action to zero without any chartering indicates the effectiveness of the proposed adaptive control method.

The effects of the changes in the unknown parameters of the system can be observed in the temporal profiles of the closed-loop 2-norm, dominant estimated mode and control action at $t = 4s$. Due to the effective performance of the two
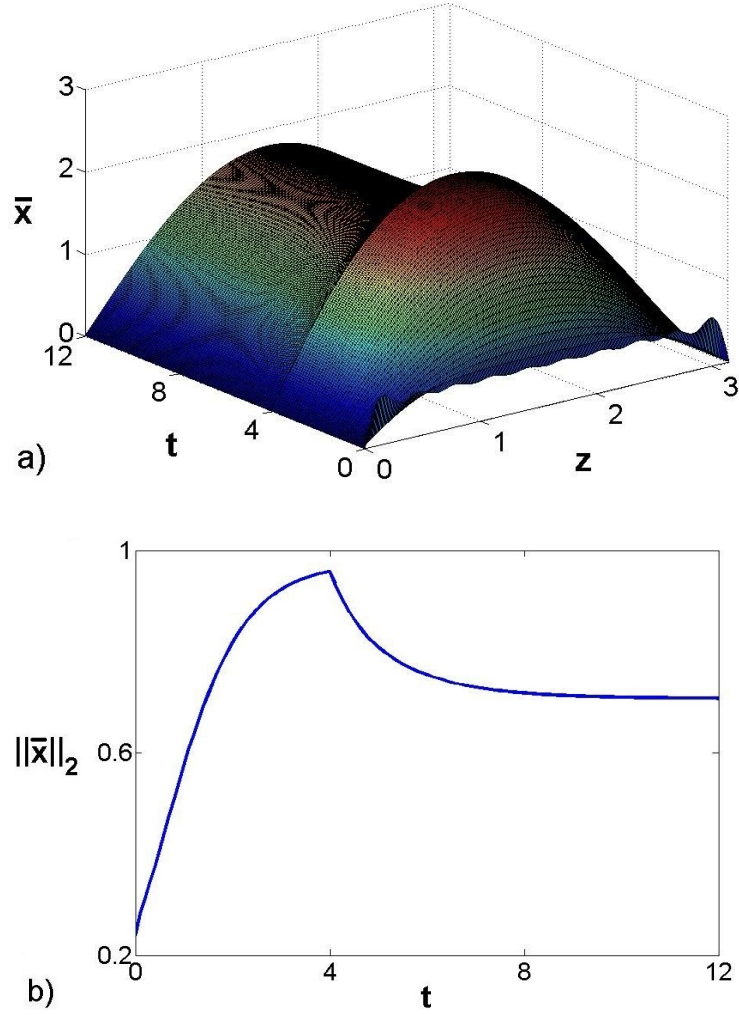
Figure 8.25: Open-loop (a) spatiotemporal profile of the system state and (b) temporal profile of its 2-norm in the presence of unknown parameters changes.

layer adaptation we do not observe significant variations in the closed-loop system when the process unknown parameters change.

The success of the designed controller in regulating the process is due to the dominant eigenspace (hence the ROM, the adaptation and the control laws) being updated as the process traverses through different regions of the state space during closed-loop operation. During the closed-loop process operation, when new
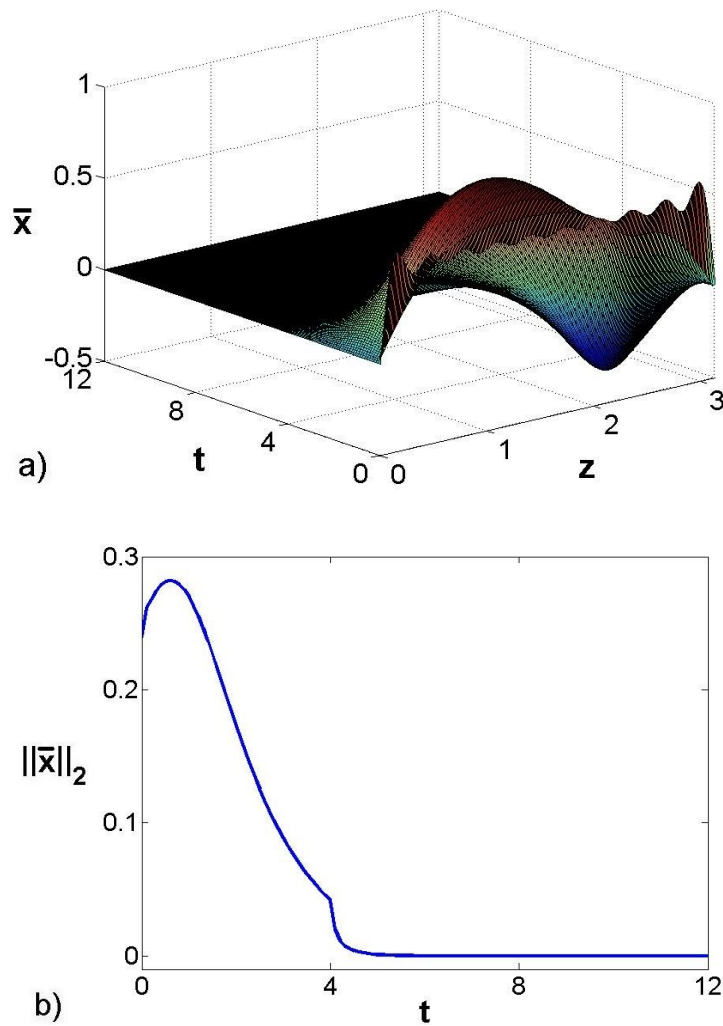
Figure 8.26: Closed-loop (a) spatiotemporal profile of the system state and (b) temporal profile of its 2-norm in the presence of unknown parameters changes.

trends appeared the dominant empirical basis functions were updated to accurately capture the process behavior.
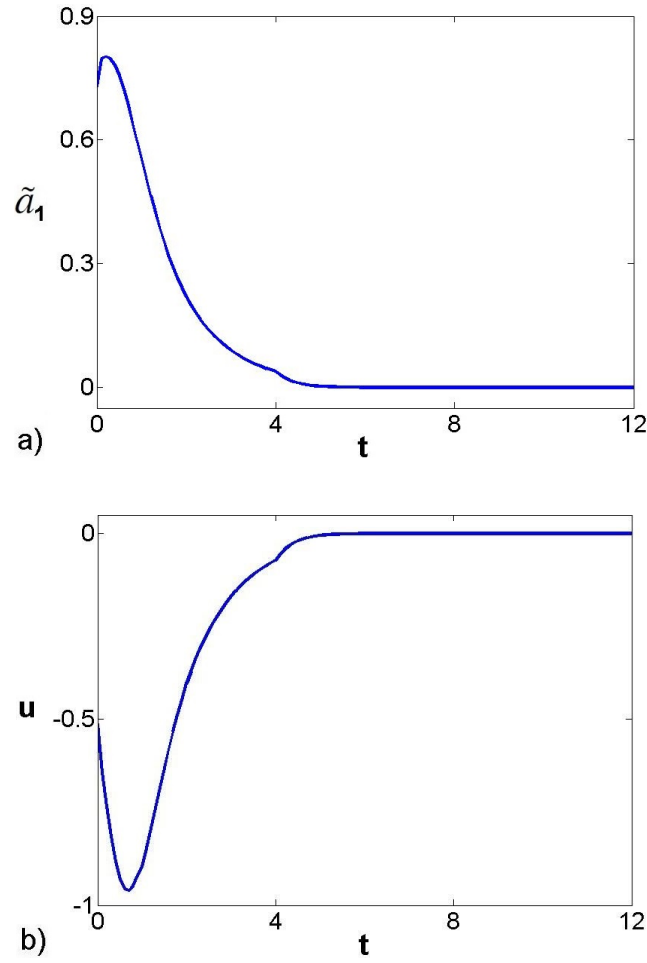
Figure 8.27: Temporal profile of (a) the estimated dominant mode of the system and (b) the required control action in the presence of unknown parameters changes.

8.4.2 Direct adaptive control

8.4.2.1 Preliminaries

We study the control problem of wave motion spatiotemporal dynamics of flow processes in the presence of unknown parameters which can be mathematically

modeled by the following nonlinear dissipative PDE,

$$\frac{\partial \bar{x}(z,t)}{\partial t} = \mathcal{F}_n\Big(\bar{x}(z,t)\Big) + \mathcal{G}_n\Big(\bar{x}(z,t)\Big)\theta + \mathcal{B}(z)u(t),$$

$$\Gamma\Big(\bar{x}(z,t), \frac{\partial \bar{x}(z,t)}{\partial z}, \ldots, \frac{\partial^{n-1}\bar{x}(z,t)}{\partial z^{n-1}}\Big)_{\partial\Omega} = 0, \tag{8.86}$$

$$\bar{x}(z,0) = \bar{x}_0(z).$$

In the PDE system of (8.86),

$\bar{x}(z,t) \in \mathbb{R}$: *system spatiotemporal state,*

$z \in \Omega$: *spatial coordinate,*

t : *time,*

Ω : *process domain,*

$\partial\Omega$: *process boundaries,*

$\mathcal{F}_n, \mathcal{G}_n^{1\times q}$: *nonlinear differential-algebraic operators of order n,*

$\theta \in \mathbb{R}^q$: *vector of unknown parameters,*

$u \in \mathbb{R}^l$: *vector of manipulated inputs,*

$\mathcal{B}(z)$: *spatial distribution of manipulated inputs,*

Γ : *vector of homogeneous boundary conditions,*

$\bar{x}_0(z)$: *initial spatial profile of the system state.*

We can reformulate the PDE of (8.86) in the infinite dimensional form,

$$\dot{x} = \mathbf{F}(x) + \mathbf{G}(x)\theta + \mathbf{B}u, \quad x(0) = x_0, \tag{8.87}$$

in an appropriate Sobolev subspace of $\mathbb{W}$,

$$\mathbb{W}(\Omega) = \Big\{ \mathcal{H} \in L_2(\Omega) : \ \forall \alpha \in \mathbb{N}, \ |\alpha| \leqslant n - 1, \ \partial^\alpha \mathcal{H} \in L_2(\Omega),$$
$$\Gamma\Big(\mathcal{H}, \frac{\partial \mathcal{H}}{\partial z}, \dots, \frac{\partial^{n-1}\mathcal{H}}{\partial z^{n-1}}\Big)_{\partial\Omega} = 0 \Big\},$$

where

$$x(t) = \bar{x}(z, t),$$

$$\mathbf{F}(x) = \mathcal{F}_n\Big(\bar{x}(z, t)\Big),$$

$$\mathbf{G}(x)\theta = \mathcal{G}_n\Big(\bar{x}(z, t)\Big)\theta,$$

$$\mathbf{B}u = \mathcal{B}(z)u(t).$$

To discretize the resulting infinite dimensional system of (8.87) in the form of ODEs of vectorized modes needed for MOR, we must calculate the set of basis functions. Such basis functions are the solution of the following nonlinear dissipative eigenproblem,

$$\mathbf{F}(\phi_j) + \mathbf{G}(\phi_j)\theta = \lambda_j \phi_j,$$
$$\Gamma(\phi_j, \frac{\partial \phi_j}{\partial z}, \dots, \frac{\partial^{n-1}\phi_j}{\partial z^{n-1}})\Big|_{\partial\Omega} = 0, \qquad (8.88)$$
$$j = 1, \dots, \infty,$$

where λ and ϕ denote the eigenvalue and corresponding analytical basis function, and $\mathbb{W} \triangleq span\{\phi_i\}_{i=1}^\infty$, i.e., the nonlinear dissipative operator is a strong generator of the defined Sobolev subspace of $\mathbb{W}$.

Assumption 8.4. *Considering the eigenspectrum of above nonlinear dissipative eigenproblem in the form of $\{\lambda_1, \lambda_2, \dots\}$ where the eigenvalues are sorted by size,*

we assume it can be decomposed to the following subsets;

1. *finite subset of p slow and possibly unstable eigenvalues,*

$$\{\lambda_1, \lambda_2, \ldots, \lambda_p\},$$

2. *complement infinite subset of the rest fast and stable eigenvalues,*

$$\{\lambda_{p+1}, \lambda_{p+2}, \ldots\}.$$

A time scale separation can be identified between such subsets as $\sigma = \dfrac{|Re(\lambda_1)|}{|Re(\lambda_{p+1})|}$ where σ is a small number and $Re(\cdot)$ shows the real part. In addition we can define two Sobolev subspaces for such subsets that includes the corresponding basis functions;

1. *slow subspace, $\mathbb{W}_s \triangleq span\{\phi_i\}_{i=1}^p$,*

2. *complement fast, $\mathbb{W}_f \triangleq span\{\phi_i\}_{i=p+1}^\infty$.*

According to Assumption 8.4 and by defining slow and fast projection operators,

$$\mathcal{P} : \mathbb{W} \to \mathbb{W}_s, \quad \mathcal{P}(\cdot) = (\cdot, \Phi_s),$$
$$\mathcal{Q} : \mathbb{W} \to \mathbb{W}_f, \quad \mathcal{Q}(\cdot) = (\cdot, \Phi_f), \tag{8.89}$$

the infinite dimensional system of (8.87) can be represented by a partitioned ODE set of vectorized slow and fast modes as follows,

$$\dot{x}_s = F_s(x_s, x_f) + G_s(x_s, x_f)\theta + B_s u, \quad x_s(0) = \mathcal{P}x_0,$$
$$\dot{x}_f = F_f(x_s, x_f) + G_f(x_s, x_f)\theta + B_f u, \quad x_f(0) = \mathcal{Q}x_0, \tag{8.90}$$

where $x = x_s \oplus x_f$, $F_s = \mathcal{P}\mathbf{F}$, $F_f = \mathcal{Q}\mathbf{F}$, $G_s = \mathcal{P}\mathbf{G}$, $G_f = \mathcal{Q}\mathbf{G}$, $B_s = \mathcal{P}\mathbf{B}$, $B_f = \mathcal{Q}\mathbf{B}$.

Based on Tykhonov's theorem [175] and using singular perturbation analysis [76], the partitioned infinite dimensional system of (8.90) can be approximated in the form of

$$\dot{x}_s = F_s(x_s, 0) + G_s(x_s, 0)\theta + B_s u, \quad x_s(0) = \mathcal{P}x_0, \tag{8.91}$$

when the residual fast and stable dynamics stabilize, $x_f \to 0$, after a finite period of time which can be identified by applying singular perturbation analysis.

Remark 8.11. *The partitioning assumption between the slow and fast dynamics of the system (Assumption 8.4) is satisfied by a majority of dissipative transport-reaction processes [76], which indicates that only a few dominant modes are adequate to approximate the long-term dynamic behavior of the system.*

8.4.2.2 Model order reduction using recursively updated empirical basis functions

The low dimensional approximation of the PDE system can be obtained by truncating the discretized system up to an appropriate number of equations when the basis functions are accessible. In general, if we can compute an appropriate set of orthonormal basis functions that capture the dominant dynamics of the system,

the spatiotemporal state of the PDE system can be approximated by

$$\bar{x}(z,t) \approx \sum_{k=1}^{m} \psi_k(z) a_k(t), \tag{8.92}$$

where $\{\psi_i(z)\}_{i=1}^{m}$ is the set of m required basis functions and $a_k(t)$ denotes the corresponding system modes.

Then, by applying a discretization method such as Galerkin projection we obtain the mth order ODEs by substituting the approximation of (8.92) in the PDE system of (8.86) and then integrating over spatial domain by considering the orthonormal basis functions as the weighting functions,

$$\dot{a}_v(t) = \int_{\Omega} \psi_v(z) \mathcal{F}(z, \sum_{k=1}^{m} \psi_k(z) a_k(t)) dz + \left(\int_{\Omega} \psi_v(z) \mathcal{G}(z, \sum_{k=1}^{m} \psi_k(z) a_k(t)) dz \right) \theta$$
$$+ \left(\int_{\Omega} \psi_v(z) b(z) dz \right) u, \tag{8.93}$$

for $v = 1, ..., m$.

The above discretization is only applicable when the orthonormal basis functions are available. However, we can not find an analytical solution for the nonlinear eigenproblem of (8.88) subject to unknown parameters and general boundary conditions. We also can not use numerical techniques to directly solve such eigenproblems due to the existence of unknown vector of θ in the nonlinear operator structure. To circumvent such essential issues we employ APOD algorithm to compute the set of empirical orthonormal basis functions. The off-line part of the

algorithm (POD) is applied to compute the initial empirical orthonormal basis functions based on limited available off-line spatially distributed state profiles of the system before the closed-loop process starts. Then, during the process evolution when new trends appear in the system dynamics the on-line part of the algorithm recursively update the empirical basis functions.

To revise the empirical basis functions during closed-loop process evolution, APOD needs the spatially distributed profile of the system state at each revision times which is called snapshot. Such required snapshots can be accessible from periodic fixed or moving spatially distributed measurement sensors, or be computed using in parallel high fidelity simulator. The corresponding measurement output can be presented by

$$y_r(z, t_k) = \int_0^t \delta(\tau - t_k)\bar{x}(z, \tau)\ d\tau, \tag{8.94}$$

where $\delta(\cdot)$ is the standard Dirac function and t_k denotes the time instance for snapshot measurement and $k = 1, 2, \ldots, \infty$.

Remark 8.12. *The structure and dimension of the ODEs of (8.93) changes during the process evolution because the APOD algorithm recursively revises the set of empirical basis functions to capture possible new dynamics. Following such revisions that change the number and spatial distribution of the empirical basis functions, the output feedback control structure (state feedback controller and observer) also*

updates.

8.4.2.3   Adaptive output feedback control

In this section we use the resulting ROM (obtained by APOD and Galerkin projection in Section 8.4.2.2) as the basis for adaptive output feedback control design assuming the approximate controllability of the dissipative DPS described by the PDE of (8.86). To simplify the controller structure notation we summarized the ROM of (8.93) as follows,

$$\dot{a} = f(a) + g(a)\theta + Bu, \qquad (8.95)$$

where $f^{m \times 1}$ and $g^{m \times q}$ are nonlinear vector functions, and $B^{m \times l}$ is a matrix whose components are presented as follows,

$$f_v = \int_\Omega \psi_v(z)\mathcal{F}(z, \sum_{k=1}^{m} \psi_k(z)a_k(t))dz,$$

$$g_{v,i} = \int_\Omega \psi_v(z)\mathcal{G}^i(z, \sum_{k=1}^{m} \psi_k(z)a_k(t))dz,$$

$$b_{v,j} = \int_\Omega \psi_v(z)b_j(z)dz.$$

To design the adaptive controller we consider the ROM of (8.95) where $a \in \mathbb{R}^m$, $\theta \in \mathbb{R}^q$, $f : \mathbb{R}^m \to \mathbb{R}^m$, $g : \mathbb{R}^m \to \mathbb{R}^{m \times q}$, $B \in \mathbb{R}^{m \times l}$ and $u \in \mathbb{R}^l$. We use the vector variable $\hat{\theta}$ as the estimation of the unknown variable of θ, where the identification error vector can be presented by $e_\theta = \theta - \hat{\theta}$. We assume that the identification error

remains bounded under the stable adaptive control design as $\|e_\theta\| < \Theta$, where Θ denotes the error upper bound.

By considering the control Lyapunov function (CLF) as $V_c(a) = \frac{1}{2}a^T a$ where V_c is a positive definite function (i.e., $V_c(a) \geq 0$ and $V_c = 0$ only when $a = 0$), we can obtain its time derivative as

$$\dot{V}_c = a^T \dot{a} = a^T \Big(f(a) + g(a)\theta + Bu \Big). \tag{8.96}$$

Then by setting

$$f(a) + g(a)\theta + Bu = -C_0 a - \|g(a)\|\Theta \, sign(a), \tag{8.97}$$

where $C_0 > 0$ and $sign(\cdot)$ denotes the sign function, we conclude

$$\dot{V}_c = -C_0 a^T a - \|g(a)\|\Theta a^T sign(a) \leq 0,$$

which presents the controller stability [148]. Thus, we obtain the controller structure from (8.97) as follows,

$$u = -B^\perp \Big(C_0 a + f(a) + g(a)\theta + \|g(a)\|\Theta \, sign(a) \Big), \tag{8.98}$$

where $B^\perp = B^T(BB^T)^{-1}$ is the Moore-Penrose pseudo-inverse. Note that such pseudo-inverse definition reduces to B^{-1} when $m = l$.

Based on certainty equivalence principle we obtain the controller formula from (8.98) by replacing θ with its estimation, $\hat{\theta}$,

$$u = -B^{\perp}\left(C_0 a + f(a) + g(a)\hat{\theta} + \|g(a)\|\Theta\, sign(a)\right). \tag{8.99}$$

Now if we consider the closed-loop positive definite Lyapunov function as combination of the identification Lyapunov function (ILF) and CLF as follows,

$$V = V_i(e_\theta) + V_c(a) = \frac{1}{2}e_\theta^T P^{-1} e_\theta + \frac{1}{2}a^T a, \tag{8.100}$$

where $P^{q \times q}$ is a symmetric positive definite matrix (i.e., $P = P^T$ and $d^T P d > 0$ for every non-zero column vector of d), we obtain

$$\dot{V} = \dot{e}_\theta^T P^{-1} e_\theta + a^T \dot{a}. \tag{8.101}$$

Assuming that the unknown variable of θ does not change continuously, $\dot{\theta} = 0$,

$$\dot{e}_\theta = \dot{\theta} - \dot{\hat{\theta}}, \tag{8.102}$$

and by considering the adaptation law as

$$\dot{\hat{\theta}} = Pg^T(a)a, \tag{8.103}$$

we conclude

$$\dot{V} = -\left(Pg^T(a)a\right)^T P^{-1}e_\theta + a^T \Big(f(a) + g(a)\theta - C_0 a$$

$$-f(a) - g(a)\hat{\theta} - \|g(a)\|\Theta\, sign(a)\Big) \qquad (8.104)$$

$$= -C_0 a^T a - \|g(a)\|\Theta a^T sign(a) \leq 0.$$

Then by integrating the resulting inequality of (8.104) over time we obtain

$$\int_0^\infty \left(C_0 a^T a + \|g(a)\|\Theta a^T sign(a)\right) dt < V(0) - V(\infty) < \infty. \qquad (8.105)$$

The stability of the closed-loop system [148] can be obtained from (8.104) and (8.105).

To compute the required control action using the controller formula (8.99) and adaptation law (8.103) we have to access the full measurements of the states of (8.95) which are the system modes. However such states can not be measured directly from the process sensors while only a limited number of continuous point measurement sensors are considered to be available. The vector of measurement output for such fixed point sensors in the process domain can be presented as follows,

$$y_w(t) = \int_\Omega \delta(z - L_s)\bar{x}(z,t)\ dz, \qquad (8.106)$$

where L_s is a vector that presents the location of fixed continuous measurement sensors.
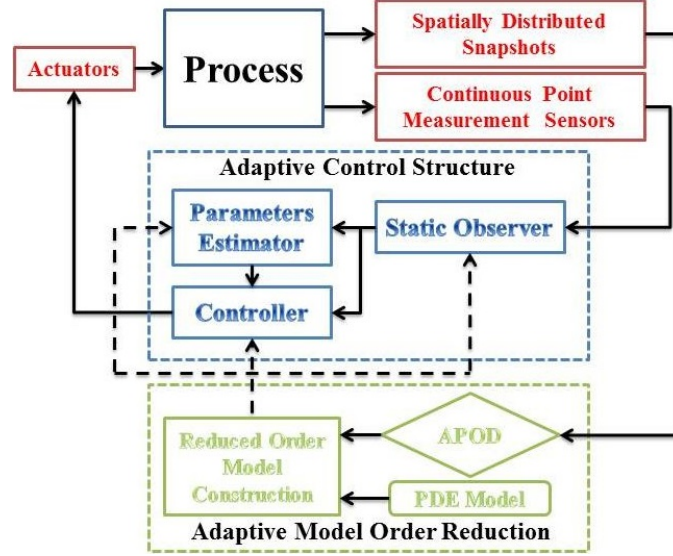
Figure 8.28: Closed-loop process operation.

By setting the number of such sensors to be supernumerary to the number of modes between ROM revisions, we apply the following static observer to estimate the required modes,

$$\hat{a} = \left(\Psi(L_s)\Psi^T(L_s) \right)^{-1} \Psi(L_s)y_m, \tag{8.107}$$

where $\Psi = [\psi_1 \ \psi_2 \ \cdots \ \psi_m]^T$. The closed-loop process block diagram is presented in Figure 8.28.

8.4.2.4 Application to wave motion suppression of a typical fluid flow process

In this section we employ the proposed output feedback adaptive control structure to suppress the wave motion dynamics in a thin film described by Korteweg-de

Vries-Burgers (KdVB) equation. The KdVB is one of the simplest nonlinear models that shows dispersion and dissipation effects in flow patterns [16, 48]. We consider the standard form of controlled KdVB equation as follows,

$$\frac{\partial \bar{x}}{\partial t} = -\frac{\partial^3 \bar{x}}{\partial z^3} + \theta \frac{\partial^2 \bar{x}}{\partial z^2} - \bar{x}\frac{\partial \bar{x}}{\partial z} + b(z)u(t), \qquad (8.108)$$

subject to the periodic boundary conditions,

$$\bar{x}(0,t) = \bar{x}(\pi,t),$$

$$\frac{\partial \bar{x}}{\partial z}(0,t) = \frac{\partial \bar{x}}{\partial z}(\pi,t), \qquad (8.109)$$

$$\frac{\partial^2 \bar{x}}{\partial z^2}(0,t) = \frac{\partial^2 \bar{x}}{\partial z^2}(\pi,t),$$

and initial condition,

$$\bar{x}(z,0) = \bar{x}_0(z), \qquad (8.110)$$

where

$\bar{x}(z,t) \in \mathbb{R} :$ *system spatiotemporal state,*

$z \in [0,\pi] :$ *spatial coordinate,*

$t :$ *time,*

$\theta :$ *unknown parameter,*

$u \in \mathbb{R}^l :$ *vector of manipulated inputs,*

$b(z) :$ *spatial distribution of manipulated inputs,*

$\bar{x}_0(z) :$ *initial spatial profile of the system state.*
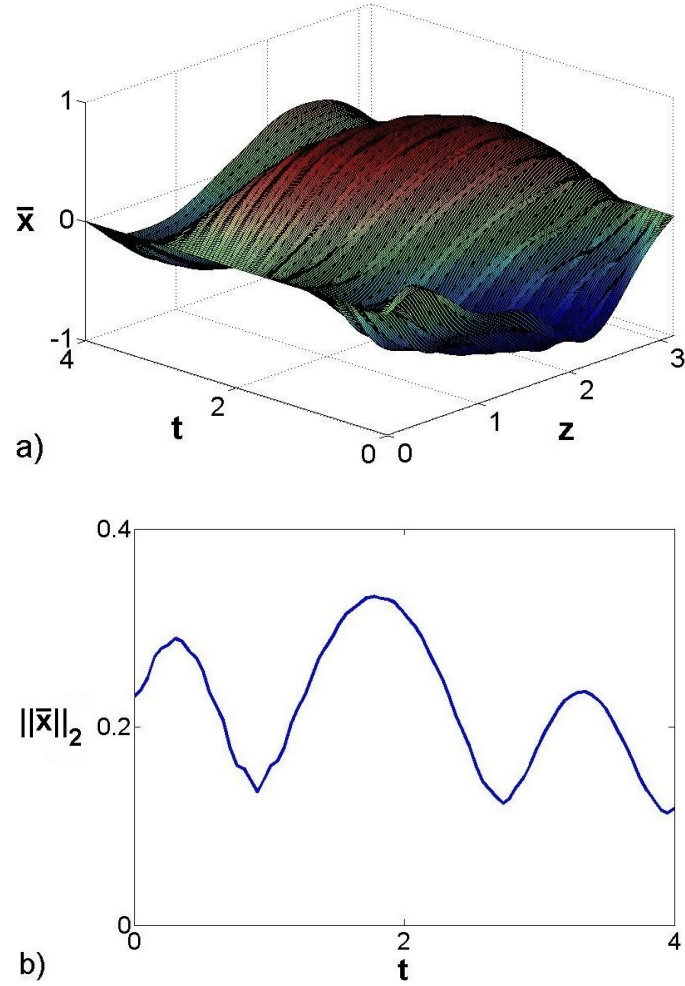
Figure 8.29: (a) Spatiotemporal profile of the system state and (b) temporal profile of its spatial 2-norm when the controller is inactivated.

8.4.2.4.1 Open-loop simulation results

The open-loop spatiotemporal profile of the system state and the temporal profile of its 2-norm for the nominal value of the unknown parameter, $\theta = 0.01$, is presented in Figure 8.29, where we observe the periodic dynamic behavior.

We considered a nonuniform initial spatial profile of the system state $\bar{x}_0(z) = -0.5\sin(z) + 0.3\sin(2z) + 0.1\sin(5z)$ which satisfies the boundary conditions. It can
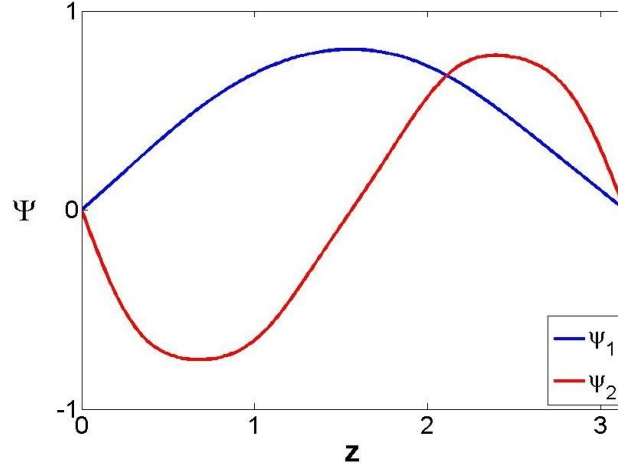
Figure 8.30: The initial orthonormal empirical basis functions.

be easily observe that the open-loop behavior of the system is under the influence of such nonuniform initial profile in the first two time steps of the process operation. We employed 10 snapshots during the time period of $t \in [0, 1]$ to compute the set of empirical basis functions using off-line APOD. Figure 8.30 shows the spatial profile of the initial set of dominant orthonormal empirical basis functions which capture 0.99 of the ensemble energy.

8.4.2.4.2 Closed-loop simulation results To implement the proposed MOR-based adaptive output feedback controller five continuous fixed point measurement sensors were considered across the process domain, $L_s = [\pi/6, \pi/3, \pi/2, 2\pi/3, 5\pi/6]$, we set four point actuators at $L_a = [\pi/5, 2\pi/5, 3\pi/5, 4\pi/5]$ where $b_i(z) = \delta(z - L_{a,i})$ for $i = 1, ..., 4$. The system snapshots were also assumed to be available every $\delta t = 1s$.

We apply $C_0 = 3$ to adjust the rate of asymptotic stabilization and $P = 1$ for
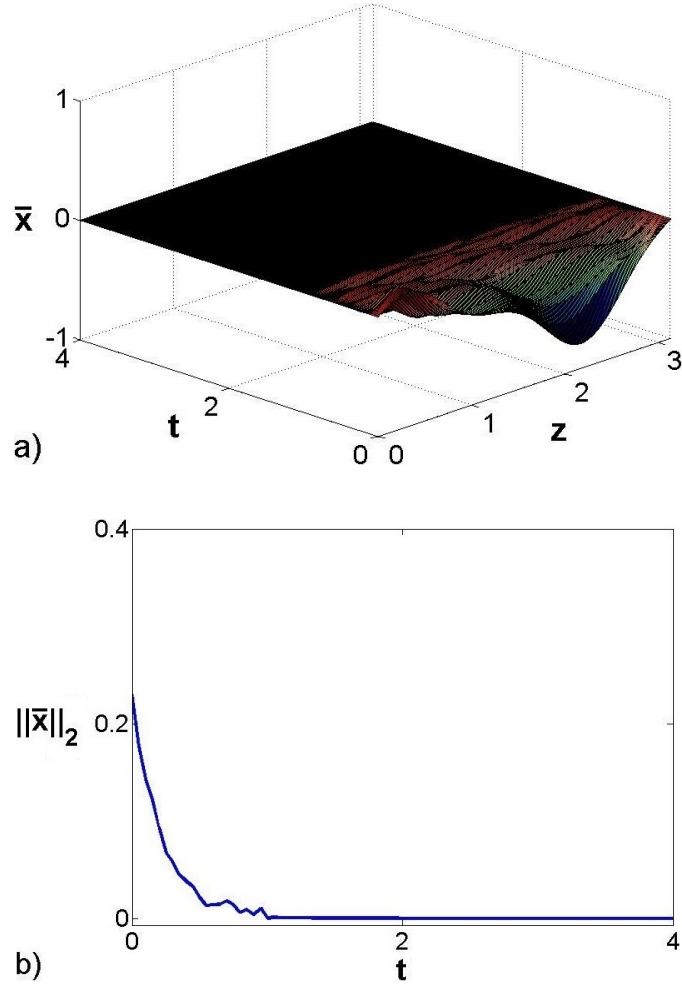
Figure 8.31: (a) Spatiotemporal profile of the system state and (b) temporal profile of its spatial 2-norm under the proposed control structure.

the identification law. Figure 8.31 shows the spatiotemporal profile of the system state and its 2-norm during the closed-loop process operation. We observe that the adaptive output feedback controller suppressed the periodic trends of the system and regulate the system state at the uniform spatial profile of $\bar{x}_d(z) = 0$. Figure 8.32 shows the required control actions applied by the four point actuators, where the components of actuation vector converged to zero.
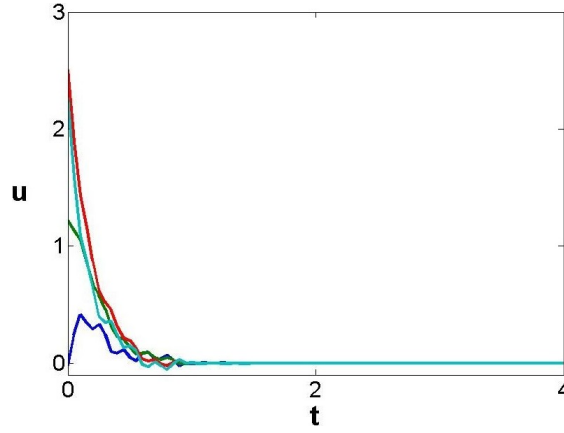
Figure 8.32: Temporal profile of the required control actions.
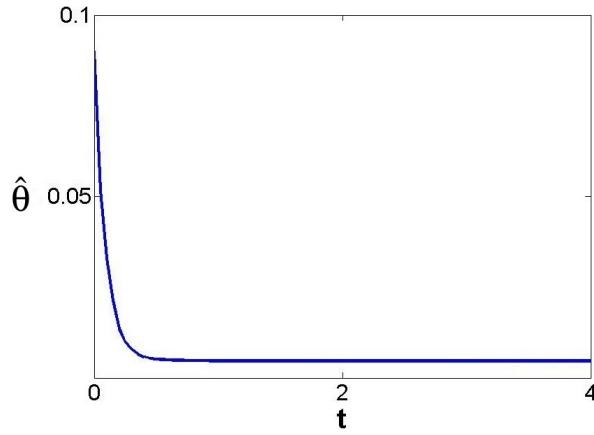
Figure 8.33: Temporal profile of $\hat{\theta}$.

The dominant empirical basis functions were recursively revised by APOD to capture the appearance of new dynamical trends during process evolution. Finally, Figure 8.33 shows the temporal profile of the estimated unknown parameter from the adaptation law. The estimated parameter converged the steady state values of $\hat{\theta} = 0.005$ which shows the adaptation law did not identify the parameter correctly due to the lack of required condition of persistent excitation for complete system identification.

CONCLUSIONS AND FUTURE RESEARCH DIRECTIONS

This dissertation focused on output feedback control of nonlinear distributed parameter systems (DPSs) via model order reduction (MOR). A wide range of analytical and proper orthogonal decomposition (POD) based statistical approaches were employed to compute the set of empirical orthonormal basis functions required by Galerkin's method to discretize the governing partial differential equations (PDEs) [28–40]. The effectiveness of the proposed output feedback control structures were successfully illustrated on a general class of chemical reactors and physico-chemical systems.

9.1 Conclusions

Chapter 1 presented the general form of PDEs which describe the DPSs in the chemical process industries and summarized the recent research work in monitoring, control and optimization of such processes.

In Chapter 2, we presented adaptive proper orthogonal decomposition (APOD) algorithm and its modification for on-line computation of the empirical basis functions required for system discretization.

In Chapter 3, we addressed the output feedback control problem of DPSs with limited measurement sensors. A combination of a robust state feedback controller with a Luenberger-type nonlinear dynamic observer of the system states was applied to synthesize a computationally efficient control structure based on adaptive proper orthogonal decomposition. The stability of the closed-loop system was proved based on Lyapunov stability theorem for hybrid systems. The effectiveness of the proposed control method was successfully employed to stabilize a physico-chemical system described by the Kuramoto-Sivashinsky equation (KSE) when the open-loop process exhibited highly nonlinear behavior.

In Chapter 4, the dynamic observer based control problem of DPSs with limited state measurements was addressed by employing a modified approach in APOD methodology. The stability of the closed-loop system was proven by Lyapunov stability criteria for hybrid systems. The proposed approach was successfully used to regulate the KSE at an spatially invariant steady state profile in the absence

and presence of uncertainty when the open loop process exhibits highly nonlinear and chaotic behavior with fast transients.

Chapter 5 focused on output tracking control issue for DPSs with limited state measurements. A computationally efficient regulator and output tracking controller structure was synthesized, by combining a globally linearizing controller (GLC) with a dynamic observer of the system states based on APOD methodology. The proposed synthesis method was successfully employed to address the output tracking problem for a catalytic reactor; specifically, the thermal dynamics of the reactor were controlled to reduce the hot spot temperature across the reactor length using a limited number of actuators and sensors to force the process evolution.

In Chapter 6, model-based controllers were designed for linear and nonlinear distributed processes based on restricted communication between the control system elements. We addressed the modeling component question via APOD algorithm to recursively compute the set of empirical basis functions. We employed APOD to properly express the system while circumventing extensive off-line computations. The main objective was to minimize snapshots transfer rate from the distributed sensors to the controller, for ROM revisions, considering closed-loop stability. The proposed control structure was illustrated on the temperature regulation problem of a tubular reactor and physico-chemical systems which can be modeled by the KSE.

In Chapter 7, the spatiotemporal dynamic shaping of semi-linear DPSs was investigated by regulating the error dynamics between the reduced order models (ROMs) of governing and target PDEs. The required ROMs were derived by applying Galerkin projection to the describing PDEs. The spatiotemporal error dynamics between the governing and target ROMs were stabilized using a sliding mode controller design combined with a Luenberger-type dynamic observer to estimate the required states. The effectiveness of the proposed control structure was illustrated on thermal dynamic shaping of a tubular flow reactor.

Chapter 8 addressed the adaptive output feedback control of chemical DPSs in the presence of unknown parameters via MOR. The reduced order model which used as the basis for the Lyapunov-based adaptive controller design is obtained by applying Galerkin's method to the governing PDEs. The basis functions required by the Galerkin projection was computed via employing analytical and statistical approaches. When the statistical methods were required, POD and APOD were applied to the set of spatiotemporal profiles of the system states obtained from open-loop process operation. The effectiveness of the proposed control structure was successfully illustrated on thermal dynamics regulation in a flow reactor and wave motion suppression in fluid flow processes.

9.2 Future research directions

According to the previous chapters, the research work in this dissertation can be extended in a broad areas of monitoring, control, optimization of DPSs in chemical and advanced material production industries. We briefly explain some direction for future research in the remainder of this chapter.

9.2.1 Controller/observer redesign based on the post processing of basis functions

In APOD and other variations of POD, the empirical basis functions computation is based on the covariance matrix of ensemble of snapshots. Then they might be different from the eigenfunctions of the spatial operator of the governing PDE. Thus, the ROM based on this strategy and the controller and dynamic observer designed based on ROM might not be accurate enough to depict the system dynamics at different regions of the state space. Therefore, a procedure is needed to find the eigenvalues and eigenfunctions of the PDE spatial operator and modify the controller/observer pair based on the new eigenfunctions as different regions of the state space are traversed. The linear part of the PDE spatial operator can be considered to find a bijective map from the space spanned by APOD empirical basis functions, $\mathbb{P}$, to the space spanned by the operator eigenfunctions, $\mathbb{W}_s$. The new basis functions will be computed using the empirical basis functions and the bijective map to improve the controller/observer pair.

9.2.2   Sensor/actuator placement & fault tolerance

An important issue when considering the controller design problem for distributed processes is where to place the sensors/actuators such that the system exhibits desired system theoretic properties such as enhanced controllability [3, 4, 21]. The complexity in this endeavor lies in the spatial dependence of the concepts of controllability and observability. At the same time, sensor/actuator and component failures have too often plagued industrial processes, often leading to deteriorating product quality and potentially dangerous process operation, such as runaway conditions [87, 118].

To address the issue of fault tolerance within the prism of an integrated sensor/controller selection and observer/controller design, a completely new direction can be embarked, whereby the objective of an sensor/actuator network is not only defined in terms of enhanced observability/controllability, improved performance or enhanced robustness with respect to disturbances or unmodeled dynamics, but with respect to fault tolerability. By taking advantage of the spatial variability that spatially distributed processes naturally enjoy, we can endeavor on an entirely new concept of optimal sensor/actuator network, in which sensor/actuator groups are physically distinct, and yet can be interchangeably used by the same observer/controller! This property is only applicable to DPSs wherein the same sensor/actuator placed at two or more different locations within the spatial domain of definition can have the same level of observability/controllability. We can cap-

italize on this property of spatially DPSs to find locations for different groups of sensor/actuator, each of which resulting in a similar observability/controllability level. When a given sensor/actuator group fails, then simply deactivating the faulty group and activating another healthy group constitutes the fault accommodation policy. Such a simple accommodation significantly reduces the costs associated with process supervision with the obvious economic and performance savings.

9.2.3 Simulation on demand and time delay compensation in sensor/controller network

The designed feedback controller requires continuous availability of measurements of the process state. Measurements of complete state profiles is usually difficult due to limited availability of sensors [256]. One of the possible solution for this issue is using a high accurate simulator that could send the snapshot to the controller structure as needed. However, there will be a time delay between snapshot demand and receiving it due to the time that is needed for highly accurate simulation. The control objective is to enforce closed-loop stability while simultaneously accounting for the delayed arrival of the state profiles from the parallel simulator. To compensate for the effect of the delay, the controller includes a finite dimensional propagation model that uses the delayed measurement, together with the past values of the control input, to provide an estimate of the current slow state which is then used to update the state of the model [270].

9.2.4 APOD error expressions, error bounds, and asymptotic results for reduced order models

As it discussed in previous sections, APOD takes simulation data or experimental data during process evolution and produces modes that can be used to reduce the model via a Galerkin projection. These reduced order APOD models are not well understood when initial conditions or parameters are changed in the reduced model, the solution of the reduced model can either be surprisingly accurate or completely unrelated to the solution of the full model. Understanding and predicting the accuracy of the reduced model is an extremely important problem.

As a first step toward this goal, Kunisch and Volkwein in [162, 163] proved error bounds for the POD reduced order model of various linear and nonlinear parabolic PDEs under the assumption that the initial conditions and parameters in the reduced model were not varied from the original PDE model. Since these works, other researchers have considered various scenarios (different PDEs, numerical methods, etc.) and modified POD model reduction schemes and have proved related error bounds (see [227] and the references therein). The derivations of existing error bounds for reduced order models of time varying partial differential equations (PDEs) constructed using proper orthogonal decomposition (POD) have relied on bounding the error between the POD data and various POD projections of that data. Furthermore, the asymptotic behavior of the model reduction error bounds depends on the asymptotic behavior of the POD data approximation error

bounds. [227].

Such work will give error indicators for the APOD reduced order model when model parameters or initial conditions are varied from those used to construct the APOD basis. It gives further insight into the behavior of APOD reduced order models for partial differential equations in the case where the model is varied. Hopefully, an increased understanding of this case will lead to additional progress in analyzing the effects of problem variations on reduced order models.

9.2.5 Moving sensors network & control

An unavoidable assumption of previously developed methodologies for controller synthesis that employ data driven model reduction techniques is the necessity for complete snapshots (in the sense the profiles must span the whole process domain). As expected, even though APOD relaxes the requirement for representative snapshot ensemble, it is also data driven methodology so it requires spatially complete snapshots. However, obtaining such information might not be feasible owing to high sensor costs and limited availability of sensors [4]. In recent years there has been considerable effort to relax this assumption in the field of model reduction as presented in the background section, substituting it with the assumption that periodically all the regions of the process domain are sampled.

The basic premise of the research work is that a set of mobile sensors achieve better estimation performance than a set of immobile sensors. To enhance the

performance of the state estimator, a network of sensors that are capable of moving within the spatial domain is utilized. Specifically, such an estimation process is achieved by using a set of spatially distributed mobile sensors. The objective is to provide mobile sensor control policies that aim to improve the state estimate. The metric for such an estimate improvement is taken to be the expected state estimation error.

A combination of scanning sensor networks and the proposed APOD methodology can be employed as a demarcation point to develop control methodologies that relax both the complete snapshot assumption and the representative ensemble requirement. To extend the applicability of APOD to situations when the availability of distributed sensing is limited, the proposed work cab be based on Gappy APOD (GAPOD) [104, 204, 265]. Briefly, GAPOD methodology scheme is outlined below.

1. Use initially available process snapshots to obtain empirical eigenfunctions using method of snapshots. If the snapshots in the ensemble are themselves damaged or incomplete, an iterative gappy method based on [104, 265] will be used to derive the empirical basis functions:

2. As a new incomplete snapshot from the process becomes available, reconstruct the snapshot via Gappy POD; solve a restricted linear optimization problem to refine the snapshot.

3. Augment the data ensemble using the reconstructed snapshot, while simul-

taneously discarding the least important snapshot available in the data ensemble.

4. Employ APOD to the modified data ensemble; update the empirical basis functions.

The primary application of GAPOD is the synthesis of feedback controllers for transport-reaction processes when only a limited set of measurements is available, e.g. due to design constraints and sensor cost. Furthermore, GAPOD is also an effective online data reconstruction tool for damaged or incomplete data sequences. This tool does not require an initial data ensemble that captures all the trends expected from a process (a requirement of gappy POD [104]) and hence is relatively easy to implement.

Based on the constructed method, issues arising from lack of distributed sensing can now be addressed. In general, there are two classes of sensor coverage control problems. The first class involves spatially fixed sensors. The goal, which has been extensively studied in the past, is to optimize sensor locations and sensor domains in fixed-sensor networks, and the problems in this class are considered to be in locational optimization [197]. In such problems, the solution is a Voronoi partition [92], where the optimal sensor domain is a Voronoi cell in the partition and the optimal sensor location is a centroid of a Voronoi cell in the partition. The second class of problems involves a set of mobile sensors. In [70], the authors present a survey of recent activities in the control and design of both static and dynamic

sensor networks. In their design criteria, they consider issues such as maximum coverage, detection of events, and minimum communication energy expenditure.

Small number of moving sensors that provide continuous local measurements will be employed to construct recursively the approximate reduced-order models. This cannot be achieved using standard techniques such as POD and Gappy POD. Such measurements are the only ones available for certain complex microelectronics processes, such as MOVPE. Beyond the obvious savings on communication costs and sensor network size, the study of this problem will provide an assessment of the robustness of the synthesized controllers and will allow us to identify the fundamental limits on the control structure tolerance to communication suspension. This is a major consideration in deciding a priori whether the desired control objectives can be met with a certain device network. The key idea is to embed a GAPOD-based model in the synthesized controller to provide an estimate of the system behavior when measurements are not transmitted, and to update the model state using the actual sensor measurements at discrete time instants [79, 100, 101, 273, 278, 279].

9.2.6   New applications

9.2.6.1   Application to microelectronics fabrication processes

To be competitive in the global market, semiconductor manufacturing increasingly relies on advanced process modeling, monitoring, and control due to shrinking feature size (less than $0.20\,\mu m$ line width) and increasing wafer diameter (up to $12\,in$).

Given these critical dimension constraints and the trend toward further miniaturization, extremely tight manufacturing tolerances are required. Achieving these specifications represents a major engineering challenge. Comprehensive modeling and control technologies are thus required to achieve satisfactory yields, maximize throughput, and reduce cost [179].

In semiconductor manufacturing processes, Metal-organic vapor phase epitaxy (MOVPE) is widely used to produce a variety of high-performance optoelectronic devices including light-emitting diodes, quantum-well lasers, heterojunction bipolar transistors and Si photovoltaic systems. Multilayered structures of group-III Nitrides form the basis of these devices. MOVPE utilizes the thermal decomposition and reaction of gaseous precursors to epitaxially grow multiple layers of group-III nitride thin films with precise thickness, composition, dopant level and surface roughness.

Photovoltaics (i.e., solar cells) play an important role in the development of sustainable energy resources. Thin-film silicon solar cells (TSSC) are the predominant choice currently. Their limitation lies in their low efficiency of 15%. In TSSC the light comes in to the hydrogenated amorphous silicon (Si) semiconductor layers (p-i-n layers) through a front transparent conducting oxide (TCO) layer and the part of the light not absorbed by these semiconductor layers is reflected back to the p-i-n layers through a back TCO layer (see figure 9.2).

The effectiveness of TSSC is directly related to the light trapping process, which

is characterized by scattering properties of thin-film interfaces especially at the front & back TCO layers, as well as at interfaces of TCO and p-i-n-layers [156, 192]. Recent studies have shown that thin-film surface and interface morphology play a significant role in increasing the absorption of incident light by the semiconductor layers of thereby enhancing TSSC's performance [157, 158, 168, 213, 274]. It is thus important during the manufacturing of TSSC to regulate the surface morphology of the thin-film. TSSC is predominantly produced [164] using MOVPE.

Recent developments on in-situ measurement technology, such as laser interferometry (LI), make real-time feedback control of MOVPE feasible. The surface morphology of the thin-film surface is characterized using root-mean-square (RMS) roughness and RMS surface slope. Thus, we can propose to regulate the surface morphology of the TSSC, by measuring RMS slope and roughness and manipulating the substrate temperature and precursor flow rates. The available Edwards-Wilkinson type models [97] that describe the evolution profiles of the surface height and surface slopes of the thin-film will be used to design the controller. A total of 7 PDEs and 10 ODEs are needed to model the process; further constraints arise from sensing and actuation limitations. The resulting process model is too computationally demanding to be used to design model based controllers for TSSC.

The proposed methodology can be employed to synthesize controllers for the production of TSSC using MOVPE. The objective will be to regulate the thin film
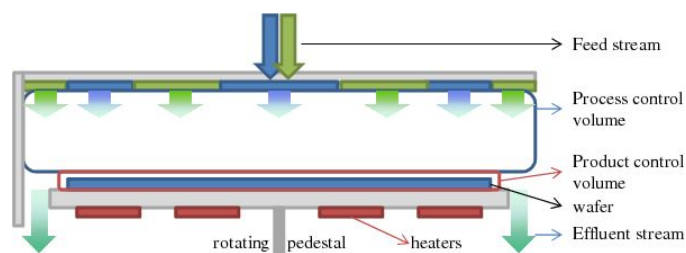
Figure 9.1: Vertical MOVPE reactor with a three concentric ring showerhead inlet configuration.
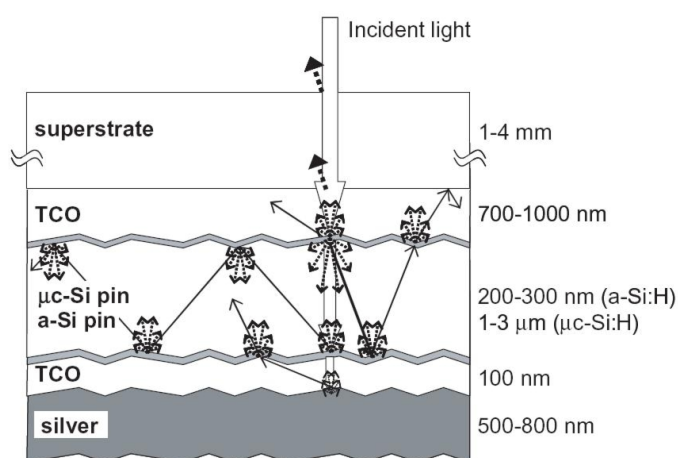
Figure 9.2: Schematic sketch of the cross section of a silicon thin film p-i-n solar cell [192].

morphology of TSSC, using LI measurements and manipulating the precursor inlet concentration and substrate temperature profiles, such that the efficiency of TSSC is maximized. However, the proposed research will not be limited to silicon based photovoltaics. Organic photovoltaics (OPVs) offer an attractive alternative to TSSC, due to their low materials and production cost. Using benzene as a building block, polyphenylene based OPVs show great promise to complement TSSC for solar energy harvesting [67, 125, 169]. Important limitations that preclude their wide use is their limited stability and efficiency. These limitations can be partially

negated by optimizing and tightly controlling the manufacturing process which is based either on spin coating or vapor deposition [67].

Upon completion of the initial objectives, the attention can be focus on organic vapor phase deposition. The process involves evaporation of the organic material over a substrate in the presence of an inert carrier gas [67, 110]. The controllers can be designed that manipulate the chamber pressure, carrier gas flow rate and heater power to force the deposited thin film morphology within strict limits. The distributed nature of the process, due to the intimate interplay between evaporation, transport and deposition phenomena necessitates the use of advanced controller design methods such as the proposed one.

9.2.6.2   Application to temperature control in batteries

Safe electric energy storage is the key objective of a wide range of battery applications from transportation systems to portable electronics. Lithium-ion batteries attracts a lots of attentions for energy storage due to their high energy density, lack of hysteresis, and low self-discharge currents [208]. These beneficial properties, as well as decreasing costs, have established Li-ion batteries as a leading candidate for the next generation of automotive and aerospace applications [11, 231, 242]. Li-ion batteries are also a promising candidate for green technology.

Electric automobiles and submarines demand large amounts of energy and power, and therefore need packs of thousands of Li-ion cells. One of the chal-
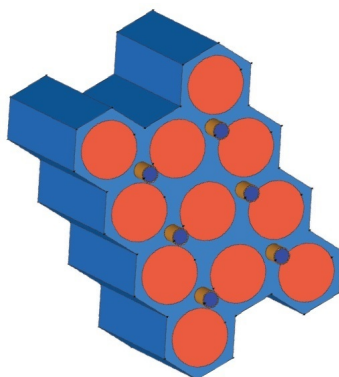
Figure 9.3: A battery pack with coolant lines [234].

lenges when dealing with battery packs (Fig. 9.3) is that after a period of usage, the state of health of individual cells will be highly non-uniform due to electrical and thermal interactions of the individual cells [234].

At high-discharge rates, Li-ion batteries generate a significant amount of heat which can detrimentally affect the overall performance of the devices. Prolonged excessive heat and uneven temperature distributions over time can damage the battery resulting in decrease in capacity, charge retention, battery lifespan, and physical deformations of the battery itself. Under more extreme conditions, the battery can undergo thermal runaway, which may result in the rupture of the battery casing, explosion, and ignition of the flammable electrolytes [43, 196, 261].

There is a large body of literature focused on the thermal analysis of Li-ion batteries which employ experimental and computation techniques to model the complex electrochemical reactions responsible for heat generation under a variety of operating conditions [52, 73, 127]. In conjunction with these studies, there are
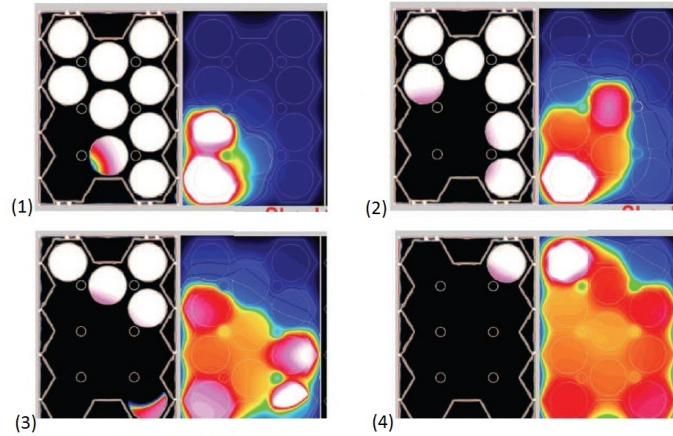
Figure 9.4: Thermal runaway in a battery pack [234]. It starts in (1) with the cell in the lower left corner drawing high current and overheating, progressing through (2), (3) and (4), where the entire pack is ignited.

complementary results discussing various approaches in the thermal management of Li-ion batteries [177, 209]. The primary means of temperature regulation are typically through exclusive and combinations of passive and active control strategies each involving air for heating/cooling, liquid for heating/cooling, and also the use of phase change materials (PCMs). The implementation of any of the aforementioned control methods are dependent on a number of factors including the battery system setup (e.g. single cell, battery pack, shape, etc.) which affects the feasibility of heating/cooling system design. In all cases, model based control design has the potential of enhancing these existing methodologies by improving controller performance.

Charging all the cells to their full capacity becomes unachievable because it would lead to some of the cells exceeding the maximum voltage, above which they become thermally unstable.

Even when a battery pack is not in use, namely, neither being charged nor discharged, a reasonable probability exists that, in an aging, or inexpensively produced battery pack, one of the many cells in a pack undergoes short circuit. This results in the cell overheating and igniting. The high temperature produced by such a cell leads to electrical and thermal transients in the neighboring cells which results in a chain reaction where an entire pack explodes. This phenomenon is called thermal runaway that is presented in Figure 9.4. While thermal runaways in battery cells in portable computers have been widely publicized, the danger from them is limited. Thermal runaway in large battery packs can result in damage on a large scale [234]. Safety is typically ensured by over-design, which amounts to packaging and passive cooling techniques designed for worst-case scenarios. Better understanding of the thermal dynamics in battery packs, state estimation to spatially locate the hot spots in the pack using temperature sensors at only a limited number of locations in the pack, and more intelligent control systems that employ parameter estimators of the uncertain thermal conductivity within and in-between cells, are crucial for developing cheaper batteries that will enable commercialization of the environmentally-friendly electric and plug-in hybrid vehicles.

Useful models emphasize the inhomogeneity of the battery pack medium, where, the cells and the materials they are enclosed in have very different thermal conductivity properties, where the thermal dynamics are coupled with the electrical dynamics which act as heat sources, and where cooling systems passive or con-

trolled may be introduced to manage the temperature distribution in a battery pack. These models are in the form of partial differential equations and capture the spatially distributed character of the thermal dynamics in a pack [234].The important issue when considering the thermal control problem for this systems is where to place the actuators (sensors) such that the system exhibits desired system theoretic properties such as enhanced controllability.

APPENDIX

A.1   Proofs of Chapter 3

A.1.1   Proof of Proposition 3.1

Let $V_o(e) = \dfrac{\zeta_o}{2} e^T P_o e$ be the observer Lyapunov function (OLF) for observer error dynamics of (3.26) with the equilibrium point of $e = 0$, where the dynamic observer of system described by (3.24). $V_o(0) = 0$ and $V_o(e) > 0$ in $\mathbb{R}^m - \{0\}$ where m denotes the number of the modes between ROM revisions. Considering the observer gain matrix, L, computed by either

(i) Eq. (3.31), where the characteristic polynomial roots are negative and $P_o = I$,

(ii) Eq. (3.35), where the Riccati equation of (3.36) has a solution, S, for positive

definite matrices, Q, R, N,

(iii) Eq. (3.46), where W and U are symmetric positive definite matrices,

and assuming that f satisfies the Lipschitz condition (3.17), we conclude that

$\dot{V}_o(e) < 0$ and $\dot{V}_o(0) = 0$. Based on Lyapunov's stability theorem (Theorem 4.1 in

[148]), $\exists \delta_o > 0 : \|e(0)\| < \delta_o$, then the observer error dynamics of (3.26) are locally

asymptotically stable.

A.1.2   Proof of Theorem 3.1

The slow system observer error with respect to modes in subspace $\mathbb{W}_s$ can be

defined as follows

$$\hat{e} = \hat{x}_s - x_s, \tag{A.1}$$

where $\hat{e} = \mathcal{M}^\perp e$ and $\hat{x}_s = \mathcal{M}^\perp \hat{a}$. From (3.26) and (A.1) we obtain

$$\dot{\hat{e}} = (A_s + \mathcal{M}^\perp L S_m)\hat{e} + \Big(F_s(\hat{x}_s, x_f) - F_s(\hat{x}_s - \hat{e}, x_f) \Big). \tag{A.2}$$

Under Assumption 3.1 (time scale separation part), the system of (3.12) can be

presented in the following singular perturbation form (sections 4.4 and 4.5 in [76])

augmented with the observation error dynamics of (A.2),

$$\dot{x}_s = A_s x_s + F_s(x_s, x_f) + B_s u,$$

$$\sigma \dot{x}_f = \sigma A_f x_f + \sigma \Big(F_f(x_s, x_f) - B_f u \Big), \tag{A.3}$$

$$\dot{\hat{e}} = (A_s + \mathcal{M}^\perp L S_m)\hat{e} + \Big(F_s(\hat{x}_s, x_f) - F_s(\hat{x}_s - \hat{e}, x_f) \Big),$$

where $\sigma = \dfrac{|\lambda_1|}{|\lambda_{p+1}|}$ is a small value that indicates the separation between the dominant and non-dominant dynamic behavior. From the definition of A_f and σ, $A_{f\sigma} = \sigma A_f$ has eigenvalues with negative real parts of $O(1)$. We assume that $F_f(x_s, x_f) + B_f u$ does not locally include terms of $O(\dfrac{1}{\sigma})$ [76], where $O(\cdot)$ indicates the order of $(\cdot)$. By defining $\tau = \dfrac{t}{\sigma}$ and setting $\sigma = 0$, we can express the fast dynamics of (A.3) in the fast time scale form

$$\frac{\partial x_f}{\partial \tau} = A_{f\sigma} x_f. \tag{A.4}$$

Thus, the solution can be obtained as

$$x_f(\tau) = x_f(0) e^{A_{f\sigma}\tau}. \tag{A.5}$$

Then from (A.5) and Schwartz inequality we conclude

$$\|x_f(\tau)\|_2 = \|x_f(0)e^{A_{f\sigma}\tau}\|_2 \leq \|x_f(0)\|_2 \|e^{A_{f\sigma}\tau}\|_2. \tag{A.6}$$

Considering the eigenspectrum bound to the fast dynamics implies that

$$\|x_f(0)\|_2 \|e^{A_{f\sigma}\tau}\|_2 \leq \|x_f(0)\|_2 e^{(\sigma\lambda_{p+1})\tau}, \tag{A.7}$$

where λ_{p+1} denotes the dominant, least negative eigenvalue of A_f which is of $O(\frac{1}{\sigma})$.

From (A.6), (A.7) and $\sigma = \frac{|\lambda_1|}{|\lambda_{p+1}|}$ we can obtain

$$\|x_f(0)\|_2 e^{(\sigma\lambda_{p+1})\tau} = \|x_f(0)\|_2 e^{-|\lambda_1|\tau} \leq O(\sigma); \tag{A.8}$$

this bound is satisfied when

$$\tau_b = \frac{t_b}{\sigma} \geq -\frac{1}{|\lambda_1|} \ln\left[O(\frac{\sigma}{\|x_f(0)\|_2})\right]. \tag{A.9}$$

Thus,

$$t_b \geq \frac{1}{|\lambda_{p+1}|} \ln\left[O(\frac{\|x_f(0)\|_2}{|\lambda_1|}|\lambda_{p+1}|)\right]. \tag{A.10}$$

We choose δt such that $\delta t > t_b$ where t_b denotes the time needed for the fast dynamics of (A.3) to be stabilized and $\delta t = t_k - t_{k-1}$ is the time interval between ROM revisions. Then the observation error can be expressed as follows

$$E_o = \hat{x}_s - x = \hat{x}_s - (x_s + x_f) = \hat{x}_s - (x_s + 0) = \hat{x}_s - x_s = \hat{e}, \tag{A.11}$$

when the infinite-dimensional system of (A.3) is approximated by the finite-dimensional slow system for $t \geq t_b$,

$$\dot{x}_s = A_s x_s + F_s(x_s, 0) + B_s u,$$
$$\dot{\hat{e}} = (A_s + \mathcal{M}^\perp L S_m)\hat{e} + \left(F_s(\hat{x}_s, 0) - F_s(\hat{x}_s - \hat{e}, 0)\right). \tag{A.12}$$

Based on Proposition 3.1 we obtain that the OLF, V_o, is negative definite, thus observer error dynamics in (3.26) is locally asymptotically stable based on Lyapunov's stability theorem, i.e., for $\|e(0)\| < \delta_o$ there is a $\delta_o' = \|\mathcal{M}^\perp\|_2 \delta_o$ the dynamics of observer error of $E_o = \hat{e}$ is locally asymptotically stable in the Lyapunov sense such that $\|E_o\|_2 = \|\hat{e}\|_2 < \delta_o'$.

A.1.3 Proof of Theorem 3.2

Consider the nonlinear uncertain system of (3.49) whose control Lyapunov function (CLF) is defined as follows

$$V_c = \frac{\zeta_c}{2} \hat{a}^T P_c \hat{a}, \tag{A.13}$$

where P_c is a positive definite matrix. It is obvious that $V_c(0) = 0$ and $V_c(\hat{a}) > 0$ in $\mathbb{R}^m - \{0\}$.

By substituting Eqs. (3.49) and (3.50) in the CLF time derivative, we obtain

$$\dot{V}_c = L_F V_c + L_B V_c u + \sum_{i=1}^{s} L_{w_i} V_c \theta_i = -c_o \Big(\|L_B V_c\| \Big)^2 - \rho \|P_c \hat{a}\| - \chi \sum_{i=1}^{s} \|L_{w_i} V_c\| \theta_{bi}$$
$$- \sqrt{ \Big(L_F V_c + \rho \|P_c \hat{a}\| + \chi \sum_{i=1}^{s} \|L_{w_i} V_c\| \theta_{bi} \Big)^2 + \Big(\|(L_B V_c)\| \Big)^4 } + \sum_{i=1}^{s} L_{w_i} V_c \theta_i. \tag{A.14}$$

Using $\sum_{i=1}^{s} L_{w_i} V_c \theta_i \le \sum_{i=1}^{s} \|L_{w_i} V_c\| \theta_{bi}$ and by adjusting the parameters as $\rho > 0$ and $\chi > 1$, the time derivative of the CLF is negative, $\dot{V}_c < 0$. Thus $\exists \delta_c > 0 :$ $\|\hat{a}(0)\| < \delta_c$, that the closed-loop system in (3.49) is locally asymptotically stable

in the Lyapunov sense (Theorem 4.1 in [148]).

In Chapter 3.2.2, we assumed that if a controller can be synthesized such that $\dot{V}_c < 0$, based on the stability of the dynamic observer the closed-loop process will be asymptotically stable, i.e., e and $\hat{a}$ will be bounded. From the definition $e = \hat{a} - \mathcal{M}a$ and the fact that we did not use the separation principle we conclude that a will be bounded. Substituting the controller (3.50) into the Sobolev representation of the infinite-dimensional system (3.12) and dynamic observer of (3.24), we obtain

$$
\begin{aligned}
\dot{x}_s &= A_s x_s + F_s(x_s, x_f) - B_s k(\hat{a}, c_o, \rho, \chi, \theta_b)(L_B V_c), \\
\dot{x}_f &= A_f x_f + F_f(x_s, x_f) - B_f k(\hat{a}, c_o, \rho, \chi, \theta_b)(L_B V_c), \\
\dot{\hat{a}} &= A\hat{a} + f(\hat{a}) - Bk(\hat{a}, c_o, \rho, \chi, \theta_b)(L_B V_c) + L(C\hat{a} - S_m x_s - S_m x_f).
\end{aligned}
\tag{A.15}
$$

Based on Assumption 3.1, (A.15) can be stated in the following singular perturbation form (sections 4.4 and 4.5 in [76])

$$
\begin{aligned}
\dot{x}_s &= A_s x_s + F_s(x_s, x_f) - B_s k(\hat{a}, c_o, \rho, \chi, \theta_b)(L_B V_c), \\
\sigma \dot{x}_f &= \sigma A_f x_f + \sigma\Big(F_f(x_s, x_f) - B_f k(\hat{a}, c_o, \rho, \chi, \theta_b)(L_B V_c)\Big), \\
\dot{\hat{a}} &= A\hat{a} + f(\hat{a}) - Bk(\hat{a}, c_o, \rho, \chi, \theta_b)(L_B V_c) + L(C\hat{a} - S_m x_s - S_m x_f),
\end{aligned}
\tag{A.16}
$$

where $\sigma = \dfrac{|Re(\lambda_1)|}{|Re(\lambda_{p+1})|}$ is a small value that presents the separation between the dominant and non-dominant eigenmodes. λ_1 and λ_{p+1} are the dominant eigenvalues of slow and stable fast subsets of eigenvalues of $\mathbf{A}$, respectively. Based on the control law (3.50) and assuming bounded control action and Lipschitz condition for

F, (3.8), then $F_f(x_s, x_f) - B_f k(\hat{a}, c_o, \rho, \chi, \theta_b)(L_B V_c)$ does not have a term of $O(\frac{1}{\sigma})$ [76]. By defining $\tau = \frac{t}{\sigma}$, it directly results from the definitions that $A_{f\sigma} = \sigma A_f$ is of order $O(1)$. Then by setting $\sigma = 0$, the fast subsystem of (A.16) can be presented in the following locally exponentially stable subsystem

$$\frac{\partial x_f}{\partial \tau} = A_{f\sigma} x_f, \tag{A.17}$$

Based on singular perturbation theory [76] after a period of time, t_b, where

$$t_b \geq \frac{1}{|\lambda_{p+1}|} \ln \left[O(\frac{\|x_f(0)\|_2}{|\lambda_1|} |\lambda_{p+1}|) \right], \tag{A.18}$$

the fast dynamics of the system stabilize to zero, $x_f \simeq 0$ and the closed-loop PDE system of (A.16) is approximated by the finite-dimensional slow system below

$$\dot{x}_s = A_s x_s + F_s(x_s, 0) - B_s k(\hat{a}, c_o, \rho, \chi, \theta_b)(L_B V_c).$$
$$\dot{\hat{a}} = A\hat{a} + f(\hat{a}) - Bk(\hat{a}, c_o, \rho, \chi, \theta_b)(L_B V_c) + L(C\hat{a} - S_m x_s). \tag{A.19}$$

The system of (A.19) is stabilized by the controller/observer design.

A.1.4 Proof of Theorem 3.3

Based on Proposition 3.1 and Theorems 3.1, 3.2 we obtained

$$\dot{V}_o < 0, \quad \dot{V}_c < 0, \tag{A.20}$$

between ROM revisions and the observer/controller structure redesigns. As a result the closed-loop system will destabilize only when A, B, C and f in (3.23) and (3.16) deviate due to appearance of new trends. In such case the structure of the ROM is revised using adaptive proper orthogonal decomposition (APOD) methodology. According to such system structure changes the extra Lyapunov stability condition of switching systems must be satisfied to guarantee the stability of the closed-loop system (Theorem 3.2 in [86]).

The supervisory strategies of (3.51) and (3.48) directly enforce the Lyapunov stability criterion for of the switching systems, (3.47), in the controller and observer designs thus the OLF and CLF satisfy the conditions of (3.47). It means that during the ROM revisions the ζ_c and ζ_o values are periodically chosen subject to $V_c(\hat{a}(t_k))$ and $V_o(e(t_k))$. Then $\dot{V} < 0$ between ROM revisions as follows

$$\dot{V} = \dot{V}_o + \dot{V}_c < 0. \tag{A.21}$$

Thus $\exists \delta > 0 : \|a(0)\| < \delta$, that the closed-loop system is locally asymptotically stable in the Lyapunov sense (Theorem 4.1 in [148]). Also the closed-loop Lyapunov function satisfies the criteria (3.47),

$$V(t_k) = V_c(\hat{a}(t_k)) + V_o(\hat{a}(t_k)) < V_c(\hat{a}(t_{k-1})) + V_o(\hat{a}(t_{k-1})) \Rightarrow V(t_k) < V(t_{k-1}). \tag{A.22}$$

where the time interval between the ROM revisions, $\delta t = t_k - t_{k-1}$, is chosen to

satisfy $\delta t > t_b$. Thus, it can be concluded that the APOD-based dynamic observer designs of (3.31), (3.35) and (3.46) and the APOD-based output feedback controller of (3.50) asymptotically stabilizes the switching closed-loop system.

A.2 Proofs and supplementary materials of Chapter 4

A.2.1 Proof of Proposition 4.1

Let $V_o = \dfrac{\zeta_o}{2} e^T e$ be the OLF for the dynamic observer system of (4.11); it can be shown that $e = 0$ is an equilibrium point for (4.13), $V_o(0) = 0$ and $V_o(e) > 0 \in \mathbb{R}^m - \{0\}$ where m is the number of the modes between ROM revisions. By substituting the observer gain which satisfies (4.18) in the system of (4.11) and assuming that the nonlinear function of f satisfies the Lipschitz condition, (4.16), it can be concluded that the OLF time derivative, $\dot{V}_o$, is negative definite and it only equals to zero at the equilibrium point. Thus based on Lyapunov's stability theorem (Theorem 4.1 in [148]), there is δ_o such that when $\|e(0)\| < \delta_o$ the observer error dynamics in (4.13) are locally asymptotically stable in the Lyapunov sense.

A.2.2 Proof of Proposition 4.2

Consider the system of (4.10) with candidate CLF defined as

$$V_c = \frac{\zeta_c}{2}\tilde{a}^T\tilde{a}. \tag{A.23}$$

It is obvious that $V_c(0) = 0$ and $V_c(\tilde{a}) > 0 \in \mathbb{R}^s - \{0\}$ where s is the number of the modes of (4.10) between ROM revisions. By substituting equations (4.10) and (4.20) in the time derivative of the CLF, we obtain

$$\dot{V}_c = L_F V_c + L_B V_c u = -c_o\Big(\|L_B V_c\|\Big)^2 - \sqrt{\Big(L_F V_c\Big)^2 + \Big(\|(L_B V_c)\|\Big)^4}. \tag{A.24}$$

Using appropriate values for the parameter c_o, it can be clearly observed that the time derivative of the CLF will be negative, $\dot{V}_c < 0$. Thus, based on Lyapunov's stability theorem (Theorem 4.1 in [148]), there is a δ_c such that for $\|\tilde{a}(0)\| < \delta_c$ the closed-loop system in (4.10) is locally asymptotically stable in the Lyapunov sense. Based on the designed fast stable observers and using the separation principle, the closed-loop process of (4.10) with the controller/observer pair will be asymptotically stable. Note that we use the observer state values, $\hat{a}$, for system states, $\tilde{a}$, in equation (4.20) based on the assumption of separation principle between dynamic observer and controller design.

A.2.3   Proof of Theorem 4.1

Part I. Closed-loop stability between ROM revisions:

Substituting the controller (4.20) based on the states of (4.4) into the Sobolev

representation of the PDE system, we obtain

$$
\begin{aligned}
\dot{a}_s &= A_s(a_s, a_f) + F_s(a_s, a_f) - B_s k(\hat{a}, c_o)(L_B V_c), \\
\dot{a}_f &= A_f(a_s, a_f) + F_f(a_s, a_f) - B_f k(\hat{a}, c_o)(L_B V_c),
\end{aligned}
\tag{A.25}
$$

where the initial conditions of the switching system in current time interval are

the final states of the system in the previous time interval, and state estimate $\hat{a}$ is

obtained from the dynamic observer of (4.11)

$$
\dot{\hat{a}} = A\hat{a} + f(\hat{a}) + Bu + L(C\hat{a} - y_m),
\tag{A.26}
$$

where

$$
y_m = S_m a_s + S_m a_f.
\tag{A.27}
$$

Under the assumption of time scale separation of the PDE dynamics, the system

of (A.25) can be expressed in the following singular perturbation form (sections

4.4 and 4.5 in [76]) with dynamic observer of (A.26)

$$\dot{a}_s = A_s(a_s, a_f) + F_s(a_s, a_f) - B_s k(\hat{a}, c_o)(L_B V_c),$$

$$\epsilon_s \dot{a}_f = \epsilon_s A_f(a_s, a_f) + \epsilon_s \Big(F_f(a_s, a_f) - B_f k(\hat{a}, c_o)(L_B V_c) \Big), \qquad \text{(A.28)}$$

$$\dot{\hat{a}} = A\hat{a} + f(\hat{a}) - Bk(\hat{a}, c_o)(L_B V_c) + L(C\hat{a} - S_m a_s - S_m a_f),$$

where $\epsilon_s = \dfrac{|\lambda_1|}{|\lambda_{s+1}|}$ is a small number that indicates the separation between the dominant and non-dominant eigenmodes. In (A.28), $A_{f\epsilon_s} = \epsilon_s A_f$ has negative eigenvalues of $O(1)$ (due to the definition of A_f and ϵ_s) and $F_f(a_s, a_f) - B_f k(\hat{a}, c_o)(L_B V_c)$ does not contain terms of $O(\dfrac{1}{\epsilon_s})$ locally for the specific controller design [76, 78]. By defining $\tau = \dfrac{t}{\epsilon_s}$ and setting $\epsilon_s = 0$, the fast subsystem dynamics of (A.28) can be expressed in the following fast time scale form

$$\frac{\partial a_f}{\partial \tau} = A_{f\epsilon_s} a_f. \qquad \text{(A.29)}$$

The solution of the locally exponentially stable system of (A.29) then is

$$a_f(\tau) = a_f(0) e^{A_{f\epsilon_s} \tau}. \qquad \text{(A.30)}$$

Focusing on the norm of a_f, from (A.30) and Schwartz inequality we obtain

$$\|a_f(\tau)\|_2 = \|a_f(0) e^{A_{f\epsilon_s} \tau}\|_2 \leq \|a_f(0)\|_2 \|e^{A_{f\epsilon_s} \tau}\|_2. \qquad \text{(A.31)}$$

The definition of $A_{f\epsilon_s}$ and the eigenspectrum bound to the fast subsystem imply that

$$\|a_f(0)\|_2\|e^{A_{f\epsilon_s}\tau}\|_2 \leq \|a_f(0)\|_2 e^{(\epsilon_s\lambda_{s+1})\tau}, \tag{A.32}$$

where λ_{s+1} represents the dominant eigenvalue of A_f which is the least negative and of $O(\dfrac{1}{\epsilon_s})$. Using singular perturbation arguments for infinite dimensional systems it is shown that within a finite time the fast system dynamics will relax to a ball of radius $O(\epsilon_s)$ around zero. Using the spectral bound of (A.31) and (A.32) for the dynamic behavior and that $\epsilon_s = \dfrac{|\lambda_1|}{|\lambda_{s+1}|}$ we can obtain

$$\|a_f(0)\|_2 e^{(\epsilon_s\lambda_{s+1})\tau} = \|a_f(0)\|_2 e^{-|\lambda_1|\tau} \leq O(\epsilon_s); \tag{A.33}$$

it implies that

$$\tau_b = \frac{t_b}{\epsilon_s} \geq -\frac{1}{|\lambda_1|} \ln\left[O(\frac{\epsilon_s}{\|a_f(0)\|_2})\right]. \tag{A.34}$$

Thus,

$$t_b \geq \frac{1}{|\lambda_{s+1}|} \ln\left[O(\frac{\|a_f(0)\|_2}{|\lambda_1|}|\lambda_{s+1}|)\right]. \tag{A.35}$$

Considering the time needed for relaxation of (A.28), t_b, and the time interval between ROM revisions, $\delta t = t_k - t_{k-1}$, we choose δt such that $\delta t > t_b$. For time, $t \geq t_b$ the closed-loop PDE system in (A.28) approximately reduces to the

finite-dimensional slow system (Proposition 1 in [78]),

$$\dot{a}_s = A_s(a_s, 0) + F_s(a_s, 0) - B_s k(\hat{a}, c_o)(L_B V_c),$$
$$\dot{\hat{a}} = A\hat{a} + f(\hat{a}) - Bk(\hat{a}, c_o)(L_B V_c) + L(C\hat{a} - S_m a_s). \tag{A.36}$$

Based on Propositions 4.1 and 4.2 we obtain that the OLF, V_o, and the CLF, V_c, are negative individually. Thus, the combined observer/controller structure can stabilize the states of (A.36) based on the assumption of separation principle between dynamic observer and controller design and considering (4.8) and (4.9). The time derivative of the Lyapunov function of the system, $\dot{V}$, is thus negative between ROM revisions

$$\dot{V} = \dot{V}_o + \dot{V}_c < 0. \tag{A.37}$$

Therefore, based on Lyapunov's stability theorem (Theorem 4.1 in [148]), there is δ such that when $\|a(0)\| < \delta$, the closed-loop system of (A.36) is locally asymptotically stable in the Lyapunov sense between ROM revisions. Thus, the nonlinear dissipative PDE system in (4.1) can be asymptotically stabilized by the dynamic observer design of (4.11) and the output feedback controller in (4.20) between ROM revisions.

Part II. Closed-loop stability of the hybrid system:

Considering ROM revisions, the closed-loop system behavior can be described by switched systems theory and the stability aspects of the closed-loop switched system need to be guaranteed using hybrid systems stability theorems. Based on the

discussion in Chapter 4.3 the obtained multiple observer and controller Lyapunov functions defined after each ROM revision need to satisfy the hybrid systems stability criteria. The supervisory control strategies in (4.22) and (4.24) directly enforce the Lyapunov stability of the switching systems criteria at the beginning of each time period, in the controller and observer designs (Theorem 3.2 in [86]) and the CLF and OLF satisfy the conditions of (4.21) in the time intervals between switching. Thus, the closed-loop Lyapunov function satisfies the Lyapunov stability of the switching systems [79, 86],

$$V(t_k) = V_c\big(\hat{a}(t_k)\big) + V_o\big(\hat{a}(t_k)\big) < V_c\big(\hat{a}(t_{k-1})\big) + V_o\big(\hat{a}(t_{k-1})\big) \Rightarrow V(t_k) < V(t_{k-1}).$$

It can be concluded that the designed observer of (4.19) and the output feedback controller in (4.20) pair using supervisory control strategies (4.22) and (4.24) asymptotically stabilize the switching closed-loop system.

A.2.4 Lipschitz condition for nonlinear term in KSE

The nonlinear term in KSE has a quadratic form of $\mathcal{F}(x) = -x\dfrac{\partial x}{\partial z}$. The important step in nonlinear analysis is finding a procedure to compute the Lipschitz parameter. We assumed that $\big\|x(z,t)\big\|_2 \leq L_1(t)$, i.e. the system state remained within a ball of radius $L_1(t)$ around the desired steady state and the spatial dynamics are bounded, i.e., $\big\|\dfrac{\partial x}{\partial z}(z,t)\big\|_2 \leq L_2(t)$ and $\big\|\dfrac{\partial x_2}{\partial z}(z,t) - \dfrac{\partial x_1}{\partial z}(z,t)\big\|_2 \leq M(t)\big\|x_2(z,t) - x_1(z,t)\big\|_2$. From the left-hand side of Lipschitz condition we ob-

tain

$$\left\| x_1 \frac{\partial x_1}{\partial z} - x_2 \frac{\partial x_2}{\partial z} \right\|_2 = \left\| x_1 \frac{\partial x_1}{\partial z} - x_2 \frac{\partial x_1}{\partial z} + x_2 \frac{\partial x_1}{\partial z} - x_2 \frac{\partial x_2}{\partial z} \right\|_2$$

$$\leq \left\| x_2 \frac{\partial x_1}{\partial z} - x_2 \frac{\partial x_2}{\partial z} \right\|_2 + \left\| x_1 \frac{\partial x_1}{\partial z} - x_2 \frac{\partial x_1}{\partial z} \right\|_2$$

$$= \| x_2 \|_2 \left\| \frac{\partial x_1}{\partial z} - \frac{\partial x_2}{\partial z} \right\|_2 + \left\| \frac{\partial x_1}{\partial z} \right\|_2 \| x_1 - x_2 \|_2$$

thus

$$\left\| x_1 \frac{\partial x_1}{\partial z} - x_2 \frac{\partial x_2}{\partial z} \right\|_2 \leq \big(L_1(t) M(t) + L_2(t) \big) \| x_1 - x_2 \|_2$$

and the Lipschitz constant in the previous equation is $K_l(t) = L_1(t) M(t) + L_2(t)$.

A.3 Proofs of Chapter 5

A.3.1 Proof of Theorem 5.1

Considering the Sobolev representation of the PDE system (5.11) and dynamic observer of (5.22), we obtain

$$\dot{x}_s = A_s x_s + F_s(x_s, x_f) + B_s u,$$

$$\dot{x}_f = A_f x_f + F_f(x_s, x_f) + B_f u, \tag{A.38}$$

$$\dot{\hat{a}} = A\hat{a} + f(\hat{a}) + Bu + \Pi_{\hat{a}}^{-1} L(y_m - C\hat{a}),$$

and based on Assumption 5.1, (A.38) can be stated in the following singular perturbation form (sections 4.4 and 4.5 in [76])

$$
\begin{aligned}
\dot{x}_s &= A_s x_s + F_s(x_s, x_f) + B_s u, \\
\sigma \dot{x}_f &= \sigma A_f x_f + \sigma \Big(F_f(x_s, x_f) + B_f u \Big), \\
\dot{\hat{a}} &= A\hat{a} + f(\hat{a}) + Bu + \Pi_{\hat{a}}^{-1} L(y_m - C\hat{a}),
\end{aligned}
\tag{A.39}
$$

where $\sigma_s = |\lambda_1|/|\lambda_{p+1}|$ is a small number that indicates the separation between the dominant and non-dominant modes. Due to the definition of A_f and σ, $A_{f\sigma} = \sigma A_f$ has negative eigenvalues of $O(1)$, where $O(\cdot)$ indicates the order of $(\cdot)$ [76]. At this point we assume that $F_f(x_s, x_f)$ and $B_f u$ (by the globally linearizing controller (GLC) design) do not contain terms of $O(\frac{1}{\sigma})$ locally. By defining $\tau = t/\sigma$ and setting $\sigma = 0$, the fast subsystem dynamics of (A.38) can be expressed in the following fast time scale form

$$
\frac{\partial x_f}{\partial \tau} = A_{f\sigma} a_f.
\tag{A.40}
$$

Then the solution of the locally exponentially stable system of (A.40) is obtained as

$$
x_f(\tau) = x_f(0) e^{A_{f\sigma} \tau}.
\tag{A.41}
$$

Focusing on the norm of x_f, from (A.41) and Schwartz inequality we obtain

$$\|x_f(\tau)\|_2 = \|x_f(0)e^{A_{f\sigma}\tau}\|_2 \leq \|x_f(0)\|_2\|e^{A_{f\sigma}\tau}\|_2. \tag{A.42}$$

The definition of $A_{f\sigma}$ and the eigenspectrum bound to the fast subsystem imply that

$$\|x_f(0)\|_2\|e^{A_{f\sigma}\tau}\|_2 \leq \|x_f(0)\|_2 e^{(\sigma\lambda_{p+1})\tau}, \tag{A.43}$$

where λ_{p+1} represents the dominant eigenvalue of A_f which is the least negative and of $O(\frac{1}{\sigma})$. Using singular perturbation arguments for infinite-dimensional systems it is shown that within a finite time the fast system dynamics will relax to a ball of radius $O(\sigma)$ around zero. Using the spectral bound of (A.42) and (A.43) for the dynamic behavior and that $\sigma = |\lambda_1|/|\lambda_{p+1}|$ we can obtain

$$\|x_f(0)\|_2 e^{(\sigma\lambda_{p+1})\tau} = \|x_f(0)\|_2 e^{-|\lambda_1|\tau} \leq O(\sigma); \tag{A.44}$$

this bound is satisfied when

$$\tau_b = \frac{t_b}{\sigma} \geq -\frac{1}{|\lambda_1|} \ln\left[O(\frac{\sigma}{\|x_f(0)\|_2})\right]. \tag{A.45}$$

Thus,

$$t_b \geq \frac{1}{|\lambda_{p+1}|} \ln\left[O(\frac{\|x_f(0)\|_2}{|\lambda_1|}|\lambda_{p+1}|)\right]. \tag{A.46}$$

Considering the time needed for relaxation of (A.38), t_b, and the time interval between ROM revisions, $\delta t = t_k - t_{k-1}$, we choose δt such that $\delta t > t_b$. In this case the complete system (slow and fast) observation error can be simplified as

$$E_o = \hat{x}_s - x = \hat{x}_s - (x_s + x_f) = \hat{x}_s - (x_s + 0) = \hat{x}_s - x_s = \hat{e}, \qquad \text{(A.47)}$$

and for $t \geq t_b$ the infinite-dimensional system in (A.38) approximately reduces to the following augmented finite-dimensional slow system,

$$
\begin{aligned}
\dot{x}_s &= A_s x_s + F_s(x_s, 0) + B_s u, \\
\dot{\hat{a}} &= A\hat{a} + f(\hat{a}) + Bu + \Pi_{\hat{a}}^{-1} L(y_m - C\hat{a}), \\
\dot{\hat{e}} &= (A_s + \mathcal{M}^{\perp}\Pi_{\hat{a}}^{-1} L S_m)\hat{e} + \left(F_s(\hat{x}_s, 0) - F_s(\hat{x}_s - \hat{e}, 0)\right).
\end{aligned}
\qquad \text{(A.48)}
$$

Then by considering Assumption 5.3 and based on the stability arguments of geometric dynamic observer and GLC in [6, 7] and [155], respectively, we conclude that the geometric observer and controller can stabilize the observation error and states of the reduced order dynamics of (A.48).

At this point, we know that the previous statement is true if and only if the Assumption 5.3 holds. However, Assumption 5.3 is correct for finite periods longer than the critical period of t_b. It may fail when new trends show during the process evolution that makes the set of basis functions and ROM inaccurate. When it happens, the APOD algorithm revises the basis functions and corrects the ROM. Following that, the controller structure redesigns the observer/controller compo-

nents to retain relevancy. This procedure is repeated during system progression to enforce closed-loop stability.

A.4 Proofs of Chapter 6

A.4.1 Proof of Proposition 6.1

The solution of the system for $t \in [t_i, t_{i+1}]$ is

$$x(t) = e^{\mathcal{G}(t-t_i)} x(t_i).$$

When resetting the error to zero at t_i, we can restate $x(t_i)$ as

$$x(t_i) = \begin{bmatrix} I & 0 \\ 0 & 0 \end{bmatrix} x(t_i^-),$$

then we obtain that

$$x(t_i) = \begin{bmatrix} I & 0 \\ 0 & 0 \end{bmatrix} e^{\mathcal{G}\delta_t} x(t_{i-1}).$$

Finally using initial condition, $x_0 = x(t_0)$, the response of the system can be presented as

$$x(t) = e^{\mathcal{G}(t-t_i)} \left(\begin{bmatrix} I & 0 \\ 0 & 0 \end{bmatrix} e^{\mathcal{G}\delta_t} \right)^i x_0 = e^{\mathcal{G}(t-t_i)} \left(\begin{bmatrix} I & 0 \\ 0 & 0 \end{bmatrix} e^{\mathcal{G}\delta_t} \begin{bmatrix} I & 0 \\ 0 & 0 \end{bmatrix} \right)^i x_0.$$

A.4.2 Proof of Theorem 6.1

Taking the 2-norm of (6.21) and using Cauchy-Schwarz inequality we obtain

$$
\|x(t)\|_2 = \|e^{\mathcal{G}(t-t_i)} \mathcal{S}^i x_0\|_2 \leq \|e^{\mathcal{G}(t-t_i)}\|_2 \ \|\mathcal{S}^i\|_2 \ \|x_0\|_2
$$
$$
\leq \|e^{\sigma_{\mathcal{G}}^{max}(t-t_i)}\|_2 \ \|\mathcal{S}^i\|_2 \ \|x_0\|_2 \leq \|e^{\sigma_{\mathcal{G}}^{max}\delta_t}\|_2 \ \|\mathcal{S}\|_2^i \ \|x_0\|_2. \tag{A.49}
$$

where $\sigma_{\mathcal{G}}^{max}$ is the largest singular value of $\mathcal{G}$. Then it is obvious that the bound-edness of the solution only depends on $\|\mathcal{S}\|_2$ and this term will be bounded if and only if the eigenvalues of $\mathcal{S}$ are inside the unit circle (sufficient condition). To prove the necessity part assume that the system is stable and $\mathcal{S}$ has at least one eigenvalue outside the unit circle. We consider the exponential term that has the general form of

$$
e^{\mathcal{G}T} = \begin{bmatrix} V_1(T) & V_2(T) \\ V_3(T) & V_4(T) \end{bmatrix}.
$$

Then the solution value just before the update will be

$$
x(t_{i+1}^-) = \begin{bmatrix} V_1(\delta_t)\Big(V_1(\delta_t)\Big)^i & 0 \\ V_3(\delta_t)\Big(V_1(\delta_t)\Big)^i & 0 \end{bmatrix} x_0 = \begin{bmatrix} \Big(V_1(\delta_t)\Big)^{i+1} & 0 \\ V_3(\delta_t)\Big(V_1(\delta_t)\Big)^i & 0 \end{bmatrix} x_0.
$$

Since $\mathcal{S}$ has at least one eigenvalue outside the unit circle (in V_1), the solution will grow with i and the system will be unstable.

A.4.3 Proof of Theorem 6.2

Under Assumption 6.1 (time scale separation part), the system of (6.8) can be expressed in the following singular perturbation form

$$
\begin{aligned}
\dot{x}_s &= A_s x_s + B_s \tilde{K} x_m, \\
\gamma \dot{x}_f &= \gamma A_f x_f + \gamma B_f \tilde{K} x_m,
\end{aligned}
\tag{A.50}
$$

where $\gamma = |\lambda_1|/|\lambda_{\alpha+1}|$ is a small number that indicates the separation between the dominant and non-dominant modes [76]. Due to the definition of A_f and γ, $A_{f\gamma} = \gamma A_f$ has negative eigenvalues of $O(1)$ and based on controller design, the manipulating term in the fast subsystem, $B_f \tilde{K} x_m$, does not contain terms of $O(\frac{1}{\gamma})$ locally, where $O(\cdot)$ indicates the order of $(\cdot)$. By defining $\tau = t/\gamma$ and setting $\gamma = 0$, the fast subsystem dynamics of (A.50) can be expressed in the following fast time scale form

$$
\frac{\partial x_f}{\partial \tau} = A_{f\gamma} x_f.
\tag{A.51}
$$

Then the solution of the locally exponentially stable system of (A.51) is obtained as

$$
x_f(\tau) = x_f(0) e^{A_{f\gamma} \tau}.
\tag{A.52}
$$

Focusing on the norm of x_f, from (A.52) and Schwartz inequality we obtain

$$
\|x_f(\tau)\|_2 = \|x_f(0) e^{A_{f\gamma} \tau}\|_2 \leq \|x_f(0)\|_2 \|e^{A_{f\gamma} \tau}\|_2.
\tag{A.53}
$$

The definition of $A_{f\gamma}$ and the eigenspectrum bound to the fast subsystem imply that

$$\|x_f(0)\|_2 \|e^{A_{f\gamma}\tau}\|_2 \leq \|x_f(0)\|_2 e^{(\gamma\lambda_{\alpha+1})\tau}, \tag{A.54}$$

where $\lambda_{\alpha+1}$ represents the dominant eigenvalue of A_f which is the least negative and of $O(\frac{1}{\gamma})$. Using singular perturbation arguments for infinite dimensional systems it is shown that within a finite time the fast system dynamics will relax to a ball of radius $O(\gamma)$ around zero [175]. Using the spectral bound of (A.53) and (A.54) for the dynamic behavior and that $\gamma = |\lambda_1|/|\lambda_{\alpha+1}|$ we can obtain

$$\|x_f(0)\|_2 e^{(\gamma\lambda_{\alpha+1})\tau} = \|x_f(0)\|_2 e^{-|\lambda_1|\tau} \leq O(\gamma); \tag{A.55}$$

this bound is satisfied when

$$\tau_b = \frac{t_b}{\gamma} \geq -\frac{1}{|\lambda_1|} \ln\left[O(\frac{\gamma}{\|x_f(0)\|_2})\right]. \tag{A.56}$$

We denote t_b with the time period needed by the fast dynamics of the process to stabilize and converge to a small neighborhood of zero,

$$t_b \geq \frac{1}{|\lambda_{\alpha+1}|} \ln\left[O(\frac{\|x_f(0)\|_2}{|\lambda_1|}|\lambda_{\alpha+1}|)\right]. \tag{A.57}$$

Considering t_b and the time interval between snapshots, $\delta_t = t_k - t_{k-1}$, we choose δ_t such that $\delta_t > t_b$. Then the infinite dimensional system in (A.50) approximately

reduces to the finite-dimensional slow system,

$$\dot{x}_s = A_s x_s + B_s \tilde{K} x_m, \tag{A.58}$$

and the complete system of (6.13) reduces to

$$
\begin{aligned}
Process: & \quad \dot{x}_s = A_s x_s + B_s u, \\
Model: & \quad \dot{x}_m = A_m x_m + B_m u, \\
Controller: & \quad u = \tilde{K} x_m.
\end{aligned}
\tag{A.59}
$$

Then by considering Assumption 6.3 and based on the stable static state feedback control law, we conclude that the controller can stabilize the reduced order dynamics of (A.59).

At this point, we know that the previous statement is true if and only if Assumptions 6.1, 6.2 and 6.3 hold. Focusing on the system dynamics Assumption 6.1 holds. Assumption 6.3 is satisfied for finite periods longer than the critical period of t_b. From this assumption we can assume that any basis functions of the slow subsystem are expressed in $\mathbb{P} \oplus \mathbb{Q}$. This assumption is not satisfied when new trends appear during the process evolution for the first time that makes the set of basis functions incomplete and the ROM inaccurate. Within a finite amount of time from when it happens, the APOD algorithm revises the basis functions and corrects the ROM. Following that, the controller is redesigned to retain rele-

vancy. This procedure is recursively repeated during system progression to enforce closed-loop stability.

A.4.4 Proof of Theorem 6.3

The general highly dissipative PDE of (6.50) can be categorized to two forms with different properties; (1) linear PDE, and (2) semilinear, quasilinear and nonlinear PDEs. According to such classification, the proof is presented for two class of governing PDEs;

Case I. Linear PDE

For the linear class, the PDE of (6.50) takes the following form,

$$
\begin{aligned}
&\frac{\partial}{\partial t}\bar{x}(z,t) = \mathcal{A}_n(z)\bar{x} + M(z,\bar{x}) + B(z)u(t), \\
&\Gamma(\bar{x}, \frac{\partial}{\partial z}\bar{x}, \ldots, \frac{\partial^{n-1}}{\partial z^{n-1}}\bar{x})\Big|_{\partial\Omega} = 0, \\
&\bar{x}(z,0) = \bar{x}_0(z),
\end{aligned}
\tag{A.60}
$$

where $\mathcal{A}_n(z)$ denotes the linear differential operator of order n and $M(z,\bar{x})$ is a linear function of $\bar{x}$. Then the infinite-dimensional representation of (A.60) in the Sobolev subspace can be presented as follows

$$
\dot{x} = \mathbf{A}x + \mathbf{M}(x) + \mathbf{B}u, \quad x(0) = x_0,
\tag{A.61}
$$

where $\mathbf{A}x = \mathcal{A}_n(z, \bar{x})$ and $\mathbf{M}(x) = M(z, \bar{x})$. According to Assumption 6.5, the ordered by size eigenspectrum of the linear operator of $\mathbf{A}$, $\{\lambda_1, \lambda_2, \dots\}$, which is the solution of the eigenproblem of

$$\mathbf{A}\psi_i - \lambda_i\psi_i = 0,$$

$$\Gamma(\psi_i, \frac{\partial \psi_i}{\partial z}, \dots, \frac{\partial^{n-1}\psi_i}{\partial z^{n-1}})\Big|_{\partial\Omega} = 0, \qquad (A.62)$$

$$i = 1, \dots, \infty,$$

and in practice computed by APOD, can be decomposed to two subsets; (1) the finite slow subset that includes the slow and possibly unstable eigenvalues, $\{\lambda_1, \lambda_2, \dots, \lambda_m\}$, where $\frac{|Re(\lambda_1)|}{|Re(\lambda_m)|} = \mathcal{O}(1)$, and $\mathcal{O}(\cdot)$ and $Re(\cdot)$ present the order of magnitude and the real part, respectively, and (2) the infinite complement fast subset that includes the remaining eigenvalues which are fast and stable, $\{\lambda_{m+1}, \lambda_{m+2}, \dots\}$. The two sets of basis functions correspond to functional subsets can be presented by $\{\psi_i\}_{i=1}^m$ and $\{\psi_i\}_{i=m+1}^\infty$, respectively. Also there is at least an order of magnitude separation between slow and fast subsets, defined by $\sigma = \frac{|Re(\lambda_1)|}{|Re(\lambda_{m+1})|}$ where σ is a small number. This separation corresponds to a time scale separation of the system dynamics.

Then considering the Galerkin projectors in the forms of (6.55), the modal vectorized representation of the infinite-dimensional system of (A.61) takes the following

form,

$$\dot{x}_s = A_s x_s + M_s(x_s) + B_s u, \quad x_s(0) = \mathcal{P} x_0,$$

$$\dot{x}_f = A_f x_f + M_f(x_f) + B_f u, \quad x_f(0) = \mathcal{Q} x_0,$$

$$(A.63)$$

where $A_s = \mathcal{P}\mathbf{A}$, $A_f = \mathcal{Q}\mathbf{A}$, $M_s = \mathcal{P}\mathbf{M}$, $M_f = \mathcal{Q}\mathbf{M}$. Then the partitioned system

of (A.63) can be described in the standard singular perturbation form [76, 148] of

$$\dot{x}_s = A_s x_s + M_s(x_s) + B_s u,$$

$$\sigma \dot{x}_f = A_{f\sigma} x_f + \sigma \big(M_f(x_f) + B_f u \big),$$

$$(A.64)$$

where $A_{f\sigma} = \sigma A_f$ is the exponentially stable unbounded linear operator. The fast

subsystem dynamics can be represented in the fast time scale of $\tau = t/\sigma$,

$$\frac{\partial x_f}{\partial \tau} = A_{f\sigma} x_f + \sigma \big(M_f(x_f) + B_f u \big), \tag{A.65}$$

by considering that the expression of $M_f(x_f) + B_f u$ does not locally contain terms

of $O(\frac{1}{\sigma})$ under a stable and non-aggressive controller design and by setting $\sigma = 0$

we obtain

$$\frac{\partial x_f}{\partial \tau} = A_{f\sigma} x_f. \tag{A.66}$$

By solving the locally exponentially stable system of (A.66) we conclude

$$x_f(\tau) = x_f(0) e^{A_{f\sigma} \tau}. \tag{A.67}$$

Then by taking the L_2 norm of x_f and applying Schwartz inequality

$$\|x_f(\tau)\|_2 = \|x_f(0)e^{A_{f\sigma}\tau}\|_2 \leq \|x_f(0)\|_2\|e^{A_{f\sigma}\tau}\|_2, \tag{A.68}$$

and the eigenspectrum bound to the exponential term of the fast dynamics we obtain

$$\|x_f(0)\|_2\|e^{A_{f\sigma}\tau}\|_2 \leq \|x_f(0)\|_2 e^{\left(\sigma\ Re(\lambda_{m+1})\right)\tau}, \tag{A.69}$$

where $Re(\lambda_{m+1}) = O(\frac{1}{\sigma})$ denotes real part of the least negative dominant eigenvalue of A_f. By applying singular perturbation theory [76, 148, 151] and Tykhonov's theorem [175] we conclude that after a finite period of time the fast dynamics of the infinite-dimensional system converges to a ball of radius $O(\sigma)$ around zero. Therefore,

$$\|x_f(0)\|_2 e^{\left(\sigma\ Re(\lambda_{m+1})\right)\tau} = \|x_f(0)\|_2 e^{-|Re(\lambda_1)|\tau} \leq O(\sigma), \tag{A.70}$$

implies that

$$\tau_b = \frac{t_b}{\sigma} \geq -\frac{1}{|Re(\lambda_1)|}\ln\left[O(\frac{\sigma}{\|x_f(0)\|_2})\right]. \tag{A.71}$$

Consequently we can obtain a lower bound for required relaxation time as follows

$$t_b \geq \frac{1}{|Re(\lambda_{m+1})|}\ln\left[O(\frac{\|x_f(0)\|_2}{|Re(\lambda_1)|}|Re(\lambda_{m+1})|)\right]. \tag{A.72}$$

The closed-loop infinite-dimensional system of (A.61) which is the functional representation of the PDE of (A.60) exponentially reduces to the finite-dimensional

slow subsystem (Proposition 1 in [78]) and when $t \geq t_b$ we can approximate the infinite-dimensional system by

$$\dot{x}_s = A_s x_s + M_s(x_s) + B_s u. \tag{A.73}$$

Then due to the exponential stability of fast subsystem, if the finite-dimensional system approximation of (A.73) is exponentially stable, the infinite-dimensional system of (A.61) is also exponentially stable.

Case II. Semilinear, Quasilinear and Nonlinear PDEs

Under the assumption of time scale separation between the slow and fast dynamics of the infinite-dimensional system (Assumption 6.5), the vectorized modal system of (6.56) can be described in the standard singular perturbation form in different time scales [76]

$$\dot{x}_s = F_s(x_s, x_f) + H_s(x_s, x_f) + B_s u,$$
$$\sigma \dot{x}_f = \sigma F_f(x_s, x_f) + \sigma \big(H_f(x_s, x_f) + B_f u\big), \tag{A.74}$$

for sufficiently small values of σ which indicates the time-scale separation between the slow (and possibly unstable) and fast (and stable) dynamics where F_f is an exponentially stable unbounded operator. Note that such separation can be recognized by statistical approached like APOD. Due to the highly dissipative nature of the spatial differential operator of $\mathcal{F}_n$, the resulting nonlinear vector function of

the fast subsystem satisfies the following local property [18, 76]

$$F_f(x_s, x_f) = f_{fs}x_s + \frac{1}{\sigma}f_f x_f + \tilde{f}_f(x_s, x_f), \tag{A.75}$$

where f_f is a stable matrix with negative eigenvalues, $\tilde{f}_f$ is a purely nonlinear vector function which does not include any linear terms and the components f_{fs}, f_f and $\tilde{f}_f$ does not contain any term of $O(\sigma)$. Then the fast subsystem dynamics can be represented in the fast time scale of $\tau = t/\sigma$,

$$\frac{\partial x_f}{\partial \tau} = f_f x_f + \sigma\big(f_{fs}x_s + \tilde{f}_f(x_s, x_f)\big) + \sigma\big(H_f(x_s, x_f) + B_f u\big). \tag{A.76}$$

According to the Lipschitz property of H_f, the expression of $H_f(x_s, x_f) + B_f u$ does not also locally contain terms of $O(\frac{1}{\sigma})$ under a stable and non-aggressive controller design. Then by setting $\sigma = 0$ we obtain

$$\frac{\partial x_f}{\partial \tau} = f_f x_f. \tag{A.77}$$

The solution of the locally exponentially stable system of (A.77) takes the following form

$$x_f(\tau) = x_f(0)e^{f_f \tau}. \tag{A.78}$$

Therefore, the infinite-dimensional dynamics of (6.53) which is the functional representation of the PDE of (6.50) exponentially converges to the finite-dimensional

slow dynamics of

$$\dot{x}_s = F_s(x_s, 0) + H_s(x_s, 0) + B_s u, \tag{A.79}$$

after a finite period of time. Then the infinite-dimensional system of (6.53) is exponentially stable if the finite-dimensional system approximation of (A.79) is exponentially stable due to the exponential stability of fast subsystem.

BIBLIOGRAPHY

[1] R.A. Adomaitis. A reduced-basis discretization method for chemical vapor deposition reactor simulation. *Math Comput. Model*, 38(1-2):159–175, 2003.

[2] F. Allgöwer and F.J. Doyle. Nonlinear process control - Which way to the promised land? In *Proceedings of 5th International Conference on Chemical Process Control*, 24–45, Tahoe City, CA, 1997.

[3] A.A. Alonso, C.E. Frouzakis, and I.G. Kevrekidis. Optimal sensor placement for state reconstruction of distributed process systems. *AICHE J.*, 50:1438–1452, 2004.

[4] A.A. Alonso, I.G. Kevrekidis, J.R. Banga, and C.E. Frouzakis. Optimal sensor location and reduced order observer design for distributed process systems. *Comp. & Chem. Eng.*, 28:27–35, 2004.

[5] A.A. Alonso and B.E. Ydstie. Stabilization of distributed systems using irreversible thermodynamics. *Automatica*, 37:1739–1755, 2001.

[6] J. Alvarez. Nonlinear state estimation with robust convergence. *J. Proc. Cont.*, 10:59–71, 2000.

[7] J. Alvarez and T. Lopez. Robust dynamic state estimation of nonlinear plants. *AIChE J.*, 45(1):107–123, 1999.

[8] A. Ammar, B. Mokdad, F. Chinesta, and R. Keunings. A new family of solvers for some classes of multidimensional partial differential equations encountered in kinetic theory modeling of complex fluids. Part II: transient simulation using space-time separated representations. *J. Non-Newtonian Fluid Mechanics*, 144(2-3):98121, 2007.

[9] A. Ammar, E. Pruliere, F. Chinesta, and M. Laso. Reduced numerical modeling of flows involving liquid-crystalline polymers. *J. Non-Newtonian Fluid Mechanics*, 160(2-3):140–156, 2009.

[10] B.D.O. Anderson. Adaptive systems, lack of persistency of excitation and bursting phenomena. *Automatica*, 21(3):247 – 258, 1985.

[11] M. Armand and J.M. Tarascon. Building better batteries. *Nature*, 451:652–657, 2008.

[12] A. Armaou, J. Baker, and P.D. Christofides. Feedback control of plasma etching reactors for improved etching uniformity. *Chem. Eng. Sci.*, 56:257–265, 2001.

[13] A. Armaou and P.D. Christofides. Nonlinear feedback control of parabolic PDE systems with time-dependent spatial domains. *J. Math. Anal. & Appl.*, 239:124–157, 1999.

[14] A. Armaou and P.D. Christofides. Plasma-enhanced chemical vapor deposition: Modeling and control. *Chem. Eng. Sci.*, 54:3305–3314, 1999.

[15] A. Armaou and P.D. Christofides. Feedback control of the Kuramoto-Sivashinsky equation. *Physica D*, 137:49–61, 2000.

[16] A. Armaou and P.D. Christofides. Wave suppression by nonlinear finite-dimensional control. *Chem. Eng. Sci.*, 55:2627–2640, 2000.

[17] A. Armaou and P.D. Christofides. Crystal temperature control in the Czochralski crystal growth process. *AIChE J.*, 47:79–106, 2001.

[18] A. Armaou and P.D. Christofides. Finite-dimensional control of nonlinear parabolic PDE systems with time-dependent spatial domains using empirical eigenfunctions. *Int. J. Appl. Math. & Comp. Sci.*, 11:287–317, 2001.

[19] A. Armaou and P.D. Christofides. Robust control of parabolic PDE systems with time-dependent spatial domains. *Automatica*, 37:61–69, 2001.

[20] A. Armaou and P.D. Christofides. Dynamic optimization of dissipative PDE systems using nonlinear order reduction. *Chem. Eng. Sci.*, 57:5083–5114, 2002.

[21] A. Armaou and M.A. Demetriou. Optimal actuator/sensor placement for linear parabolic PDEs using spatial H_2 norm. *Chem. Eng. Sci.*, 61(22):7351–7367, 2006.

[22] A. Armaou and A. Varshney. Dynamic optimization of dissipative PDEs using control vector parameterization: Application to GaN thin film epitaxy. In *Proceedings of the American Control Conference*, 279–286, Boston, MA, 2004.

[23] J. Aseltine, A. Mancini, and C. Sarture. A survey of adaptive control systems. *Automatic Control, IRE Transactions on*, 6(1):102–108, 1958.

[24] P. Astrid, S. Weiland, K. Willcox, and T. Backx. Missing point estimation in models described by proper orthogonal decomposition. *IEEE Trans. Autom. Contr.*, 53:2237–2251, 2008.

[25] K. Astrom. Theory and applications of adaptive-control - A survey. *Automatica*, 19(5):471–486, 1996.

[26] A.N. Atassi and H.K. Khalil. A separation principle for the control of a class of nonlinear systems. *IEEE Trans. Automatic Control*, 46(5):742–746, 2001.

[27] J.A. Atwell, J.T. Borggaard, and B.B. king. Reduced order controllers for Burger's equation with a nonlinear observer. *Int. J. Appl. Math. Comput. Sci.*, 11:1311–1330, 2001.

[28] D. Babaei Pourkargar and A. Armaou. Control of dissipative partial differential equation systems using APOD based dynamic observer designs. In *Proceedings of the American Control Conference*, 502–508, Washington, DC, 2013.

[29] D. Babaei Pourkargar and A. Armaou. Modification to adaptive model reduction for regulation of distributed parameter systems with fast transients. *AIChE J.*, 59(12):4595–4611, 2013.

[30] D. Babaei Pourkargar and A. Armaou. Feedback control of linear distributed parameter systems via adaptive model reduction in the presence of device network communication constraints. In *Proceedings of the American Control Conference*, 1667–1673, Portland, OR, 2014.

[31] D. Babaei Pourkargar and A. Armaou. Geometric output tracking of non-

linear distributed parameter systems via adaptive model reduction. *Chem. Eng. Sci.*, 116:418–427, 2014.

[32] D. Babaei Pourkargar and A. Armaou. Output tracking of spatiotemporal thermal dynamics in transport-reaction processes via adaptive model reduction. In *Proceedings of the American Control Conference*, 3364–3370, Portland, OR, 2014.

[33] D. Babaei Pourkargar and A. Armaou. A refined adaptive model reduction approach for control of fast evolving distributed parameter systems. In *Proceeding of the 21st International Symposium on Mathematical Theory of Networks and Systems*, 140–147, Groningen, Netherlands, 2014.

[34] D. Babaei Pourkargar and A. Armaou. Adaptive control of chemical distributed parameter systems. In *Proceeding of the IFAC International Symposium on Advanced Control of Chemical Processes*, 682–687, Whistler, Canada, 2015.

[35] D. Babaei Pourkargar and A. Armaou. APOD-based control of linear distributed parameter systems under sensor/controller communication bandwidth limitations. *AIChE J.*, 61(2):434–447, 2015.

[36] D. Babaei Pourkargar and A. Armaou. Control of spatially distributed processes with unknown transport-reaction parameters via two layer system adaptations. *AIChE J.*, 61(8):2497–2507, 2015.

[37] D. Babaei Pourkargar and A. Armaou. Design of APOD-based switching dynamic observers and output feedback control for a class of nonlinear distributed parameter systems. *Chem. Eng. Sci.*, http://dx.doi.org/10.1016/j.ces.2015.02.032, 2015.

[38] D. Babaei Pourkargar and A. Armaou. Dynamic shaping of transport-reaction processes with a combined sliding mode controller and luenberger-type dynamic observer design. *Chem. Eng. Sci.*, to appear, 2015.

[39] D. Babaei Pourkargar and A. Armaou. Low-dimensional adaptive output feedback controller design for transport-reaction processes. In *Proceeding of the European Control Conference*, Linz, Austria, to appear, 2015.

[40] D. Babaei Pourkargar and A. Armaou. Wave motion suppression in the presence of unknown parameters using recursively updated empirical basis functions. In *Proceedings of the American Control Conference*, 2619–2624, Chicago, IL, 2015.

[41] E.W. Bai and S.S. Sastry. Persistency of excitation, sufficient richness and parameter convergence in discrete time adaptive control. *Systems & Control Letters*, 6(3):153 – 163, 1985.

[42] J. Baker, A. Armaou, and P.D. Christofides. Nonlinear control of incompressible fluid flow: Application to Burgers' equation and 2D channel flow. *J. Math. Anal. Appl.*, 252:230–255, 2000.

[43] P. Balakrishnan, R. Ramesh, and T.P. Kumar. Safety mechanisms in Lithium-ion batteries. *Journal of Power Sources*, 155(2):401–414, 2006.

[44] M.J. Balas. Feedback control of linear diffusion processes. *Int. J. Control*, 29:523–533, 1979.

[45] M.J. Balas. Trends in large scale structure control theory: Fondest hopes, wildest dreams. *IEEE Trans. Automat. Contr.*, 27:522–535, 1982.

[46] M.J. Balas. The Galerkin method and feedback control of linear distributed parameter systems. *J. Math. Anal. Appl.*, 91:527–546, 1983.

[47] M.J. Balas. Nonlinear finite-dimensional control of a class of nonlinear distributed parameter systems using residual mode filters: A proof of local exponential stability. *J. Math. Anal. Appl.*, 162:63–70, 1991.

[48] A. Balogh and M. Krstic. Boundary control of the Kortewegde VriesBurgers equation: Further results on stabilization and wellposedness, with numerical demonstration. *IEEE Trans. Automatic Control*, 45(9):1739–1745, 2000.

[49] E. Balsa-Canto, A.A. Alonso, and J.R. Banga. Reduced-order models for nonlinear distributed process systems and their application in dynamic optimization. *Ind. & Eng. Chem. Res.*, 43:3353–3363, 2004.

[50] E. Balsa-Canto, A.A. Alonso, and J.R. Banga. Dynamic optimization of complex distributed process systems. *Chem. Eng. R& D.*, 83:724–729, 2005.

[51] E. Balsa-Canto, J.R. Banga, and A.A. Alonso. A novel, efficient and reliable method for thermal process design and optimization. parts I and II. *Journal of Food Engineering*, 52:227–247, 2002.

[52] T. Bandhauer, S. Garimella, and T. Fuller. A critical review of thermal issues in Lithium-ion batteries. *Journal of The Electrochemical Society*, 158(3):R1–R25, 2011.

[53] B. Bandyopadhyay and S. Janardhanan. *Discrete-time sliding mode control: A Multirate output feedback approach, Lecture Notes in Control and Information Sciences.* Springer-Verlag, Berlin, 2006.

[54] H.T. Banks and M.A. Demetriou. Adaptive parameter estimation of hyperbolic distributed parameter systems: Non-symmetric damping and slowly time varying systems. *ESAIM: Control, Optimisation and Calculus of Variations*, 3:133–162, 2010.

[55] V.L. Barrio, G. Schaub, M. Rohde, S. Rabe, F. Vogel, J.F. Cambra, P.L. Arias, and M.B. Guemez. Reactor modeling to simulate catalytic partial oxidation and steam reforming of methane. Comparison of temperature profiles and strategies for hot spot minimization. *Int. J. Hydro. Ener.*, 32:1421–1428, 2007.

[56] G. Bartolini, A. Ferrara, and S. Spurgeon (Eds.). Special issue: New trends in sliding mode control. *Int. J. Robust Nonlinear Control*, 7(4), 1997.

[57] A. Bartoszewicz, O. Kaynak, and V.I. Utkin (Eds.). Special issue: Sliding mode control in industrial applications. *IEEE Trans. Ind. Electron.*, 55(11), 2008.

[58] R. Bellman. *Adaptive control processes: a guided tour*. Princeton University Press, Princeton, NJ, 1961.

[59] E. Bendersky and P.D. Christofides. Optimization of transport-reaction processes using nonlinear model reduction. *Chem. Eng. Sci.*, 55:4349–4366, 2000.

[60] J. Bentsman and Y. Orlov. Reduced spatial order model reference adaptive control of spatially varying distributed parameter systems of parabolic and hyperbolic types. *Int. J. Adapt. Control Signal Process.*, 15:679–696, 2001.

[61] W.B. Bequette. Nonlinear control of chemical processes: A review. *Ind. Eng. Chem. Res.*, 30:1391–1413, 1991.

[62] L.G. Bleris and M.V. Kothare. Low-order empirical modeling of distributed parameter systems using temporal and spatial eigenfunctions. *Comp. & Chem. Eng.*, 29:817–827, 2005.

[63] M. Bohm, M.A. Demetriou, S. Reich, and I.G. Rosen. Model reference adaptive control of distributed parameter systems. *SIAM J. Control Optim.*, 36(1):33–81, 1998.

[64] S. Boyd, E. Feron, L. El-Ghaoui, and V. Balakrishnan. *Linear matrix inequality in system and control theory.* SIAM, Philadelphia, 1994.

[65] S. Boyd and S. Sastry. On parameter convergence in adaptive control. *Systems & Control Letters*, 3(6):311 – 319, 1983.

[66] S. Boyd and S.S. Sastry. Necessary and sufficient conditions for parameter convergence in adaptive control. *Automatica*, 22(6):629 – 639, 1986.

[67] C. Brabec, U. Scherf, and V. (Eds.) Dyakonov. *Organic Photovoltaics: Materials, Device Physics, and Manufacturing Technologies.* Wiley-VCH, 2008.

[68] C. Brezinski. *Computational aspects of linear control.* Kluwer, Dordrecht, 2002.

[69] B. Brogliato, R. Lozano, B. Maschke, and O. Egeland. *Dissipative systens analysis and control.* Springer, London, 2007.

[70] C.G. Cassandras and W. Li. Sensor networks and cooperative control. *European J. Control*, 11:436463, 2005.

[71] H.C. Chang. Nonlinear waves on liquid film surfaces. I. Flooding in vertical tube. *Chem. Eng. Sci.*, 41:2463–2476, 1986.

[72] K.K. Chen, J.H. Tu, and C.W. Rowley. Variants of dynamic mode decomposition: Boundary condition, koopman, and fourier analyses. *Journal of Nonlinear Science*, 22(6):887–915, 2012.

[73] S. Chen, C. Wan, and Wang Y. Thermal analysis of Lithium-ion batteries. *Journal of Power Sources*, 140(1):111–124, 2005.

[74] F. Chinesta, A. Ammar, A. Leygue, , and R. Keunings. An overview of the proper generalized decomposition with applications in computational rheology. *J. Non-Newtonian Fluid Mechanics*, 166(11):578–592, 2011.

[75] P.D. Christofides. Robust control of parabolic pde systems. *Chem. Eng. Sci.*, 16:2949–2965, 1998.

[76] P.D. Christofides. *Nonlinear and robust control of PDE systems.* Birkhäuser, New York, 2000.

[77] P.D. Christofides and A. Armaou. Global stabilization of the Kuramoto-Sivashinsky equation via distributed output feedback control. *Sys. & Contr. Lett.*, 39:283294, 2000.

[78] P.D. Christofides and P. Daoutidis. Finite-dimensional control of parabolic PDE systems using approximate inertial manifolds. *J. Math. Anal. Appl.*, 216:398–420, 1997.

[79] P.D. Christofides and N.H. El-Farra. *Control of nonlinear and hybrid process systems: Designs for uncertainty, constraints and time-delays.* Springer-Verlag, Berlin, Germany, 2005.

[80] R.W. Chylla, R.A. Adomaitis, and A. Cinar. Stability of tubular and autothermal packed-bed reactors using phase plane analysis. *Ind. & Eng. Chem. Res.*, 26:1356–1362, 1987.

[81] R.F. Curtain. Stabilizability and controllability of spatially invariant PDE systems. *IEEE Trans. Automatic Control*, 60(2):383–392, 2015.

[82] R.F. Curtain, M.A. Demetriou, and I. Kazufumi. Adaptive compensators for perturbed positive real infinite-dimensional systems. *Int. J. Appl. Math. Comput. Sci.*, 13(4):441–452, 2003.

[83] R.F. Curtain and K. Glover. *Balanced realisations for infinte-dimensional systems: Operator theory and system.* Birkhäuser, Basel, 1986.

[84] R.F. Curtain and H. Zwart. *An Introduction to Infinite-Dimensional Linear Systems Theory.* Springer-Verlag, New York, 1995.

[85] A. Datta and P.A. Ioannou. Performance improvement versus robust stability in model reference adaptive control. In *Decision and Control, 1991., Proceedings of the 30th IEEE Conference on*, 748–753, 1991.

[86] R.A. Decarlo, M.S. Branicky, S. Pettersson, and B. Lennartson. Perspectives and results on the stability and stabilizability of hybrid systems. *Proc IEEE.*, 88:10691082, 2000.

[87] M.A. Demetriou and A. Armaou. Dynamic online nonlinear robust detection and accommodation of incipient component faults for nonlinear dissipative distributed processes. *Int. J. Robust. Nonlinear Control*, 22(1):3–23, 2012.

[88] M.A. Demetriou and I.I. Hussein. Estimation of spatially distributed pro-

cesses using mobile spatially distributed sensor network. *SIAM J. CONTROL OPTIM.*, 48(1):266–291, 2009.

[89] M.A. Demetriou and N. Kazantzis. Compensation of spatiotemporally varying disturbances in nonlinear transport processes via actuator scheduling. *Int. J. Rob. & Nonl. Contr.*, 14:181–197, 2004.

[90] M.A. Demetriou and I.G. Rosen. On the persistence of excitation in the adaptive estimation of distributed parameter systems. *IEEE Trans. Automatic Control*, 39(5):1117–1123, 1994.

[91] M.A. Demetriou and I.G. Rosen. On-line robust parameter identification for parabolic systems. *Int. J. Adapt. Control Signal Process.*, 15(6):615–631, 2001.

[92] Q. Du, V. Faber, and M. Gunzburger. Centroidal Voronoi tessellations: Applications and algorithms. *SIAM Rev.*, 41:637676, 1999.

[93] S. Dubljevic. Boundary model predictive control of Kuramoto-Sivashinsky equation with input and state constraints. *Comp. & Chem. Eng.*, 34(10):1655–1661, 2010.

[94] S. Dubljevic, P.D. Christofides, and I.G. Kevrekidis. Distributed nonlinear control of diffusion-reaction processes. *Int. J. Robust Nonlinear Control*, 14:133–156, 2004.

[95] T.E. Duncan and B. Pasik-Duncan. Adaptive control of continuous-time linear stochastic systems. *Mathematics of Control, Signals and Systems*, 3(1):45–60, 1990.

[96] C. Edwards and S.K. Spurgen. *Sliding mode control: Theory and applications.* Taylor and Francis Ltd., London, 1998.

[97] S.F. Edwards and D.R. Wilkinson. The surface statistics of a granular aggreate. In *Proceedings of the Royal Society of Lond Series A-Mathematical Physical and Engineering Sciences*, 381, 17–31, 1982.

[98] B. Egardt. *Stability of adaptive controllers.* Springer-Verlag, Berlin, 1979.

[99] N.H. El-Farra, A. Armaou, and P.D. Christofides. Analysis and control of parabolic PDE systems with input constraints. *Automatica*, 39(4):715–725, 2003.

[100] N.H. El-Farra and P.D. Christofides. Robust inverse optimal control of nonlinear systems. *Int. J. Rob. & Nonl. Contr.*, 13:1371–1388, 2003.

[101] N.H. El-Farra and S. Yulei. Quasi-decentralized control of process systems using wireless sensor networks with scheduled sensor transmissions. In *Proceedings of the American Control Conference*, 3390–3396, St. Louis, MO, 2009.

[102] H. Elliott, R. Cristi, and M. Das. Global stability of adaptive pole placement algorithms. *IEEE Trans. Automatic Control*, 30(4):348–356, 1985.

[103] L.C. Evans. *Partial differential equations.* American Mathematical Society, Providence, RI, 2010.

[104] R. Everson and L. Sirovich. The karhunen loẽve procedure for gappy data. *J. Opt. Soc. Am*, 12:1657–1664, 1995.

[105] A. Feuer and A.S. Morse. Adaptive control of single-input, single-output linear systems. *IEEE Trans. Automatic Control*, 23(4):557–569, 1978.

[106] A.F. Filippov. *Differential equations with discontinuous righthand sides.* Kluwer, Dordrecht, 1988.

[107] C. Foias, M.S. Jolly, I.G. Kevrekidis, G.R. Sell, and E.S. Titi. On the computation of inertial manifolds. *Phys. Lett. A*, 131:433–437, 1989.

[108] C. Foias, G.R. Sell, and R. Temam. Inertial manifolds for nonlinear evolutionary equations. *J. Diff. Equs.*, 73:309–353, 1988.

[109] C. Foias, G.R. Sell, and E.S. Titi. Exponential tracking and approximation of inertial manifolds for dissipative equations. *J. Dynamics and Differential Equations*, 1:199–244, 1989.

[110] S.R. Forrest. The path to ubiquitous and low-cost organic electronic appliances on plastic. *Nature*, 428:911–918, 2004.

[111] L.M. Fridman (Ed.). Special issue: Dedicated to Vadim Utkin on the occasion of his 65th birthday. *Int. J. Control*, 76(9-10), 2003.

[112] B. Friedland. *Control system design: An introduction to state-space methods.* McGraw-Hill, New York, 1986.

[113] C.E. Frouzakis, Y.G. Kevrekidis, J. Lee, K. Boulouchos, and A.A. Alonso. Proper orthogonal decomposition of direct numerical simulation data: Data reduction and observer construction. In *Proceedings of the Combustion Institute*, 28, 75–81, 2000.

[114] L. Fu and S. Sastry. Slow-drift instability in model reference adaptive systems: An averaging analysis. *International Journal of Control*, 45(2):503–527, 1987.

[115] K. Fukunaga. *Introduction to statistical pattern recognition.* Academic Press, New York, 1990.

[116] D.H. Gay and W.H. Ray. Identification and control of distributed parameter systems by means of the singular value decomposition. *Chem. Eng. Sci.*, 50:1519–1539, 1995.

[117] G. Georgakis, R. Aris, and N.R. Amundson. Studies in the control of tubular reactors: Part I & II & III. *Chem. Eng. Sci.*, 32:1359–1387, 1977.

[118] S. Ghantasala and N.H. El-Farra. Active fault-tolerant control of sampled-data nonlinear distributed parameter systems. *Int. J. Robust Nonlinear Control*, 22(1):24–42, 2012.

[119] G.C. Goodwin and R.S. Long. Generalization of results on multivariable adaptive control. *IEEE Trans. Automatic Control*, 25(6):1241–1245, Dec 1980.

[120] G.C. Goodwin, P.J. Ramadge, and P.E. Caines. Discrete-time multivariable adaptive control. *IEEE Trans. Automatic Control*, 25(3):449–456, 1980.

[121] G.C. Goodwin and K.S. Sin. *Adaptive filtering prediction and control.* Prentice-Hall, Englewood Cliffs, NJ, 1984.

[122] M.D. Graham and I.G. Kevrekidis. Alternative approaches to the Karhunen-Loève decomposition for model reduction and data analysis. *Comp. & Chem. Eng.*, 20:495–506, 1996.

[123] W.R. Graham, J. Peraire, and K.Y. Tang. Optimal control of vortex shedding using low-order models. Part I- Open-loop model development. *Int. J. for Numerical methods in Engineering*, 44:945–972, 1999.

[124] W.R. Graham, J. Peraire, and K.Y. Tang. Optimal control of vortex shedding using low-order models. Part II- Model-based control. *Int. J. for Numerical methods in Engineering*, 44:973–990, 1999.

[125] A.C. Grimsdale and K. Mllen. 1-, 2-, and 3-dimensional polyphenylenes–from molecular wires to functionalised nanoparticles. *Chem. Rec.*, 1:243–257, 2001.

[126] L.T. Gruyitch. *Tracking control of linear systems.* CRC Press, Boca Raton, 2013.

[127] W. Gu and C. Wang. Thermal-electrochemical modeling of battery systems. *Journal of The Electrochemical Society*, 147(8):2910–2922, 2000.

[128] L. Guo. Self-convergence of weighted least-squares with applications to stochastic adaptive control. *IEEE Trans. Automatic Control*, 41(1):79–89, 1996.

[129] L. Guo. On critical stability of discrete-time adaptive nonlinear control. *IEEE Trans. Automatic Control*, 42(11):1488–1499, 1997.

[130] M.A. Henson and D.E. Seborg. *Nonlinear Process Control.* Prentice-Hall, Englewood Cliffs, NJ, 1997.

[131] J.P. Hespanha, P. Naghshtabrizi, and Y. Xu. A survey of recent results in networked control systems. *Proceedings of IEEE*, 95(1):138–162, 2007.

[132] J.B. Hoagg and D.S. Bernstein. Retrospective cost model reference adaptive control for nonminimum-phase systems. *Journal of Guidance, Control, and Dynamics*, 35(6):17671786, 2013.

[133] P. Holmes, J.L. Lumley, and G. Berkooz. *Turbulence, Coherent Structures, Dynamical Systems and Symmetry.* Cambridge University Press, New York, 1996.

[134] C. Homescu, L.R. Petzold, and R. Serban. Error estimation for reduced-order models of dynamical systems. *SIAM Review.*, 49:277–299, 2007.

[135] K.S. Hong and J. Bentsman. Direct adaptive control of parabolic systems: Algorithm synthesis, and convergence, and stability analysis. *IEEE Trans. Automatic Control*, 39:2018–2033, 1994.

[136] P.A. Ioannou and P.V. Kokotovi. *Adaptive systems with reduced models.* Springer-Verlag, Berlin, 1983.

[137] P.A. Ioannou and G. Tao. Dominant richness and improvement of performance of robust adaptive control. *Automatica*, 25(2):287 – 291, 1989.

[138] A. Isidori. *Nonlinear Control Systems.* Springer-Verlag, New York, 1995.

[139] M. Izadi and S. Dubljevic. Order-reduction of parabolic PDEs with time-varying domain using empirical eigenfunctions. *AIChE J.*, 59(11):4142–4150, 2013.

[140] C.A. Jacobson and C.N. Nett. Linear state-space systems in infinite-dimensional space: The role and characterization of joint stabilizability/detectability. *IEEE Trans. Autom. Contr.*, 33:541–551, 1988.

[141] S.M. Joshi, G. Tao, and P. Patre. Direct adaptive control using an adaptive reference model. *International Journal of Control*, 84(1):180–196, 2011.

[142] T. Kailath. *Linear systems.* Prentice-Hall, Englewood Cliffs, N.J., 1980.

[143] R.E. Kalman. Design of a self-optimizing control system. *Transactions on ASME*, 80:468478, 1958.

[144] I. Kanellakopoulos, P.V. Kokotovic, and A.S. Morse. Systematic design of adaptive controllers for feedback linearizable systems. *IEEE Trans. Automatic Control*, 36(11):1241–1253, 1991.

[145] I. Karafyllis and P. Doutidis. Control of hot spots in plug flow reactors. *Comput. Chem. Eng.*, 26:1087–1094, 2002.

[146] I.G. Kevrekidis, B. Nicolaenko, and J.C. Scovel. Back in the saddle again: A computer assisted study of the Kuramoto-Sivashinsky equation. *SIAM J. Appl. Math.*, 50:760–790, 1990.

[147] H.K. Khalil. Adaptive output feedback control of nonlinear systems represented by input-output models. *IEEE Trans. Automatic Control*, 41(2):177–188, 1996.

[148] H.K. Khalil. *Nonlinear systems*. Prentice-Hall, New Jersey, 2002.

[149] B.B. King, N. Hovakimyan, K.A. Evans, and M. Buhl. Reduced order controllers for distributed parameter systems: LQG balanced truncation and an adaptive approach. *Mathematical and Computer Modelling*, 43:1136–1149, 2005.

[150] A. Koji and A.M. Annaswamy. Adaptive control of nonlinearly parameterized systems with a triangular structure. *Automatica*, 38(1):115 – 123, 2002.

[151] P. Kokotovic, H.K. Khalil, and J. O'Reilly. *Singular Perturbation Methods in Control: Analysis and Design.* SIAM, Philadelphia, 1999.

[152] R.L. Kosut, B.D.O. Anderson, and I. Mareels. Stability theory for adaptive systems: Methods of averaging and persistency of excitation. In *Decision and Control, 1985 24th IEEE Conference on*, 478–483, 1985.

[153] C. Kravaris and Y. Arkun. Geometric nonlinear control - an overview. In *Proceedings of 4th International Conference on Chemical Process Control*, 477–515, Padre Island, TX, 1991.

[154] C. Kravaris and J.C. Kantor. Geometric methods for nonlinear process control 1. Background. *Ind. Eng. Chem. Res.*, 29:2295–2310, 1990.

[155] C. Kravaris and J.C. Kantor. Geometric methods for nonlinear process control 2. Controller synthesis. *Ind. Eng. Chem. Res.*, 29:2310–2323, 1990.

[156] J. Krc, F. Smole, and M. Topic. Analysis of light scattering in amorphous Si:H solar cells by a one-dimensional semi-coherent optical model. *Progress in Photovoltaics*, 11(1):15–26, 2003.

[157] J. Krc, M. Zeman, O. Kluth, E. Smole, and M. Topic. Effect of surface roughness of ZnO: Al films on light scattering in hydrogenated amorphous silicon solar cells. *Thin Solid Films*, 426(1-2), 2003.

[158] J. Krc, M. Zeman, E. Smole, and M. Topic. Optical modelling of thin-film silicon solar cells deposited on textured substrates. *Thin Solid Film*, (451-452):298302, 2004.

[159] G. Kreisselmeier and G. Rietze-Augst. Richness and excitation on an interval-with application to continuous-time adaptive control. *IEEE Trans. Automatic Control*, 35(2):165–171, 1990.

[160] M. Krsti, I. Kanellakopoulos, and P.V. Kokotovi. Adaptive nonlinear control without overparametrization. *Systems & Control Letters*, 19(3):177 – 185, 1992.

[161] M. Krstic and A. Smyshlyaev. Adaptive boundary control for unstable parabolic PDEs - Part I: Lyapunov design. *IEEE Trans. Automatic Control*, 53:1575–1591, 2008.

[162] K. Kunisch and S. Volkwein. Galerkin proper orthogonal decomposition methods for parabolic problems. *Numer. Math.*, 90:117–148, 2001.

[163] K. Kunisch and S. Volkwein. Galerkin proper orthogonal decomposition methods for a general equation in fluid dynamics. *SIAM J. Numer. Anal.*, 40:492–515, 2002.

[164] S. Kurtz, D. Friedman, J. Geisz, and W. McMahon. Using MOVPE growth to generate tomorrow's solar electricity. *Journal of Crystal Growth*, 298:748–753, 2007.

[165] S. Lall, J. Marsden, and S. Glavaski. Empirical model reduction of controlled nonlinear systems. In *Proceedings of the IFAC World Congress, International Federation of Automatic Control*, F, 473–478, 1999.

[166] L. Lao, M. Ellis, and P.D. Christofides. Economic model predictive control of transport-reaction processes. *Ind. Eng. Chem. Res.*, 53(18):7382–7396, 2014.

[167] I. Lasiecka. Control of systems governed by partial differential equations: A historical perspective. In *Proceedings of 34th IEEE Conference on Decision and Control*, 2792–2797, New Orleans, LA, 1995.

[168] F. Leblanc, J. Perrin, and J. Schmitt. Numerical modeling of the optical-properties of hydrogenated amorphous-silicon-based p-i-n solar-cells deposited on rough transparent conducting oxide substrates. *Journal of Applied Physics*, 75(2):1074–1087, 1994.

[169] C. Li, M. Liu, N.G. Pschirer, M. Baumgarten, and K. Mllen. Polyphenylene-based materials for organic photovoltaics. *Chem. Rev.*, 110:6817–6855, 2010.

[170] J. Lin and I. Kanellakopoulos. Nonlinearities enhance parameter convergence in strict feedback systems. *IEEE Trans. Automatic Control*, 44(1):89–94, 1999.

[171] W. Lin and C. Qian. Adaptive control of nonlinearly parameterized systems: the smooth feedback case. *IEEE Trans. Automatic Control*, 47(8):1249–1266, 2002.

[172] Y.H. Lin and R.A. Adomaitis. Simulation and model reduction methods for an RF plasma glow discharge. *J. Comput. Phys.*, 171(2):731–752, 2001.

[173] Z. Lin and G. Tao. Adaptive control of a weakly nonminimum phase linear system. *IEEE Trans. Automatic Control*, 45(4):824–829, 2000.

[174] L. Liu, B. Huang, and S. Dubljevic. Model predictive control of axial dispersion chemical reactor. *J. Process Contr.*, 24(11):1671–1690, 2014.

[175] C. Lobry, T. Sari, and S. Touhami. On Tykhonov's theorem for convergence of solutions of slow and fast systems. *Electronic Journal of Differential Equations (EJDE)*, 1998(19):1–22, 1998.

[176] R. Lozano and X. Zhao. Adaptive pole placement without excitation probing signals. *IEEE Trans. Automatic Control*, 39(1):47–58, 1994.

[177] L. Lu, X. Han, J. Li, J. Hua, and M. Ouyang. A review on the key issues for Lithium-ion battery management in electric vehicles. *Journal of Power Sources*, 226:272–288, 2013.

[178] P. Lu, J.H. Edgar, O.J. Glembocki, P.B. Klein, E.R. Glaser, J. Perrin, and J. Chaudhuri. High-speed homoepitaxy of SiC from methyltrichlorosilane by chemical vapor deposition. *J. Cryst. Growth*, 285(4):506–513, 2005.

[179] V.M. Martinez and T.F. Edgar. Model-based run-to-run controllers for improved yields. *IEEE Control System Magazine*, December:46–55, 2006.

[180] D.Q. Mayne, J.B. Rawlings, C.V. Rao, and P.O.M. Scokaert. Constrained model predictive control: Stability and optimality. *Automatica*, 36:789–814, 2000.

[181] I. Mezic. Spectral properties of dynamical systems, model reduction and decompositions. *Nonlinear Dyn.*, 41(1-3):309–325, 2005.

[182] I. Mezic and A. Banaszuk. Comparison of systems with complex behavior. *Physica D*, 197(1-2):101–133, 2004.

[183] P. Mhaskar and A. Kennedy. Robust model predictive control of nonlinear process systems: Handling rate constraints. *Chem. Eng. Sci.*, 63:366–375, 2008.

[184] R.H. Middleton, G.C. Goodwin, D.J. Hill, and D.Q. Mayne. Design issues in adaptive control. *IEEE Trans. Automatic Control*, 33(1):50–58, 1988.

[185] D.E. Miller and E.J. Davison. An adaptive controller which provides an arbitrarily good transient and steady-state response. *IEEE Trans. Automatic Control*, 36(1):68–81, 1991.

[186] E.A. Misawa and V.I. Utkin (Eds.). Special issue: Variable structure systems. *J. Dyn. Syst. Meas. Control*, 122, 2000.

[187] R.V. Monopoli. Model reference adaptive control with an augmented error signal. *IEEE Trans. Automatic Control*, 19(5):474–484, 1974.

[188] L.A. Montestruque and P. Antsaklis. On the model-based control of networked systems. *Automatica*, 39:1837–1843, 2003.

[189] M. Morari and J.H. Lee. Model predictive control: past, present and future. *Comp. & Chem. Eng*, 23:667–682, 1999.

[190] A.S. Morse. Global stability of parameter-adaptive control systems. *IEEE Trans. Automatic Control*, 25(3):433–439, 1980.

[191] A.S. Morse, D.Q. Mayne, and G.C. Goodwin. Applications of hysteresis switching in parameter adaptive control. In *Proceedings of the 30th IEEE Conference on Decision and Control*, 1, 767–772, 1991.

[192] J. Muller, B. Rech, J. Springer, and M. Vanecek. TCO and light trapping in silicon thin film solar cells. *Solar energy*, 77(6):917–930, 2004.

[193] K.S. Narendra and J. Balakrishnan. Adaptive control using multiple models. *IEEE Trans. Automatic Control*, 42(2):171–187, 1997.

[194] K.S. Narendra and L.S. Valavani. Stable adaptive controller design-direct control. *IEEE Trans. Automatic Control*, 23(4):570–583, 1978.

[195] K.S. Narendra, Lin Y., and L.S. Valavani. Stable adaptive controller design, part ii: Proof of stability. *IEEE Trans. Automatic Control*, 25(3):440–448, 1980.

[196] J. Ng and S. Dubljevic. Boundary control synthesis for a Lithium-ion battery thermal regulation problem. *AIChE J.*, 59(10):3782–3796, 2013.

[197] A. Okabe and A. Suzuki. Locational optimization problems solved through Voronoi diagrams. *European J. Oper. Res.*, 98:445456, 1997.

[198] Y. Orlov and D. Dochain. Discontinuous feedback stabilization of minimum-phase semilinear infinite-dimensional systems with application to chemical tubular reactor. *IEEE Trans. Automatic Control*, 47(8):1293–1304, 2002.

[199] Z. Pan and T. Basar. Adaptive controller design for tracking and disturbance attenuation in parametric strict-feedback nonlinear systems. *IEEE Trans. Automatic Control*, 43(8):1066–1083, 1998.

[200] I.N.M. Papadakis and S.C.A. Thomopoulos. Improved performance model reference adaptive control with parameter mismatch compensation. *IEEE Trans. Automatic Control*, 41(2):224–227, 1996.

[201] P. Parks. Lyapunov redesign of model reference adaptive control systems. *IEEE Trans. Automatic Control*, 11(3):362–367, Jul 1966.

[202] R. Penrose. A generalized inverse for matrices. *Proceedings of the Cambridge Philosophical Society*, 51:406–413, 1955.

[203] S. Pitchaiah and A. Armaou. Output feedback control of distributed parameter systems using adaptive proper orthogonal decomposition. *Ind. Eng. Chem. Res.*, 49:10496–10509, 2010.

[204] S. Pitchaiah and A. Armaou. Output feedback control of dissipative PDE systems with partial sensor information based on adaptive model reduction. *AIChE J.*, 59(3):747–760, 2013.

[205] A.D. Polyanin and V.F. Zaitsev. *Handbook of nonlinear partial differential equations.* Chapman & Hall/CRC, Boca Raton, 2004.

[206] L. Praly. Robust model reference adaptive controllers, part i: Stability analysis. In *The 23rd IEEE Conference on Decision and Control*, 1009–1014, 1984.

[207] C. Qian and W. Lin. Output feedback control of a class of nonlinear systems: A nonseparation principle paradigm. *IEEE Trans. Autom. Cont.*, 47(10):1710–1715, 2002.

[208] V. Ramadesigan, P.W.C. Northrop, S. De, S. Santhanagopalan, R.D. Braatz, and V.R. Subramaniana. Modeling and simulation of Lithium-Ion batteries from a systems engineering perspective. *Journal of The Electrochemical Society*, 159(3):R31–R45, 2012.

[209] Z. Rao and S. Wang. A review of power battery thermal energy management. *Renewable and Sustainable Energy Reviews*, 15(9):4554–4571, 2011.

[210] M. Rathinam and L.R. Petzold. A new look at proper orthogonal decomposition. *SIAM J. Numer. Anal.*, 41:1893–1925, 2003.

[211] J.B. Rawlings, E.S. Meadows, and K.R. Muske. Nonlinear model predictive control: A tutorial and survey. In *Proceedings of International Symposium on Advanced Control of Chemical Processes*, 203–214, Kyoto, Japan, 1994.

[212] W.H. Ray. *Advanced process control.* McGraw-Hill, Stoneham, 1981.

[213] S.F. Rowlands, J. Livingstone, and C.P. Lund. Optical modeling of finely textured amorphous silicon solar cells. *Solar Energy Materials and Solar Cells*, 71(3):399–405, 2002.

[214] C.W. Rowley. Model reduction for fluids, using balanced proper orthogonal decomposition. *International Journal of Bifurcation & Chaos in Applied Sciences & Engineering*, 15(3):997–1013, 2005.

[215] C.W. Rowley, I. Mezic, S. Bagheri, P. Schlatter, and Henningson D.S. Spectral analysis of nonlinear flows. *J. Fluid Mech.*, 641:115–127, 2009.

[216] D.L. Russell. Controllability and stabilizability theory for linear partial differential equations: Recent progress and open questions. *SIAM Review*, 20:639–739, 1978.

[217] Y. Saad. *Iterative methods for sparse linear systems, in Transition and Turbulence.* Academic press, New York, 1981.

[218] S.S. Sastry and A. Isidori. Adaptive control of linearizable systems. *IEEE Trans. Automatic Control*, 34(11):1123–1131, 1989.

[219] C. Scherer, P. Gahinet, and M. Chilali. Multiobjective output-feedback control via LMI optimization. *IEEE Trans. Automatic Control*, 42:896–911, 1997.

[220] P.J. Schmid. Dynamic mode decomposition of numerical and experimental data. *J. Fluid Mech.*, 656:5–28, 2010.

[221] P.J. Schmid. Application of the dynamic mode decomposition to experimental data. *Exp. Fluids*, 50(4):1123–1130, 2011.

[222] P.J. Schmid, L. Li, M.P. Juniper, and O. Pust. Applications of the dynamic mode decomposition. *Theor. Comput. Fluid Dyn.*, 25(1-4):249–259, 2011.

[223] A. Serrani. An output regulation perspective on the model reference adaptive control problem. *International Journal of Adaptive Control and Signal Processing*, 27(1-2):22–34, 2013.

[224] S.Y. Shvartsman and I.G. Kevrekidis. Low-dimensional approximation and control of periodic solutions in spatially extended systems. *Phys. Rev. E*, 58:361–368, 1998.

[225] S.Y. Shvartsman and I.G. Kevrekidis. Nonlinear model reduction for control of distributed parameter systems: A computer assisted study. *AIChE J.*, 44:1579–1595, 1998.

[226] S.Y. Shvartsman, C. Theodoropoulos, R. Rico-Martinez, I.G. Kevrekidis, E.S. Titi, and T.J. Mountziaris. Order reduction for nonlinear dynamic models of distributed reacting systems. *J. Process Contr.*, 10:177–184, 2000.

[227] J.R. Singler. New POD error expressions, error bounds, and asymptotic results for reduced order models of parabolic PDEs. *SIAM J. Numer. Anal.*, 52(2):852–876, 2014.

[228] L. Sirovich. Turbulence and the dynamics of coherent structures: Parts I, II and III. *Quarterly of Applied Mathematics*, XLV:561–590, 1987.

[229] M. Skliar and P. Tathireddy. Approximation of evolutional system using singular forcing. *Comp. & Chem. Eng.*, 26:1013–1021, 2002.

[230] J.J.E. Slotine and W. Li. *Applied nonlinear control.* Prentice-Hall, New Jersey, 1991.

[231] K. Smith, C.D. Rahn, and C. Wang. Model-based electrochemical estima-

tion and constraint management for pulse operation of Lithium-ion batteries. *IEEE Trans. Cont. Sys. Tech.*, 18(3):654–663, 2010.

[232] R.C. Smith and M.A. Demetriou. *Research directions in distributed parameter systems.* SIAM Frontiers in Applied Mathematics, Philadelphia, PA, 2003.

[233] A. Smyshlyaev and M. Krstic. *Adaptive control of parabolic PDEs.* Princeton Univ. Press, Princeton, NJ, 2010.

[234] A. Smyshlyaev, M. Krstic, N. Chaturvedi, J. Ahmed, and A. Kojic. PDE model for thermal dynamics of large Li-ion battery pack. In *Proceedings of the American Control Conference*, 959–964, San Francisco, CA, 2011.

[235] E. Sontag. A universal construction of Artsteins theorem on nonlinear stabilization. *Sys. & Contr. Lett.*, 13:117–123, 1989.

[236] C. Su, Y. Stepanenko, J. Svoboda, and T.P. Leung. Robust adaptive control of a class of nonlinear systems with unknown backlash-like hysteresis. *IEEE Trans. Automatic Control*, 45(12):2427–2432, 2000.

[237] J. Sun. A modified model reference adaptive control scheme for improved transient performance. *IEEE Trans. Automatic Control*, 38(8):1255–1259, 1993.

[238] Y. Sun, S. Ghantasala, and N.H. El-Farra. Networked control of specially distributed processes with sensor-controller communication constraints. In *Proceedings of the American Control Conference*, 2489–2494, St. Louis, MO, 2009.

[239] X. Tan and J.S. Baras. Adaptive identification and control of hysteresis in smart materials. *IEEE Trans. Automatic Control*, 50(6):827–839, 2005.

[240] Y. Tang, E.F. Camacho, and J.J. Flores. Frequency domain adaptive control: Band-wise compensation. *Automatica*, 31(5):735 – 740, 1995.

[241] G. Tao. Multivariable adaptive control: A survey. *Automatica*, 50(11):2737 – 2764, 2014.

[242] J.M. Tarascon and M. Armand. Issues and challenges facing rechargeable Lithium batteries. *Nature*, 414:359–367, 2001.

[243] I.H. Tarman and L. Sirovich. Extensions to Karhunen-Loèvebased approximation of complicated phenomena. *Comput. Methods. Appl. Mech. Engrg.*, 155:359–368, 1998.

[244] R. Temam. *Infinite-dimensional dynamical systems in mechanics and physics.* Springer-Verlag, New York, 1988.

[245] G. Teschl. *Ordinary differential equations and dynamical systems: Graduate Studies in Mathematics.* Amer. Math. Soc., Providence, 2012.

[246] T. Tezcan I.E., Basar. Disturbance attenuating adaptive controllers for parametric strict feedback nonlinear systems with output measurements. *J. Dyn. Sys., Meas., Control*, 121(1):48–57, 1999.

[247] T.B. Thanh, M. Damodaram, and K. Willcox. Aerodynamic data reconstruction and inverse design using proper orthogonal decomposition. *AIAA. J.*, 42:1505–1516, 2004.

[248] A. Theodoropoulou, R.A. Adomaitis, and E. Zafiriou. Model reduction for optimization of rapid thermal chemical vapor deposition systems. *IEEE Trans. Semicond. Manuf.*, 11(1):85–98, 1998.

[249] A. Tronci, F. Bezzo, M. Barolo, and R. Baratti. Geometric observer for a distillation column: Development and experimental testing. *Ind. Eng. Chem. Res.*, 44:9884–9893, 2005.

[250] H.S. Tsien. *Engineering cybernetics.* McGraw-Hill, New York, 1954.

[251] D. Ucinski. *Measurement Optimization for Parameter Estimation in Distributed Systems.* Technical University Press, Zielona Gora, 1999.

[252] D. Ucinski. *Optimal Measurement Methods for Distributed Parameter System Identification.* CRC Press, Boca Raton, 2005.

[253] V.I. Utkin. *Sliding modes in control and optimization.* Springer-Verlag, Berlin, 1992.

[254] B. van Keulen. H_∞-*Control for Distributed Parameter Systems: A State-Space Approach.* Birkhäuser, Boston, 1993.

[255] A. Varshney and A. Armaou. Optimal operation of GaN thin film epitaxy employing control vector parameterization. *AIChE J.*, 52:1378–1391, 2006.

[256] A. Varshney, S. Pitchaiah, and A. Armaou. Feedback control of dissipative distributed parameter systems using adaptive model reduction. *AIChE J.*, 55:906–918, 2009.

[257] R.J. Veillette. Reliable linear-quadratic state feedback control. *Automatica*, 31:137–143, 1995.

[258] D. Venturi and G.M. Karniadakis. Gappy data and reconstruction procedures for flow past a cylinder. *J. Fluid Mech*, 519:315–336, 2004.

[259] F. Wang, N. Jin, D. Liu, and Q. Wei. Adaptive dynamic programming for finite-horizon optimal control of discrete-time nonlinear systems with ε-error bound. *IEEE Trans. Neural Networks*, 22(1):24–36, 2011.

[260] J. Wang and Z. Qu. Robust adaptive control of time-varying uncertain systems with nonlinear parameterization. *IET Control Theory & Applications*, 3(6):617630, 2009.

[261] Q. Wang, P. Ping, X. Zhao, G. Chu, J. Sun, and C. Chen. Thermal runaway caused re and explosion of Lithium-ion battery. *Journal of Power Sources*, 208:210–224, 2012.

[262] C. Wen. An indirect robust continuous-time adaptive controller with minimal modifications. *Automatica*, 31(2):293 – 296, 1995.

[263] J. Wen and M.J. Balas. Robust adaptive control in hilbert space. *Journal of Mathematical Analysis and Applications*, 143(1):1 – 26, 1989.

[264] N. Wiener. *Cybernetics: or control and communication in the animal and the machine.* MIT Press, Cambridge, MA, 1948.

[265] K. Willcox. Unsteady flow sensing and estimation via the gappy proper orthogonal decomposition. *Computers & Fluids*, 35:208–226, 2006.

[266] L.C. Windes, A. Cinar, and W.H. Ray. Dynamic estimation of temperature and concentration profiles in a packed-bed reactor. *Chem. Eng. Sci.*, 44:2087–2106, 1989.

[267] H. Wu, J. Hu, and Y. Xie. Characteristic model-based all-coefficient adaptive control method and its applications. *IEEE Trans. Systems, Man, and Cybernetics, Part C: Applications and Reviews*, 37(2):213–221, 2007.

[268] L. Xie and L. Guo. Fundamental limitations of discrete-time adaptive nonlinear control. *IEEE Trans. Automatic Control*, 44(9):1777–1782, 1999.

[269] A. Yakhot, T. Anor, and G.M. Karniadakis. A reconstruction method for gappy and noisy arterial flow data. *IEEE transactions on medical imaging*, 26:1681–1697, 2007.

[270] Z. Yao and N.H. El-Farra. Networked control of specially distributed processes using an adaptive communication policy. In *Proceedings of the 49th IEEE Conference on Decision and Control*, Atlanta, GA, 2010.

[271] Z. Yao, S. Sun, and N.H. El-Farra. Resource-aware scheduled control of distributed process systems over wireless sensor networks. In *Proceedings of the American Control Conference*, 4121–4126, Baltimore, MD, 2010.

[272] E.B. Ydstie and A.A. Alonso. Process systems and passivity via the Clausius-Planck inequality. *Syst. & Contr. Lett.*, 30:253–264, 1997.

[273] S. Yulei, S. Ghantasala, and N.H. El-Farra. Networked control of spatially distributed processes with sensor-controller communication constraints. In *Proceedings of the American Control Conference*, 2489–2494, St. Louis, MO, 2009.

[274] M. Zeman, R. vanSwaaij, J.W. Metselaar, and R.E.I. Schropp. Optical modeling of a-Si:H solar cells with rough interfaces: Effect of back contact and interface roughness. *Journal of Applied Physics*, 88(11):6436–6443, 2000.

[275] C. Zhang and R.J. Evans. Continuous direct adaptive control with saturation input constraint. *IEEE Trans. Automatic Control*, 39(8):1718–1722, 1994.

[276] J.F. Zhang. Robust stabilization of lti systems via indirect adaptive controllers. *IEEE Trans. Automatic Control*, 40(5):900–906, 1995.

[277] J.F. Zhang and L.Y. Wang. Performance lower bounds in stochastic robust and adaptive control. *IEEE Trans. Automatic Control*, 46(7):1137–1141, 2001.

[278] Y. Zhiyuan and N.H. El-Farra. Networked control of spatially distributed processes using an adaptive communication policy. In *49th IEEE Conference on Decision and Control*, 13–18, Atlanta, GA, 2010.

[279] Y. Zhiyuan and N.H. El-Farra. Robust stabilization of sampled-data distributed processes using a dynamic sensor-controller communication logic. In *Proceedings of the American Control Conference*, 2982–2987, San Francisco, CA, 2011.

[280] K. Zhou, J.C. Doyle, and K. Glover. *Robust and optimal control.* Prentice-Hall, Englewood Cliffs, NJ, 1996.

[281] A.S. Zinober. *Deterministic control of uncertain systems.* Peter Peregrinus Ltd., London, 1990.

Vita

Davood Babaei Pourkargar

Education

Ph.D., Chemical Engineering, Penn State University, University Park, 2011-2015. Thesis title: "Synthesis of advanced control structures for complex chemical processes using sensor networks", Advisor: Professor A. Armaou.

M.S., Chemical Engineering - Process Modeling, Simulation and Control, Sharif University of Technology, Tehran, 2008-2010. Thesis title: "Simulation, control and synchronization of chaotic chemical reactors", Advisor: Professor M. Shahrokhi.

B.S., Chemical Engineering, Sharif University of Technology, Tehran, 2004-2008. Thesis title: "Dynamic simulation of multiphase transport-reaction processes", Advisor: Professor R. Bozorgmehry Boozarjomehry.

Awards and Honors

1. O. Hugo Schuck Best Paper Award in the Application Category, American Automatic Control Council (AACC), 2014.

2. Finalist Best Paper Award, Department of Chemical Engineering, PennState University, 2014.

3. Society of Industrial and Applied Mathematics Graduate Student Travel Grant, 2014.

4. AACC Student Travel Awards, 2013 & 2014 & 2015.

5. Best Session Presentation Awards in American Control Conferences (Session MoA14, 2013 and Session ThA16, 2015).

6. Walter R. and Aura Lee Supina Graduate Fellowship in Chemical Engineering, PennState University, 2011.

Journal Papers

1. Pourkargar D.B., Armaou A., "Spatiotemporal dynamic shaping of nonlinear dissipative distributed parameter systems using empirical basis functions", *Journal of Process Control*, 2015, under review.

2. Pourkargar D.B., Armaou A., "Lyapunov-based control of dissipative distributed parameter systems via adaptive model order reduction with minimum feedback information", *IEEE Transaction on Automatic Control*, 2015, under review.

3. Pourkargar D.B., Armaou A., "Dynamic shaping of transport-reaction processes via sliding mode controller designs", *Chemical Engineering Science*, 2015, accepted.

4. Pourkargar D.B., Armaou A., "Design of APOD-based switching dynamic observers and output feedback control for a class of nonlinear distributed parameter systems", *Chemical Engineering Science, Special Issue on Smart Plants*, 2015, in press, DOI:10.1016/j.ces.2015.02.032.

5. Pourkargar D.B., Armaou A., "Control of spatially distributed processes with unknown transport-reaction parameters via two layer system adaptations", *AIChE Journal*, **61(8)**, 2497-2507, 2015.

6. Pourkargar D.B., Armaou A., "APOD-based control of general linear distributed parameter systems in the presence of network communication constraints", *AIChE Journal*, **61(2)**, 434-447, 2015.

7. Pourkargar D.B., Armaou A., "Geometric output tracking of nonlinear distributed parameter systems via adaptive model reduction", *Chemical Engineering Science*, **116**, 418-427, 2014.

8. Pourkargar D.B., Armaou A., "Modification to adaptive model reduction for regulation of distributed parameter systems with fast transients", *AIChE Journal*, **59(12)**, 4595-4611, 2013.